SYNTHESIS AND CHARACTERIZATION OF DNA NANO-MESO-MICROSPHERES AS DRUG DELIVERY CARRIERS FOR INTRATUMORAL CHEMOTHERAPY

By

IRIS VANESSA ENRIQUEZ SCHUMACHER

A DISSERTATION PRESENTED TO THE GRADUATE SCHOOL
OF THE UNIVERSITY OF FLORIDA IN PARTIAL FULFILLMENT
OF THE REQUIREMENTS FOR THE DEGREE OF
DOCTOR OF PHILOSOPHY

UNIVERSITY OF FLORIDA

2007

To my sister Laura Susana and my parents Iris and Pedro Enriquez, for being a source of constant strength and unconditional love and support through all of life's endeavors.
To my grandparents Cecilio and Susana Cartagena and Pablo and Carmen Enriquez, for instilling in our families the value and importance of a great education.
To my husband Jim, for walking by my side through this journey.

ACKNOWLEDGMENTS

I must acknowledge the many advisors, family members, colleagues, and friends whose support made it possible for me to complete my doctoral studies and research. I express my most sincere gratitude to my advisor and committee chairman, Dr. Eugene P. Goldberg for challenging and guiding me through this research and for always being present as a mentor in science and in life. His support, guidance, caring, and patience allowed me to complete this research and to grow as a scientist. I also thank the other members of my committee, Dr. Anthony Brennan, Dr. Chris Batich, Dr. Wolfgang Streit, Dr. Hassan El-Shall, and Dr. Ronald Baney, who have each individually guided, encouraged, and supported me through this graduate school journey. I extend a special thanks to Gill Brubaker for his friendship and support and for always sharing his knowledge on particle characterization techniques and analysis. In addition, special thanks are extended to the faculty and staff at the Particle Engineering Research Center, especially Gary Scheiffele and Sophie Leone for providing training on equipment and providing access to their facilities. I also thank Drs. Olajompo Moloye, Taili Thula, and John Azeke from the Batich research group for offering their assistance and knowledge in cell culture and DNA purity analysis. Additionally, I thank the Major Analytical Instrumentation Center, especially Wayne Acree for always preparing my samples to exact specification and for providing access to their instrumentation.

I acknowledge my appreciation of Paul Martin for his friendship, lively discussions, assistance with SEM, and for patiently sharing his knowledge of cell culture. I also gratefully acknowledge Jennifer Wrighton whom has not only provided considerable administrative assistance throughout my graduate studies, but whom has also provided a solid foundation of support through her caring and friendship. A very special thanks is extended to Dr. Richard

"Doc" Connell for his caring mentorship, friendship, support, discussions of materials science, and lessons of life that will be carried with me always.

I would like to acknowledge several key individuals who laid the initial building blocks and opened the door for this research. First, I extend a special acknowledgement to Dr. Brian Cuevas, who provided a tremendous amount of mentorship and encouragement when I first started graduate school despite the fact that he was in the middle of completing his doctoral research and writing his dissertation. Second, I extend a special thanks to Dr. Joshua Stopek who also provided encouragement and support during my first two years in the Goldberg research group and offered a multitude of knowledge on DNA, biomaterials, and the scientific thought process. Third, I wish to acknowledge Dr. Amanda York who took the time to teach me microsphere synthesis and characterization techniques. Fourth, I sincerely thank the undergraduate research assistants, Karly Jacobsen, Jeanney Lew, and Nathan Hicks, who taught me, as much as I taught them, and whose help and hard work facilitated in the completion of this research. Lastly, I acknowledge the other members of the Goldberg research group including Shema Freeman, Dr. Amin Elachchabi, Samesha Barnes, Dr. Lynn Peck, Hungyen Lee, Drs. Margaret and Daniel Urbaniak, and Dr. Adam Reboul whose either support, unconditional friendship, or enthusiasm have made the completion of this work possible.

I also express a very special thanks to the following friends Drs. Brian and Robin Hatcher, Dr. Brett Almond, Erica Kennedy, Dr. Adam Feinberg, Ayelet Feinberg, Dr. Clay Bohn, Christa Partridge, Dr. Thomas Estes, Nancy Estes, Dr. Leslie Wilson, Dr. Cliff Wilson, Dr. Michelle Carman, Dr. Marie Kane, Kevin Kane, Dr. Jeff Wrighton, Jason Ely, Julie Reboul, Kenneth Chung, Chris Long, Victoria Salazar, Jim Seliga, Anika Odukale Edwards, Nelly Volland, Thierry Dubroca, David Jackson, Julian Sheats, Chelsea Magin, and the family of committee

members including Lehua Goldberg, Kathy Brennan, and Abby Brennan, whose love, support, encouragement, and unconditional friendship have made this process that much more worth while.

I am indebted to my family for their unconditional love, encouragement, and support which have truly made it possible for me to reach my goals and obtain my dreams. I thank my younger sister and guardian angel, Laura Susana Enriquez, who has always been by my side when I have needed it most. I especially thank my parents, Iris and Pedro Enriquez, for setting an amazing example for my sister and me and whose love and encouragement helped me persevere through each challenge and obstacle placed in my path. I could not have done this without their love and support. I extend a special thanks to my grandparents Susana and Cecilio Cartagena and Carmen and Pablo Enriquez for their life lessons and unconditional love and support. I also thank the rest of my family members whose love and encouragement were also close by. In addition, I thank my in-laws, Susan, Fred, and Jennele Schumacher, Grandpa Bob and Grandma Carole Bevilacqua, Grandma Schumacher, and the rest of the family for their generous love and support.

I express my most sincere appreciation to my husband, James Schumacher, whose unending love, patience, encouragement, and support made this journey possible.

TABLE OF CONTENTS

LIST OF TABLES

LIST OF FIGURES

LIST OF ABBREVIATIONS

$\%M_{EQ}$	Percent molar equivalence
% (w/v)	Percent weight per volume
% (w/w)	Percent weight per weight
%Yield	Percent yield
µg	Microgram (1×10^{-6}g)
µL	Microliter (1×10^{-6}L)
µm	Micrometer (1×10^{-6}m)
ρ_{DNA}	Density of aqueous DNA solution used in MS preparation
5-FU	5-Fluorouracil
ANOVA	Analysis of variance
BSA	Bovine serum albumin
BSA-MS	BSA nano-meso-microsphere(s)
BSS	Balanced salt solution
CAB	Cellulose acetate butyrate dissolved in 1,2-dichloroethane
Cr	Chromium trivalent cation
C_{DNA}	Concentration of the aqueous DNA solution used in MS preparation
d	Particle diameter
D_D	Dry DNA-MS diameter
D_H	Hydrated DNA-MS diameter
DMEM	Dulbecco's Modified Eagle's Media with L-glutamine
DNA	Deoxyribonucleic acid
DNA-MS	DNA nano-meso-microsphere(s)
DNA-MXN-MS	Mitoxantrone *in situ* loaded DNA nano-meso-microsphere(s)

EDS	Energy dispersive x-ray spectroscopy
EDTA	Ethylenediamine tetraacetic acid
EMEM	Eagle's Minimum Essential Modified Media
FBS	Fetal bovine serum
Fe	Iron trivalent cation
FSEM	Field emission scanning electron microscope
G_0	Quiescence or non-proliferating phase of the cell cycle
G_1	Intermitotic phase of the cell cycle
G_2	Premitotic phase of the cell cycle
Gd	Gadolinium trivalent cation
GEL	Gelatin
GEL-MS	Gelatin nano-meso-microsphere(s)
Genipin	GEN
GTA	Glutaraldehyde
hr	Hour(s)
KeV	Kiloelectron volt (1×10^3eV)
LDH	Lactate dehydrogenase
M	Molar or Mitotic phase in the cell cycle
MEM	Minimum essential media
mg	Milligram (1×10^{-3}g)
min	Minute(s)
mL	Milliliter (1×10^{-3}L)
mLLC	Murine Lewis lung carcinoma

mm	Millimeter
mM	Millimolar (1×10^{-3}M)
MS	Nano-meso-microsphere(s)
MTS	Colorimetric cell growth or viability assay
MTX	Methotrexate
mV	Millivolts
MXN	Mitoxantrone
NADH	Nicotinamide adenine dinucleotide linked dehydrogenase
NAD^+	Nicotinamide adenine dinucleotide
NEAA	Non-essential amino acid
nm	Nanometer (1×10^{-9}m)
PBS	Phosphate buffered saline
rpm	Revolutions per minute
S	DNA synthesis phase of the cell cycle
SEM	Scanning electron microscopy
TCA	Trichloroacetic acid
UV-Vis	Ultraviolet – visible spectroscopy
V_{DNA}	Volume of aqueous DNA solution used in MS preparation
W_F	Final weight of DNA-MS
W_{TSOLID}	True solid weight of BSA or DNA
W_{TDNA}	True solid weight of DNA
W_X	Solid weight of crosslinking agent added during MS synthesis
W_Y	Weight of the *in situ* loaded mitoxantrone

XgDrug	Weight of methotrexate or 5-fluorouracil
XgMXN	Weight of mitoxantrone

Abstract of Dissertation Presented to the Graduate School
of the University of Florida in Partial Fulfillment of the
Requirements for the Degree of Doctor of Philosophy

SYNTHESIS AND CHARACTERIZATION OF DNA NANO-MESO-MICROSPHERES AS DRUG DELIVERY CARRIERS FOR INTRATUMORAL CHEMOTHERAPY

By

Iris Vanessa Enriquez Schumacher

August 2007

Chair: Eugene P. Goldberg
Major: Materials Science and Engineering

Conventional cancer chemotherapy results in systemic toxicity which severely limits effectiveness and often adversely affects patient quality of life. There is a need to find new drugs and delivery methods for less toxic therapy.

Previous studies concerning DNA complexing with chemotherapy drugs suggest unique opportunities for DNA as a mesosphere drug carrier. The overall objective of this research was devoted to the synthesis and evaluation of novel DNA-drug nano-mesospheres designed for localized chemotherapy via intratumoral injection. My research presents DNA nano-meso-microspheres (DNA-MS) that were prepared using a modified steric stabilization method originally developed in this lab for the preparation of albumin MS. DNA-MS were prepared with glutaraldehyde covalent crosslinking (genipin crosslinking was attempted) through the DNA base pairs. In addition, novel crosslinking of DNA-MS was demonstrated using chromium, gadolinium, or iron cations through the DNA phosphate groups. Covalent and ionic crosslinked DNA-MS syntheses yielded smooth and spherical particle morphologies with multimodal size distributions.

Optimized DNA-MS syntheses produced particles with narrow and normal size distributions in the 50nm to 5μm diameter size range. In aqueous dispersions approximately 200% swelling was observed with dispersion stability for more than 48 hours. Typical process conditions included a 1550rpm initial mixing speed and particle filtration through 20μm filters to facilitate preparation.

DNA-MS were *in situ* loaded during synthesis for the first time with mitoxantrone, 5-fluorouracil, and methotrexate. DNA-MS drug incorporation was 12%(w/w) for mitoxantrone, 9%(w/w) for methotrexate, and 5%(w/w) for 5-fluorouracil. *In vitro* drug release into phosphate buffered saline was observed for over 35 days by minimum sink release testing. The effect of gadolinium crosslink concentration on mitoxantrone release was evaluated at molar equivalences in the range of 20% to 120%. The most highly crosslinked DNA-MS exhibited the longest sustained release.

The drug efficacy of mitoxantrone loaded DNA-MS was evaluated *in vitro* using a murine Lewis lung carcinoma cell line and a significant cytotoxic response was found at mitoxantrone doses as low as 1ppm. Drug release properties, DNA biodegradability, and observed cancer cell cytotoxicity of drug loaded DNA-MS suggest that they are appropriate for intratumoral chemotherapy evaluation aimed at improved and less toxic cancer therapy.

CHAPTER 1
INTRODUCTION

Research Rationale

Cancer is the second most common cause of death in the United States, following heart disease, and accounts for every 1 in 4 deaths nationwide according to the 2005 and 2006 cancer statistic reports published by the American Cancer Society.[1, 2] Over one-half of these reported deaths can be attributed to cancers of the breast, prostate, lung and bronchus, and colon and rectum for both men and women.[1] Leukemia and cancer of the brain and central nervous system account for one-half of all children's fatalities.[2] Primary modalities of treatment for these and other forms of cancer include surgery, radiation, and systemic chemotherapy.[3] Conventional systemic chemotherapy is often used as the standard of care for most cancer cases, and, in many circumstances, is given in combination with surgery or radiation therapy in order to decrease the size of the tumor prior to excision or enhance the effects of radiation on cancerous cells.[3]

Conventional systemic chemotherapy functions by attacking rapidly dividing cancer cells while traveling through the bloodstream. When used as a sole form of treatment, conventional systemic chemotherapy often provides limited effectiveness and compromises the quality of life for its patients.[4] Patients undergoing systemic chemotherapy not only experience a variety of acute side effects such as nausea, mouth sores, alopecia (hair loss), irritation of the veins, and induced menopause, but may also experience debilitating long term effects such as multiple organ failure and even death.[3, 5] Adverse side effects, such as those just previously mentioned, arise because chemotherapeutic agents are incapable of differentiating between cancerous cells and healthy rapidly dividing cells such as hair follicle, gastrointestinal, and bone marrow cells.

The inability for chemotherapy agents to differentiate between healthy cells and cancerous cells are not solely to blame for their lack of therapeutic efficacy. When delivered

intravenously, chemotherapeutic agents are very effective against blood borne cancers such as leukemia and lymphoma, however, they tend to be less effective against solid tumor cancers such as that of the breast, lung and bronchus, prostate, colon and rectum, and head and neck.[6, 7] The therapeutic deficiency of systemic chemotherapy against solid tumor cancers can be attributed to the inability for chemotherapy agents to penetrate the tumor cells due to their intricate vasculature and interstitium.[6, 7]

It is estimated that there will be 1,399,760 new cases of cancer diagnosed this year resulting in a vast demand for conventional treatment modalities such as systemic chemotherapy.[2] This large demand for systemic chemotherapy produces an urgent need for researchers to develop new delivery methods to localize chemotherapy to thereby reduce its systemic toxicity and increase its therapeutic efficacy.

The idea of localizing chemotherapy has been around since the onset of its use in the 1940s.[8] In the 1950s, scientists such as C.T. Klopp and others experimented with localizing chemotherapy agents such as nitrogen mustard by intra-arterial infusion.[8, 9] They found that the intra-arterial infusion of these agents led to increased efficacy, however, the dose required for this type of administration did not eradicate problems with systemic toxicity. Over the next 40 years, these findings led to the development of drug delivery carriers in the form of microspheres synthesized from proteins, polysaccharides, and synthetic polymers.[10] The most successful of the aforementioned microsphere formulations were those synthesized with bovine serum albumin or human serum albumin.[10] The success of albumin protein as a microsphere drug carrier can be attributed to its high stability, biodegradability, and ease of processing.[10] Past research has shown the ability of albumin to load various drugs such as doxorubicin, mitomycin C, cisplatin, 5-fluorouracil, and mitoxantrone.[4, 10, 11] Recently it has been shown that the intratumoral

delivery of mitoxantrone loaded albumin microspheres localized the activity of mitoxantrone and increased survival time in a murine mammary adenocarcinoma model.[4, 12] This research also indicated that the maximum tolerable dose of mitoxantrone increased 8-fold when delivered intratumorally rather than intravenously.[12]

The use of albumin as a chemotherapy drug carrier has been successful with a variety of anti-tumor agents, however, it has one major disadvantage in that it has a low drug-carrying capacity.[10] The maximum drug payload for mitoxantrone loaded albumin microspheres has been limited to 15% (w/w).[4, 11] Studies have been conducted to increase the payload of cationic drugs, such as doxorubicin, into albumin microspheres by incorporating anionic constituents into the albumin carrier matrix.[10] These studies have shown that the incorporation of anionic materials help to increase the loading capacity of the albumin microspheres by 4 times the original value, however, the downfall was that the release of drug via ionic binding was rapid.[10] Recent research has shown similar results except that drug release was prolonged.[13] Studies conducted recently illustrated that the incorporation of anionic poly(glutamic) acid into gelatin microspheres did not increase the payload of cationic mitoxantrone, however, it did extend its release over 100 days.[13]

Many know DNA for its role as a carrier of genetic information; however, very few have given thought to the possible biomaterial functions of this supramolecular biopolymer. For the past 30 years scientists have focused their efforts on the delivery of viral DNA, otherwise known as plasmid DNA, for its function as a gene expressor and for its novel use as a therapeutic for cancer and genetic disorders.[14-16] With most attention focused on plasmid DNA, scientists have overlooked the attractive properties that chromosomal DNA has to offer. It has only been within

the past decade that scientists have shown interest in the biomaterial functions of chromosomal DNA.

In the late 1990s, the use of DNA as a natural occurring functional biopolymer surfaced. Scientists began to report the successful coating of non-soluble DNA-alginic acid films on Millipore filters for the successful absorption and removal of toxic intercalating pollutants such as benzopyrene.[17] Insoluble DNA films cast on polysulfone dialysis membranes were also researched and scientists illustrated that the DNA films increased the hydrophilicity and hemocompatibility of the hydrophobic polysulfone surfaces.[18] Scientists have even shown that DNA-lipid films can be used as drug delivery vehicles and antimicrobial surfaces by incorporating agents such as ethidium bromide and silver ions into the film.[19, 20] Most recently, scientists have shown that DNA may be used as a structural biopolymer for the development of biodegradable scaffolds for tissue engineering.[21] In the early 1980s, Trouet et al complexed DNA to adriamycin and daunorubicin chemotherapeutic agents and injected the DNA-drug complex intravenously into rabbit and mice models.[22, 23] These studies found that the DNA-drug complexes reduced the cardiotoxicity and improved the half-lives of the drugs.[22, 23]

The novelty of the use of DNA as a functional biopolymer and the need for developing new methods for delivering chemotherapy is what inspired the research presented in this dissertation. The research presented here describes the development and use of DNA nano-meso-microspheres as drug carriers. Shortly after these studies began, a collaboration with Dr. Amanda York looked at incorporating 1.5% (w/w) DNA into albumin microspheres.[24] The results from these studies indicated that DNA blended albumin microspheres not only loaded the same amount of drug as the albumin microspheres, but also extended release over 1000 hours.[13, 24] The optimistic payload and release characteristics of the DNA blended albumin microspheres,

which had not yet been reported in the literature, further solidified the concept of using DNA as a sole drug carrying material.

Specific Aims

The research presented in this dissertation was devoted to the development of a novel drug delivery carrier for localized or regional chemotherapy using DNA.

Aim 1: Synthesis and Characterization of DNA Nano-Meso-Microspheres

Nano-meso-microspheres from DNA derived from herring testes (DNA-MS) were synthesized to a target dry mean diameter range of 50nm to 20μm, where at least 60% of all particles prepared were within the mesosphere size range of 1μm to 10μm and < 5% of all particles were greater than 10μm in size. Particles less than 1μm in diameter were also acceptable. Hydrated particle diameters were to be less than 25μm. DNA-MS were sought to obtain aqueous dispersion stability of over 24 hours and elicit minimal toxic effect on fibroblast cells in culture.

DNA-MS were prepared using a modified steric stabilization process developed in this lab and were either covalently crosslinked with genipin or glutaraldehyde or ionically crosslinked with chromium (III) potassium sulfate, gadolinium (III) chloride, or iron (III) nitrate. A crosslinking reaction study was conducted, prior to any synthesis studies, to determine the time needed to establish DNA crosslinking with the covalent or ionic crosslinking agents. Crosslinking time was estimated by measuring the time required for each agent to precipitate DNA from solution. The crosslinking reaction study was conducted at room temperature with a maximum crosslink time of two hours to mimic conditions observed during DNA-MS synthesis. Preliminary studies were also conducted to determine the optimal concentration of the stabilizing agent used during DNA-MS synthesis.

The morphology and topography of the DNA-MS were examined by optical microscopy and scanning electron microscopy. The presence of trivalent cations in the DNA-MS was assessed by energy dispersive x-ray spectroscopy. Crosslinking was confirmed through DNA-MS dispersability testing in 0.05M phosphate buffered saline at a pH of 7.4. Dry and PBS swollen particle sizes were quantitatively characterized using an LS Coulter 13 320 particle size analyzer. The DNA-MS surface charge was measured by zeta potential analysis in 0.01M PBS at a pH of 7.4. Normal human dermal BJ fibroblast cells were used in culture to evaluate the effect of DNA and crosslinked DNA-MS on cell growth. Concentrations of 100µg and 500µg for DNA, and 25µg and 100µg for crosslinked DNA-MS were tested. A colorimetric MTS assay was used to measure fibroblast growth at the 0, 24, and 72 hour time points.

Aim 2: Optimization of DNA Nano-Mesosphere Synthesis

The process parameters for DNA-MS synthesis were optimized to produce controlled particle size distributions with mean dry diameters in the mesosphere size range of 1µm to 10µm and mean hydrated diameters of less than 25µm. DNA-MS were prepared to where at least 60% of all particles fell within the mesosphere size range of 1µm to 10µm and < 5% of all particles were greater than 10µm in size. Particles less than 1µm in diameter were also acceptable. DNA-MS were sought to obtain hydrated particle diameters of less than 25µm with aqueous dispersion stabilities of over 24 hours.

DNA-MS synthesis parameters were optimized by incorporating a filtration step at the end of the MS synthesis process with a filter pore size of 20µm to reduce or eliminate the presence of aggregates from the yield. The DNA-MS synthesis parameters were further optimized by analyzing the effects of mixer speed and crosslink concentration on particle diameter, swelling, morphology, and size distribution. Mixer speeds of 950rpm, 1250rpm, and 1550rpm with ionic crosslink concentrations of 20%, 50%, and 120% molar equivalence (M_{EQ}) were assessed for

these studies. Synthesized DNA-MS were characterized using the characterization techniques employed in Aim 1.

Aim 3: *In Vitro* Evaluations of Mitoxantrone *In Situ* Loaded DNA Nano-Mesospheres

Mitoxantrone *in situ* loaded DNA-MS (DNA-MXN-MS) were prepared using optimized synthesis conditions from Aim 2 to obtain particles with controlled size distributions where at least 60% of all particles prepared were within the mesosphere size range of 1μm to 10μm and < 5% of all particles were greater than 10μm in size. Particles less than 1μm in diameter were also acceptable and hydrated particle diameters were to be less than 25μm. In addition, MXN *in situ* loaded DNA-MS were sought to obtain loadings of ≥ 12% (w/w) MXN and release MXN for 24 hours or more in phosphate buffered saline under minimum sink conditions. DNA-MXN-MS at MXN concentrations of 1μg/mL, 10μg/mL, and 25μg/mL were also sought to elicit a cytotoxic response ≥ to that of free drug at the same MXN concentrations on murine Lewis lung carcinoma (mLLC) cells in culture.

Gadolinium cation crosslinked DNA-MS were *in situ* loaded with mitoxantrone using 20%M_{EQ}, 50%M_{EQ}, and 120%M_{EQ} crosslink concentrations. The particle diameter, size distribution, morphology, drug loading, and percent drug release of the DNA-MXN-MS were evaluated with respect to the crosslink concentration.

The particle diameter, size distribution, morphology, and presence of gadolinium trivalent cations were assessed using characterization techniques from Aim 2. Drug loading was determined by incubating the DNA-MXN-MS under stirred conditions in an enzymatic digestion buffer at 37ºC for 48 hours. DNA-MXN-MS were prepared to obtain mitoxantrone loadings of ≥ 12% (w/w). The released drug concentrations were then analyzed using UV-visible spectroscopy against a MXN standard curve. The percent drug release was measured under minimum sink conditions (i.e. low volume, 1.25mL) to simulate the tumor environment. Drug

release data was obtained by incubating the DNA-MXN-MS in phosphate buffered saline under constant agitation at 37ºC for a minimum of fourteen days in triplicate. At specific time points, aliquots were taken and measured using UV-visible spectroscopy against a MXN standard curve to determine drug concentration. The cytotoxicity of DNA-MXN-MS crosslinked with 120% M_{EQ} gadolinium was evaluated using a murine Lewis lung carcinoma cell line at concentrations of 1μg/mL, 10μg/mL, and 25μg/mL. These concentrations were used to determine the effects of MXN dose on the tumor cell line. The cytotoxicity of free drug and blank DNA-MS were also evaluated. An MTS assay was used to measure the cellular viability of the mLLC cells at days 0 through 4.

Aim 4: *In Vitro* Evaluations of Methotrexate or 5-Fluorouracil *In Situ* Loaded DNA and BSA Nano-Mesospheres

Deoxyribonucleic acid (DNA) and bovine serum albumin (BSA) nano-meso-microspheres (MS) were *in situ* loaded with methotrexate (MTX) or 5-fluorouracil (5-FU) using optimized DNA-MS synthesis conditions from Aim 2 to further analyze the drug loading capabilities of DNA and BSA. MTX and 5-FU *in situ* loaded DNA-MS and BSA-MS were synthesized to produce particles with controlled size distributions where at least 60% of all particles prepared were within the mesosphere size range of 1μm to 10μm and < 5% of all particles were greater than 10μm in size. Particles less than 1μm in diameter were also acceptable and hydrated particle diameters were to be less than 25μm. In addition, DNA-MS and BSA-MS were sought to obtain drug loadings of ≥ 5% (w/w) MTX or 5-FU and release drug for more than 24 hours in phosphate buffered saline under minimum sink conditions. MTX or 5-FU *in situ* loaded DNA-MS and BSA-MS were compared with respect to particle diameter, size distribution, morphology, topography, drug loading, and percent drug release.

DNA-MXN-MS were also prepared with a 120%M_{EQ} gadolinium crosslink concentration and were *in situ* loaded with 10% (w/w), 15% (w/w), and 25% (w/w) MXN to determine the maximum drug loading ability of DNA. The particle diameter, size distribution, morphology, topography, drug loading, and percent drug release of the DNA-MXN-MS were evaluated with respect to MXN concentration. In addition, DNA-MXN-MS were prepared with no gadolinium crosslinking to determine if MXN serves as a crosslinking agent for DNA-MS. DNA-MXN-MS were prepared to obtain *in situ* MXN loadings of ≥ 10% (w/w). The DNA-MXN-MS were characterized as mentioned above and compared with respect to crosslinking.

The particle diameters and size distributions and morphologies and topographies were obtained using characterization techniques from Aim 2. Drug loading and release were determined by using the analysis techniques from Aim 3. MTX, 5-FU, and MXN standard curve were constructed to determine drug concentration and release from the drug loaded DNA-MS and BSA-MS.

CHAPTER 2
BACKGROUND

Introduction

There are over 100 types of cancers known to man which may arise from a variety of organs within the body.[25, 26] The American Cancer Society estimates that in the USA, there will be 1,444,920 new cases of cancer and over 1 million cases of basal and squamous cell skin cancers diagnosed this year (2007), which will result in approximately 560,000 deaths.[27] These estimates are consistent with data collected in 2005 and 2006 by the National Cancer Advisory Board.[28] Cancer continues to be a national and worldwide problem and since 1999 has surpassed heart disease as the leading cause of death for people of age 85 and under.[1] In addition, cancer is the second leading cause of death for children between ages 1 and 14.[1] The global incidence of cancer is expected to increase from 10.3 million to 14.7 million by the year 2020.[29]

The increase in cancer incidence places a financial burden on national and international economies. In 2006, the National Institutes of Health estimated that the overall cancer medical, indirect morbidity, and indirect mortality costs were over $206 billion.[27] The incurred cost of cancer treatments such as radiation and chemotherapy was approximately $72.1 billion in 2004 and is expected to increase in the forthcoming years.[30] Primary treatment modalities such as radiation and chemotherapy not only place a financial burden on cancer patients, but also impact their quality of life due to the systemic toxicity and limited effectiveness of the treatments. The increasing rates of new cancer cases, their attributed costs, and impact on human life generate a significant demand to develop inexpensive drugs and new treatment modalities.

Conventional chemotherapy is delivered orally or intravenously which results in systemic toxicity. Traditional alkylating and antimetabolite cancer drugs function by attacking rapidly dividing cells such as those seen in tumor cells, however, many normal tissue cells also divide

rapidly and thus normal tissue toxicity occurs.[5] Normal tissue toxicity results from poor tumor cell specificity which may be remedied through localized delivery techniques such as those obtained with intratumoral delivery.[4, 5] The potential benefits of intratumoral therapy (IT) are a localized super dose delivery to the tumor, greatly reduced systemic toxicity, and the opportunity to prolong local drug effectiveness. Recent research has shown that the intratumoral delivery of biodegradable carriers loaded with mitoxantrone greatly improved survival and decreased toxicity in a murine breast cancer model.[12] These findings suggest that IT may be a useful alternative to conventional chemotherapy.

Previous studies concerning the intravenous delivery of DNA complexed with anthracycline chemotherapy drugs have shown that DNA reduces the cardiotoxicity and increases the half-life of the chemotherapy drugs *in vivo*.[22, 23, 31-33] The therapeutic value of the DNA-drug complexes was also found to be comparable to that of free drug.[22, 23, 31-33] These studies suggested that crosslinked but biodegradable DNA mesosphere compositions, which have not been previously reported, might have interesting and useful IT drug delivery properties.

Cancer

Types of Cancer

The most common cancers found in humans arise from mutations in epithelial cells leading to the formation of solid tumor carcinomas.[34] Solid tumor carcinomas account for 80% of all cancer-related deaths and include cancers of the mouth, stomach, esophagus, skin, mammary glands, pancreas, lung, liver, ovary, gallbladder, urinary bladder, and the small and large intestines.[34] There are two major classifications of carcinomas which include squamous cell carcinomas and adenocarcinomas.[34] Squamous cell carcinomas arise from mutations in epithelial cells that serve as a protective lining for underlying cells such as the skin and esophagaus.[34] Adenocarinomas arise from secretory cells that are contained within epithelial

cells that protect the cavities or channels that they line such as mammary glands, lung, uterus, and cervix.[34]

Nonepithelial tumors account for the remaining 20% of all malignant cancers and include sarcomas, lymphomas, leukemias, neuroectodermal tumors (i.e. gliomas, neuroblastomas, schwannomas, etc.), melanomas, and small-cell lung carcinomas.[34] Sarcomas arise due mutations in connective tissue cells such as fibroblasts (secrete collagen), osteoblasts (form bone), and myocytes (form muscle).[34] Furthermore, sarcomas may also arise from alterations in adipocyte cells whose primary functions are to store fat from cytoplasm.[34] Lymphomas and leukemias develop from blood-forming cells which include the red and white blood cells and are usually classified as systemic cancers.[34] Neuroectodermal tumors account for 2.5% of all cancer deaths (~14,000 deaths/year) and arise from cells derived from the central and peripheral nervous systems.[28, 34, 35] Melanomas derive from pigmented cells that line the skin and retina whereas small-cell lung carcinomas originate from endodermal cells that line the lung.

Tumor Development

Cancer is a progressive disease displaying benign, malignant, and metastatic stages.[25, 34-37] Initially, cancer was thought to be a disease defined by uncontrolled cell proliferation, however, the identification of many malignant tumors which are slow growing in humans and diseases that demonstrate very rapid cell proliferation with no evidence of neoplastic transformation, have proven otherwise.[36] Current models have shown that cancer develops due to genetic alterations that result in a cell's inability to respond to intra- and extracellular signals that control proliferation, differentiation, and death. [35-38] Genetic alterations may arise due to inherited gene mutations, ionizing or UV radiation, exposure to physical or chemical carcinogens, free radical attacks, or errors during DNA synthesis.[35, 37]

Two to six types of genetic alterations arise with respect to each individual type of cancer with each alteration having a specific capability.[25, 35] Normal cell proliferation is attained through the successful progression through the cell life cycle.[38-42] The normal life cycle of a cell involves four phases including the Gap_1 or "G_1" phase, the DNA Synthesis or "S" phase, the Gap_2 or "G_2" phase, and the Mitosis or "M" phase, Figure 2-1.[41-43] Normal cells will grow (G_1), replicate and synthesize their DNA (S), continue to grow with two sets of DNA with matching chromosomes (G_2), and finally divide to produce two cells with matching DNA (M).[38-43]

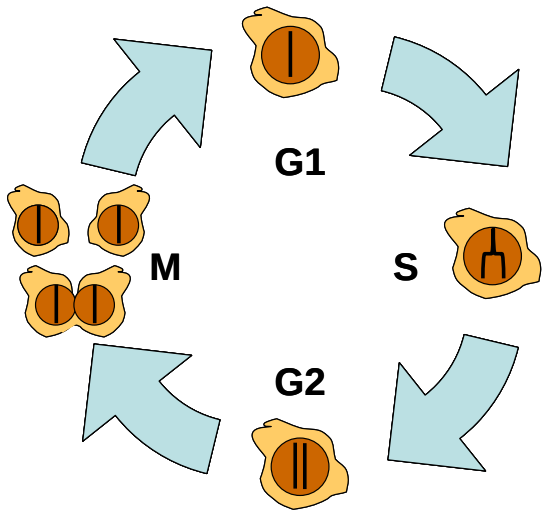

Figure 2-1. The 4 phases of the life cycle of a cell.[41-43]

Genetically altered cells also progress through the cell life cycles; however, they attain new capabilities with each alteration that lead to the development of malignant growth, Figure 2-2.[25, 44] These six new capabilities include self-sufficiency in growth signals (SS), insensitivity to anti-growth signals (IAS), tissue invasion and metastasis (TI&M), limitless replication potential (LRP), sustained angiogenesis (SA), and apoptosis evasion (AE).[25, 45]

These six new capabilities allow cancerous cells to self-stimulate into an active proliferative state (SS) and desensitize themselves to anti-growth signals (IAS).[25] Genetically altered cancer cells thus divide and grow quicker than normal cells.[25, 44] The formation of large

cancerous cell colonies allow them to invade surrounding tissues and detach to become systemic (TI&M).[25, 37] Their acquisition of limitless replication potential and their ability to evade apoptosis represent the truly devastating effects of this disease and introduces the urgent demand for new chemotherapy drug and delivery methods.[25, 37]

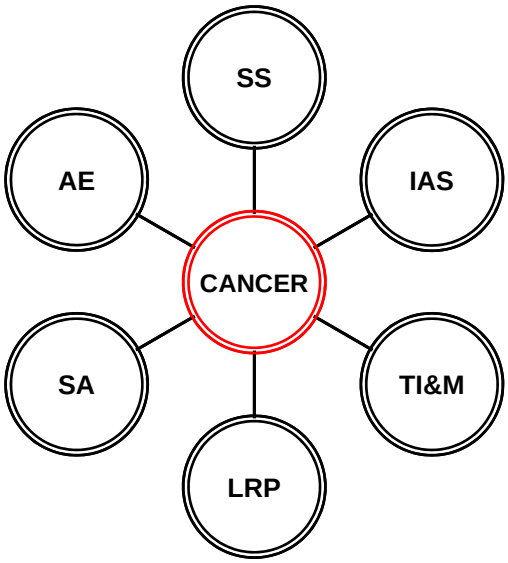

Figure 2-2. Physiological capabilities of genetically altered cancerous cells.

Conventional Treatments

Conventional cancer treatments include surgery, radiation, and chemotherapy and improvements in cancer survival often result in using a combination of the three.[3, 26, 45, 46] The choice of treatment regimen varies with each patient and is dependent on the type and location of the cancer and the physical condition of the patient.[3] Radiation therapy and surgery are localized forms of treatment whereas chemotherapy is a systemic treatment.[3, 46]

Surgery and radiation

Surgery is the oldest form of cancer treatment known dating back to Egyptian times when benign lipomas and polyps were surgically removed with a knife or red-hot iron.[47] Instances of excisions and cauterizations of tumors and ulcers have also been documented dating back to the Medieval time period between 500 and 1500 A.D..[47] This form of localized treatment continued

on through the Renaissance and Reformation periods to current day.[47] Surgery is a very common form of cancer treatment and is often used to confirm the diagnosis of cancer, determine the cell type, and to reduce the size of the tumor through excision.[3, 26] Advances in surgical technologies have lead to less invasive forms of surgery which spare as much normal tissue as possible. In some cases, radiation or chemotherapy will be used before surgery to decrease the size of the tumor and after surgery to eliminate any further traces of the cancer.[3]

Radiation therapy is the second oldest of the three conventional cancer treatments and involves the administration of x-rays or gamma rays directly to the tumor.[3] The localization of radiation therapy destroys cancer cells and minimizes toxic effects on healthy adjacent cells.[3] Radiation therapy functions by damaging the DNA of the cancer cell thus hindering it from functioning normally.[3] The first treatment of cancer using radiation was in 1896 following the discovery of the radioactivity of uranium by Becquerel.[47] The treatment of uterine carcinoma with radium soon followed in 1905 after radium's initial discovery by Marie and Pierre Curie in 1898.[47]

Chemotherapy

The first use of "anti-cancer" drugs was found during the Medieval time period when arsenic pastes were used to locally treat tumors.[47] Arsenic pastes continued to be used until 1865 when a potassium arsenite solution was given to a patient to treat chronic leukemia.[45, 47] At the turn of the twentieth century, Paul Ehrlich, "the father of chemotherapy", made tremendous advances in the field of chemotherapy and tested many new systemic chemical agents based on arsenic compounds on rodent models to predict their effectiveness in humans.[47, 48] Later during the early 1940s, the first successful clinical studies using systemic chemotherapy were reported.[45, 47] Patients at Yale University with Hodgkin's disease were treated with nitrogen mustard, a derivative of mustard gas, and were found to respond positively to the systemic

treatments (i.e. tumor size decreased).[47] However, patients relapsed after a short period of time and no true successes were found with systemic chemotherapy agents until 1956 when methotrexate cured over 50% of patients with choriocarcinoma.[47]

Chemotherapy is most commonly administered intravenously, however it may also be delivered orally in pill form or through other methods such as muscular, subcutaneous, or intra-arterial injections.[3, 46] The route of chemotherapy administration depends strongly on the drug's *in vivo* pharmacological properties such as half-life and metabolim.[46] The ultimate clinical objective of systemic chemotherapy is to kill cancer cells in the body while leaving all other healthy and normal functioning cells intact.[46] This is difficult to accomplish since chemotherapy drugs function by attacking rapidly dividing cells while circulating throughout the bloodstream. Since many normal functioning cells also divide rapidly such as hair cells, bone marrow cells, and cells that line the mouth and gastrointestinal tract, toxic side effects result such as hair loss, nausea, and even death.[3, 45, 46, 49] Systemic chemotherapy is most effective against systemic cancers such as leukemia and lymphomas and is less effective against solid tumor cancers such as the most prominent breast, lung, colon, and rectum cancers because these cancers have a lower number of rapidly dividing cells.[45] It is therefore important to find new delivery methods that localize the cancer drugs in order to increase their effectiveness and decrease systemic side effects.

Intratumoral Chemotherapy

Rationale for Intratumoral Chemotherapy

It has long been noted the therapeutic effectiveness of many chemotherapy drugs is often limited by their inability to reach the location of solid tumor cells and permeate the tumor cells' membranes.[6, 50] Intratumoral chemotherapy, through drug loaded microsphere delivery, offers one possible solution to this reoccurring problem. The main goal of intratumoral chemotherapy

is to increase the exposure of the chemotherapy drugs to the cancer cells by means safer than those achieved through systemic intravenous or oral delivery.[12, 51] Conventional systemic chemotherapy is constantly balancing the administration of a toxic dose with an effective therapeutic dose, generally described as the therapeutic ratio, which for most chemotherapy drugs has a value of one.[4, 46, 52, 53] A therapeutic ratio value of one implicates that damage to normal tissues is dose dependent which in turn limits the frequency of chemotherapy regimens.[26, 46] Thus, most chemotherapy treatments are given at concentrations below the therapeutic ratio in order to not comprise healthy rapidly dividing cells and are given in cycles long enough to allow cells in the bone marrow to recover.[46]

Advances in cancer care have led to longer patient survivals, however, it has also exposed long-term chemotherapy side effects such as infertility and carcinogenicity which have been predominant in young patients who have been cured of leukemia, testicular cancer, and Hodgkin's disease.[46] Therefore, great attention has been placed on the development of localized drug delivery methods, such as intratumoral chemotherapy, that incorporate zero-ordered controlled release devices, such as microspheres, that can maintain a desired concentration of drug at the site of the tumor without reaching toxic or minimum effective levels, Figure 2-3.[52, 54]

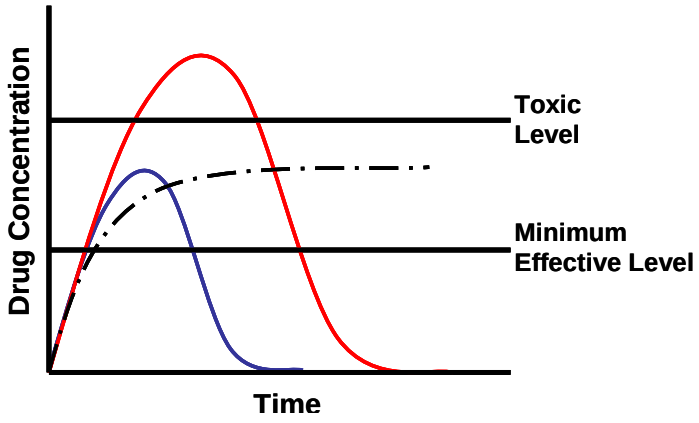

Figure 2-3. Therapeutic dose chart illustrating a toxic dose (red line), moderate dose (blue line), and a controlled release curve (dashed line).[52, 54]

Intratumoral chemotherapy using controlled release devices increase cancer patient quality of life by enhancing the safety and efficacy of chemotherapy drugs and decreasing chemotherapy frequency.[4, 55]

Controlled Release Microspheres

Controlled release devices in the form of microspheres have been prepared using biodegradable materials such as albumin, gelatin, casein, and deoxyribonucleic acid.[11, 24, 56-59] Biodegradable materials are capable of being loaded with cytotoxic drugs and can be prepared in microsphere form. The spherical morphology of these devices make them ideal for intratumoral injections since locally delivered drug loaded microspheres are trapped in the micro-circulation of tumors and release cytotoxic agents slowly with minimal systemic exposure.[60] Decrease in systemic toxicities have been proven through pharmacokinetic studies which have shown that cytotoxic agent serum levels after microsphere injections are much lower than those obtained when free drug is administered intravenously and also locally.[5, 7, 60-65] Locally delivered drug loaded microspheres also increase drug efficacy not only by increasing drug half-lives, but by also prolonging drug exposure to newly replicating cancer cells.[61, 66]

The drive to use microspheres as drug delivery vehicles may be explained by the enhanced permeability and retention (EPR) effect that was introduced in 1986.[67, 68] The EPR effect states that drug loaded microspheres improve the half-life of chemotherapy agents because microspheres do not exhibit the same lymphatic clearance rates as free drug and are capable of being trapped within the tumor vasculature.[67, 68] The question that then arises is: "What is the optimal particle size for microspheres used in intratumoral chemotherapy?". The general consensus appears to be that microspheres smaller than 25μm in diameter are preferred since they have a high surface area-to-volume ratio, are able to be entrapped in tumor tissue, and are also small enough to pass through dilated tumor vessels.[69] Microspheres in the 20μm to 40μm

size range are also preferable since they are also able to be entrapped in tumor tissue and can be administered intratumorally without complications.[9] For studies presented in this dissertation, particles were prepared in the injectable mesosphere size range (i.e. 1μm < d < 10μm).

Drug Release Kinetic Models

Release profiles

Drug elution from drug delivery devices may occur either through drug diffusion or through the erosion of the drug carrier matrix.[67, 70] The drug release profiles for each system will be different and it is possible for a drug carrier to release drug through a combination of diffusion and erosion.[67] The profile for diffusion based release will display an initial burst followed by a continual slow release over time as shown in Figure 2-4. The profile for erosion based release will initially release slowly and then increase exponentially over time, Figure 2-4.

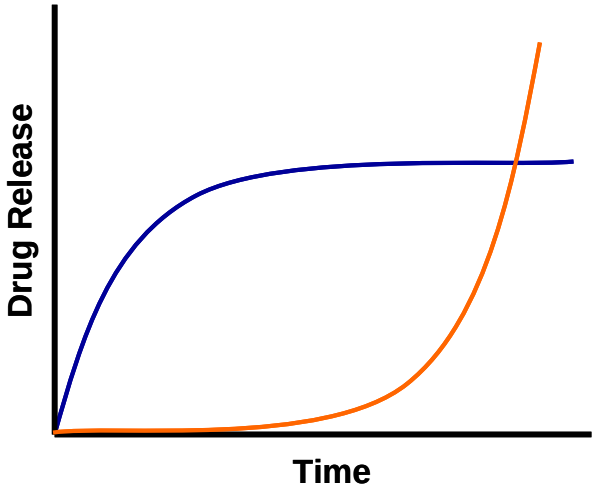

Figure 2-4. Diffusion (blue line) and erosion (orange line) drug release profiles.[67, 70]

The initial burst release illustrated in the diffusion release profile is attributed to the quick diffusion of the drug molecules that are entrapped on the carrier surface and hydrophilic outer layers, Figure 2-5.[67, 70] The quick release exhibited towards the end of the erosion release profile

is attributed to the release of the drug molecules that are entrapped within the carrier matrix due to the dissolution or erosion of the matrix, Figure 2-5.

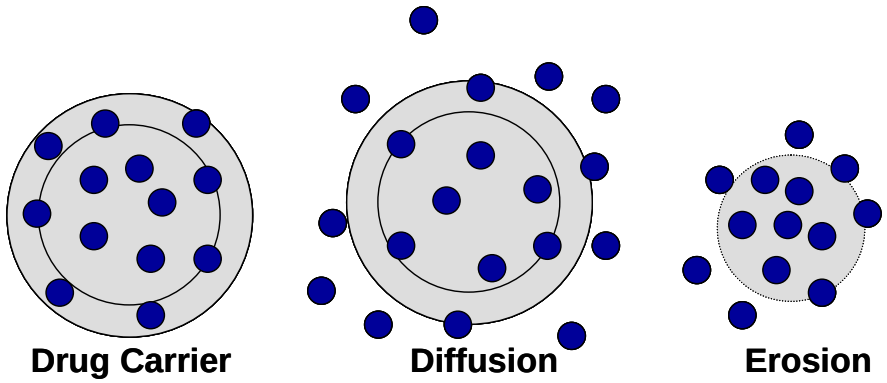

Figure 2-5. Drug release due to diffusion or erosion.[67, 70]

Release kinetics

Drug release from biodegradable controlled release matrix devices (i.e. microspheres) generally follow first order release meaning that the drug release rate is proportional to the remaining drug concentration.[71] First order release kinetics are typically observed with diffusion based release where the drug release rate decreases over time, Figure 2-6 (A).[71] The first order release kinetics model is described by plotting the log of the amount of drug remaining in the carrier versus the amount of time released and is distinguished as a linear curve, Figure 2-6 (B).[72-74]

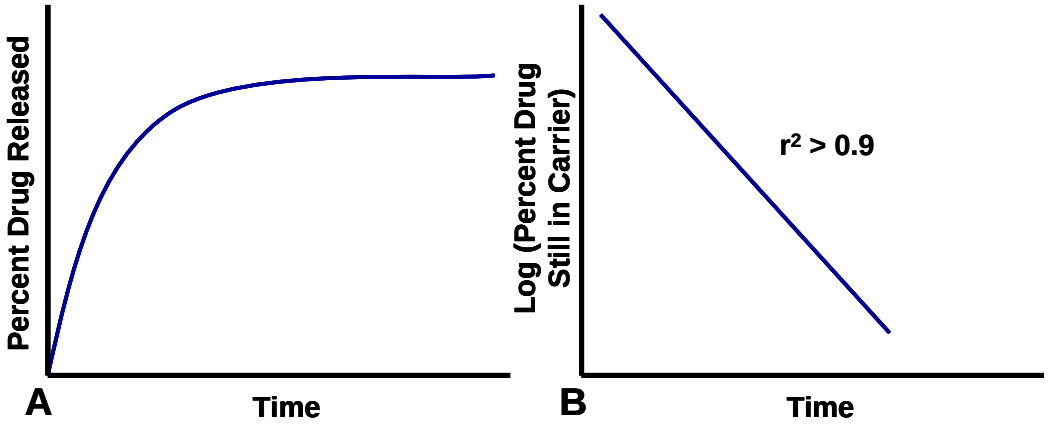

Figure 2-6. First order profiles for (A) drug release and (B) release kinetics.

Ideal drug delivery release is obtained when the drug release curve is linear and is generally described using zero order and Higuchi drug release kinetics models.[67] Zero order release is obtained when the active drugs are released over time at a constant rate and is distinguished as a linear curve on a percent drug released versus time plot, Figure 2-7 (A).[67, 71]

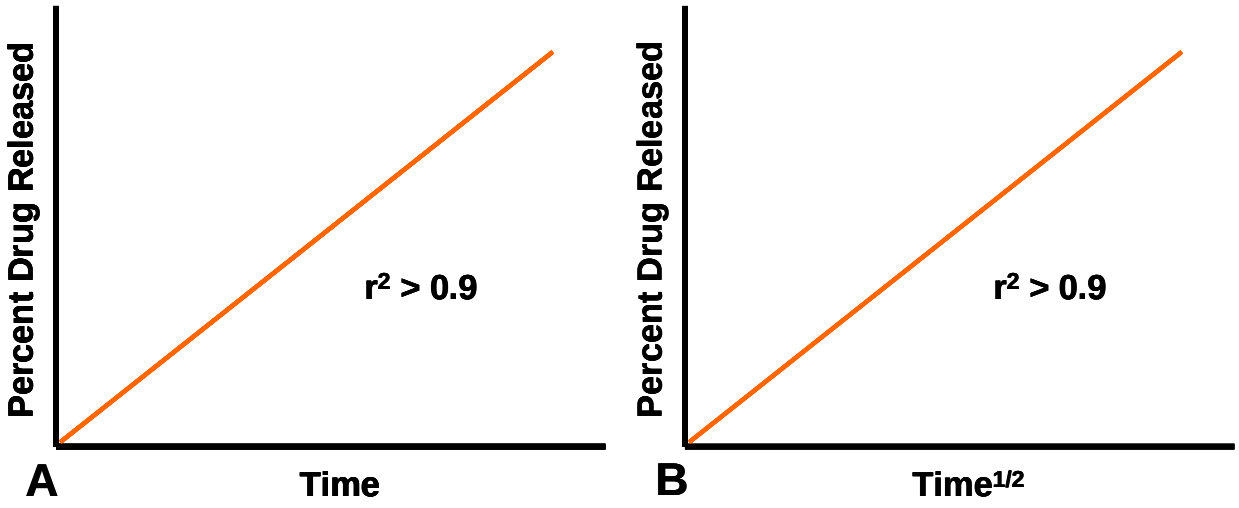

Figure 2-7. Drug release profiles for A) zero order release kinetics and B) Higuchi release kinetics.

The Higuchi release model was created in the early 1960s by Takeru Higuchi and was one of the first models ever used to describe the release of therapeutic drugs from a matrix carrier based on Fickian diffusion principles.[75-77] The Higuchi release model is one of the models most commonly used to describe drug release for controlled drug delivery devices and is obtained when the active drugs are released at a constant rate over the square root of time, Figure 2-7 (B).[75-77]

Chemotherapy Drugs

Chemotherapeutic drugs function by interfering with one or more processes involved with cell replication.[46, 49] This interference causes either cancer cell apoptosis (cytotoxic drugs) or cessation of cancer cell growth (cytostatic drugs).[46, 49] There are five major standard classes of anticancer agents which include the antimetabolites, covalent DNA binding drugs, noncovalent

DNA binding drugs, chromatin function inhibitors, and drugs affecting endocrine function.[78] The standard classes of anticancer agents with their respective subclasses are given in Table 2-1. The majority of chemotherapy drugs fall under the antimetabolite and noncovalent DNA binding drug classes and are known for their effectiveness against systemic and solid tumor cells with a high ratio of dividing cells.[26] Mitoxantrone, methotrexate, and 5-fluorouracil which are drugs in the antimetabolite and noncovalent DNA binding classes, were chosen for the research presented in this dissertation due to their broad treatment spectrum and their ease of availability.

Table 2-1. Classes and subclasses of anticancer agents.[78]

Antimetabolites	Covalent DNA binding drugs	Noncovalent DNA binding drugs	Chromatin function inhibitors	Endocrine function drugs
Folate antagonists	Nitrogen mustards	Anthracyclines	Topoismerase inhibitors	Glucocorticoids
Pyrimidine antagonists	Aziridines	Mitoxantrone	Microtubule inhibitors	Estrogens
Purine antagonists	Alkane sulfonates	Dactinomycin		Antiestrogens
Sugar-modified analogs	Nitrosoureas	Bleomycin		Progesterins
Ribonucleotide reductase inhibitors	Platinum compounds	Plicamycin		Androgens
	Monoalkylating agents			Antiandrogens
				Aromatase inhibitors

Mitoxantrone

Principle attention throughout the research presented in this dissertation was given to the use of mitoxantrone due to its broad treatment spectrum, blue chromaphore for analysis, and excellent *in vivo* murine adenocarcinoma results that were obtained in this lab.[11, 12, 56]

Mitoxantrone is a synthetic anthracenedione which is a member of the anthracycline class of antitumor antibiotics.[78-81] It has a planar tetracyclic aromatic ring structure that can easily intercalate into DNA.[78, 79] Mitoxantrone has two symmetrical aminoalkyl side arms with no

sugar moiety which is common in most anthracycline agents, Figure 2-8.[78-81] Its trade name is Novantrone™ and is also known as dihydroxyanthracenedione dihydrochloride.[81] Mitoxantrone has a molecular weight of 517.4 g/mol and is available as a blue powder that is hygroscopic and soluble in water and ethanol.[81] In a clinical setting, mitoxantrone has been shown to produce less cardiac toxicity and a diminished potential to attack healthy rapidly dividing cells as compared to other anthracyclines.[79]

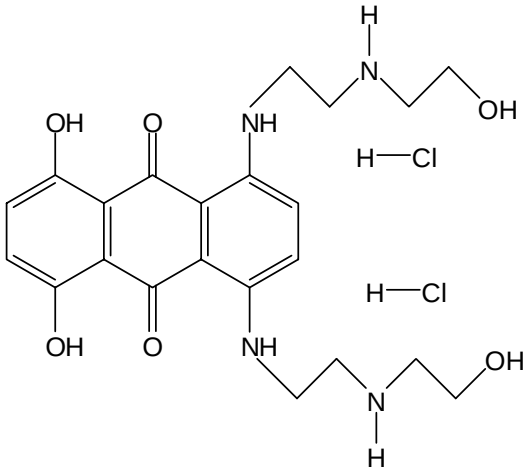

Figure 2-8. Chemical structure for mitoxantrone hydrochloride.

Mitoxantrone produces antitumor activity through two main interactions with DNA.[79, 81] The first interaction is considered a combination of high-affinity intercalation of the planar mitoxantrone structure into opposing DNA strands and lower-affinity electrostatic binding.[78, 79, 81] Intercalation occurs most preferentially at the G-C base pairs, which disrupts DNA synthesis.[78, 79, 81] This intercalation is thought to be further stabilized through electrostatic interactions between the positively charged nitrogens on the two alkyl side chains and the negatively charged ribose phosphates on the DNA.[79, 81] The second interaction involves impairment of cell division through the inhibition of topoisomerase II activity which is an enzyme most prominently found in the G_2 phase of the cell cycle.[78, 79, 81]

Mitoxantrone is administered by intravenous injection and is primarily used to treat leukemias, lymphomas, and advanced or recurrent breast cancer.[78, 81] The therapeutic dosage for mitoxantrone ranges from 10 to 14 mg/m^2 daily for 1 to 3 days.[80] Mitoxantrone is known to cause dose-limiting toxic side effects even though it has lower cardiac toxicity as compared to other commonly used anthracycline drugs.[79, 81] The most significant side effects are nausea, vomiting, and stomatitis, however, myelosuppression, alopecia, and phlebitis may also occur.[79-81]

Methotrexate

Methotrexate was discovered in the late 1940s after leukemic children went into cancer remission after being treated with folic acid antagnonists.[78, 80, 82] Methotrexate is categorized as a folate antagonist in the antimetabolite cancer drug class. It is a weak acid with a chemical structure that consists of 95% N-[4-[[2,4-diamino-6-pteridinyl)methyl]methylamino]benzoyl]-L-glutamic acid, Figure 2-9.[81] Methotrexate has a molecular weight of 452.5 g/mol and is available as sodium methotrexate which is readily soluble in water.[81]

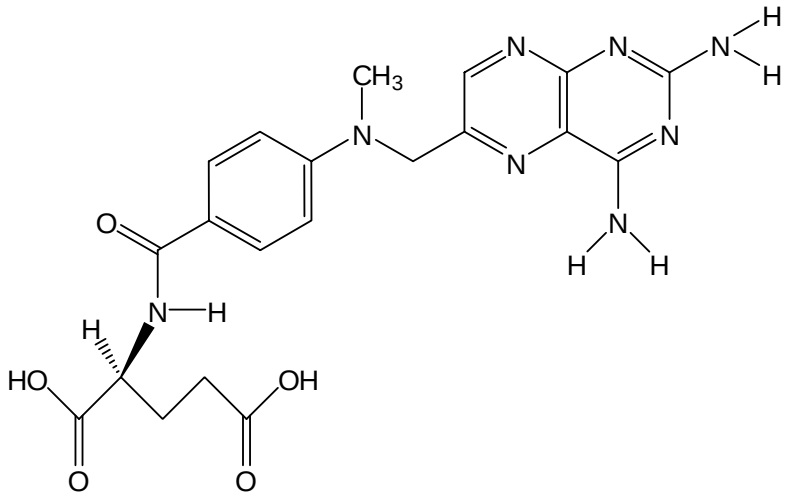

Figure 2-9. Chemical structure of methotrexate.

Methotrexate produces antitumor activity by binding to dihydrofolate reductase (DHFR) which is a key enzyme in DNA synthesis.[78, 80-82] When methotrexate is bound to DHFR, DHFR

activity is inhibited and dihydrofolate is not reduced to tetrahdyrofolic acid which ceases *de novo* purine synthesis.[78, 80, 81] For this reason, methotrexate is considered an S phase cell cycle specific drug.[80]

Methotrexate is most frequently administered intravenously; however, it may also be administered through intratumoral or intramuscular injections.[80] The dosage range for each administration method is given in Table 2-2. Methotrexate is a first-line drug for the treatments of breast cancer, osteogenic sarcoma, gestational choriocarcinoma, and leukemia and under high doses, can cross the blood brain barrier to treat cancers of the brain.[80, 82] Methotrexate has been clinically shown to be as effective as and less toxic than its folic acid antagonist counterpart aminopterin; however, it still causes toxic side effects.[78] The two major sites of methotrexate toxicity are located in the bone marrow and in the endothelium of the oropharynx and gastrointestinal tract.[78] This leads to a variety of toxic side effects which include myelosuppression, mucositis, renal tubular obstruction, hepatoxicity, pneumonitis, hypersensitivity, and neurotoxicity.[82]

Table 2-2. Methotrexate dosage ranges for various administration routes.

Administration method	Dosage range (mg/m^2)
Intravenous – low dose	10 to 50
Intravenous – medium dose	100 to 500
Intravenous – high dose	> 500
Intratumoral	10 to 15
Intramuscular	25

5-Fluorouracil

5-fluorouracil is a fluorinated pyrimidine uracil within with a fluorine atom substituted for a hydrogen atom at the carbon number 5 position on the pyrimidine ring, Figure 2-10.[81, 83] 5-fluorouracil falls within the antimetabolite cancer drug class and has a molecular weight of 5-fluorouracil is 130.08 g/mol.[80, 81, 83] Its full chemical name is 5-fluoro-2,4(1H,3H)-

pyrimidinedione and its registered name is Adrucil®.[80, 81] 5-Fluorouracil is sensitive to light and easily precipitates out of solution at low temperatures or if let standing at room temperature for prolonged periods of time.[80, 81] It is partially soluble in water or ethanol, Table 2-3, and is commercially available as an alkaline buffered solution with a pH of 9.[81]

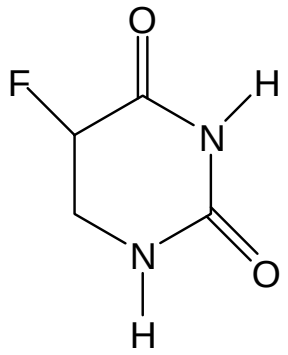

Figure 2-10. Chemical structure of 5-fluorouracil.[81, 83]

Table 2-3. 5-fluorouracil solubility in various media.[81]

Media	Solubility (mg/mL)
Water	12.2
Ethanol	5.5
Chloroform	0.1

5-Fluorouracil produces antitumor activity by behaving as a "false" pyrimidine ultimately inhibiting the formation of thymidine synthetase, an enzyme necessary for DNA synthesis.[78, 80, 81] The antitumor activity of 5-fluorouracil is governed by three main mechanisms which include 1) the inhibition of thymidine synthetase by the generation of fluorodeoxyuridine monophosphate (FdUMP), 2) the incorporation of fluorouridine triphosphate (FUTP) into RNA, and 3) the incorporation of FUTP into DNA.[81, 83] During its primary mechanism of action, FdUMP binds tightly to thymidine synthetase and prevents the formation of thymidylate.[83] Thymidylate is one of the four essential deoxyribonucleotides required for DNA synthesis and without it causes toxicity in actively dividing cell.[81, 83] Therefore, 5-fluorouracil is considered as an S phase cell cycle specific drug.[78, 81, 83]

5-fluorouracil is primarily administered intravenously; however it may also be administered by hepatic or by head and neck infusions.[78, 80, 81] The dosage ranges varies for each different administration method and are given in Table 2-4.[80, 81]

Table 2-4. 5-fluorouracil dosage ranges for various administration routes.[80, 81]

Administration method	Schedule	Dosage range
Intravenous	Once a week	12 to 15 mg/kg
Intravenous	Every day for 5 days every 4 weeks	12 mg/kg
Intravenous	Every week for 5 weeks	500 mg/m^2
Hepatic infusion	Eight hours for 5 to 21 consecutive days	22 mg/kg in 100mL D_5W
Head and neck infusion	Continuous for 4 to 5 days	1,000 mg/m^2

5-fluorouracil was discovered in 1958 and since then has been used to treat a variety of solid tumor cancers including commonly occurring cancers such as breast, head and neck, colorectal, gastric, and pancreatic cancers.[78, 81] 5-fluorouracil is also used to treat renal cell carcinoma, squamous cell carcinoma of the esophagus, prostate cancer, bladder cancer, and basal cell carcinoma; however, it is not recommended for invasive skin cancers.[78, 81] The most dose-limiting toxic side effects of 5-fluorouracil are stomatitis, nausea, vomiting, diarrhea, and anorexia since 5-fluorouracil frequently attacks rapidly dividing cells within the gastrointestinal tract.[80, 81, 83] In addition, 5-fluorouracil causes such toxic side effects as myelosuppression, dermatologic toxicity, ocular toxicity, neurotoxicity, bone marrow suppression, cardiac toxicity, and biliary sclerosis.[78, 81, 83]

Deoxyribonucleic Acid

Many know DNA for its role as a carrier of genetic information; however, very few have given thought to the possible biomaterial functions of this supramolecular biopolymer. For the past 30 years scientists have focused their efforts on the delivery of viral DNA, otherwise known as plasmid DNA, for its function as a gene expressor.[15, 16] Plasmid DNA, unlike chromosomal or genomic DNA, are small circular DNA molecules that are regarded as genetic mobile elements

because they have the ability to independently replicate themselves and have their genetic information transferred between cells.[84] The delivery of plasmid DNA has been sought after for such applications as biosensing for the detection of chemical contaminants, gene expression for its use as a novel therapeutic for cancer and genetic disorders, and tissue engineering as bone, skin, and nerve cell regenerative stimuli.[15,14,85] With all of this attention focused on plasmid DNA, scientists have overlooked the attractive properties that chromosomal DNA has to offer. It has only been within the past decade that scientists have shown interest in the biomaterial functions of chromosomal DNA.

Chromosomal DNA is a macromolecular polynucleotide with a rigid right-handed double helical molecular conformation, Figure 2-11.[86] The molecular structure of chromosomal DNA was discovered in 1953 by James Watson and Francis Crick and consists of two phosphodiester deoxyribose backbone chains that connect together through adenine-thymine and cytosine-guanine base pairs, Figure 2-12.[87] This naturally occurring biopolymer has a unique base pair configuration for each individual living creation, from humans to plants, bacteria, etc. In addition, the molecular weights of DNA range from the hundreds of thousands to easily into the hundreds of millions which is also dependent on the original source of the DNA.[86]

Figure 2-11. A drawing of DNA.

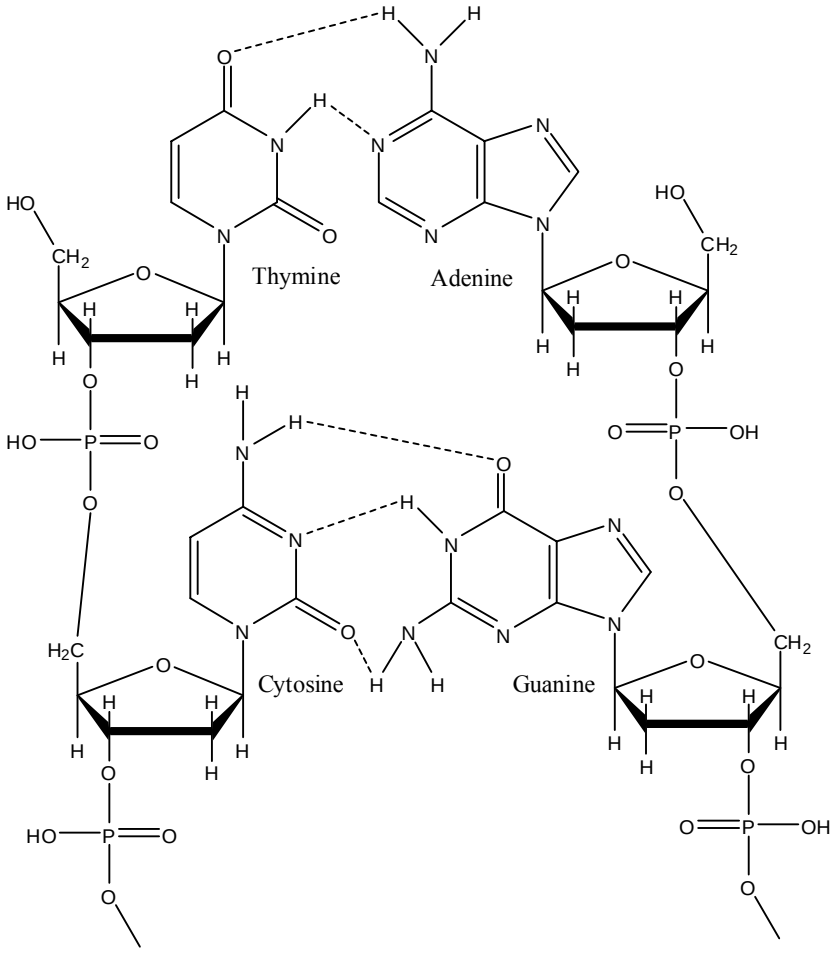

Figure 2-12. Cartoon of the molecular structure of a DNA subunit (Note: Bonds are not drawn to scale).

In the late 1970s and early 1980s, scientists began to explore the use of chromosomal DNA for biomedical purposes.[22, 23, 32, 33, 88] During this time, chromosomal DNA was used as a conjugated carrier for chemotherapy drugs such as doxorubicin and was found that DNA helped to reduce the cardiotoxicity of such drugs when injected intravenously.[22, 23, 32, 33, 88] Into the late 1990s, scientists further explored the biomaterial properties of DNA and used DNA-lipid films as drug delivery vehicles for ethidium bromide.[19, 20] DNA-alginate films were also shown to have been cast onto Millipore filters and remove contaminants such as benzopyrene and acridine orange from aqueous solutions.[17] DNA films have also been coated onto nonwoven cellulose fabrics and loaded with silver ions to give the fabric surface antibacterial properties.[20] In

addition, in 2003 DNA films were shown to increase the blood compatibility of hemodialysis membrane polysulfone fiber surfaces.[18] DNA films increased the hydrophilicity and decreased the protein absorption of the polysulfone fibers.[18] In 2003, DNA was used to produce regenerative tissue scaffolds and in 2006, DNA films were cast onto titanium medical devices.[21, 89] The combination of the biomaterial properties of DNA presented in this section suggest that DNA may be a desirable exploratory material for mesosphere synthesis for intratumoral chemotherapy applications.

DNA Mesosphere Synthesis

Steric Stabilization

The DNA microspheres (i.e. d > 10μm), mesospheres (i.e. 1μm > d > 10μm), and nanospheres (i.e. d < 1μm) (DNA-MS) presented in this dissertation were prepared using a steric stabilization process developed in this lab for the synthesis of albumin microspheres.[11, 56-59] This process creates a sterically stable colloidal microemulsion through the complete solvation of a stabilizing agent (i.e. cellulose acetate butyrate in 1,2-dichloroethane) at the surface of aqueous DNA droplets.[90]

In brief, the DNA-MS synthesis process involves adding a small volume of an aqueous DNA solution to a large volume of an organic polymer solution and mixing these two solutions at high speed (i.e. speeds greater than or equal to 900rpm) for 20 minutes in order to create a DNA microemulsion. The DNA microemulsion is then crosslinked using covalent or ionic crosslinking agents and the mixer speed is reduced to 600rpm. Crosslinking reactions continue for another hour and 40 minutes at which time acetone is added to the system to compensate for any evaporation during synthesis and to initiate the DNA microsphere washing process, Figure 2-13. The synthesis process continues for an additional hour and then the DNA-MS are washed in acetone four times, collected through centrifugation, and allowed to air dry over night at room

temperature. All DNA-MS synthesis processes are carried out at room temperature and are given in more detail in each subsequent chapter in this dissertation.

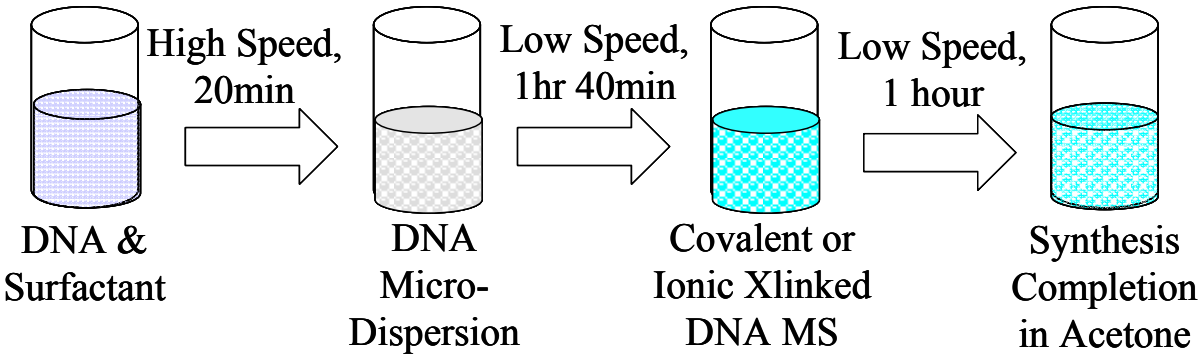

Figure 2-13. A brief schematic of the DNA-MS synthesis process.

DNA Crosslinking

Ionic crosslinking

It has long been shown that multivalent metal cations have the ability to crosslink plasmid or chromosomal DNA via the phosphate groups found along the DNA backbone or via the electron-donor groups found within the base pairs.[91, 92] Recent studies cited in the literature have shown that divalent cations, such as Co^{2+} and Zn^{2+}, and multivalent cations, such as spermidine (tertiary valence) and spermine (quaternary valence) destabilize the double helix of DNA by disrupting the base pairing of DNA due to metal ion crosslinks.[93] Therefore, the concept to use trivalent cations, such as those obtained in chromium (III) potassium sulfate, gadolinium (III) chloride, and iron (III) nitrate, as crosslinking agents for DNA-MS synthesis was developed in this lab and set forth in this dissertation. The mechanisms describing possible DNA-MS crosslinking with each of the aforementioned trivalent cations is given in detail in Chapter 3.

Covalent crosslinking

Glutaraldehyde has been the primary crosslink agent used in this lab for the preparation of albumin, gelatin, poly(glutamic acid) and blended microspheres since the early 1980s.[11, 13, 56-59,

[94] Glutaraldehyde is a dialdehyde, Figure 2-14, that reacts easily with primary amine sites commonly found in the biomaterials mentioned above through a Schiff base reaction.[11, 13] Therefore, glutaraldehyde was chosen as an experimental covalent crosslinking agent for DNA-MS synthesis due to the amino groups found on the adenine, guanine, and cytosine base groups within DNA, Figure 2-15. Possible crosslink mechanisms between glutaraldehyde and DNA are given in detail in Chapter 3.

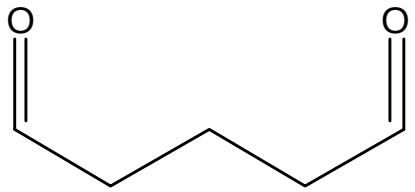

Figure 2-14. Chemical structure of glutaraldehyde.

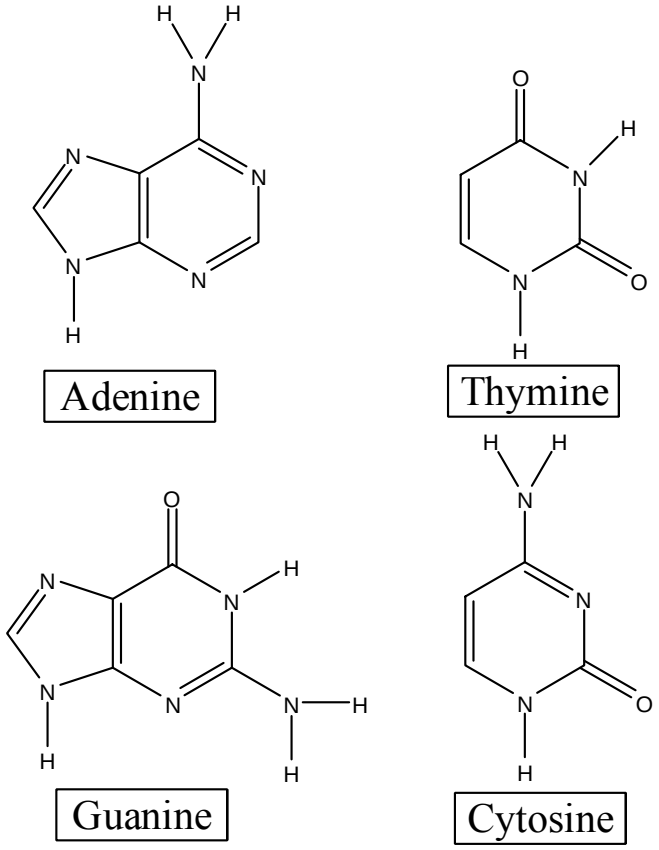

Figure 2-15. Chemical structures of the four DNA base groups.

More recently, the use of genipin as a naturally occurring biomaterial crosslinking agent has been receiving much attention due to its significantly lower *in vitro* cytotoxicity as compared to glutaraldehyde.[57, 95] Genipin is an iridoid glucoside extract from the fruits of the *Gardenia jasminoides* Ellis, Figure 2-16.[95, 96] It also has the ability to react with primary amines and was thus chosen as an experimental covalent crosslinking agent for DNA-MS synthesis. Possible crosslink mechanisms between genipin and DNA are given in detail in Chapter 3.

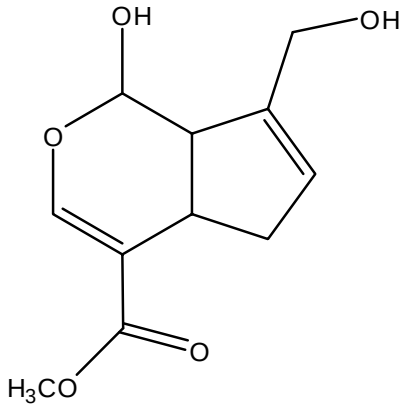

Figure 2-16. Chemical structure of genipin.

Research Goals

The increase in cancer incidence rates and financial burdens on worldwide economies places an urgent need on new cancer diagnostics, drugs, and treatment modalities. The limited effectiveness of chemotherapy agents on solid tumor cancers suggest that localized treatment through intratumoral chemotherapy may provide increased drug therapeutic efficacy and may improve the quality of life for cancer patients. The possible biomaterial applications of DNA are limitless and its demonstrated ability to load drugs such as ethidium bromide and doxorubicin make it a very desirable material for mesospheres synthesis for intratumoral chemotherapy applications. Therefore, the objective of the research presented in this dissertation was the synthesis and characterization of drug loaded DNA nano-meso-microspheres for intratumoral cancer therapy. Studies were aimed at producing DNA-MS with > 60% of all particle diameters

prepared falling in the mesosphere size range (i.e. 1μm > d > 10μm), < 5% of all particles greater than 10μm in diameter, swollen diameters < 25μm, and dispersion times of ≥ 24 hours for injectability and stability purposes. Studies were also aimed at preparing DNA-MS capable of loading ≥ 12% (w/w) MXN, loading ≥ 5% (w/w) MTX or 5-FU, releasing drug for ≥ 24 hours, and producing cytotoxic effects on murine Lewis lung carcinoma cells at concentrations as low as 1μg/mL MXN.

CHAPTER 3
DNA NANO-MESO-MICROSPHERE SYNTHESIS

Introduction

This chapter is devoted to the studies conducted on the synthesis and characterization of nano-meso-microspheres (MS) prepared from deoxyribonucleic acid (DNA) and crosslinked with covalent and ionic agents. To date, there is little in the literature regarding the use of DNA as a biopolymer for chemotherapy applications.

DNA-MS were prepared using a steric stabilization process that was developed in this lab for the synthesis of albumin (BSA) and gelatin (GEL) MS.[11, 57] This steric stabilization process was adapted to prepare DNA-MS that were crosslinked while in suspension covalently with either genipin or glutaraldehyde or ionically with either chromium (III) potassium sulfate, gadolinium (III) chloride, or iron (III) nitrate. The steric stabilization process involved a 20 minute microemulsion process followed by a one hour and 40 minute crosslink process based on previous results obtained with glutaraldehyde crosslinked BSA-MS and genipin crosslinked GEL-MS synthesis.[11, 57] DNA-MS were prepared by increasing the concentration of the stabilizing agent from 3% (w/v) to 5% (w/v) in order to obtain better steric repulsion between the higher molecular weight DNA-MS. DNA-MS were crosslinked via the aqueous phase unlike BSA-MS and GEL-MS which are crosslinked with glutaraldehyde or genipin via the continuous organic phase.[11, 57] Crosslinking through the continuous organic phase was attempted with the DNA-MS, however, crosslinking via the aqueous phase yielded particles that were less aggregated and agglomerated and more spherical in morphology.

The objectives for this chapter were to synthesize DNA-MS to a target dry mean diameter range of 50nm to 20μm, where at least 60% of all particles prepared were within the mesosphere size range of 1μm to 10μm and < 5% of all particles were greater than 10μm in size. Particles

less than 1μm in diameter were also acceptable. Hydrated particle diameters were to be less than 25μm. DNA-MS were sought to obtain aqueous dispersion stability of over 24 hours and elicit minimal toxic effect on fibroblast cells in culture.

The morphology and topography of the DNA-MS were examined by optical microscopy and scanning electron microscopy. The presence of trivalent cations in the DNA-MS was assessed by energy dispersive x-ray spectroscopy. Crosslinking was confirmed through DNA-MS stability testing in 0.05M phosphate buffered saline (PBS) at a pH of 7.4. Dry and PBS swollen particle sizes were quantitatively characterized using an LS Coulter 13 320 particle size analyzer. The DNA-MS surface charge was measured by zeta potential analysis in 0.01M PBS at a pH of 7.4 . Normal human dermal BJ fibroblast cells were used in culture to evaluate the effect of DNA and crosslinked DNA-MS on cell growth. Concentrations of 100μg and 500μg for DNA, and 25μg and 100μg for crosslinked DNA-MS were tested. A colorimetric MTS assay was used to measure fibroblast growth at the 0, 24, and 72 hour time points.

Materials and Methods

Materials

Synthesis and characterization

The following were purchased from the Sigma-Aldrich Company: DNA sodium salt derived from herring testes Type XIV, cellulose acetate butyrate, HPLC grade 1,2-dichloroethane, methanol, chromium (III) potassium sulfate dodecahydrate, gadolinium (III) chloride hexahydrate, iron (III) nitrate nonahydrate, 25% (w/w) Grade II aqueous glutaraldehyde solution, and Grey's Balanced Salt Solution. Acetone, sodium phosphate monobasic monohydrate, sodium phosphate dibasic anhydrous, and sodium chloride, each A.C.S. certified, 60mm by 15mm polystyrene radiation sterilized petri dishes, Fisherbrand microscope slides, and 50mL and 15mL polypropylene centrifuge tubes were purchased from Fisher Scientific

International. Genipin was obtained from Challenge Bioproducts Co., Ltd. Type I and Type II deionized ultrapure water was prepared using a Barnstead NANOpure Ultrapure Water System and is termed ultrapure water throughout. The resistivity of the ultrapure water was at least 16 $M\Omega\text{-}cm^{-1}$ for all aqueous solutions prepared.

Cell culture

Corning $75cm^2$ cell culture flasks, Fisherbrand clear polystyrene 96-well plates, MEM non-essential amino acid solution, Cellgro heat inactivated fetal bovine serum, and 0.22μm Corning cellulose nitrate filters were purchased from Fisher Scientific International. The CellTiter 96 Non-Radioactive Cell Proliferation Assay was purchased from the Promega Corporation. Normal human dermal BJ fibroblast cells, Eagle's Minimum Essential Modified Media (EMEM), L-glutamine, trypsin-EDTA solution, and penicillin-streptomycin were obtained from the American Type Culture Collection (ATCC, Manassas, VA).

Synthesis equipment

Solutions prepared or washed by vortex mixing were conducted on a Genie 2 vortex. Centrifugation used a Dynac II bench top centrifuge. General microsphere syntheses were carried out using Caframo Model BDC6015 and Lightnin Model LIU08 mechanical lab mixers in 300mL Labconco lyophilization flasks.

Methods

Solution preparation

Deoxyribonucleic acid. Aqueous 5% (w/v) DNA solutions were prepared at room temperature by adding 0.5g of DNA to 5mL of ultrapure water in a 50mL polypropylene centrifuge tube. The solution was mixed on a vortex mixer for 30 seconds. Three milliliters of ultrapure water was then added to the DNA and placed on the rotary shaker for at least two hours until the DNA had completely dissolved. Once the DNA had dissolved, the volume was brought

up to 10mL and vortexed for 30 seconds. The DNA solution was then placed in the refrigerator over night to ensure the complete collapse of bubbles generated during vortex and rotary mixing. The percent solid concentration of the DNA solution was quantified using a Metler LJ16 Moisture Analyzer at 130ºC for 60 minutes. The concentration of the DNA solution was then adjusted until the concentration was within 10% of the desired concentration. Once the desired concentration was reached, the aqueous DNA solution was placed in the refrigerator until further use.

Cellulose acetate butyrate. Solutions of cellulose acetate butyrate in 1,2-dichloroethane (CAB) were used as the water-immiscible continuous phase for the emulsion stabilization process during DNA-MS synthesis. The CAB solutions were used at a concentration of 5% (w/v) and prepared by adding 25g of cellulose acetate butyrate to 500mL of 1,2-dichloroethane. The CAB solution was mixed at room temperature on a magnetic stir plate on high until the cellulose acetate butyrate had completely dissolved in the 1,2-dichloroethane. The resulting CAB solution was capped, parafilmed, and stored at room temperature.

Genipin. Aqueous genipin solutions were prepared to a concentration of 5% (w/v) by adding 1.25g of genipin to 25mL of ultrapure water. The genipin solutions were mixed on a vortex at room temperature until the genipin had completely dissolved in the ultrapure water. The genipin solutions were capped, parafilmed, and stored in the refrigerator.

Glutaraldehyde. Aqueous glutaraldehyde solutions were prepared to a concentration of 5% (w/v) by diluting the 25% (w/w) aqueous glutaraldehyde solution purchased from the Sigma Aldrich Company. The aqueous glutaraldehyde solution was diluted by adding 20mL of ultrapure water to 5mL of the 25% (w/w) solution. The glutaraldehyde solutions were prepared

in 30mL glass jars and mixed on a vortex at room temperature for 1 minute. After mixing, the aqueous glutaraldehyde solutions were parafilmed and stored in the refrigerator.

Chromium (III) potassium sulfate. Aqueous chromium (III) potassium sulfate solutions were prepared to a concentration of 0.1M by adding 24.97g of chromium (III) potassium sulfate dodecahydrate to 500mL of ultrapure water. The chromium (III) solutions were mixed on a magnetic stir plate over night at room temperature until all the chromium had dissolved in the water. After complete mixing, the 0.1M chromium (III) solution was parafilmed and stored at room temperature.

Gadolinium (III) chloride. Aqueous gadolinium (III) chloride solutions were prepared to a concentration of 0.1M by adding 18.59g of gadolinium (III) chloride hexahydrate to 500mL of ultrapure water. The gadolinium (III) solutions were mixed on a magnetic stir plate over night at room temperature until all the gadolinium had dissolved in the water. After complete mixing, the 0.1M gadolinium (III) solution was parafilmed and stored at room temperature.

Iron (III) nitrate. Aqueous iron (III) nitrate solutions were prepared to a concentration of 0.1M by adding 2.02g of iron (III) nitrate nonahydrate to 50mL of ultrapure water. The iron (III) solutions were mixed in a 50mL polypropylene centrifuge tube on a rotary shaker over night at room temperature until all the iron had dissolved in the water. After complete mixing, the 0.1M iron (III) solution was parafilmed and stored at room temperature.

Phosphate buffered saline. Four liters of a 0.05M phosphate buffered saline (PBS) solution with a pH of 7.4 was prepared in the lab for measuring the swelling properties of the DNA-MS. The PBS solution was prepared by mixing 2.9L of a 0.05M sodium phosphate dibasic solution with 1L of a 0.05M sodium phosphate monobasic solution. During mixing, the pH of

the PBS solution was measured and sodium phosphate monobasic solution was added until the target pH of 7.4 was reached.

A PBS solution with a concentration of 0.01M at a pH of 7.4 was used for the zeta potential measurements and was prepared by diluting a 0.1M PBS solution and adjusting the pH back to 7.4. The 0.1M PBS solution was prepared by mixing 2.9L of a 0.1M sodium phosphate dibasic solution with 1L of a sodium phosphate monobasic solution. The two solutions were mixed and the pH of the resulting solution was brought to 7.4 by adding monobasic solution. The prepared PBS solutions were stored at room temperature until needed.

Cell culture media. Cell culture media was prepared by adding 50mL of fetal bovine serum (FBS), 10mL of non-essential amino acid solution, 10mL of L-glutamine, and 10mL of penicillin-streptomycin to 500mL of Eagle's Minimum Essential Modified Media (EMEM) in order to obtain a 10%FBS, 2%non-essential amino acid (NEAA), 2% L-glutamine, and 2% penicillin-streptomycin treated media and will be referred to as treated media from this point forward. The treated media solutions were mixed manually and placed in the refrigerator until further use. DNA solutions used in the cell culture study were prepared as mentioned above; however; they were sterilized with a 0.22μm filter immediately prior to adding treatment.

Crosslinking reaction study

The time to crosslink DNA with covalent or ionic crosslinking agents was estimated by measuring the time needed for each agent to precipitate DNA from solution. For these studies, genipin and glutaraldehyde covalent crosslinking agents were tested by adding 2mL of the 5% (w/v) crosslinking agent solutions to 3mL of the 5% (w/v) aqueous DNA solution. For ionic crosslinking, 2mL of the 0.1M chromium (III), gadolinium (III), or iron (III) solutions were added to 3mL of the 5% (w/v) aqueous DNA solution. The amount of time required for the individual agent to crosslink the DNA, as measured by the precipitation of the DNA, was then

recorded. These studies were conducted at room temperature with a two hour reaction time in order to mimic conditions observed during MS synthesis.

Pilot microsphere synthesis study

DNA-MS were initially prepared using chromium (III) potassium sulfate dodecahydrate to determine if the chromium (III) cations (Cr^{3+}) could ionically crosslink the DNA molecule. For this study, DNA-MS were synthesized using a 1% (w/v) aqueous DNA solution, a 0.1M Cr^{3+} solution, and a 3% (w/v) CAB solution. DNA-MS were prepared by adding 2mL of the 1% (w/v) aqueous DNA solution to 16mL of the 3% (w/v) CAB solution in a 50mL polypropylene centrifuge tube. The centrifuge tube was capped and then mixed on the vortex at level 8 for 2 minutes. After 2 minutes, 1mL of the 0.1M Cr^{3+} solution was added and mixed on the vortex at level 8 for an additional 5 minutes. After 5 minutes, the DNA-MS suspension was separated into three separate 50mL polypropylene centrifuge tubes and acetone was added up to 35mL. The DNA-MS were then rinsed in the acetone for 30 seconds using the vortex at level 8 and collected by centrifugation at 2000rpm for 10 minutes. After centrifugation, the acetone was decanted and the DNA-MS were combined into two centrifuge tubes. The acetone rinse was repeated and then the DNA-MS were combined into one centrifuge tube and the acetone rinse was repeated. After the final rinse, the acetone was decanted and the DNA-MS were allowed to air dry at room temperature by securing a Kimwipe over the mouth of the open centrifuge tube with a rubber band.

General microsphere synthesis

Based on results obtained from the pilot study and previous research conducted on BSA-MS and GEL-MS synthesis, DNA-MS were prepared using an emulsion stabilization technique that sterically stabilizes the DNA molecule into spherical conformations and crosslinks them while in suspension. This emulsion stabilization process involved dispersing 3mL of a 5% (w/v)

aqueous DNA solution (i.e. the aqueous phase) into 47mL of a 5% (w/v) CAB solution (i.e. the continuous phase) in a 300mL Labconco lyophilization flask. After dispersion, a DNA microemulsion was created by vigorously mixing the two solutions at 1250rpm for 20 minutes at room temperature, using a paddle mixer with a two inch, two blade propeller. The DNA microemulsion was then covalently or ionically crosslinked while in suspension by reducing the speed of the paddle mixer to 600rpm and adding 2mL of a crosslinking agent. In the case where genipin was used as a crosslinking agent, 9mL was added instead of 2mL because the amount of genipin needed to establish the same amount of crosslinking as glutaraldehyde in albumin was found to be 4.5 times more.[57] Therefore, the amount of genipin used for these studies was also increased by a factor of 4.5. The DNA microemulsion then underwent crosslinking for 1 hour and 40 minutes at which time 50mL of acetone was added and any further reactions were allowed to reach completion for another hour. After synthesis was complete, the DNA-MS underwent four rinses in acetone to remove any residual organic phase or crosslinking agent. The DNA-MS were rinsed by separating the resultant DNA-MS suspension into four separate 50mL polypropylene centrifuge tubes. To these tubes, acetone was added up to 35mL and the tubes were capped and vortexed on high for 30 seconds. After vortexing, the DNA-MS were collected by centrifuging the tubes at 2600rpm for 10 minutes. After centrifugation, the acetone was decanted and fresh acetone was added again up to 35mL. The acetone rinse was repeated once more as mentioned above and then twice more by consolidating the contents of 4 tubes to 2 tubes and then 2 tubes to one tube. After the final acetone rinse, the centrifuge tube was uncapped, the acetone was decanted, and a Kimwipe was secured over the mouth of the tube using a rubber band. The DNA-MS were then allowed to dry overnight at room temperature.

Crosslinking determination

DNA-MS were crosslinked by either ionic bonding through the phosphate groups on the DNA backbone or by covalent bonding presumably through the amino groups within the base pairs of the DNA molecule. Crosslinking efficiency was estimated on the basis of percent molar equivalence ($\%M_{EQ}$) of crosslink agent to moles of possible reactive sites found within one DNA repeat unit.

For these crosslinking estimates, a generic repeat unit structure, independent of DNA source, was established and considered to include phosphate, deoxyribose, adenine, thymine, cytosine, and guanine groups as shown in Figure 3-1. The number of repeat units within a DNA molecule was estimated from the molecular weight of the DNA molecule and the molecular weight of the repeat unit. A molecular weight of 1.3million Daltons was used for these calculations as reported from the Sigma-Aldrich Company.

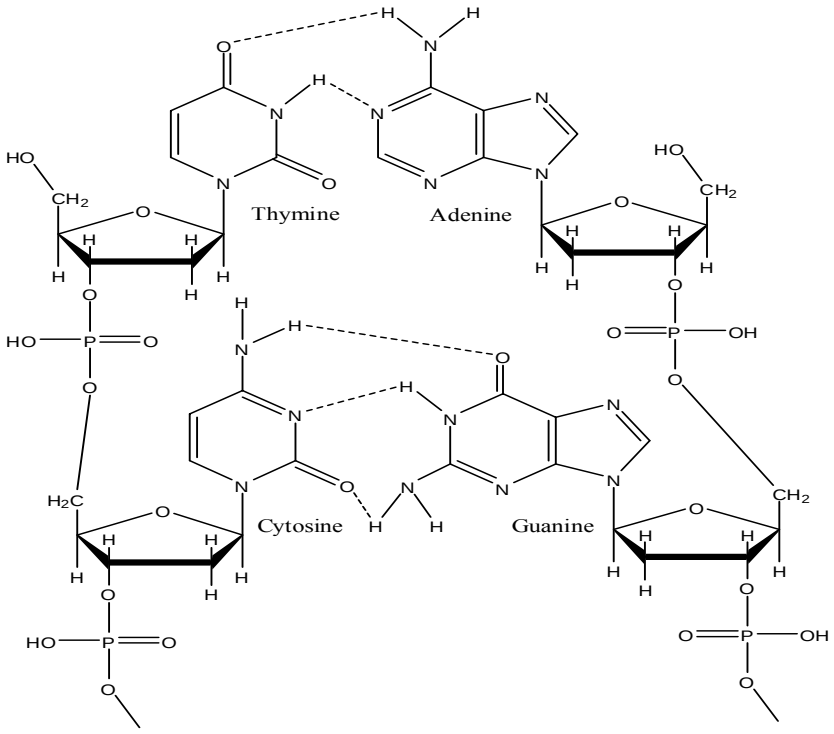

Figure 3-1. A cartoon of the DNA generic repeat unit used for all crosslink calculations (Note: Bonds are not drawn to scale).

Using the generic repeat unit model, the number of amino groups and phosphate groups per repeat unit were calculated to obtain the number of sites available for possible covalent or ionic crosslinking. The number of amino groups and phosphate groups per repeat unit was multiplied by the total number of DNA repeat units in the 1.3 million Daltons chain to obtain the total number of possible reactive sites; which were 3,231 amino groups and 4,308 phosphate groups. The extent of crosslinking was estimated from these available sites. Ionic crosslinking was based on the assumption that the trivalent cations can bind to 3 possible phosphate groups as shown in Figure 3-2.

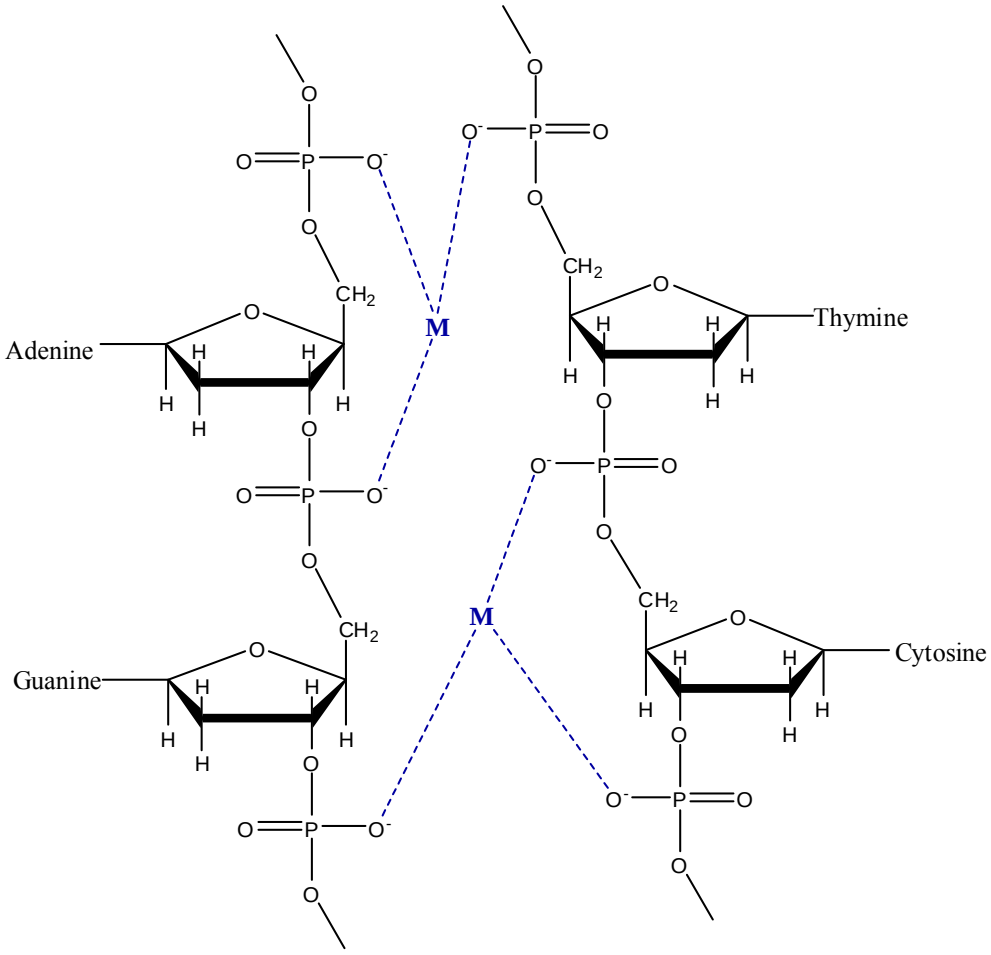

Figure 3-2. Schematic drawing of possible DNA crosslinking sites for trivalent cations, M = Gd^{3+}, Cr^{3+}, or Fe^{3+}. (Note: Bonds are not drawn to scale.)

For covalent crosslinking conditions, it was assumed that one glutaraldehyde molecule could establish a crosslinking unlike genipin for which it was assumed that two genipin molecules would be needed for crosslinking.[11, 96] Glutaraldehyde crosslinking was assumed to occur through a Schiff base reaction with the amino groups found within the adenine, cytosine, and guanine nucleobases of DNA. A possible mechanism for DNA covalently crosslinking with glutaraldehyde is shown in Figure 3-3. Future studies should be conducted to determine the true mechanism for DNA to crosslink with glutaraldehyde. A possible schematic drawing for DNA covalently crosslinking with genipin was not included since genipin was found to not crosslink DNA efficiently (i.e. DNA-MS did not turn blue and immediately dissolved in water.).

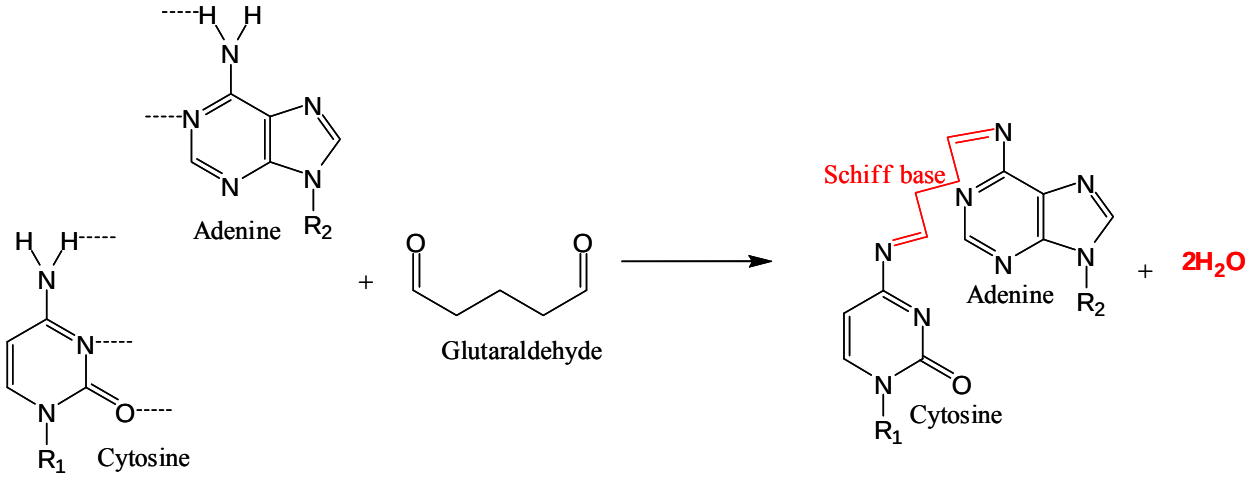

Figure 3-3. Schematic drawing of a possible mechanism for glutaraldehyde to covalently crosslink DNA. (Note: R_1 and R_2 represent the remainder of DNA molecule.)

Microsphere characterization

Yield analysis. The yield of each DNA-MS condition was calculated and expressed as a percent yield value. The percent yield was calculated by dividing the final weight of the DNA-MS by the amount of weight used to synthesize the MS. Equation 3-1 illustrates the expression for calculating the percent yield where W_F is the final weight of the DNA-MS, V_{DNA}, ρ_{DNA}, and

C_{DNA} are the volume, density, and concentration of the aqueous DNA solution used, and W_X is the weight of the crosslinking agent added during synthesis

$$\%\text{Yield} = \left(\frac{W_F}{((C_{DNA} \times V_{DNA} \times \rho_{DNA}) + W_X}\right) \times 100\,\% \quad (3\text{-}1)$$

Dry particle size analysis. The mean dry diameters and particle size distributions of the DNA-MS were obtained using a Coulter LS 13 320 particle size analyzer. Approximately 2mg of the dried DNA-MS were suspended in 2mL of methanol. The suspension was then sonicated for 30 seconds in order to break up any aggregates and tested. The Coulter LS 13 320 particle size analyzer was set to run at a pump speed of 73% using a protein/DNA particle diffraction model. Standards were tested in methanol before the first run of the first batch to ensure that the instrument was performing adequately. Each condition was tested three times in which each test consisted of two runs. This method of testing produced six independent particle diameters and size distributions. Data collected from these experiments were statistically analyzed using SigmaStat 3.0 software.

Hydrated particle size analysis. The mean swollen diameters and particle size distributions of the DNA-MS were obtained using a Coulter LS 13 320 particle size analyzer. Approximately 2mg of the DNA-MS were suspended in 2mL of 0.05M PBS with a pH of 7.4. The suspension was then sonicated for 30 seconds in an attempt to break up any MS aggregates. The DNA-MS were then allowed to swell in the PBS for an additional two minutes and thirty seconds. After swelling the DNA-MS were tested in the Coulter LS 13 320 particle size analyzer using a pump speed of 73% and a protein/DNA particle diffraction model. Standards were tested in PBS before the first run to ensure that the instrument was performing adequately. Each condition was tested three times in which each test consisted of two runs. This method of testing produced six independent particle diameters and size distributions. After obtaining the mean

swollen particle diameters, the data was used to calculate the percent change in size following Equation 3-2, where D_D is the dry diameter and D_H is the swollen or hydrated diameter. A negative percent change in size depicted a decrease in particle size (i.e. degradation) whereas a positive percent change in size depicted an increase in particle size (i.e. swelling). Data collected from these experiments were statistically analyzed using SigmaStat 3.0 software.

$$\%\ \text{Change in Size} = \left(\frac{D_H - D_D}{D_D}\right) \times 100 \tag{3-2}$$

Surface charge analysis. DNA-MS surface charge was characterized to determine dispersability and obtained using a Brookhaven ZetaPlus zeta potential analyzer with ZetaPALS software. Approximately 2mg of dry DNA-MS were suspended in 1.5mL of 0.01M PBS with a pH of 7.4. Each DNA-MS condition was sampled three times in which each sample underwent ten runs. This method of testing produced thirty independent zeta potential values. The data collected from zeta potential analysis was statistically analyzed using SigmaStat 3.0 software.

Dispersability. The dispersability of the DNA-MS was measured by suspending approximately 13mg of dried DNA-MS in 20mL of cold Grey's Balanced Salt Solution (BSS) in a 50mL polypropylene centrifuge. The centrifuge tube was capped and the DNA-MS were mixed on a vortex at level 8 for thirty seconds. After mixing, the centrifuge tube was placed in a stand and the time for DNA-MS to fall out of dispersion was measured using a stop watch. Each condition was sampled three times resulting in three separate dispersability measurements.

Optical microscopy. The morphology of the DNA-MS was observed through optical microscopy. Approximately 1mg of the DNA-MS were spread over a Fisherbrand microscope slide and observed under a Zeiss Axioplan2 optical microscope. Images were taken with a Carl Zeiss AxioCam HR camera under 40x magnification and saved using AxioVision 3.1 software.

Scanning electron microscopy. The morphology and surface topography of the DNA-MS were observed using scanning electron microscopy (SEM). Approximately 1mg of dry DNA-MS was mounted onto aluminum SEM stubs using double sided tape. The DNA-MS were then coated with gold-palladium for 2 minutes using a Technix Hummer V sputter coater. Images were taken either on a JEOL 6400 SEM using an accelerating voltage of 5KeV, condenser lens setting of 10, objective lens setting of 117, and a working distance of 15mm, or on a JEOL 6335F Field Emission SEM at an accelerating voltage of 5KeV and a working distance of 15mm.

Energy dispersive x-Ray spectroscopy. The presence of trivalent cations in the DNA-MS after washing and drying was observed using energy dispersive x-ray spectroscopy (EDS). DNA-MS were mounted onto a piece of silicon wafer. The silicon wafer was then secured to aluminum SEM stubs using carbon double sided tape. The DNA-MS were then coated with carbon for 2 minutes using a Technix Hummer V sputter coater. EDS spectra on the DNA-MS were collected using a JEOL 6400 SEM at an accelerating voltage of 15KeV and working distance of 15mm. A dead time of 20% to 40% was allowed for each condition tested.

Evaluation of fibroblast growth

Synopsis. Normal human dermal BJ fibroblast cells were used in culture to determine the effects DNA and crosslinked DNA-MS on cellular growth. DNA was evaluated at concentrations of 100μg and 500μg, and DNA-MS were tested at concentrations of and 25μg and 100μg. The effects of DNA and DNA-MS on fibroblast growth was determined using a colorimetric MTS assay which measures the number of metabolically active cells in culture.[35] The MTS tetrazolium salt, which is also known as Owen's reagent, is bioreduced to a colored formazan product through the functioning electron transport systems of viable cells.[35, 97, 98] This conversion is assumed to take place through the interaction of the tetrazolium salt with

nicotinamide adenine dinucleotide (NADH) linked dehydrogenases, which are produced during cellular respiration.[35, 99] This interaction results in the oxidized form of nicotinamide adenine dinucleotide (NAD^+) and a colored formazan product which absorbs at the 490nm wavelength, Figure 3-4.[35] The fibroblast cells were evaluated at the 1, 24, and 72 hour time points. An increase in cell growth was defined by an increase in absorbance at 490nm for any given treatment group.

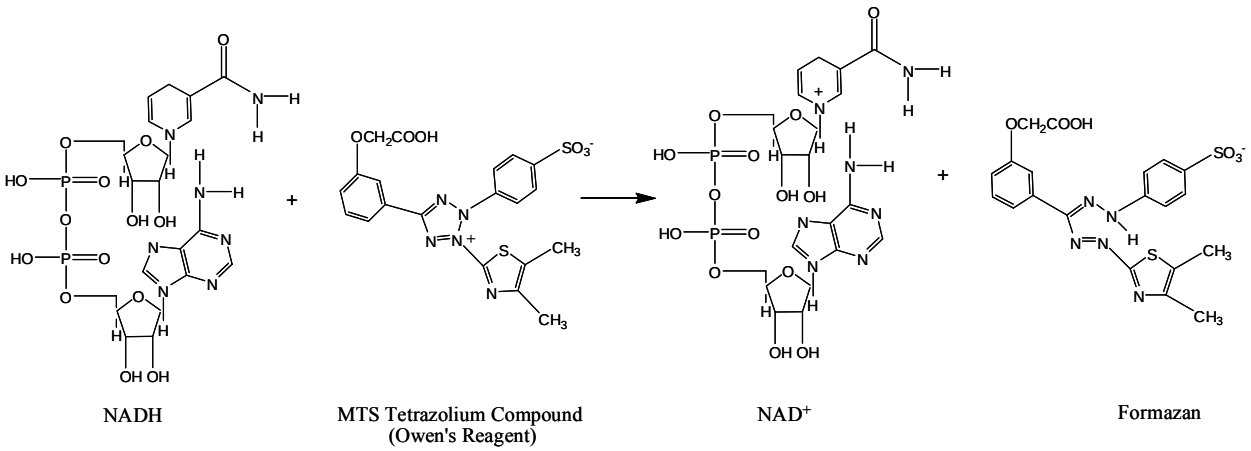

Figure 3-4. The chemical conversion of MTS to formazan.[35, 97, 99]

Culture. Fibroblast cells were cultured in 75cm^2 cell culture flasks with 20mL of treated media. The cells were incubated at 37ºC in humidified air with 5% carbon dioxide for at least 24 hours. After 24 hours, the cells were monitored daily until the cells reached 95% confluency. The cells were then trypsinized and counted in order to determine the cell density. If the cell density was below a concentration of 1 x 10^4 cells/mL, the cells were split and re-cultured until the cell density was between 1 x 10^4 cells/mL and 1 x 10^5 cells/mL. Once the desired cell density was obtained, the cell suspension was used to seed the corresponding 96-well plates used for the study.

Cell seeding. A cell density of 4.4 x 10^4 cells/mL was obtained for these studies and 100µL of the acquired cell suspension were added to specified wells in six separate 96-well

plates. Eight well plates were used for this study representing the two control plates used to measure the absorbance of treatment groups in the absence of cells and the six treatment plates representative of the 1, 24, and 72 hour time points. The six seeded well plates used to evaluate the cytotoxicity of the treatment groups were incubated at 37ºC in humidified air with 5% carbon dioxide in order to reach adequate attachment for at least 24 hours before adding the first treatment. After 24 hours the media was removed from the wells and the treatments were added. The cell culture procedures for this proliferation study were conducted with the help and guidance of Paul Martin.

Treatment groups. The treatment groups for this study evaluated the effects of DNA and crosslinked DNA-MS on fibroblast growth. To evaluate DNA as a sole biomaterial without the influence of possible cytotoxic crosslinking agents, 0.50g of DNA derived from herring testes was dissolved in 10mL of ultrapure water. The aqueous DNA solution was then sterilized using a 0.22µm filter and 2µL of the sterile DNA solution was added to 98µL of the treated media to obtain a concentration of 100µg of DNA in the wells. Similarly, 10µL of the filtered DNA solution was added to 90µL of the treated media to obtain a concentration of 500µg.

DNA-MS synthesized with covalent and ionic crosslinking agents were assessed at concentrations of 25µg and 100µg to determine if the leaching of the crosslinking agents during DNA-MS degradation caused a negative response on fibroblast growth. For these conditions, 2mg of crosslinked DNA-MS were sterilized by thoroughly rinsing the DNA-MS with 1mL of 70% ethanol by vortexing them on high for 30 seconds. The DNA-MS were then centrifuged at 3,000rpm for 5 minutes and collected by decanting the ethanol and allowing the sterilized DNA-MS to air dry over night. The sterilized DNA-MS were then resuspended in 1mL of treated media and added to designated cells using appropriate volumes to reach desired treatment group

concentrations. For the 25μg treatment conditions, 13μL of the MS/media suspension was added to 87μL of the treated media. For the 100μg treatment conditions, 50μL of the MS/media suspension was added to 50μL of the treated media.

There were three control groups used in this study which consisted of 1) treated media in the absence of cells, 2) treated media with cells, 3) treatment groups in treated media in the absence of cells. Absorbance values taken of the media and treatment groups in the absence of cells were used to correct cell culture data obtained in the study.

To access the morphology of the fibroblast cells after treatment, the cells were fixed with 10% formalin and stained with crystal violet immediately following the proliferation assay. All control, DNA, and DNA-MS conditions were evaluated in replicates of six. All cellular proliferation data collected was statistically analyzed using SigmaStat 3.0 Software.

Results

Pilot Microsphere Synthesis Study

Synopsis

A pilot study was conducted to determine if DNA-MS could be prepared through chromium trivalent cation crosslinking. Synthesis procedures were carried out in a 50mL polypropylene centrifuge tube at room temperature. Prepared chromium crosslinked DNA-MS were analyzed via scanning electron microscopy.

Scanning electron microscopy

The pilot study was successful in producing chromium trivalent cation crosslinked DNA-MS. Evidence of successful chromium bonding was visually denoted by the blue color of the resultant DNA-MS. It was visually observed that during the synthesis process, the chromium crosslinked DNA-MS aggregated during washing and furthermore upon drying. SEM micrographs confirmed aggregation and discrete particles were not produced. However, the

SEM micrographs also illustrated that the pilot study produced DNA-MS with spherical morphologies as shown in Figure 3-5.

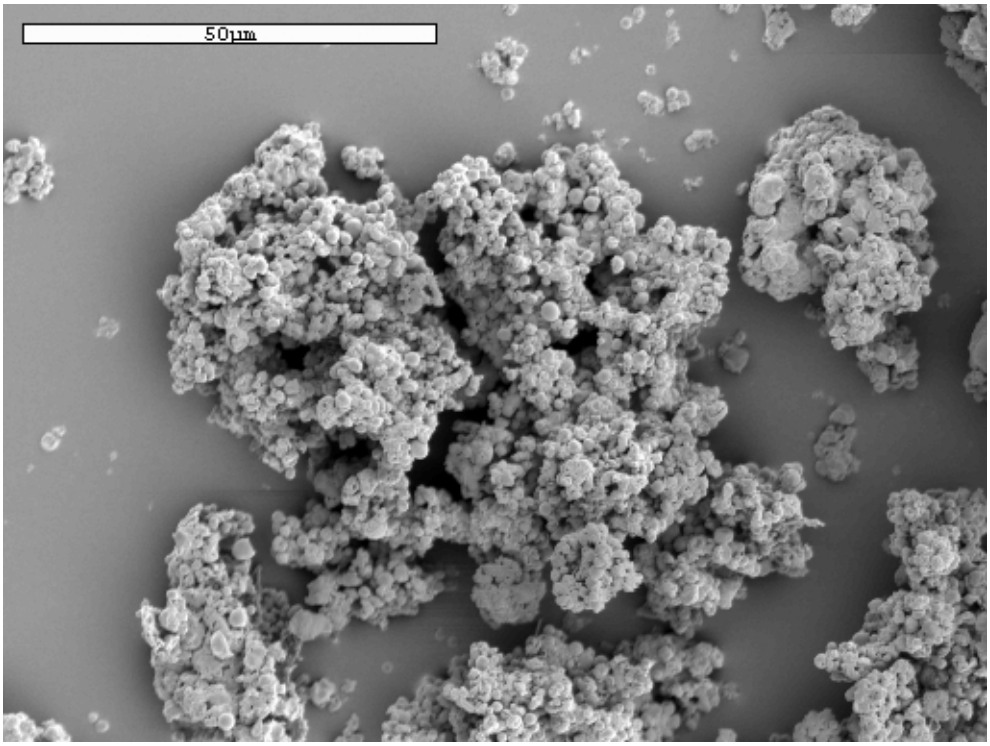

Figure 3-5. SEM micrograph of chromium crosslinked DNA-MS (Magnification:1,000x).

Stabilizing Agent Study

Synopsis

A study was designed to evaluate the effects of the stabilizing agent concentration (CAB) on synthesized DNA-MS particle discreteness due to particle aggregation encountered in the pilot study. The concentrations of the CAB solutions were varied for this study and assessed at 3% (w/v), 5% (w/v), 10% (w/v), and 25% (w/v). In order to increase the yield of the synthesized DNA-MS, the concentration of the aqueous DNA solution was increased from 1% (w/v) to 3% (w/v). Prepared DNA-MS were characterized using scanning electron microscopy.

Scanning electron microscopy

SEM micrographs displayed varied results for the CAB concentrations used for this study. The 5% (w/v) CAB condition produced DNA-MS that were disperse during washing and dried into nice discreet powders. DNA-MS prepared with the 3% (w/v), 10% (w/v), and 25% (w/v) CAB concentrations produced particles that aggregated during acetone rinsing which resulted in agglomerated clumps upon drying. SEM visually confirmed these observations as shown in Figure 3-6.

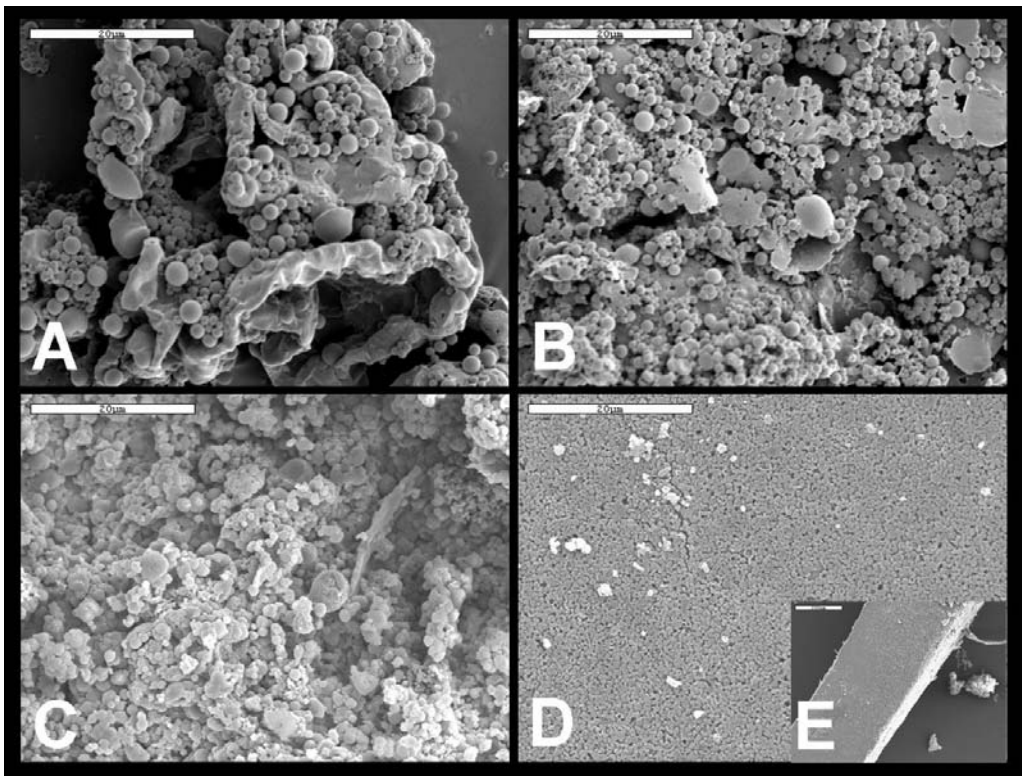

Figure 3-6. SEM micrographs of DNA-MS prepared with CAB concentrations of A) 3% (w/v), B) 5% (w/v), C) 10% (w/v), D) 25% (w/v) (Magnifications: 2,000x), and E) 25% (w/v) (Magnification: 130x; Scale bar: 200μm).

The 5% (w/v) CAB condition produced the most discrete DNA-MS particles as compared with the other three conditions examined. The 25% (w/v) CAB condition produced the highest level agglomeration, followed by the 10% (w/v) and 3% (w/v) CAB conditions. SEM micrographs also illustrated a trend in decreasing particle diameter size as the CAB

concentration increased with the 25% (w/v) CAB condition producing DNA-MS with the smallest diameters.

Crosslinking Reaction Study

The time to crosslink DNA with covalent or ionic crosslinking agents used for general microsphere synthesis was investigated. Crosslinking time was estimated by measuring the time needed for each agent to precipitate DNA from solution. This study found that the ionic crosslinking agents displayed the quickest reaction with DNA, with the glutaraldehyde and genipin following after. The chromium and gadolinium crosslinking agents reacted instantaneously with the DNA and appeared to produce films that were crosslinked homogenously. The iron reacted with the DNA rapidly; however, the reaction was not homogeneous and produced clumps of iron crosslinked DNA instead of a uniform DNA film. It took approximately two hours for the glutaraldehyde to react with the DNA and produce a crosslinked film. The film appeared to be crosslinked homogenously. The genipin crosslinking agent did not appear to react with the DNA since no noticeable change in color was observed (i.e. The DNA solution did not turn from white to blue which is indicative of genipin reacting with openly functional primary amine sites.[95]).

It was speculated that the genipin solution was no longer reactive since there was no interaction between the DNA and genipin. A side study was therefore conducted to determine if the genipin solution was still reactive. To test this, 9mL of the 5% (w/v) genipin solution was added to 3mL of 5% (w/v) lysine, 3mL of irradiated 5% (w/v) DNA, and 3mL of 5% (w/v) DNA separately. The genipin and lysine and genipin and DNA solutions were mixed on the vortex mixer on level 8 for 30 seconds and then placed on a rotary mixer. The genipin reacted completely with the lysine solution after two hours. The color of the lysine solution changed from white to a dark purplish blue. On the other hand, it took approximately 72 hours for the

genipin to react with both DNA solutions and the reaction never reached completion. It was assumed that the genipin would react quicker with the irradiated DNA since it would be degraded and thus have functional amino sites more readily accessible than the non-degraded DNA, but this was not the case. Both DNA solutions changed from a white color to a reddish brown to finally a dark bluish yellow indicating a small reaction between the genipin and the amino groups within the DNA molecule.

General Microsphere Synthesis

Synopsis

Full scale studies were designed to evaluate and characterize DNA-MS synthesized with covalent and ionic crosslinking agents based on the successes encountered with the pilot and stabilizing agent studies. The concentration of the beginning aqueous DNA solution was increased from 3% (w/v) to 5% (w/v) to increase the resulting DNA-MS yield for these studies.

Particle analysis

Percent yield. DNA-MS synthesis appeared to be successful with each crosslink agent condition producing yields over 50%. The gadolinium and genipin crosslinked DNA-MS conditions produced discrete particle yields; however, the iron, chromium, and glutaraldehyde conditions produced aggregates upon washing and drying. The gadolinium crosslinked DNA-MS performed the best producing a yield of 82%. The percent yield values for each condition are tabulated in Table 3-1.

Table 3-1. The yields, dry mean particle diameters, and crosslink concentrations for DNA-MS prepared with ionic and covalent crosslinking agents.

Crosslinking agent	Percent yield (%)	Crosslink concentration (%M_{EQ})
Chromium	77	120
Gadolinium	82	120
Iron	54	120
Glutaraldehyde	61	540
Genipin	63	1070

Dry particle size analysis. The dry particle sizes of the DNA-MS were obtained in methanol. DNA-MS prepared with covalent and ionic crosslinking agents produced particles with mean dry diameters of less than 20μm. Statistical analysis using a one way analysis of variance test (ANOVA) found there to be no significant differences among the mean particle diameter values for all conditions tested. However, the gadolinium and genipin crosslinked DNA-MS conditions appear to have performed the best, producing the highest percentage of particles in the mesosphere size range and the lowest percentage of particles with diameters greater than 10μm. The gadolinium condition produced mean dry particle diameters of 2.6μm ± 2.8μm and the genipin condition produced mean dry particle diameters of 3.1μm ± 2.9μm. The glutaraldehyde crosslink condition performed similarly well with a mean dry particle diameter of 6.4μm ± 9.7μm; however produced over 5% of particles with diameters greater than 10μm. Both the chromium and iron crosslink agent conditions produced the largest mean particle diameters as compared to all other conditions tested with values of 10.3μm ± 13.9μm and 14.1μm ± 16.7μm, respectively. The mean dry particle diameters and the size ranges for each of the synthesized DNA-MS conditions are shown in Table 3-2.

Table 3-2. The dry mean particle diameters and size ranges for DNA-MS prepared with ionic and covalent crosslinking agents.

Crosslinking agent	Mean dry particle diameter (μm)	DNA-MS in 1μm to 10μm range (%)	DNA-MS larger than 10μm (%)
Chromium	10.3 ± 13.9	32	44
Gadolinium	2.6 ± 2.8	81	2
Iron	14.1 ± 16.7	31	50
Glutaraldehyde	6.4 ± 9.7	64	16
Genipin	3.1 ± 2.9	73	3

The gadolinium condition produced the most controlled and narrow particle size distribution of the three ionic crosslinking agent conditions tested. The chromium crosslink agent condition displayed an irregular and multimodal distribution over a very broad range of

particle diameter sizes. The iron condition exhibited a bimodal distribution with a larger volume percent of DNAMS over a range of larger particle sizes. Each of the three ionic agent crosslink conditions produced particles within the nano-mesosphere range of 67nm to 2µm, with the gadolinium crosslink condition producing the highest volume percent of the three. The particle size distributions for ionically crosslinked DNA-MS is shown in Figure 3-7.

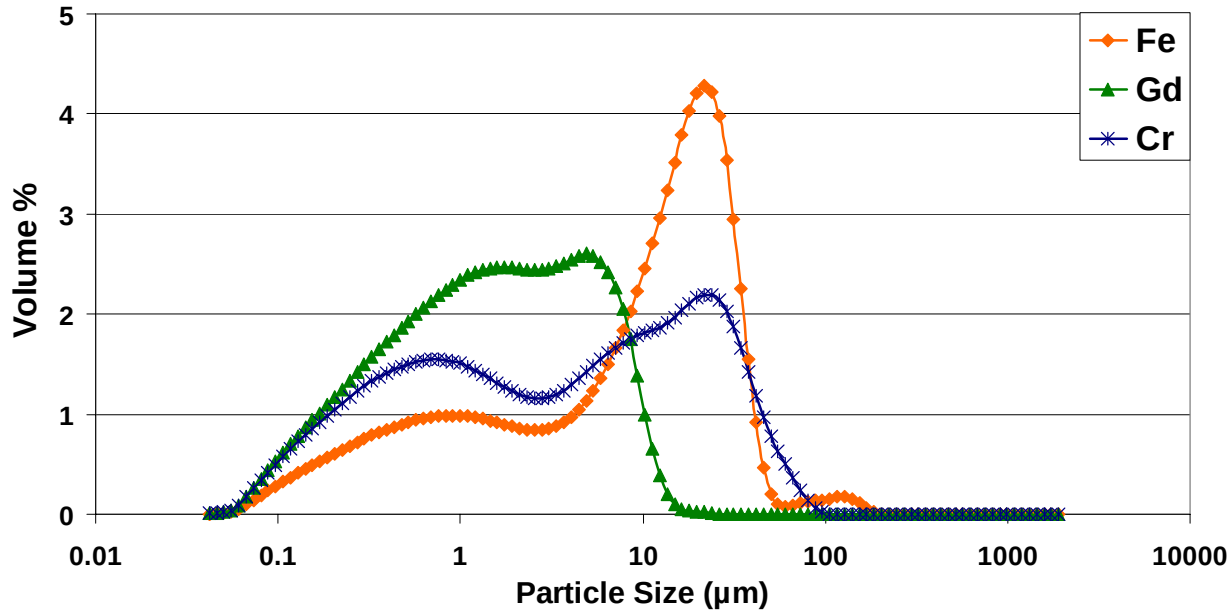

Figure 3-7. Particle size distributions of ionically crosslinked DNA-MS under dry conditions.

The covalently crosslinked DNA-MS performed similarly well with dry mean diameters less than 10µm and mostly normalized particle size distributions. DNA-MS covalently crosslinked with glutaraldehyde displayed a narrow particle size distribution; however, aggregates were visually noted above 10µm. DNA-MS prepared with genipin also exhibited a normalized and narrow particle size distribution; however, resulting DNA-MS were white in color instead of blue indicating a lack of reaction between the genipin and DNA. Similar to DNA-MS synthesized with ionic crosslinking agents, the covalent crosslinking agent conditions also produced nano-mesospheres in the 60nm to 2µm range. Particle size distributions for covalently crosslinked DNA-MS can be found in Figure 3-8.

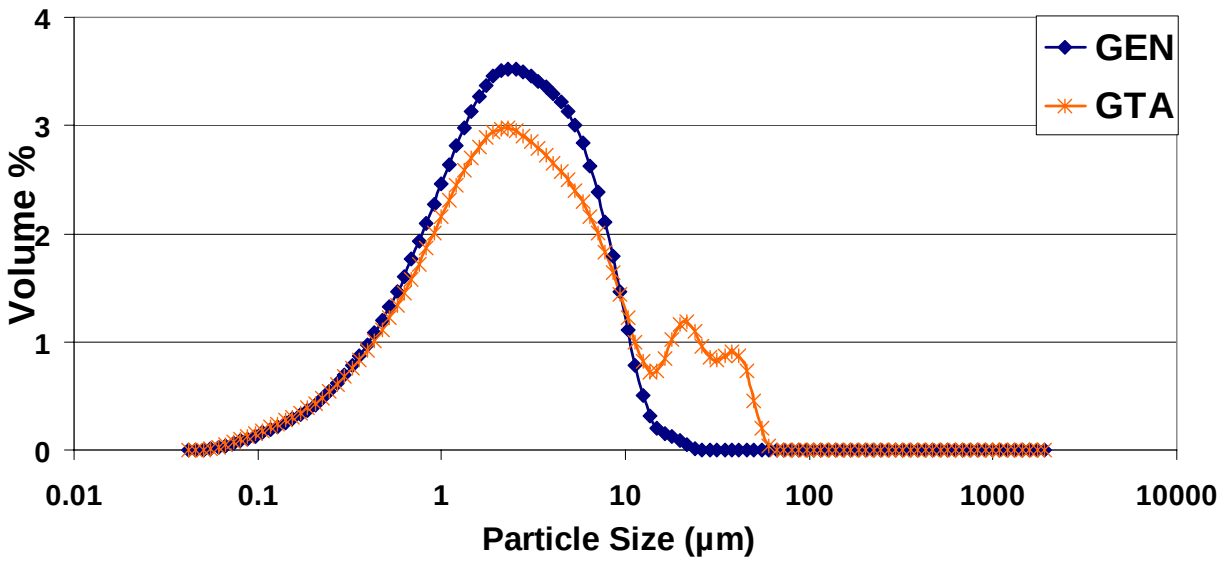

Figure 3-8. Particle size distributions for covalently crosslinked DNA-MS under dry conditions.

Hydrated particle size analysis. DNA-MS synthesized with covalent and ionic crosslinking agents also underwent particle size analysis under hydrated conditions in 0.05M PBS at a pH of 7.4. Approximately 2mg of the DNA-MS were suspended in PBS and sonicated for 30 seconds in a 15mL centrifuge tube. Upon suspension into PBS, it was noted that the DNA-MS began to stick to the walls of the centrifuge tube and the particles began to clump or aggregate together. The samples were sonicated to disperse the DNA-MS; however, hydrated particle size analysis for both ionic and covalent conditions illustrated that sonication was not successful in breaking up aggregates.

Hydrated particle diameters for the ionically crosslinked DNA-MS ranged from 11µm to 45µm and each condition, with the exception of the iron condition, displayed hydrated diameters of greater than 25µm. However, it was suspected that these values mostly represented the aggregates that formed during hydration instead of the true values of hydrated DNA-MS. Upon closer observation, it appeared that the median particle diameter values better represented the

true hydrated size of the DNA-MS and were therefore tabulated and compared to mean hydrated particle size values, Table 3-3.

Table 3-3. Mean and median hydrated particle size values for ionically crosslinked DNA-MS.

Crosslinking Agent	Mean dry particle diameter (μm)	Mean hydrated Particle diameter (μm)	Median hydrated particle diameter (μm)
Chromium	10.3 ± 13.9	25.8 ± 29.6	14.9
Gadolinium	2.6 ± 2.8	45.1 ± 85.7	12.1
Iron	14.2 ± 17.1	11.9 ± 10.9	9.3
Glutaraldehyde	6.4 ± 9.7	128 ± 222	27.6
Genipin	3.1 ± 2.9	0 ± 0	0 ± 0

The ionic crosslink agent conditions produced mostly normalized hydrated particle size distributions with evidence of aggregation most noted in the chromium and gadolinium conditions, Figure 3-9. The iron particle size distribution did not illustrate signs of aggregation, however, it was noted that during particle size analysis, the size of the DNA-MS began to decrease rapidly suggesting that the iron crosslinked DNA-MS were dissolving or degrading in the PBS.

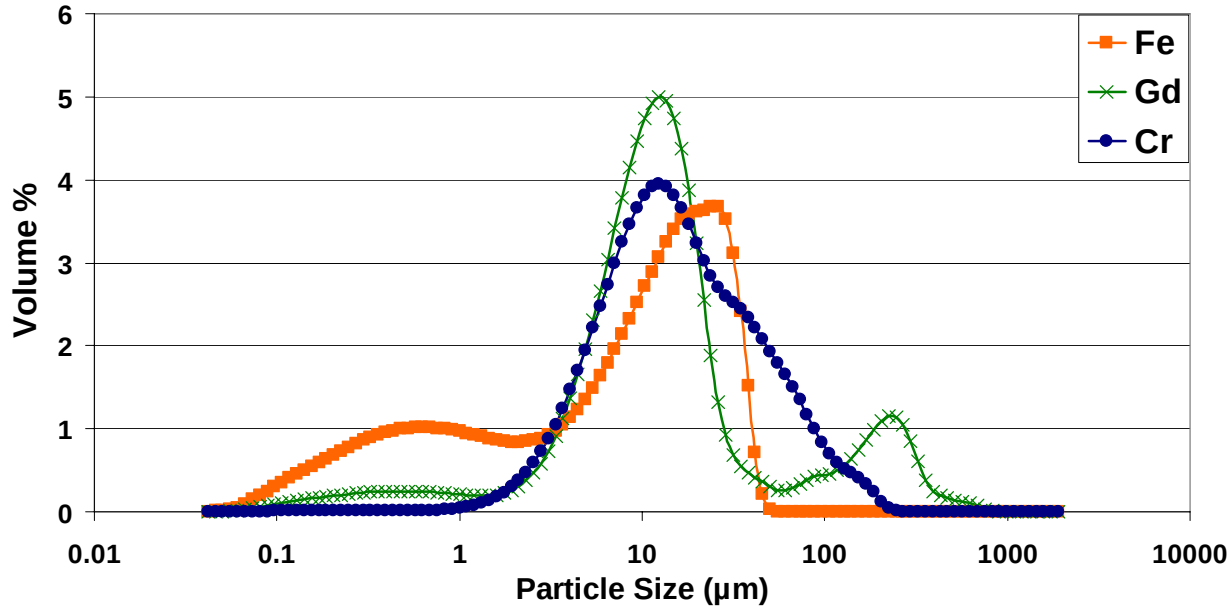

Figure 3-9. Particle size distributions of ionically crosslinked DNA-MS under hydrated conditions.

The glutaraldehyde crosslink agent condition produced a mean hydrated particle size of 128µm. However, it was also suspected that this value was a better representation of the aggregates that formed upon hydration instead of the true swollen diameter size of the DNA-MS. Therefore, the median hydrated particle size diameter was tabulated and compared to the mean hydrated value, Table 3-3.

The glutaraldehyde crosslink agent condition was the only condition to display stability in PBS. The DNA-MS prepared with genipin immediately dissolved and were unable to undergo hydrated particle size analysis. Glutaraldehyde crosslinked DNA-MS illustrated multimodal hydrated particle size distributions with a large percent of DNA-MS exhibiting hydrated diameter values over the 100µm to 1000µm size range, indicative of a high degree of aggregation upon hydration, Figure 3-10.

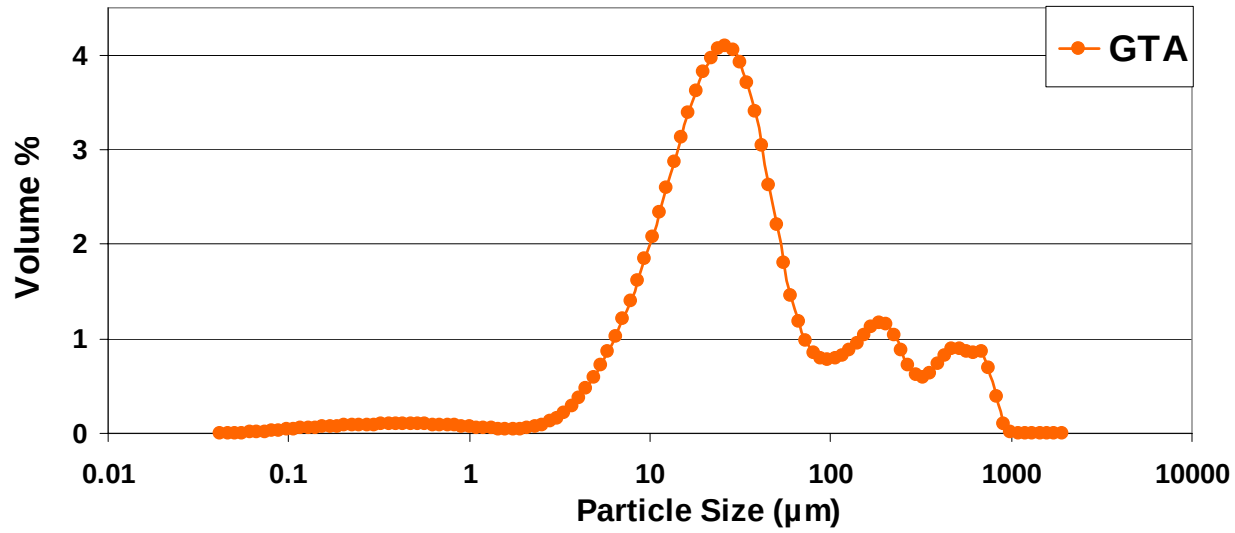

Figure 3-10. Particle size distribution of the glutaraldehyde crosslinked DNA-MS under hydrated conditions.

Statistical analysis was conducted on all collected mean and median hydrated data to further compare each DNA-MS condition under hydration. A one way ANOVA found no significant differences among all mean and median hydrated particle size values tested. The lack

of statistical difference among mean and median values can be attributed to the variability of sizes due to the formation of aggregates upon hydration.

In order to quantify the effect of hydration on particle size, the mean and median percent change in size values were calculated for all DNA-MS conditions tested using the mean dry, mean hydrated, and median hydrated diameter values. Equation 3-2 was used for all percent change in size calculations and values for each DNA-MS condition tested are given in Table 3-4.

Table 3-4. Percent change in size values for ionically and covalently crosslinked DNA-MS.

Crosslinking Agent	Mean percent change in size (%)	Median percent change in size (%)
Chromium	(+) 151	(+) 45
Gadolinium	(+) 1640	(+) 365
Iron	(-) 19	(-) 35
Glutaraldehyde	(+) 1900	(+) 331
Genipin	(-) 100	(-) 100

The gadolinium crosslinked DNA-MS condition produced the highest percent increase in size under hydrated conditions, with glutaraldehyde and chromium following after due to the formation of aggregates upon hydration. The chromium crosslinked DNA-MS condition performed the best with only a 151% mean or 45% median increase in size under hydrated conditions. The iron crosslink agent condition displayed the least stability under aqueous conditions of all the ionic crosslink agent conditions tested with a 19% mean or 35% median decrease in size. The genipin crosslinked DNA-MS condition displayed the least stability and immediately dissolved upon hydration producing a 100% decrease in size.

Surface charge and dispersability

Surface charge. The surface charge was measured for DNA-MS that were stable under hydrated conditions. Therefore, only the glutaraldehyde, chromium, and gadolinium crosslinked DNA-MS were evaluated. The surface charges of the DNA-MS were measured using a zeta potential analyzer in 0.01M PBS at a pH of 7.4 and expressed in millivolts (mV). The

gadolinium crosslinked DNA-MS condition displayed the most negative zeta potential values, -45.3mV, as compared to the chromium and glutaraldehyde crosslinked conditions, Figure 3-11.

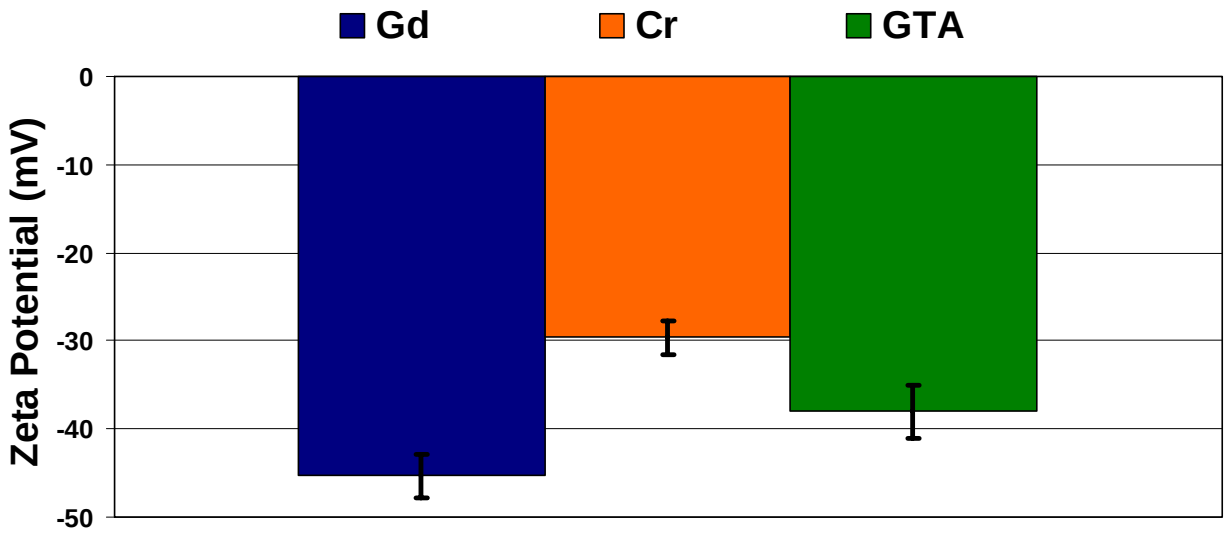

Figure 3-11. Zeta potential chart for DNA-MS crosslinked with gadolinium (Gd), chromium (Cr), and glutaraldehyde (GTA).

The glutaraldehyde crosslinked condition displayed the second most negative zeta potential value of -38.0mV, followed by the chromium crosslinked DNA-MS which displayed the least negative zeta potential, -29.6mV. Statistical analysis using a one way ANOVA test found the zeta potential values for all conditions to be significantly different from one another ($p < 0.001$). Further analysis using a Tukey Test for all pairwise multiple comparisons found the zeta potential values for chromium to be significantly lower from those obtained for the gadolinium ($p < 0.001$) and glutaraldehyde ($p < 0.001$) conditions, and the zeta potential values for glutaraldehyde to be significantly lower than those obtained for the gadolinium ($p = 0.002$) condition. The zeta potential values with their respective standard errors for each condition tested are given in Table 3-5.

Table 3-5. Zeta potential values and dispersability times for DNA-MS crosslinked with gadolinium, chromium, and glutaraldehyde.

Crosslinking agent	Zeta potential (mV)	Dispersability time (hr)
Gadolinium	-45.3 ± 2.4	48 ± 3
Chromium	-29.6 ± 1.9	12 ± 1
Glutaraldehyde	-38.0 ± 3.0	1 ± 1

Dispersability. It is important for DNA-MS to be stable and dispersible under aqueous conditions for their intended application of intratumoral chemotherapy. Therefore, gadolinium, chromium, and glutaraldehyde crosslinked DNA-MS were tested in Grey's balanced salt solution for dispersability. The gadolinium crosslinked DNA-MS displayed the most stable dispersability with dispersion times exceeding 24 hours. The gadolinium crosslinked DNA-MS maintained their dispersion for 48 hours upon which slight agitation could resuspend the microspheres for another 48 hours. The chromium crosslinked DNA-MS did not perform as well as the gadolinium crosslinked MS and displayed dispersion times that only lasted 12 hours. For this condition, approximated 25% of all dispersed MS fell out of solution within the first two minutes; and within four hours, approximately 60% of the MS were out of dispersion. The remaining DNA-MS continued to fall out of dispersion for the remaining eight hours. The glutaraldehyde crosslinked DNA-MS conditions performed the worst as compared to all other conditions tested in which 60% of all MS clumped together during vortex mixing and fell out of dispersion within the first two minutes. The remaining 40% fell out of dispersion within the first hour. Dispersability times for each DNA-MS condition tested are given in Table 3-5.

Microscopy

Optical microscopy. Dried DNA-MS were observed under optical microscopy to evaluate their discreteness, morphology, and particle size after synthesis. Optical images of the ionically crosslinked DNA-MS displayed particles with small diameters and spherical morphologies, Figure 3-12. Each ionic crosslink agent condition produced discrete particles with

the exception of the iron crosslink agent condition which appeared to exhibit a moderate amount of aggregation. Optical images of the chromium crosslink agent condition also displayed some particles that appeared aggregated and had slightly irregular shapes. Optical images also confirmed data obtained through particle size analysis illustrating that the chromium crosslinked condition produced DNA-MS with larger particle sizes than the gadolinium condition.

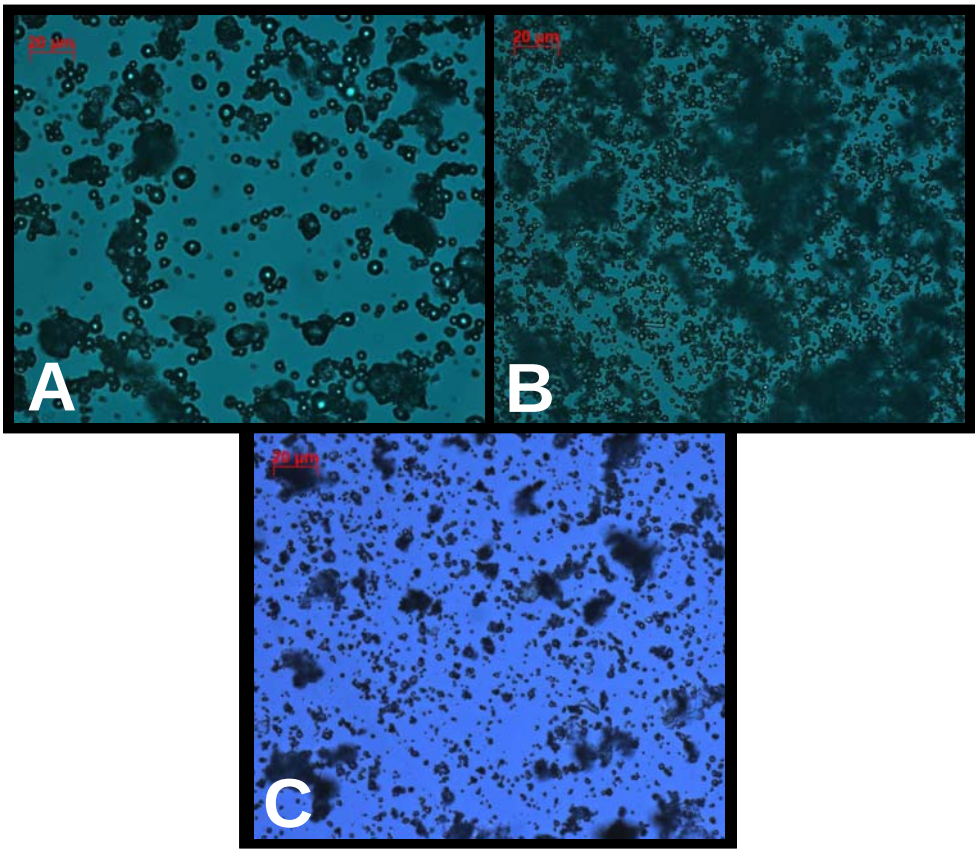

Figure 3-12. Optical microscopy images of DNA-MS ionically crosslinked with A) chromium, B) gadolinium, and C) iron trivalent cations (Magnification: 400x).

The optical images of the ionically crosslinked DNA-MS revealed particles sizes that were much smaller than those produced with covalent crosslinking agents. The DNA-MS that were covalently crosslinked with glutaraldehyde produced the largest microsphere sizes as compared to all other conditions tested. Optical images of DNA-MS crosslinked with genipin displayed images of spherical particles and strands of un-crosslinked DNA further indicating that the

genipin did not fully react with the DNA in solution during synthesis. DNA-MS that were covalently crosslinked produced discrete particles with spherical morphologies and are shown in Figure 3-13.

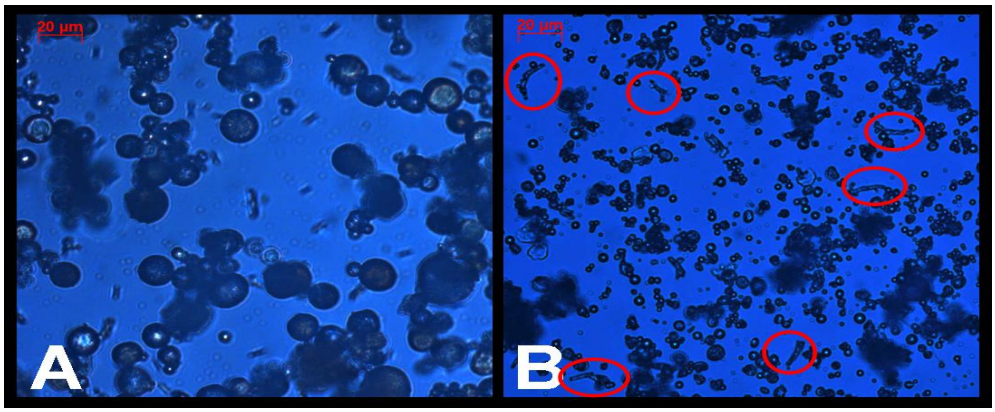

Figure 3-13. Optical microscopy images of DNA-MS covalently crosslinked with A) glutaraldehyde, and B) genipin (Magnification: 400x). Note: Red circles highlight un-crosslinked DNA strands.

Scanning electron microscopy. SEM images were taken of the DNA-MS to characterize their morphology and surface topography. SEM images illustrated that the ionically crosslinked DNA-MS displayed spherical morphologies and smooth surface topographies, with the exception of the iron crosslink agent condition which produced an agglomerate of aggregated DNA and iron crosslinked MS, Figures 3-14 to 3-16.

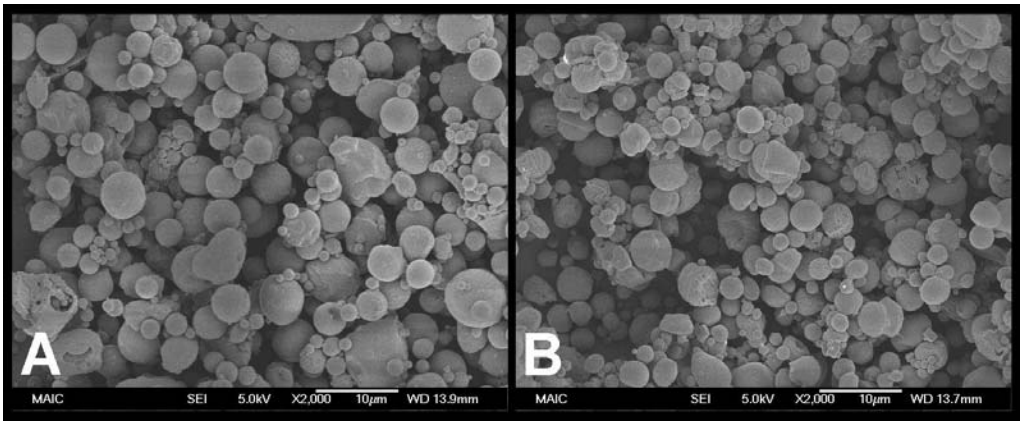

Figure 3-14. SEM images of DNA-MS prepared with A) chromium and B) gadolinium trivalent cationic crosslinking agents (Magnification: 2000x).

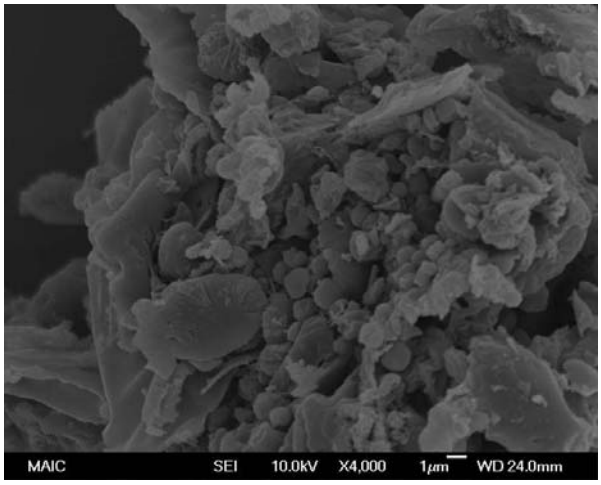

Figure 3-15. SEM image of a DNA-MS aggregate crosslinked with trivalent iron cations (Magnification: 4,000x).

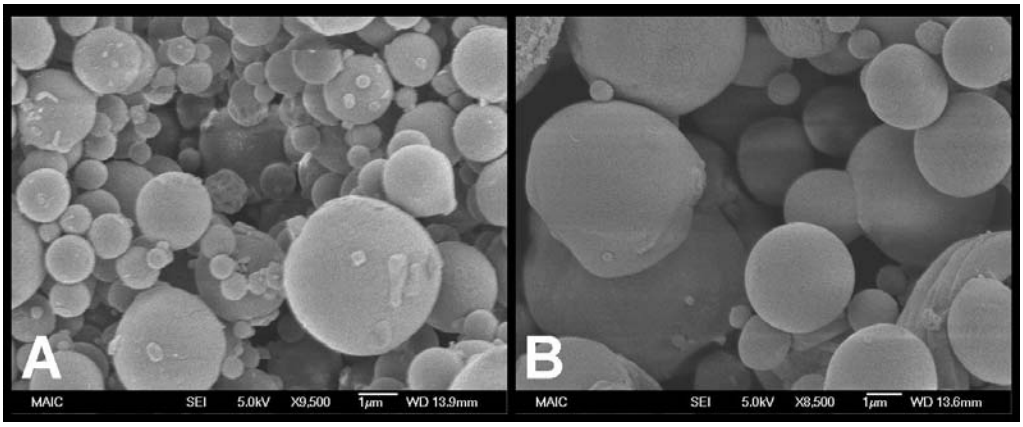

Figure 3-16. SEM images of ionically crosslinked DNA-MS with smooth surface topographies in the nano-mesosphere size range: A) chromium (Magnification: 9,500x) and B) gadolinium crosslinked DNA-MS (Magnification: 8,500x).

SEM images taken of the DNA-MS crosslinked with chromium and gadolinium also illustrated particle sizes under 10μm which visually confirmed results obtained with the particle size analyzer. These SEM images also depicted particles that fell within the nano-mesosphere particle size range (i.e. d < 10μm). Upon further observation of the chromium and gadolinium crosslink agent conditions, SEM images illustrated that the gadolinium crosslink agent condition produced discrete particles, whereas the chromium crosslink agent condition produced aggregated particles, Figure 3-17.

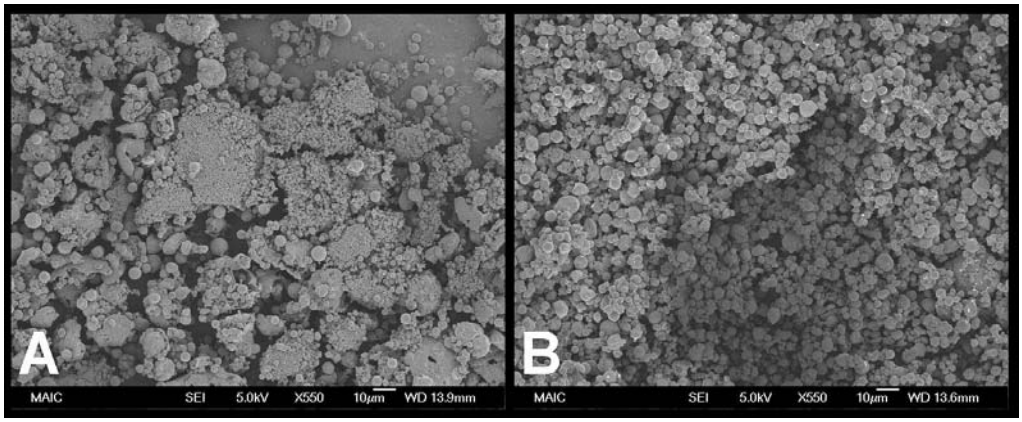

Figure 3-17. SEM images of ionically crosslinked DNA-MS: A) aggregated chromium and B) discrete gadolinium crosslinked DNA-MS (Magnification: 550x).

SEM images taken of the covalently crosslinked DNA-MS produced spherical morphologies confirming observations made with the optical microscope, Figure 3-18.

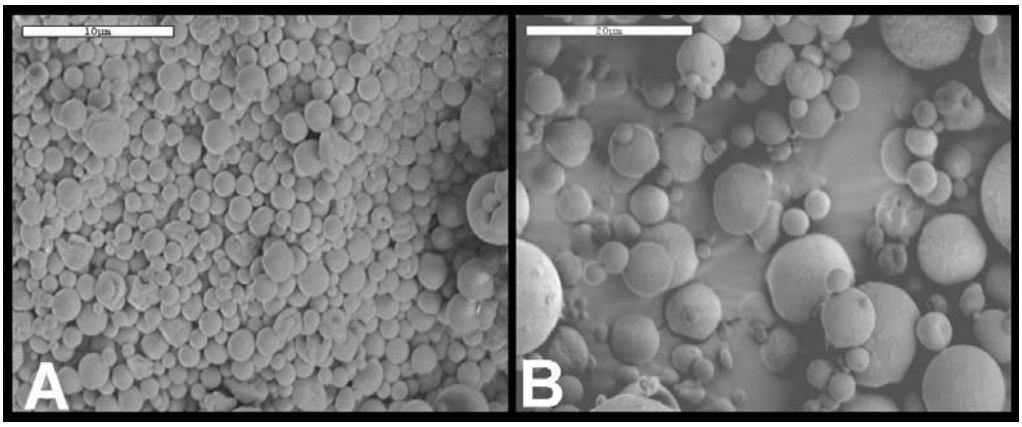

Figure 3-18. SEM images of DNA-MS prepared with A) genipin (Magnification: 4,000x) and B) glutaraldehyde (Magnification: 2,000x) covalent crosslink agents.

The SEM images also displayed variations in particle size between the genipin and glutaraldehyde crosslink agent conditions. These images illustrated that the glutaraldehyde crosslink condition produced microspheres with larger diameters and a broader size distribution than that of the genipin, further confirming results obtained with the particle size analyzer. Upon closer observation of the SEM images, it was also noted that the glutaraldehyde crosslink

condition produced DNA-MS with rougher surface topographies than the DNA-MS synthesized with the genipin crosslink condition.

Energy dispersive x-ray spectroscopy. The presence of the trivalent cations in the DNA-MS were confirmed using EDS. EDS spectra collected on the chromium, gadolinium, and iron crosslinked DNA-MS conditions confirmed the presence of the trivalent cations in the dried DNA-MS indicating that the cations are not being washed out by acetone during rinsing indicating that they are indeed chemically bonding with the DNA. The EDS spectra also depicted large phosphorous peaks indicative of the phosphate groups in the DNA molecule. Silicon peaks were also seen in the spectra due to the silicon wafer used for EDS sample preparation. The collected EDS spectra for each ionic crosslink condition can be found in Figures 3-19 to 3-21.

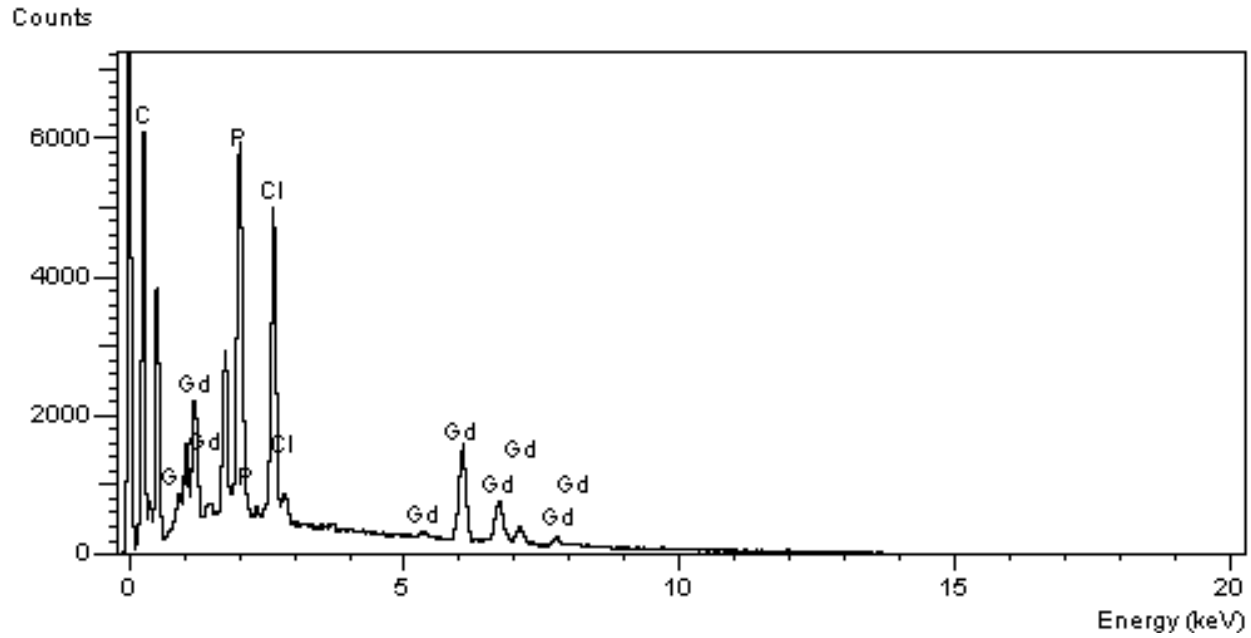

Figure 3-19. EDS spectra collected on DNA-MS crosslinked with gadolinium.

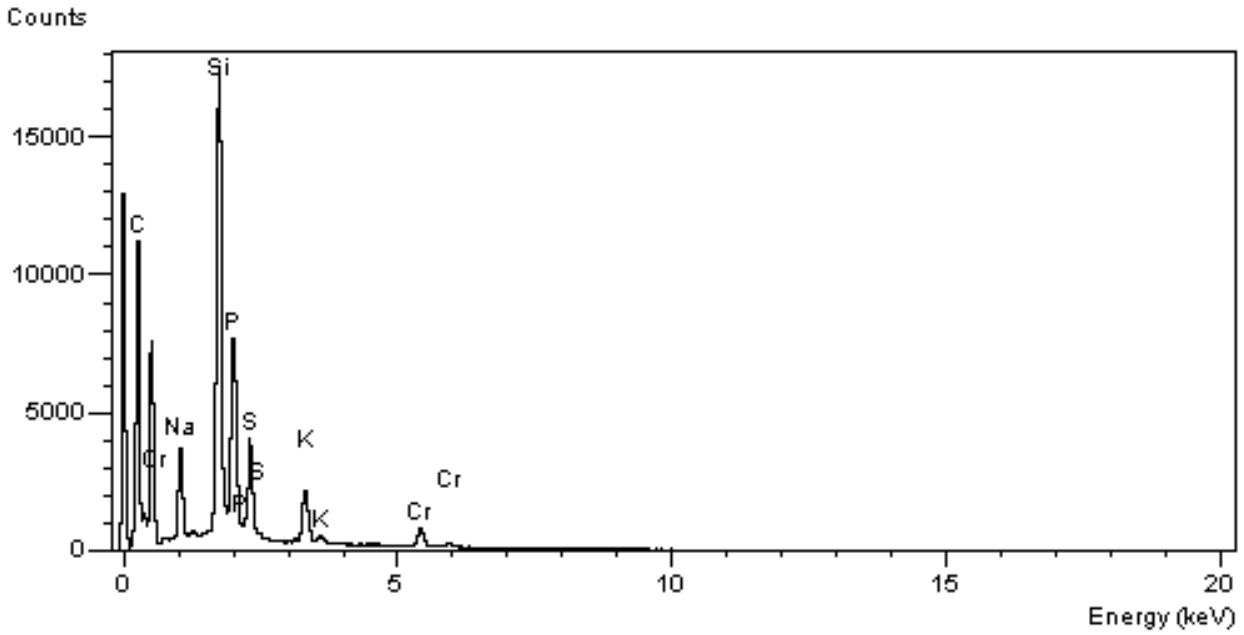

Figure 3-20. EDS spectra collected on DNA-MS crosslinked with chromium.

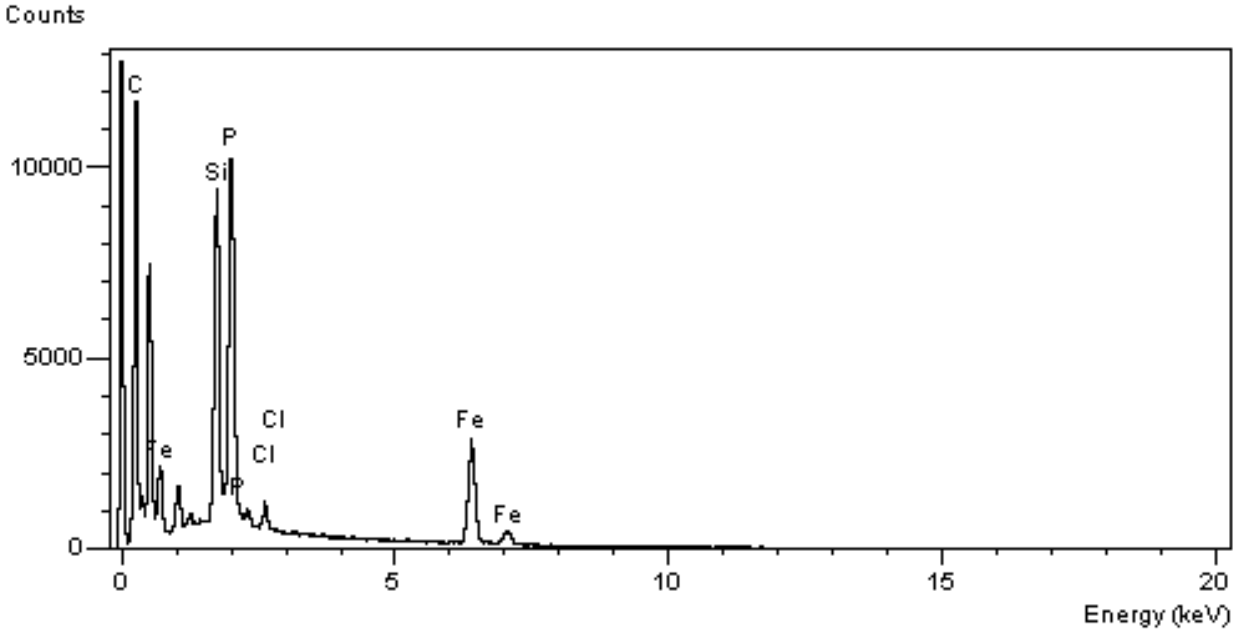

Figure 3-21. EDS spectra collected on DNA-MS crosslinked with iron.

Evaluation of fibroblast growth

DNA. The effect of DNA on the cell growth of normal human dermal BJ fibroblast cells was assessed in culture using an MTS proliferation assay. Results from the assay indicated that

fibroblast proliferation decreased at the 100µg and the 500µg DNA conditions between hours 1 and 24, but increased between hours 24 and 72, Figure 3-22.

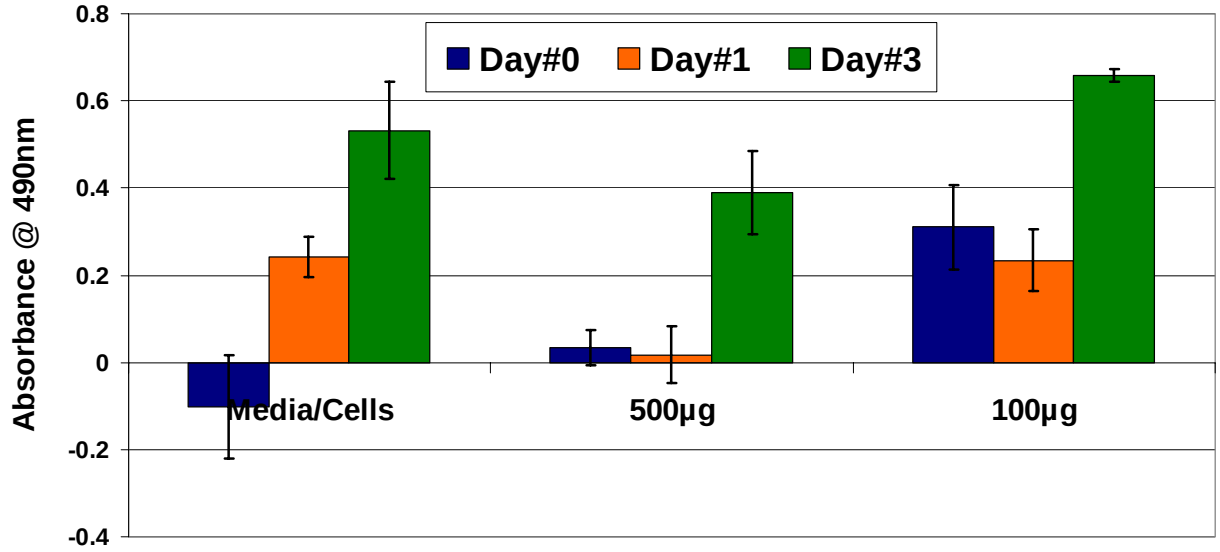

Figure 3-22. Fibroblast proliferation profiles for DNA treatment conditions.

Statistical analysis of these values, however, illustrated that at Day#0 (Hour 1), the 100µg DNA condition produced significantly higher proliferation rates than the control ($p < 0.001$) and the 500µg condition ($p = 0.021$). Statistical analysis also illustrated that by Day#1 (Hour 24), the 500µg condition produced significantly lower proliferation rates than the control ($p < 0.001$) and the 100µg condition ($p = 0.003$). There were no significant differences between the control and the 100µg or 500µg conditions by Day#3 (hour 72); however, the 100µg condition did produce significantly higher proliferation rates than the 500µg condition ($p = 0.017$). Further analysis using optical microscopy images displayed fibroblast cells that were very similar in morphology and confluency, Figure 3-23.

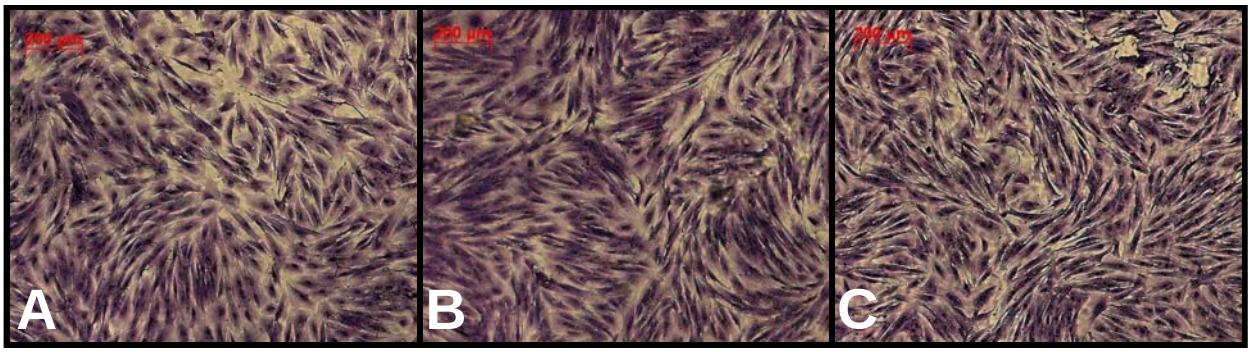

Figure 3-23. Optical microscopy images of crystal violet stained normal human dermal BJ fibroblast cells exposed to A) media with cells, B) 100µg DNA, and C) 500µg DNA treatment conditions (Magnification: 50x).

Microsphere treatment groups. At the 100µg DNA-MS condition, the gadolinium and glutaraldehyde treatment groups displayed increased cellular proliferation from hour 1 to hour 72. The chromium, iron, and DNA treatment groups illustrated a slight decrease in proliferation between hours 1 and 24; however, they displayed an increase in proliferation between hours 24 and 72. The iron crosslinked DNA-MS condition was the only condition to demonstrate proliferation values lower than the media with cells control treatment group, Figure 3-24.

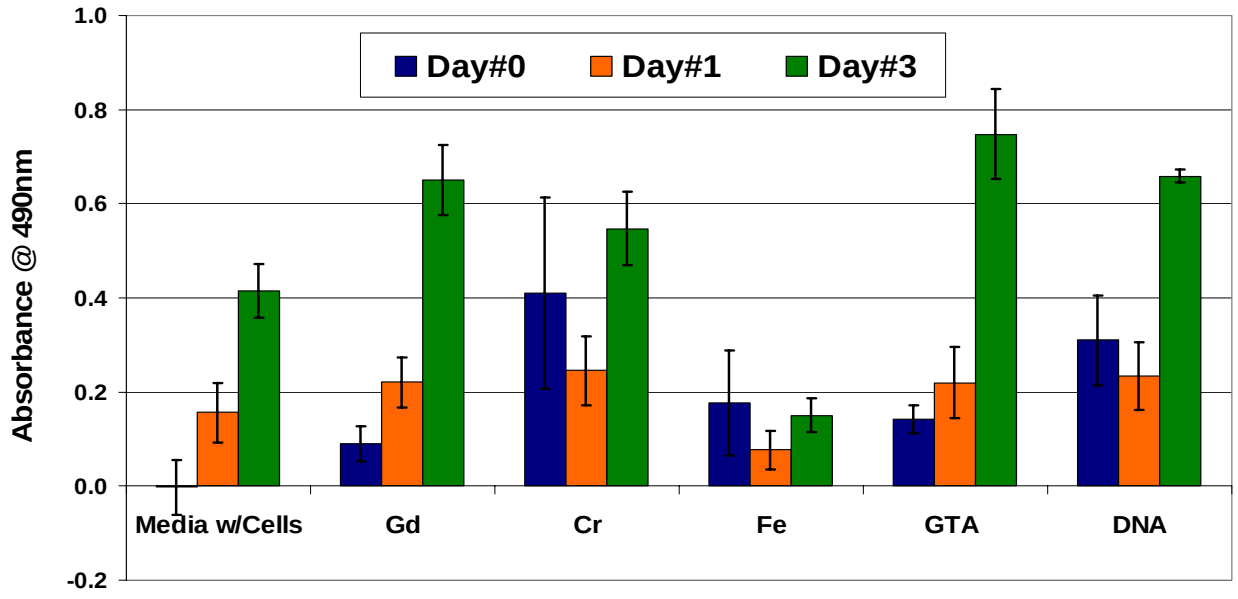

Figure 3-24. Fibroblast proliferation values for crosslinked DNA-MS and DNA treatment groups at the 100µg condition.

Statistical analysis of these values using a one way ANOVA followed by Tukey's test of all pairwise multiple comparisons illustrated that at 1) Day#0 (Hour 1), only the chromium and DNA conditions produced higher proliferation rates than the media with cells control treatment group ($p < 0.001$). On Day#1 (Hour 24), there were no significant differences among the DNA, crosslinked DNA-MS, and media with cells control treatment groups. By Day#3 (Hour 72), the gadolinium, glutaraldehyde, and DNA treatment group conditions all produced significantly higher proliferation rates than the media with cells control treatment group ($p < 0.001$). The chromium treatment group condition also produced significantly higher proliferation rates ($p = 0.016$) and the iron treatment group condition produced significantly lower proliferation rates ($p < 0.001$) than the media with cells control treatment group.

Further analysis using optical microscopy images displayed fibroblast cells at the gadolinium, chromium, and iron treatment group conditions that were very similar in morphology and confluency to the media with cells control treatment group condition, Figure 3-25. The gadolinium condition appeared to have the closest resemblance to the media with cells control group. The cell density for the chromium condition was similar to the cell density found in the control condition, however, the cells appeared to be more dehydrated or stretched than those seen in the control condition. The iron condition exhibited similar cell morphologies to the control group as well; however, in some wells, the cell density was slightly lower than the control. The glutaraldehyde condition exhibited similar cellular morphology as the control condition; however, a lower concentration of cells were present in the images which indicate that the fibroblast cells were less adherent under this condition and may have experienced a slight cytotoxic response to the glutaraldehyde in the crosslinked DNA-MS.

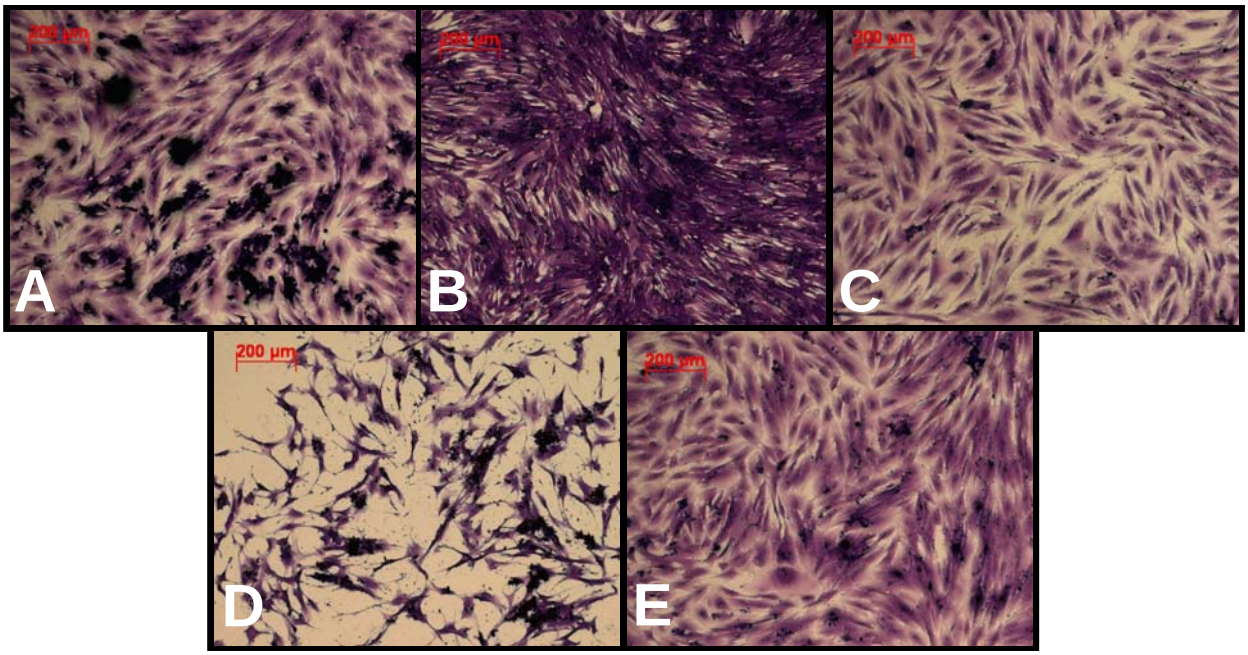

Figure 3-25. Optical microscopy images of crystal violet stained normal human dermal BJ fibroblast cells exposed to DNA-MS prepared with A) gadolinium, B) chromium, C) iron, and D) glutaraldehyde crosslinking agents at the 100µg condition and E) media with cells control group condition (Magnification: 50x).

At the 25µg DNA-MS conditions, each crosslink agent exhibited a slight decrease in cellular proliferation from hour 1 to hour 24, however, displayed an increase in proliferation from hour 24 to hour 72, Figure 3-26. Cellular proliferation profile for each DNA-MS crosslink agent treatment group also exhibited higher proliferation rates than the media with cells control treatment group. Statistical analysis using a one way ANOVA followed by Tukey's test for all pairwise multiple comparisons displayed that at Day#0 (Hour 1), the gadolinium($p < 0.001$), chromium ($p < 0.001$), and iron ($p = 0.002$) treatment groups produced significantly higher proliferation rates than the media with cells control treatment group. On Day#1 (Hour 24), statistical analysis found no significant differences between the DNA-MS treatment conditions and the media with cells control treatment group. By Day#3 (Hour 72), the gadolinium DNA-MS treatment group was the only condition to display higher proliferation rates than the media with cells control treatment group ($p < 0.001$).

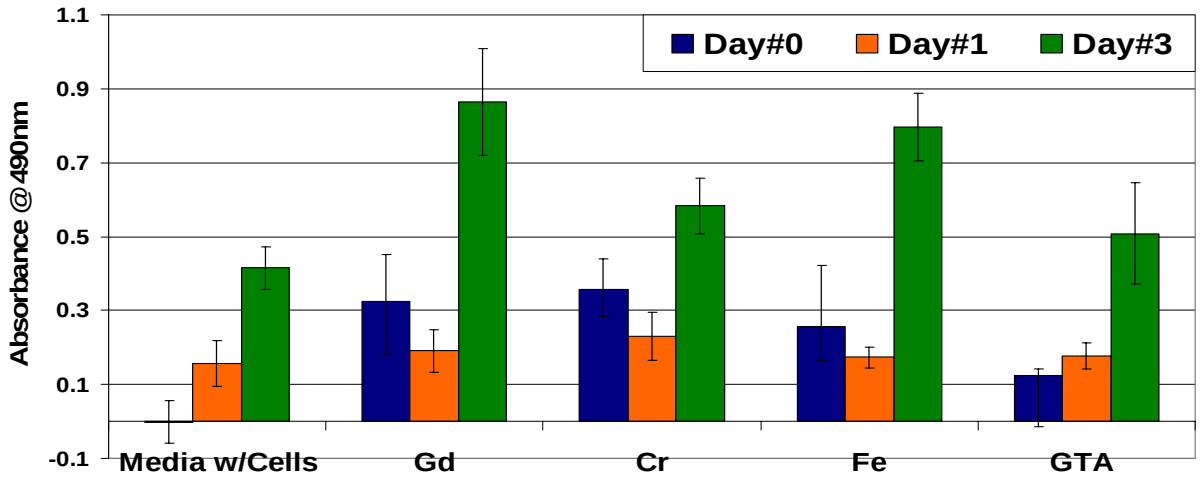

Figure 3-26. Fibroblast proliferation values for the crosslinked DNA-MS treatment groups at the 25µg condition.

Further analysis using optical microscopy images displayed fibroblast cells at the gadolinium, chromium, and glutaraldehyde treatment group conditions with similar cellular morphologies as the fibroblast cells present in the media with cells control treatment group, Figure 3-27. Analyses of the iron treatment groups produced images with no cells present indicating that the cells were washed off during fixation and/or staining suggesting that the fibroblast cells were less adherent under this condition.

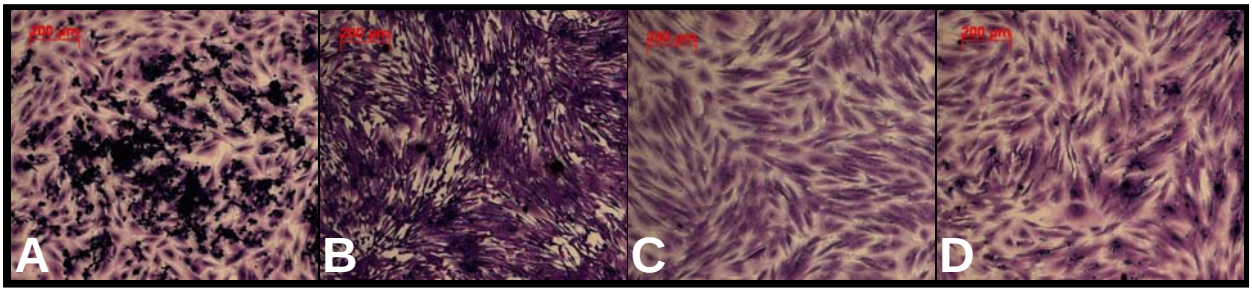

Figure 3-27. Optical microscopy images of crystal violet stained normal human dermal BJ fibroblast cells exposed to DNA-MS prepared with A) gadolinium, B) chromium, and C) glutaraldehyde crosslinking agents at the 25µg condition and D) media with cells control group condition (Magnification: 50x).

Discussion

Pilot Microsphere Synthesis Study

The pilot study that was conducted to determine if DNA-MS could be prepared through chromium trivalent cation crosslinking was successful. Chromium crosslinked DNA-MS were prepared with spherical morphologies with diameters that fell within the 1μm to 10μm diameter range, Figure 3-5. These results were expected since DNA behaves as a polyanion under aqueous conditions and therefore attracts multivalent cations, such as Cr^{3+}, under the same conditions.[92] Evidence of successful chromium bonding was visually confirmed by the blue coloration of the dried synthesized DNA-MS. It is believed that the trivalent chromium cations crosslinked the DNA via electrostatic binding with the phosphate groups on the DNA backbone. This mechanism has been cited as the principal mechanism for multivalent metal ion binding with DNA at neutral pHs.[92]

Stabilizing Agent Study

Chromium crosslinked DNA-MS produced favorable morphological and particle size results, however, upon washing and drying, the DNA-MS became aggregated and discrete particles were not produced. It was therefore believed that the steric repulsions created with the stabilizing agent used was not enough to disperse the DNA-MS during synthesis thus causing the formation of agglomerations due to crosslinking of adjacent particles. A stabilizing agent study was conducted to determine if higher stabilizing agent concentrations could better disperse the DNA-MS during synthesis and reduce particle aggregation.

Stabilizing agent concentrations of 3% (w/v), 5% (w/v), 10% (w/v), and 25% (w/v) were evaluated for this study. It was observed that the particle agglomeration increased as the stabilizing agent concentration increased with the exception of the DNA-MS prepared at the 5% (w/v) CAB condition. It was also interesting to note that the particle diameter size decreased as

the CAB concentration increased which is consistent with findings obtained with protein MS.[11] A resulting decrease in particle size is a result of the emulsifying stabilizing agent viscosity increasing as its concentration is increased.[10] In this case, increasing the concentration of cellulose acetate butyrate in the 1,2-dichloroethane increased the viscosity of the stabilizing agent thus decreasing the resultant size of the synthesized DNA-MS.

The onset of MS aggregation was first noticed during the acetone rinsing step in the synthesis procedure where larger degrees of aggregation were present as the CAB concentrations increased. A possible explanation for this may be attributed to the fact that the stabilizing agent was soluble in acetone. As the stabilizing agent concentration increased, the DNA-MS particle size decreased, and DNA-MS packing increased. This increased packing caused the DNA-MS to collapse on one another upon removal of the dispersing agent. Therefore, lower stabilizing agent concentrations allowed for lesser DNA-MS packing thus creating a more stable system for removal of the stabilizing agent. Based on these findings and the data obtained, it was determined the 5% (w/v) CAB was the most optimal stabilizing agent concentration for DNA-MS synthesis.

Crosslinking Reaction Study

The study to determine the time for covalent or ionic agents to crosslink DNA illustrated that the ionic crosslinking agents reacted quickest with the DNA followed by glutaraldehyde and genipin. The instantaneous reaction between the trivalent cations and the DNA was to be expected since it has been well documented in the literature that DNA is known to interact electrostatically with multivalent cations within the millisecond time range.[100] It took approximately two hours for the glutaraldehyde to crosslink the DNA, whereas it took the genipin over 72 hours to slightly crosslink the DNA molecules. Signs of the genipin interacting with the DNA molecules after 72 hours was consistent with similar studies found in the literature

which state that glutaraldehyde crosslinks significantly faster than genipin and that genipin undergoes changes in color from yellow, to brownish-red, to blue when interacting with amino groups.[96, 101] The slow interaction of these two covalent crosslinking agents may be explained by examining the theoretical crosslinking mechanism assumed to occur between DNA and glutaraldehyde or DNA and genipin. It was hypothesized that the glutaraldehyde and genipin would react with the amino groups in the base pairs of the DNA molecule as it has been presented in the literature and shown in Figure 3-3 for glutaraldehyde.[95, 96] Under static aqueous conditions and neutral pHs, these amino groups are unavailable for bonding because the base pairs within the DNA molecule are held together through hydrogen bonding between hydrogen groups and oxygen and nitrogen groups.[102] Therefore, the reactive sites on the glutaraldehyde and genipin molecules were unable to react with the amino groups found within the base pairs due to hydrogen bonding. However, it was expected for these covalent crosslinking agents to perform better during DNA-MS synthesis. During synthesis, the DNA molecules would be subjected to high shear rates which would in turn unzip the DNA double helix, exposing the amino groups within the base pairs to the covalent crosslinking agents.

The chromium and gadolinium crosslinking agents reacted instantaneously with the DNA and produced films that appeared homogenously crosslinked. The iron crosslinking agent reacted rapidly with the DNA; however, the reaction did not appear to be homogeneous and produced clumps of iron crosslinked DNA instead of a uniform film. Trivalent cations are known to crosslink or collapse DNA by interacting with either the phosphate backbone, the base pairs of the DNA molecule (more specifically the N7 nitrogen on the guanine and/or adenine nucleosides), or with both the phosphate and base pairs of DNA.[92, 103, 104] It has been cited that different trivalent cation complexes can have differing effects on the confirmation of the DNA

molecule upon interaction.[92] These various changes in confirmation of the DNA molecule can lead to its aggregation and collapse thus leading to the appearance of non-uniform crosslinking as observed with the iron crosslinking agent condition. Based on this ideology, it may be safe to assume that gadolinium and chromium cation complexes used for these studies interact more favorably with the DNA molecule used than the iron cation complex because the formation of aggregation was less evident with these two crosslinking agents.

General Microsphere Synthesis Studies

Particle analysis

Dry particle size. DNA-MS prepared with both covalent and ionic crosslinking agents produced particles with mean diameters less than 20μm. The gadolinium and genipin crosslink DNA-MS conditions produced the most discrete particles with the highest percentage of particles in the mesosphere size range and the lowest percentage of particles with diameters greater than 10μm. Gadolinium and genipin crosslinked DNA-MS conditions appear to have performed the best and displayed more controlled and narrower size distributions than the DNA-MS prepared with the chromium, iron, and glutaraldehyde conditions, Figures 3-7 and 3-8. The chromium, iron, and glutaraldehyde crosslinked DNA-MS became visibly aggregated upon washing and drying, however, it was unclear if these or other aggregates had formed during synthesis. Thus the mean particle dry diameters and size distributions reported for these conditions better reflect particle aggregation rather than the true diameter of the individual DNA-MS.

The formation of aggregates during synthesis with the chromium and iron crosslinking agents may have arisen due to the different interactions each cationic complex had with the DNA molecule.[92] Most trivalent cations are known to collapse or aggregate DNA into various condensed structures, such as spheres or toroids.[92] The type of structure that DNA will condense into is dependent on the classification of the interacting metal ion. Metal ions fall into two

different classifications: Class A or "hard" metal ions which prefer interactions with the oxygen donor atoms found on the phosphate groups of the DNA backbone, and the Class B or "soft" metal ions which prefer binding with the nitrogen donor atoms found within the base pairs of the DNA molecule.[92, 103, 105] Chromium and iron fall between classes A and B and are considered borderline ions with both hard and soft metal ion properties.[92] Metal ions with these characteristics can form bonds with both the phosphate oxygens and N7 nitrogen atoms found within the guanine and adenine base pair groups of DNA, Figure 3-28.

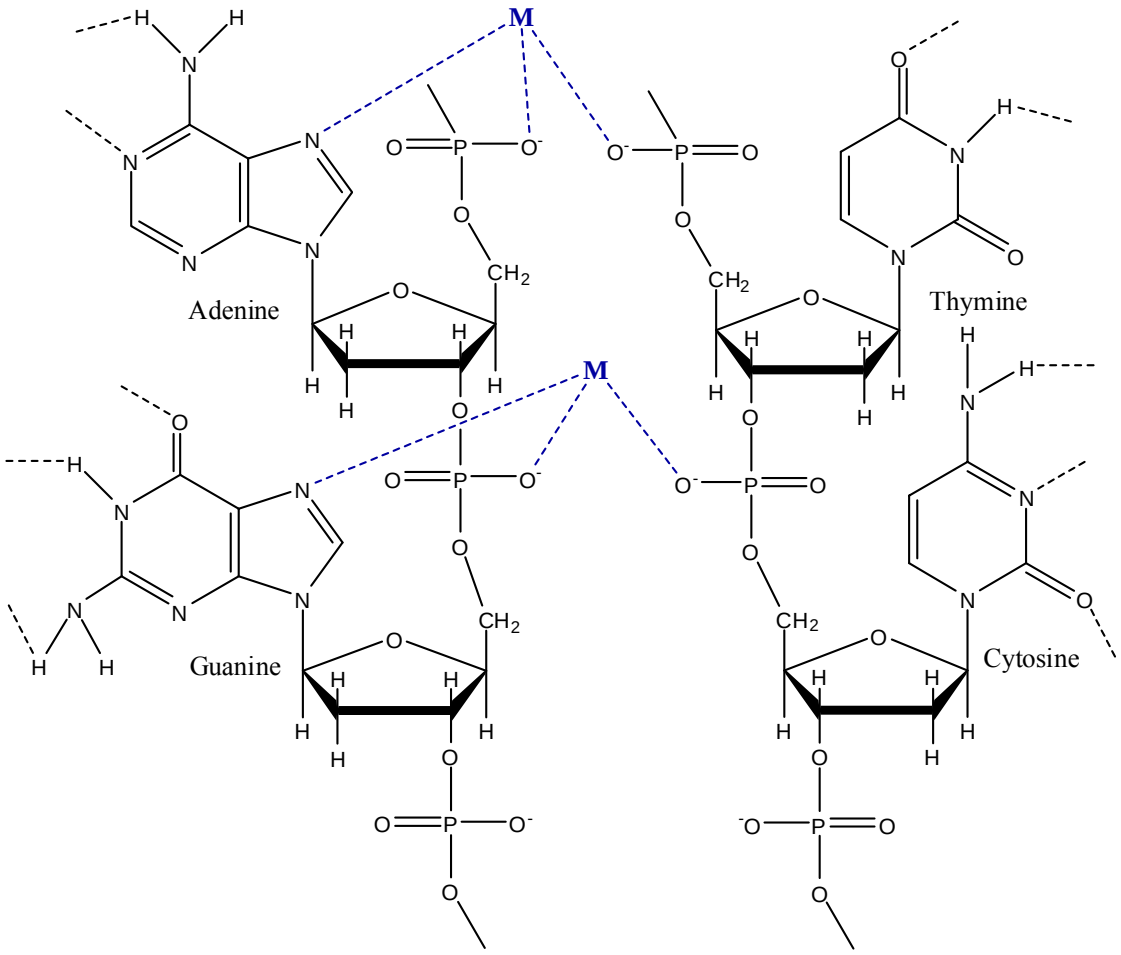

Figure 3-28. Schematic drawing of possible interactions between chromium and iron trivalent cations and phosphate oxygens and base pair guanine and adenine N7 nitrogen atoms. (Note: M = Cr^{3+} or Fe^{3+}.)

The ability of the metal ions to bind at both oxygen and nitrogen sites can cause a destabilizing effect on the DNA molecule and lead to more aggregated structures, such as toroids instead of spheres.[92] These aggregated structures arise more frequently when there is joint bonding between phosphate and base pair groups. The trivalent cationic nature of chromium and iron allow them to interact instantaneously with the phosphate oxygen and since the nitrogen atoms found within the base pairs interact the strongest and more frequently with d orbital transition metals such as chromium and iron, it allows them to interact with the base pairs as well.[105] The ability for chromium and iron to bind with both oxygen and nitrogen groups explains the broad particle diameter ranges and multimodal size distributions produced with these two crosslinking agents. Gadolinium on the other hand is a class A hard metal lanthanide cation which predominantly binds ionically to the oxygen atoms found on the phosphate groups of the DNA backbone and will never thermodynamically bind to the nitrogen atoms found within the DNA base pairs.[92, 103, 105] It has also been noted that even though lanthanides (i.e. gadolinium) are known to favorably bind with phosphate oxygen groups, they are also known to prevent complementary interactions between single DNA strands and in this case interactions between neighboring DNA-MS.[92] For this reason, gadolinium crosslinked DNA-MS produced discrete particles with more normalized particle size distributions.

The amount of aggregate formation seen for the chromium and iron crosslink agent conditions during the washing and drying steps of the DNA-MS synthesis procedure may be attributed to further ionic interactions between un-reacted cationic crosslinking agents and free phosphate group sites. The ionic radii of the trivalent cations used in this study led to either electrostatic interactions (as in the case of the chromium and iron crosslinking agents) or electrostatic repulsions (as in the case of the gadolinium crosslinking agent) during the washing

and drying steps of the DNA-MS synthesis process. Electrostatic interactions led to particle aggregation, whereas electrostatic repulsions led to particle discreteness. The extent of particle aggregation or discreteness may then be explained by the amount of electrostatic interaction or repulsion each cationic crosslinking agent presents which can be measured by their respective ionic radii. The ionic radius for the trivalent cations are 0.63 angstroms for chromium, 0.64 angstroms for iron, and 0.938 angstroms for gadolinium.[106] The ionic radii for the chromium and iron were similar in size and smaller than that of gadolinium. This may explain why the chromium and iron crosslinking agent conditions produced more aggregates than the gadolinium crosslink agent condition. Since the chromium and iron cations had smaller ionic radii, the smaller radii allowed the DNA-MS to be closer and interact more with one another. The size of the gadolinium trivalent cation may have been large enough to generate sufficient electrostatic repulsion among the DNA-MS to produce a discrete particle distribution.[90]

The broad size distributions and the slightly larger particle diameters obtained using the glutaraldehyde crosslinking agent may be attributed to the amount of time needed to obtain an interaction between glutaraldehyde and the amino groups in DNA. It has been cited in the literature that glutaraldehyde interacts more efficiently with DNA at higher temperatures because the hydrogen bonds holding the DNA tertiary structure together are broken.[96] The same case can be made for the ability of glutaraldehyde to interact with DNA when it is exposed to high shear rates during DNA-MS synthesis. The shear rates are large enough to disrupt hydrogen bonding between DNA base pairs thus exposing the amino groups for glutaraldehyde interaction. Since the interaction between glutaraldehyde and the amino groups within the base pairs is a lot slower than that seen between cationic crosslinking agents and the phosphate oxygen groups, it is to be expected to obtain particles that are larger and less homogeneous in size than those as seen with

the cationic crosslinking agents. The multimodal size distributions obtained with the glutaraldehyde suggest that it may be an unfavorable crosslinking agent for DNA-MS.

Hydrated particle size. The stability of dispersions can be best described using two major colloidal dispersion systems: 1) a lyocratic system which requires solvation at the surface for dispersion stability and 2) an electrocratic system which requires electrostatic repulsion between particles for dispersion stability.[90] During synthesis, a DNA-MS emulsion is created via a lyocratic system in which cellulose acetate butyrate dissolved in 1,2-dichloroethane completely wets each individual DNA-MS and sterically stabilizes it in that form. During hydrated particle size analysis, the system changes from a lyocratic system to an electrocratic system. The stability of the dispersion is then dependent on the electrostatic repulsion between the particles instead of the steric repulsions. In an electrocratic system, it is noted in the literature that the addition of a small amount of salt to the dispersion will cause the particles in the system to coagulate or aggregate if there is insufficient electrostatic repulsions between the particles.[90] DNA-MS prepared with glutaraldehyde produced the most multimodal hydrated particle size distributions indicating the there were insufficient electrostatic repulsions between the particles to prevent aggregate formation.

Surface charge and dispersability

The zeta potential is the measurement of the electric potential at the plane of shear of a particle and is used to determine the net interparticle forces in a dispersion.[90] The lifetime of a stable dispersion can therefore by estimated by measuring the zeta potential of the particles in dispersion. Particles with large zeta potential values have large magnitudes for interparticle repulsion and thus have longer and more stable dispersion lifetimes.[90] Dispersability experiments conducted in Grey's BSS indicated that the gadolinium crosslinked DNA-MS displayed the most stable dispersability with dispersion times exceeding 48 hours. The

chromium and glutaraldehyde crosslink agent conditions both displayed dispersion times of 12 hours or less. The dispersion stability of the gadolinium crosslinked DNA-MS may be attributed to its zeta potential values which were much larger than the those obtained for the chromium and glutaraldehyde crosslink agent conditions (-45.3mV for gadolinium as compared to -38.0mV for chromium and -29.6mV for glutaraldehyde). At these larger zeta potential values, the gadolinium crosslinked DNA-MS condition may have produced large enough interparticle repulsions to create a stable dispersion.[90, 107]

Microscopy

Optical and scanning electron microscopy. Images acquired using optical microscopy and SEM further confirmed crosslinking reaction observations and results obtained during dry particle size analysis. As seen in the Crosslinking Reaction Study, DNA-MS that were prepared with gadolinium produced small, discrete, spherical particles with smooth topographies suggesting homogeneous crosslinking of the gadolinium, Figures 3-14, 3-16, and 3-17. DNA-MS prepared with chromium produced particles that were mostly spherical, however, there were a few particles that were aggregated and irregularly shaped as similarly seen in the iron crosslink agent condition, Figures 3-15 and 3-17. The aggregations seen in the chromium and iron conditions may be attributed to the instantaneous collapse or condensing of the DNA molecule upon interaction with these different cationic complexes since it is well stated in the literature that most trivalent cationic complexes collapse DNA into condensed toroidal or non-spherical confirmations.[92] Agglomerations observed in the chromium and iron conditions may also be a result of multi-site crosslinking since the chromium and iron complexes are capable of binding or crosslinking with the nitrogen at the N-7 coordination site in the guanine nucleobase.[103, 105, 108, 109] The gadolinium chloride cationic complex, however, was only capable of binding with

phosphate oxygen groups found along the DNA backbone and thus generated spherical particles.[92, 103, 105]

Optical and scanning electron microscopy images also illustrated that glutaraldehyde crosslinked DNA-MS produced larger particle sizes than the ionically crosslinked conditions. The larger size of the glutaraldehyde DNA-MS may be attributed to the time required for glutaraldehyde to bond with the amino groups in DNA. Since literature and experiments conducted have shown that glutaraldehyde takes much longer to interact with DNA than the cationic crosslinking agents, it may be safe to assume that the glutaraldehyde is not interacting with the DNA base pairs until the latter part of the synthesis procedure which is conducted at 600rpm rather than 1250rpm. At these lower stir rates, the DNA particles are capable of existing at a larger size and thus are crosslinked at a larger size. When using cationic crosslinking agents, the interaction with DNA is instantaneous. This quicker interaction with DNA leads to smaller particle sizes since the cationic agents are able to crosslink the DNA-MS immediately after mixing at 1250rpm.

Energy dispersive x-ray spectroscopy. Elemental analysis via EDS utilizes inelastic electron scattering to cause inner shell excitations that result in emissions of characteristic x-rays of an element.[110] The energies obtained for each x-ray signal given is specific to each individual element.[110] EDS analysis of DNA-MS confirmed the presence of the cationic crosslinking agents strongly suggesting that the trivalent cations are indeed chemically bonding with the DNA molecule, Figures 3-19 to 3-21. The emitted x-ray energies obtained from the EDS spectra were compared against x-ray wavelength energies for each element examined. Energy values for characteristic x-rays were confirmed for each element analyzed and are summarized in Table A-1 in Appendix A.

Evaluation of fibroblast growth

Overview. The effects of DNA and crosslinked DNA-MS normal human dermal BJ fibroblast cell growth in culture was measured using a colorimetric MTS cell proliferation assay. In order for a cell to proliferate or reproduce, it must go through the life cycle of a cell.[38-42] The life cycle of a cell involves four phases including the Gap_1 or "G_1" phase, the DNA Synthesis or "S" phase, the Gap_2 or "G_2" phase, and the Mitosis or "M" phase, Figure 3-29.[41-43]

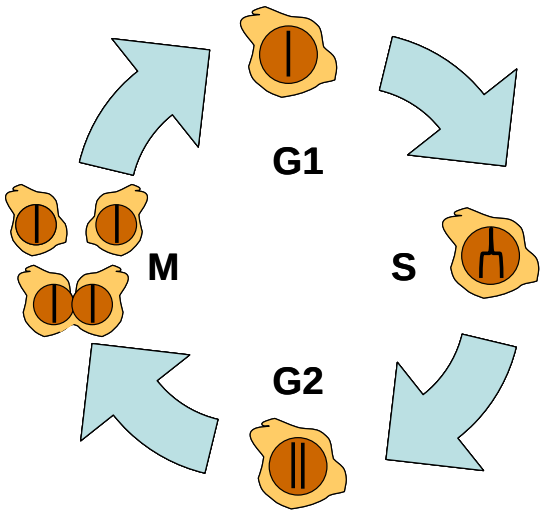

Figure 3-29. A drawing of the 4 phases of the cell life cycle.

The proliferation of a cell involves all four phases of the cell life cycle. The cell will grow while in the G_1 phase. Then during the S phase, the DNA from the parent cell is synthesized and duplicated and the cell moves on to the G_2 phase where the existing cell now carries two sets of DNA and matching chromosomes. Finally in the M phase, the duplicated chromosomes separate and the cell divides or reproduces to create two cells with matching DNA. [38-43]

A cell population will continue to undergo cellular proliferation through the cell cycle as long as their environment is untouched and has all the necessary nutrients for growth and reproduction. The addition of foreign agents or materials to the media sustaining a cell population can cause enough of an imbalance to alter the amount of time necessary to complete

the cell cycle. Altering the environment of a cell population can lead some cells to enter the Gap_0 or "G_0" phase as shown in Figure 3-30, where the cell enters a resting or quiescent state in which it ceases to proliferate, but retains its capacity to re-initiate its progress through the cell cycle at a later time.[41]

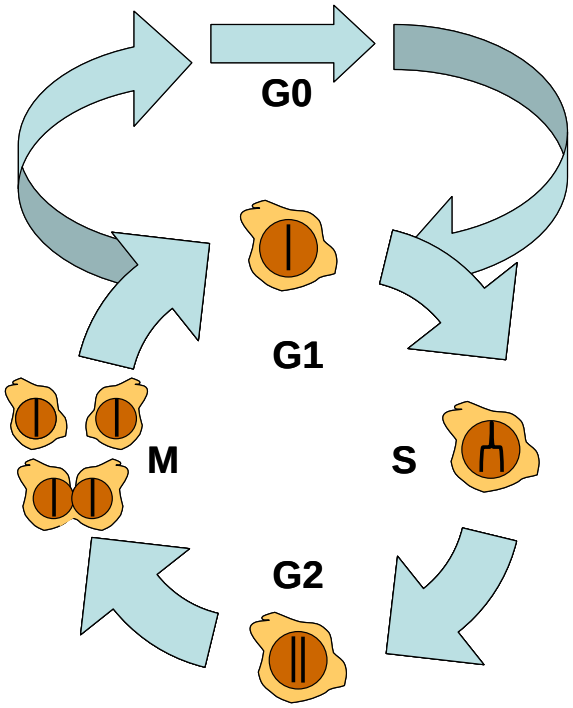

Figure 3-30. A drawing of the 4 phases of the cell life cycle, including the G_0 quiescence phase.

This phase is often seen in the culturing of fibroblast cells which can enter the G_0 phase upon alteration of their culture media.[39] The environmental alteration of a cell population can also cause a change in the G_1 phase duration leading to a longer or shorter cell cycle.[41] However, if the cell decides to not re-enter the cell cycle, the cells will round up and break their surface attachments within their culture environment and undergo apoptosis or cell death.[39] A cell responding to an environmental change in this fashion would indicate that the new environment has become cytotoxic.

DNA. Results obtained from the cell proliferation studies conducted on DNA displayed a slight decrease in proliferation between the first two time points, hour 1 and hour 24, Figure 3-22. The control group consisting of the cells with media alone did not display this same trend and instead exhibited a significant increase in proliferation between the first two and last two time points. The decrease in proliferation noted within the treatment groups may be attributed to the cells entering a short G_0 phase or a lengthened G_1 phase due to the temporary destabilization of their environment (i.e. addition of the DNA treatment). However, by the third time point, hour 72, proliferation had increased significantly and the treatment groups displayed no statistical differences in proliferation from the control group indicating that the DNA does not elicit an anti-proliferative response or a cytotoxic response *in vitro*. Optical images of each treatment group illustrated similar cellular densities and morphologies to the control group further confirming this conclusion.

Microsphere treatment groups. At the 100μg condition, the gadolinium and glutaraldehyde conditions continued to increase in proliferation through all three time points similar to the media with cells control group. On the other hand, the chromium and iron treatment conditions demonstrated similar trends as seen above for the DNA conditions in which proliferation decreased between the first two time points, hour 1 and hour 24, and then significantly increased between the last two time points, hour 24 and hour 72, Figure 3-24. As mentioned before, the observed decrease in fibroblast proliferation may be attributed to the disturbance of the culture media upon adding treatment leading to a change in the cell growth cycle.[38-41] The same trends were seen in the 25μg treatment groups for the gadolinium, chromium, and iron conditions.

The glutaraldehyde treatment group was the only condition to exhibit the trend of continued cellular proliferation through all three time points at both 25µg and 100µg conditions; however, upon further observation of the glutaraldehyde condition at the 100µg concentration, optical images displayed wells with lower cell densities than those seen in the media with cells control condition indicating that the fibroblasts cells were less adherent. These observations suggested that the glutaraldehyde elicited a cytotoxic response at the 100µg concentration and not at the 25µg concentration.[39] The cytotoxic response of the glutaraldehyde observed at the 100µg concentration was expected since glutaraldehyde has been shown to decrease normal human dermal fibroblast proliferation and elicit cytotoxic responses *in vitro* at concentrations as low as 1ppm.[95]

At both treatment concentrations, the iron condition produced significantly lower proliferation rates than the media with cells control group and all other conditions indicating that the iron concentration in the DNA-MS may be enough to elicit a an anti-proliferative response *in vitro*. Optical micrographs taken of the iron treatment conditions tend to support this conclusion illustrating that there was a slightly lower cell density at the 100µg condition than the media with cells control condition and that at the 25µg condition there were no cells present in the images indicating a lack of adherence of the cells to the 96-well plate. The lack of cellular adherence at the 25µg condition indicates that the iron concentration in the DNA-MS was enough to elicit a cytotoxic response.[39] A cytotoxic response *in vitro* was expected since it has been noted in the literature that iron (III) (Fe^{3+}) is known to be highly cytotoxic and cause massive cell death at concentrations greater than 10µM.[111] In *vivo*, Fe^{3+} would be expected to be even more cytotoxic since Fe^{3+} is known catalyze the Haber-Weiss reaction and create highly reactive and toxic hydroxyl radicals through Fenton Chemistry, Equations 3-3 and 3-4. [112, 113]

$$Fe^{3+} + O_2^{\bullet -} \rightarrow Fe^{2+} + O_2 \quad (3\text{-}3)$$

$$Fe^{2+} + H_2O_2 \rightarrow Fe^{3+} + OH^- + OH^{\bullet} \quad (3\text{-}4)$$

Reactive hydroxyl radicals are know to cause oxidative damage under physiological conditions and are the main cause of several neurodegenerative diseases such as Alzheimer's Disease and Parkinson's Disease.[112-115]

Overall the chromium and gadolinium conditions at both the 25µg and 100µg concentrations produced not only proliferation rates that either exceeded or were comparable to the media with cells control condition, but also comparable cell densities and morphologies to the control. The positive results obtained in this study were further supported by literature that indicates that certain complexes of chromium (III) are known to be non-cytotoxic and that many gadolinium (III) complexes are used at low concentrations with minimal cytotoxic responses *in vivo* for magnetic resonance imaging of tumor physiology of various cancers such as breast and prostate cancer.[116-119]

Conclusions

The objectives of these studies were to synthesize DNA-MS in good yield with covalent (i.e. glutaraldehyde or genipin) or ionic (i.e. chromium, gadolinium, or iron) crosslinking and to produce particles with a target dry mean diameter range of 50nm to 20µm, where at least 60% of all particles prepared were within the mesosphere size range of 1µm to 10µm and < 5% of all particles were greater than 10µm in size. Hydrated particle diameters were to be less than 25µm. In addition, DNA-MS were sought to obtain aqueous dispersion stability of over 24 hours and elicit minimal toxic effect on fibroblast cells in culture.

Pilot studies were conducted to determine the optimum processing conditions to achieve these goals. Pilot studies focused on determining an optimal stabilizing agent concentration for DNA-MS synthesis and on verifying the amount of time required to establish DNA crosslinking

with the covalent and ionic crosslink agents. General DNA-MS synthesis studies were then conducted and resulting particle diameters, size distributions, morphologies, topographies, and surface charges were evaluated and compared. In addition, normal human dermal BJ fibroblast cells were used in culture to evaluate the effect of DNA and crosslinked DNA-MS on cell growth at concentrations of 100μg and 500μg for DNA, and 25μg and 100μg for crosslinked DNA-MS. A colorimetric MTS assay was used to measure fibroblast growth at the 0, 24, and 72 hour time points.

Particle Analysis

DNA-MS were successfully synthesized with ionic and covalent crosslinking agents with mean dry diameters of less than 20μm. Pilot studies found that a concentration of 5% (w/v) CAB produced the most optimal conditions for DNA-MS synthesis. Crosslinking reactions studies found that ionic crosslinking agents displayed an instantaneous reaction with DNA, whereas it took glutaraldehyde 2 hours to react with DNA and genipin 72 hours. EDS analysis of DNA-MS confirmed the presence of the cationic crosslinking agents strongly suggesting that the trivalent cations are indeed chemically bonding with the DNA molecule.

The gadolinium crosslinked DNA-MS produced the smallest particles (2.6μm ± 2.8μm), with the most narrow size distributions and the largest percentage of particles that fell within the mesosphere size range (i.e. 1μm to 10μm) of all the crosslinking agents tested. The gadolinium crosslinked DNA-MS also produced excellent median hydrated particle size values of 12.1μm. The multimodal dry particle size distributions obtained with chromium, iron, and glutaraldehyde suggest that they may not be optimal crosslinking agents for DNA-MS; however, the glutaraldehyde condition did come close to matching the goals of the initial particle size objectives and future studies should focus on optimizing its processing conditions to obtain

DNA-MS with at least 60% of all particles with diameters in the mesosphere size range and less than 5% of all particles with diameters greater than 10μm.

The genipin crosslinked DNA-MS produced excellent dry particle sizes and distributions; however, they were unstable in PBS and immediately dissolved. Their instability in PBS was indicative of the inefficient crosslinking between genipin and DNA. The crosslink reaction time used to prepare genipin DNA-MS was insufficient and future studies will have to be conducted with longer reaction times to see if genipin can be used as a crosslinking agent for DNA-MS.

Dispersability experiments conducted in Grey's BSS indicated that the gadolinium crosslinked DNA-MS displayed the most stable dispersability with dispersion times exceeding 48 hours. The dispersion stability of the gadolinium crosslinked DNA-MS were attributed to their zeta potential values which were much larger than those obtained for the chromium and glutaraldehyde crosslinked DNA-MS.

In Vitro Human Dermal Fibroblast Growth

Human dermal fibroblast proliferation data and optical microscopy images obtained suggest that DNA derived from herring testes does not elicit an anti-proliferative response or a cytotoxic response *in vitro*. Iron crosslinked DNA-MS produced significantly lower proliferation rates than the media with cells control group indicating that the iron concentration in the DNA-MS may be enough to elicit an anti-proliferative response *in vitro*. The glutaraldehyde crosslinked DNA-MS also elicited a negative response at the 100μg concentration and not at the 25μg concentration. DNA-MS crosslinked with chromium and gadolinium produced the best *in vitro* results with proliferation rates that either exceeded or were comparable to the media with cells control condition at both the 25μg and 100μg concentrations. Since the chromium condition did not produce a toxic response on the fibroblast cells in culture, future studies should focus on optimizing the synthesis parameters for chromium crosslinked DNA-MS

in order to obtain at least 60% of all particles with diameters in the mesosphere size range and less than 5% of all particles with diameters greater than 10μm.

CHAPTER 4
OPTIMIZATION OF DNA NANO-MESOSPHERE SYNTHESIS

Introduction

This chapter presents studies conducted on the optimization of processing parameters for DNA nano-mesospheres (DNA-MS) synthesis. DNA-MS synthesis parameters were optimized to produce controlled size distributions where at least 60% of all particles prepared fell within the mesosphere size range of 1μm to 10μm and < 5% of all particles were greater than 10μm in size. Particles less than 1μm in diameter were also acceptable and DNA-MS were sought to obtain hydrated particle diameters of less than 25μm.

DNA-MS synthesis parameters were optimized with a filtration study to eliminate aggregates from the yield and narrow particle size distributions. A filtering step was added at the end of the synthesis process using a nylon filter with a pore size of 20μm. The resulting particle diameters and size distributions were then evaluated and compared to non-filtered controls.

DNA-MS processing parameters were further optimized by analyzing the effects of mixer speed and crosslink concentration on particle diameter, swelling, morphology, and size distribution. Mixer speeds of 950rpm, 1250rpm, and 1550rpm with ionic crosslink concentrations of 20%, 50%, and 120% molar equivalence (M_{EQ}) were assessed for these studies. The dry and swollen particle sizes of the DNA-MS were quantitatively characterized using an LS Coulter 13 320 particle size analyzer. The morphology and topography of the DNA-MS were analyzed using optical microscopy and scanning electron microscopy. The presence of trivalent cations was assessed using energy dispersive x-ray spectroscopy and crosslinking was confirmed through stability studies in 0.05M phosphate buffered saline at a pH of 7.4.

Materials and Methods

Materials

DNA sodium salt derived from herring testes Type XIV, cellulose acetate butyrate, HPLC grade 1,2-dichloroethane, methanol, chromium (III) potassium sulfate dodecahydrate, gadolinium (III) chloride hexahydrate, iron (III) nitrate nonahydrate, and 25% (w/w) Grade II aqueous glutaraldehyde solution were purchased from the Sigma-Aldrich Company. Sodium phosphate monobasic monohydrate, sodium phosphate dibasic anhydrous, and sodium chloride, each A.C.S. certified, were purchased from Fisher Scientific International. Acetone, 20μm and 70μm Spectra/Mesh Nylon filters, and 50mL and 15mL polypropylene centrifuge tubes were also obtained from Fisher Scientific International. Type I and Type II deionized ultrapure water were prepared with a resistivity of at least 16 $M\Omega\text{-}cm^{-1}$ using the Barnstead NANOpure Ultrapure Water System in the lab and is termed ultrapure water throughout.

Methods

Solution preparation

Deoxyribonucleic acid. Aqueous 5% (w/v) solutions of DNA were prepared at room temperature by adding 0.5g of DNA to 5mL of ultrapure water in a 50mL polypropylene centrifuge tube. The solution was mixed on a vortex for 30 seconds. Three milliliters of ultrapure water were then added to the DNA and placed on the rotary shaker for at least two hours until the DNA had completely dissolved. Once the DNA had fully dissolved, the volume was brought up to 10mL and vortexed for 30 seconds. The DNA solution was then placed in the refrigerator over night to ensure the complete collapse of bubbles generated during vortex and rotary mixing. The percent solid concentration of the DNA solution was quantified using a Metler LJ16 Moisture Analyzer at 130ºC for 60 minutes. The concentration of the DNA solution was then adjusted until the concentration was within 10% of the desired concentration. Once the

desired concentration was reached, the aqueous DNA solution was placed in the refrigerator until further use.

Cellulose acetate butyrate. Solutions of cellulose acetate butyrate in 1,2-dichloroethane (CAB) were used as the water-immiscible continuous phase for the emulsion stabilization process during DNA-MS synthesis. The CAB solutions were used at a concentration of 5% (w/v) and prepared by adding 25g of cellulose acetate butyrate to 500mL of 1,2-dichloroethane. The CAB solution was mixed at room temperature on a magnetic stir plate on high until the cellulose acetate butyrate had completely dissolved in the 1,2-dichloroethane. The resulting CAB solution was capped, parafilmed, and stored at room temperature.

Glutaraldehyde. Aqueous glutaraldehyde solutions were prepared to a concentration of 4% (w/v) by diluting the 25% (w/w) aqueous glutaraldehyde solution purchased from the Sigma-Aldrich Company. The aqueous glutaraldehyde solution was diluted by adding 21mL of ultrapure water to 4mL of the 25% (w/w) solution. The glutaraldehyde solutions were prepared in 30mL glass jars and mixed on a vortex at room temperature for 1 minute. After mixing, the aqueous glutaraldehyde solutions were parafilmed and stored in the refrigerator.

Chromium (III) and gadolinium (III). Aqueous solutions of chromium (III) potassium sulfate and gadolinium (III) chloride were prepared to a concentration of 0.1M by adding 24.97g of chromium (III) potassium sulfate dodecahydrate or 18.59g of gadolinium (III) chloride hexahydrate to 500mL of ultrapure water. The chromium (III) and gadolinium (III) solutions were mixed on a magnetic stir plate over night at room temperature until all the chromium or gadolinium had dissolved in the water. After complete mixing, the 0.1M ionic crosslinking agent solutions were parafilmed and stored at room temperature.

Phosphate buffered saline. Four liters of a 0.05M phosphate buffered saline (PBS) solution with a pH of 7.4 was prepared in the lab for measuring the swelling properties of the DNA- MS. The PBS solution was prepared by mixing 2.9L of a 0.05M sodium phosphate dibasic solution to 1L of a 0.05M sodium phosphate monobasic solution. The pH of the resulting solution was measured and the sodium phosphate monobasic solution was added until the target pH of 7.4 was reached.

A PBS solution with a concentration of 0.01M at a pH of 7.4 was used for zeta potential measurements and was prepared by diluting a 0.1M PBS solution and adjusting the pH back to 7.4. The 0.1M PBS solution was prepared by mixing 2.9L of a 0.1M sodium phosphate dibasic solution with 1L of a sodium phosphate monobasic solution. The two solutions were mixed and the pH of the resulting solution was brought to 7.4 by adding monobasic solution. The prepared PBS solutions were left out at room temperature until needed.

DNA nano-mesosphere synthesis

Filtration study procedure. DNA-MS were prepared using an emulsion stabilization technique that sterically stabilizes the DNA molecule into spherical conformations and crosslinks them while in suspension. This emulsion stabilization process involved dispersing 3mL of an aqueous DNA solution (i.e. the aqueous phase) into 47mL of a CAB solution (i.e. the continuous organic phase) in a 300mL Labconco lyophilization flask. A DNA microemulsion was then created by vigorously mixing the two solutions at 1250rpm for 20 minutes at room temperature using a paddle mixer with a two inch, two blade propeller. The DNA microemulsion was covalently or ionically crosslinked while in suspension by reducing the speed of the paddle mixer to 600rpm and adding 2mL of the crosslinking agent. The DNA microemulsion then underwent crosslinking for 1 hour and 40 minutes at which time 50mL of acetone was added and any further reactions were allowed to reach completion for another hour. After synthesis was

complete, the DNA-MS underwent four rinses in acetone to remove any residual organic phase or crosslinking agent. The DNA-MS were rinsed by separating the resultant DNA-MS suspension into four separate 50mL polypropylene centrifuge tubes. To these tubes, acetone was added up to 40mL and the tubes were capped and vortexed on high for 30 seconds. The DNA-MS were then collected by centrifuging the tubes at 2600rpm for 10 minutes. After centrifugation, the acetone was decanted and fresh acetone was added again up to 40mL. The acetone rinse was repeated once more as mentioned above and then twice more by consolidating the contents of 4 tubes to 2 tubes and then 2 tubes to one tube. After the final acetone rinse, the DNA-MS were resuspended in 30mL of acetone and vortexed on high for 30 seconds. The resuspended DNA-MS were then filtered using a stainless steel vacuum filtration device with a 20μm Spectra/Mesh Nylon filter. The device was then rinsed with 10mL of acetone to further filter any remaining DNA-MS under 20μm. After the final filter rinse, the centrifuge tube was capped, vortexed on high for 30 seconds, and centrifuged at 2600rpm for 5 minutes to collect the microspheres. The acetone was then decanted and a Kimwipe was secured over the mouth of tube using a rubber band in order to allow the DNA-MS to dry overnight at room temperature.

Mixer speed and crosslink concentration study procedure. DNA-MS were prepared using the same emulsion stabilization technique described above for the Filtration Study, however, mixer speeds and crosslink agent concentrations were varied in order to determine the effects of these factors on the diameters of the resulting DNA-MS and their respective size distributions. This emulsion stabilization process involved dispersing 3mL of the aqueous DNA solution (i.e. the aqueous phase) into 47mL of the CAB solution (i.e. the continuous organic phase) in a 300mL Labconco lyophilization flask. A DNA microemulsion was then created by vigorously mixing the two solutions at 950rpm, 1250rpm, or 1550rpm for 20 minutes at room

temperature, using a paddle mixer with a two inch, two blade propeller. The DNA microemulsion was then ionically crosslinked with trivalent gadolinium cations while in suspension by reducing the speed of the paddle mixer to 600rpm and adding 0.3314mL, 0.8285mL, or 2mL of the 0.1M aqueous gadolinium solution to obtain the 20%M_{EQ}, 50%M_{EQ}, or 120%M_{EQ} crosslink concentration conditions. The DNA microemulsion then underwent crosslinking for 1 hour and 40 minutes at which time 50mL of acetone was added and any further reactions were allowed to reach completion for another hour. After synthesis was complete, the DNA-MS underwent four rinses in acetone to remove any residual organic phase or crosslinking agent. The DNA-MS were rinsed using the same washing procedure as mentioned above for the Filtration Study, however, a 70μm Spectra/Mesh Nylon filter was used in place of the 20μm filter in order to not completely eliminate the possible size effects of the varying mixer speeds and gadolinium crosslink concentrations. The 70μm filter was also used to minimize the number of aggregates in the resulting yield.

Mesosphere characterization

Yield analysis. The yield of each condition synthesized was calculated and expressed as a percent yield value. The percent yield was calculated by dividing the final weight of the DNA-MS by the amount of weight used to synthesize the DNA-MS. The equation for the percent yield is expressed in Equation 4-1 where W_F is the final weight of the DNA-MS, V_{DNA}, ρ_{DNA}, and C_{DNA} are the volume, density, and concentration of the aqueous DNA solution used respectively, and W_X is the weight of the crosslinking agent added during synthesis.

$$\%\ \text{Yield} = \left(\frac{W_F}{((V_{DNA} \times C_{DNA} \times \rho_{DNA}) + W_X)}\right) \times 100 \qquad (4\text{-}1)$$

Dry particle size analysis. The particle size distributions and diameters of the DNA-MS were obtained under dry conditions using a Coulter LS 13 320 particle size analyzer. DNA-MS

were sonicated for 10 to 30 seconds prior to analysis to aerate the particles and then approximately 2mg of the DNA-MS were suspended in 2mL of methanol. The suspension was then sonicated for 30 seconds to break up any aggregates and tested. The Coulter LS 13 320 particle size analyzer was set to run at a pump speed of 73% using a protein/DNA particle diffraction model. Standards were tested in methanol before the first run to ensure that the instrument was performing adequately. Each condition was tested three times in which each test consisted of two runs. This method of testing produced six independent and size distributions. Data collected from these experiments were statistically analyzed using SigmaStat 3.0 software.

Hydrated particle size analysis. The mean swollen diameters and particle size distributions of the DNA-MS were obtained using a Coulter LS 13 320 particle size analyzer. Approximately 2mg of the DNA-MS were suspended in 2mL of 0.05M PBS with a pH of 7.4. The suspension was then sonicated for 30 seconds to break up any DNA-MS aggregates. The DNA-MS were then allowed to swell in the PBS for an additional two minutes and thirty seconds. After swelling, the DNA-MS were tested in the Coulter LS 13 320 particle size analyzer using a pump speed of 73% and a protein/DNA particle diffraction model. Standards were tested in PBS before the first run of the first batch to ensure that the instrument was performing adequately. Each condition was tested three times in which each test consisted of two runs. This method of testing produced six independent particle diameters and size distributions.

After obtaining the mean particle swollen diameters, the data was used to calculate the percent change in size using Equation 4-2, where D_D is the dry diameter and D_H is the swollen or hydrated diameter. A negative percent change in size depicted a decrease in particle size (i.e. degradation) whereas a positive percent change in size depicted an increase in particle size (i.e.

swelling). Data collected from these experiments were statistically analyzed using SigmaStat 3.0 software.

$$\%\ \text{Change in Size} = \left(\frac{D_H - D_D}{D_D}\right) \times 100 \qquad (4\text{-}2)$$

Surface charge analysis. The surface charge of DNA-MS prepared in the Mixer Speed and Crosslink Concentration Study was measured to determine the effects of crosslink concentration on surface charge. The surface charge of the DNA- MS was obtained using a Brookhaven ZetaPlus zeta potential analyzer with ZetaPALS software. Approximately 2mg of the DNA-MS were suspended in 1.5mL of 0.01M PBS solution with a pH of 7.4. Each condition was sampled three times in which each sample underwent ten runs. This method of testing produced thirty independent zeta potential values. The data collected from the zeta potential analyzer was statistically analyzed using SigmaStat 3.0 software.

Scanning electron microscopy. The morphology and surface topography of the DNA-MS were observed using scanning electron microscopy (SEM). Approximately 1mg of dry DNA-MS were mounted onto a small piece of silicon wafer which in turn was mounted onto an aluminum SEM stub using double sided tape. The DNA-MS were then coated with gold-palladium for 2 minutes using a Technix Hummer V sputter coater. Images were taken either on a JEOL 6400 SEM using an accelerating voltage of 5KeV, condenser lens setting of 10, objective lens setting of 117, and a working distance of 15mm, or on a JEOL 6335F Field Emission SEM at an accelerating voltage of 5KeV and a working distance of 15mm.

Energy dispersive x-ray spectroscopy. The presence of trivalent cations in the DNA-MS after washing and drying was observed using energy dispersive x-ray spectroscopy (EDS). DNA-MS were mounted onto a piece of silicon wafer. The silicon wafer was then secured to an aluminum SEM stub using carbon double sided tape. The DNA-MS were then coated with

carbon for 2 minutes using a Technix Hummer V sputter coater. EDS spectra on the DNA-MS were collected using a JEOL 6400 SEM at an accelerating voltage of 15KeV and working distance of 15mm. A dead time of 20% to 40% was allowed for each condition tested.

Results & Discussion

Filtration Study

Synopsis

A filtration study was conducted to optimize DNA-MS synthesis parameters, eliminate aggregates from the yield, and narrow particle size distributions. A filtering step was added at the end of the synthesis process using a nylon filter with a pore size of 20μm. Since a particle size of less than 25μm is desired for optimal intratumoral delivery, a Spectra/Mesh Nylon filter with a 20μm pore size was used for this study.[69, 120]

Particle analysis

Percent yield. The filtration step used in this study successfully tailored the particle size of the DNA-MS that were prepared with both covalent and ionic crosslinking agents by reducing the yields in most cases over 50%. The gadolinium crosslinked DNA-MS produced the best particle yields after filtration with a yield of 67%. However, the chromium and glutaraldehyde crosslinking agent conditions continued to produce aggregates upon washing and drying and their yields were reduced after filtration to 24% from 77% for chromium and to 23% from 61% for glutaraldehyde. The percent yield values as calculated by Equation 4-1 for each condition with their respective decreases due to filtration are tabulated in Table 4-1.

Table 4-1. The yields and percent decrease in yield values for DNA-MS synthesized with ionic and covalent crosslinking agents.

Crosslinking agent	Percent yield after filtration (%)	Percent yield before filtration (%)	Percent decrease in yield due to filtration (%)
Chromium	24	77	69
Gadolinium	67	82	18
Glutaraldehyde	23	61	62

Dry particle size analysis. The dry particle sizes of the DNA-MS were obtained in methanol. Filtered DNA-MS prepared with both ionic and covalent crosslinking agents produced particles with mean diameters less than 10μm in size consistent with observations presented in Chapter 3. The filtered gadolinium and glutaraldehyde crosslinked DNA-MS conditions performed similarly to their non-filtered counter parts, producing dry mean particle diameters of 3.3μm ± 2.8μm and 5.5μm ± 6.5μm, respectively with the same percentage of particles falling within the mesosphere size range (i.e. 1μm to 10μm) and particles greater than 10μm. The gadolinium condition still produced the most controlled size distributions of the three. The chromium crosslink condition displayed the most significant deviance from its non-filtered counter part with a mean particle diameter of 4.2μm ± 6.2μm from 10.3μm ± 13.9μm and an increase in particles within the mesosphere size range from 32% to 55%. However, the chromium condition still produced the largest particle diameters of the three conditions tested.

A one way analysis of variance (ANOVA) test was conducted on all collected data to quantify the differences between filtered and non-filtered particle size values and illustrated that all differences between filtered and non-filtered mean dry particle diameters were not significant. The test also illustrated no significant particle size differences among the crosslink agent conditions used. Table 4-2 lists each condition with their respective non-filtered and filtered dry mean particle diameter values and their particle diameter size ranges.

Table 4-2. The dry mean particle diameter values for the 20μm-filtered and the non-filtered DNA-MS synthesized with ionic and covalent crosslinking agents.

Crosslinking agent	Non-filtered mean dry particle diameter (μm)	20μm-filtered mean dry particle diameter (μm)	DNA-MS in 1μm to 10μm size range (%)	DNA-MS larger than 10μm (%)
Chromium	10.3 ± 13.9	4.2 ± 6.0	55	16
Gadolinium	2.6 ± 2.8	3.3 ± 2.8	81	2
Glutaraldehyde	6.4 ± 9.7	5.5 ± 6.5	64	16

The addition of the filtration step not only decreased the resultant mean particle diameter values for the chromium crosslink agent condition tested, but it also normalized and narrowed the particle size distributions by reducing the amount of aggregates in the yield, Figure 4-1. The filtered gadolinium crosslinked DNA-MS condition displayed a normal and narrow particle size distribution as well, Figure 4-2, which was very similar to its non-filtered distribution seen in Chapter 3. However, the filtered glutaraldehyde crosslinked DNA-MS condition still displayed evidence of aggregate formation within the 50µm to 70µm range even though it too demonstrated a more normalized distribution, Figure 4-3.

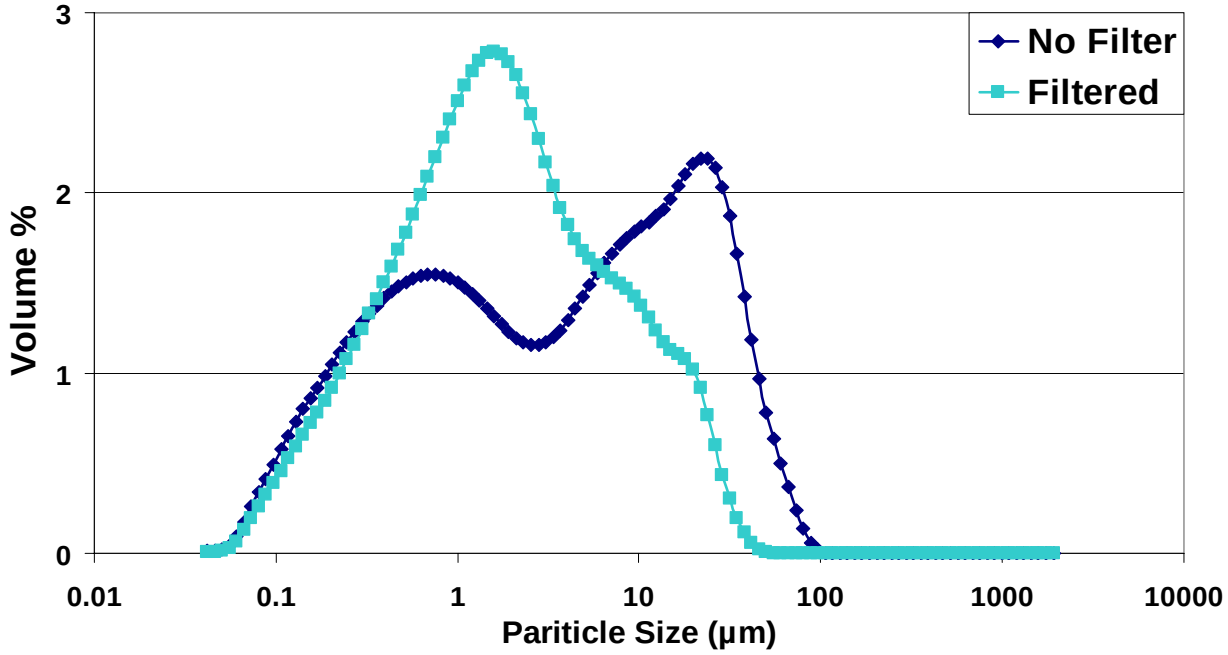

Figure 4-1. A particle size distribution comparison of non-filtered and 20µm-filtered chromium crosslinked DNA-MS under dry conditions.

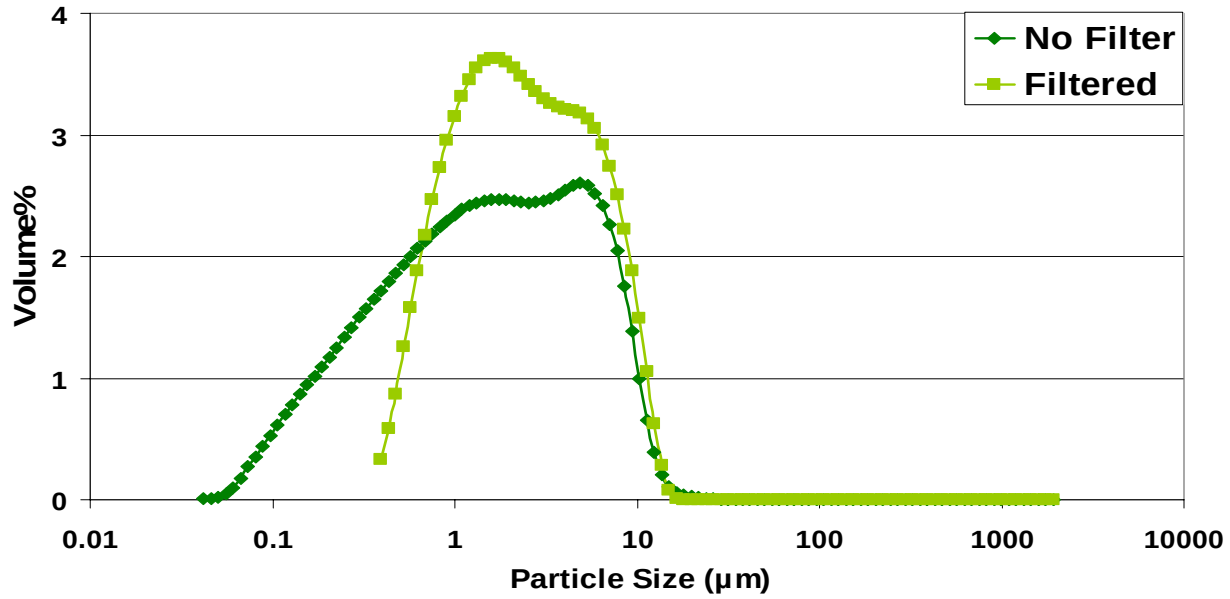

Figure 4-2. A particle size distribution comparison of non-filtered and 20µm-filtered gadolinium crosslinked DNA-MS under dry conditions.

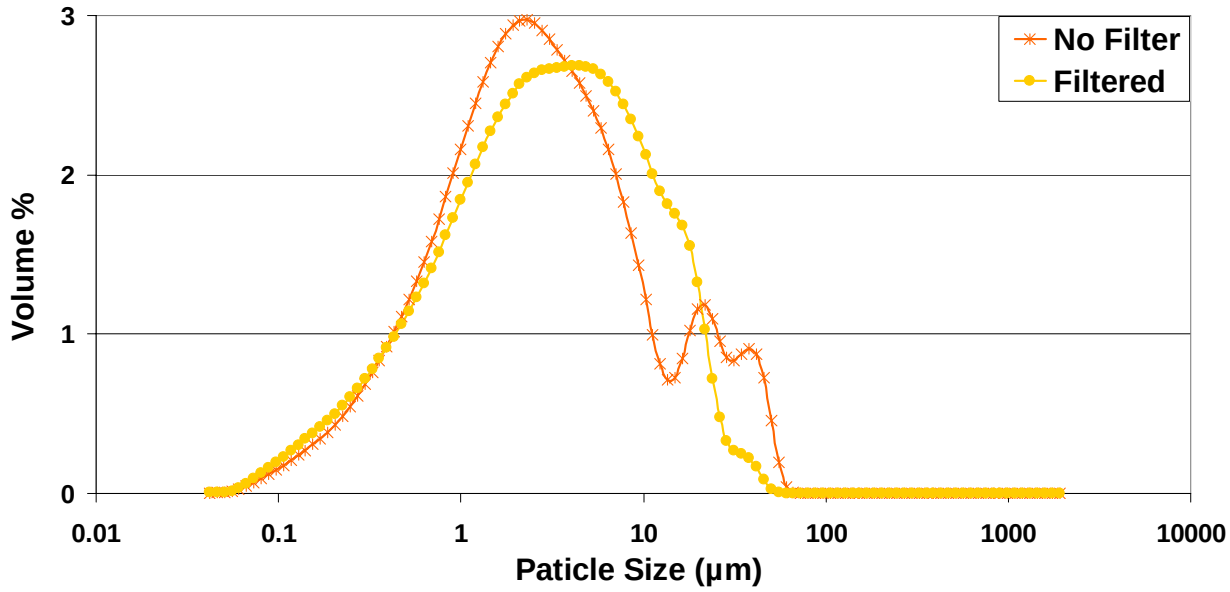

Figure 4-3. A particle size distribution comparison of non-filtered and 20µm-filtered glutaraldehyde crosslinked DNA-MS under dry conditions.

Overall, the filtration step appeared to have had two benefits: 1.) the 20µm filter helped to remove particles and aggregates over 20µm in diameter and 2.) the 20µm filter helped to separate or disperse the DNA-MS in a process somewhat similar to sifting. The filtration step

mechanically facilitated the break up of DNA-MS aggregates within the yield and thus subsequent particle diameters appeared reduced because the true diameters of the DNA-MS were measured and reported instead of the diameters of the aggregates. Reported sizes for the DNA-MS decreased by 59% for the chromium and 14% for the glutaraldehyde conditions, and increased by 27% for the gadolinium condition, Table 4-3.

Table 4-3. The dry mean particle diameter values for the 20μm-filtered and the non-filtered DNA-MS synthesized with ionic and covalent crosslinking agents.

Crosslinking agent	Non-filtered mean dry particle diameter (μm)	20μm-filtered mean dry particle diameter (μm)	Percent change in size (%)
Chromium	10.3 ± 13.9	4.2 ± 6.0	(-) 59
Gadolinium	2.6 ± 2.8	3.3 ± 2.8	(+) 26
Glutaraldehyde	6.4 ± 9.7	5.5 ± 6.5	(-) 14

The normalization effect illustrated in the particle size distributions for the DNA-MS may have not only been attributed to the filtration step added in the synthesis procedure, but also to the sonication step added prior to particle size analysis. This additional sonication step may have further broken up aggregates and aerated the DNA-MS prior to analysis by rupturing intermolecular bonds between the particles that formed during synthesis or drying.

When particle powders are synthesized or prepared, cohesive forces tend to join the particles together through an adhesive bridge.[121] This adhesive bridging leads to particle agglomerations which occur more frequently in powders with higher volume fractions of small particles as those seen when preparing DNA-MS.[122, 123] There are five mechanisms which can bring about interparticle bonding which include solid bridges which arise from the melting of the particles or from the diffusion of molecules between particles, liquid bridges which arise from surface tension or capillary pressure, van der Waals forces which result from dipole interactions on the molecular level over short distances, electrostatic forces which are longer ranging and

result from the surface charge of a particle, and interlocking bonds which arise from mechanical interlocking between particles due to surface irregularities and protrusions, Figure 4-4.[122]

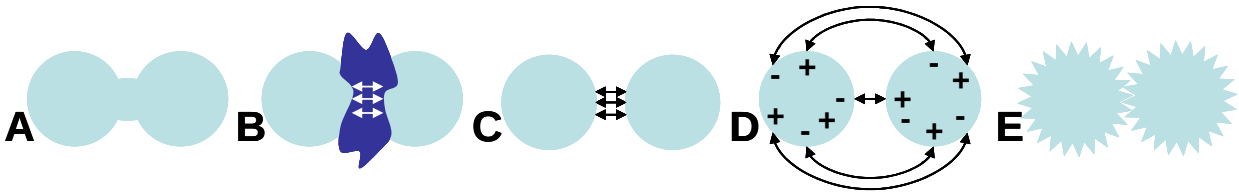

Figure 4-4. An illustrative depiction of the five mechanisms responsible for interparticle bonding: A.) solid bridges, B.) liquid bridges, C.) van der Waals forces, D.) electrostatic forces, and E.) interlocking bonds.[122]

The aggregates seen in the particle size distributions presented in this section may have been attributed to electrostatic forces between particles since this type of interaction plays a significant role for interparticle bonding in particles ≤ 10μm in diameter.[124, 125] The production of aggregates may have also been attributed to liquid bridging interactions between the particles which arise during DNA-MS drying or van der Waals attractions which arise once the particles are placed in the methanol and sonicated. However, the van der Waals interactions were probably the least contributive of the three mentioned.

The normalization of the particle size distributions presented in this study may have been produced during sonication both before and after the DNA-MS were added to the methanol analysis. The normalization effect may have arisen by the temporary disruption of the electrostatic forces between DNA-MS, which created a more disperse system than those that were obtained in Chapter 3.[125-127] It is also believed that the van der Waals and electrostatic interparticle interactions were further disrupted with the use of the filtration step immediately after synthesis which caused a sifting or dispersion effect on the particles.

Hydrated particle size analysis. The particle size of the DNA-MS synthesized with covalent or ionic crosslinking agents was also tested under hydrated conditions in 0.05M PBS at

a pH of 7.4. Each crosslink agent condition produced hydrated mean diameters of less than 25µm. The ionically crosslinked DNA-MS displayed similar normalization trends under hydrated conditions as compared to their dry distributions and swelled to approximately 200% of their original size as shown in Figures 4-5 to 4-7. The normalization trend seen in the ionically crosslinked DNA-MS suggests that the DNA-MS were disperse and dominated by electrostatic repulsions between the particles.[90, 107, 122, 124] The glutaraldehyde crosslinked DNA-MS condition did not follow the same normalization trend and continued to display multimodal particle size distributions indicating that this condition was dominated by particle aggregation. Glutaraldehyde crosslinked DNA-MS aggregated because the particles were more influenced by the attractive van der Waals interparticle forces within the PBS more so than the ionically crosslinked DNA-MS, Figure 4-8. [90, 107, 125, 128, 129] Aside from the aggregation present, the glutaraldehyde condition also performed well exhibiting a 14.4µm mean hydrated particle diameter and only a 150% increase in size.

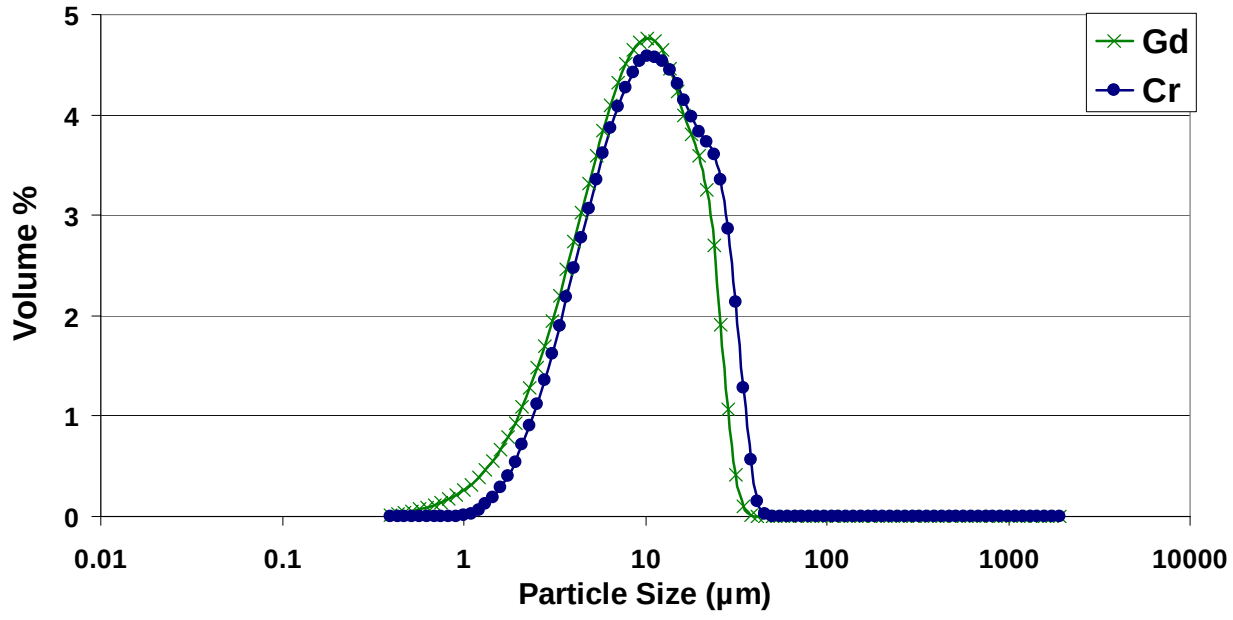

Figure 4-5. Hydrated particle size distribution comparisons of the 20µm-filtered ionically crosslinked DNA-MS.

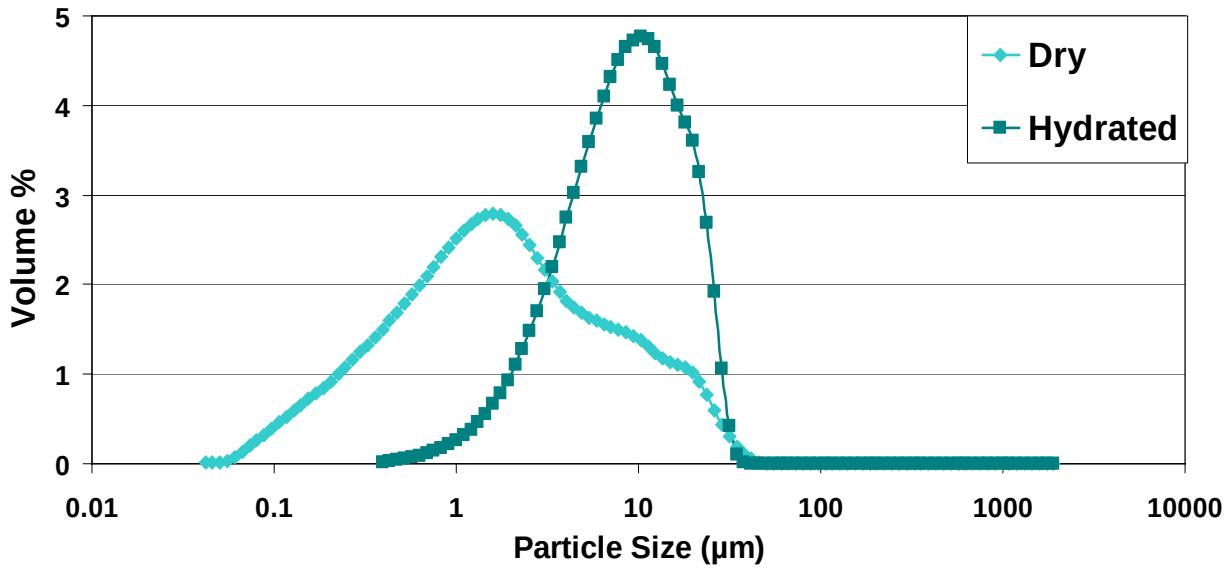

Figure 4-6. A particle size distribution comparison of the 20µm-filtered, chromium crosslinked DNA-MS under dry and hydrated conditions.

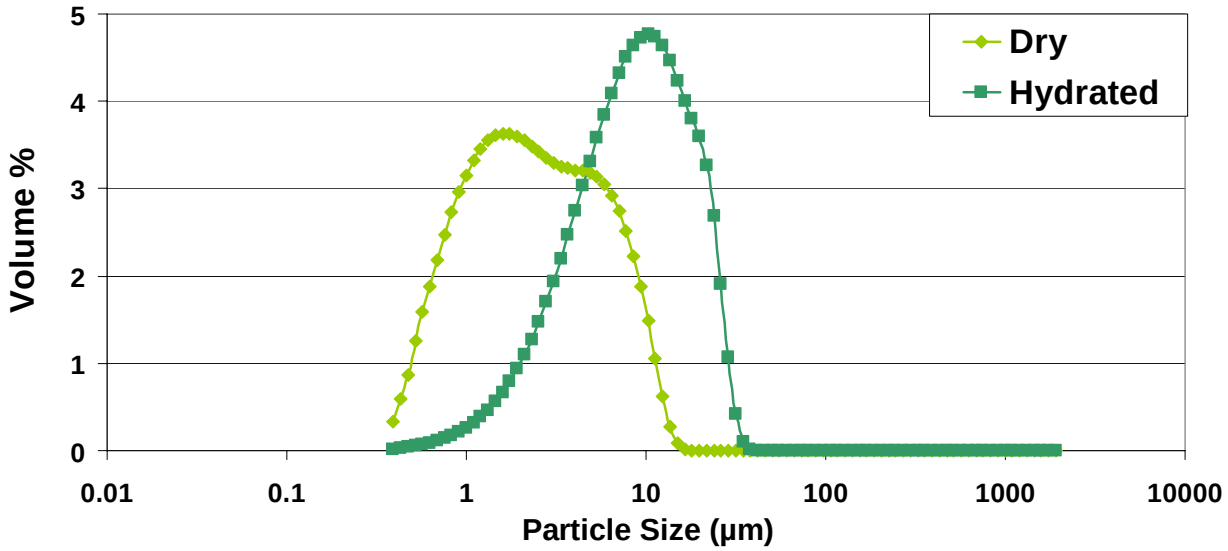

Figure 4-7. A particle size distribution comparison of 20µm-filtered, gadolinium crosslinked DNA-MS under dry and hydrated conditions.

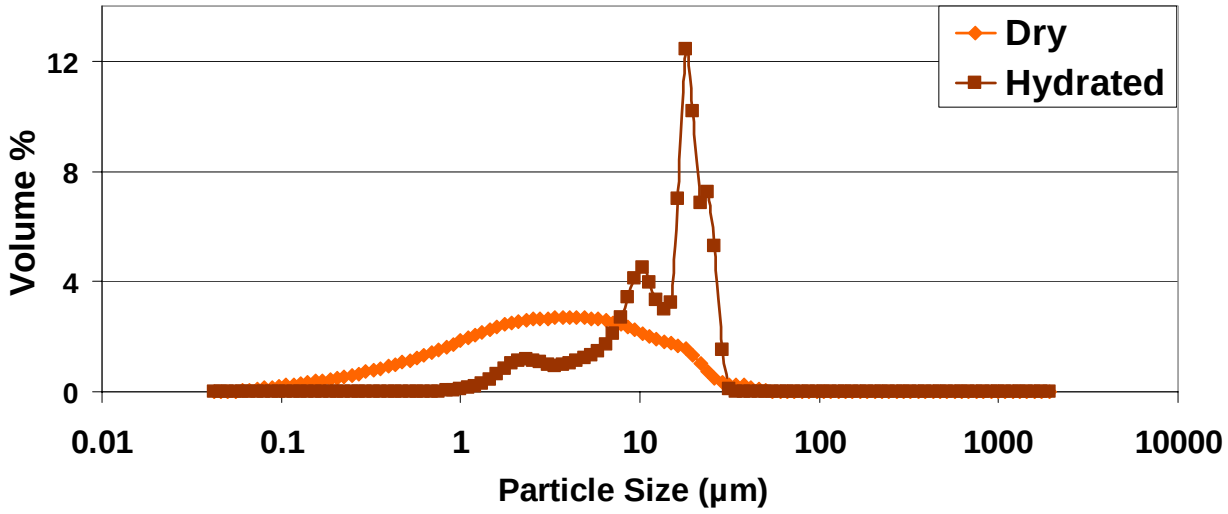

Figure 4-8. A particle size distribution comparison of 20µm-filtered, glutaraldehyde crosslinked DNA-MS under dry and hydrated conditions.

Statistical analysis was conducted on all data collected to quantify the effects of the filtered DNA-MS on hydrated particle size values. A t test was conducted on all hydrated data illustrated no significant differences between the filtered and non-filtered hydrated mean particle size values. However, particle size distributions illustrate that the filtration step normalized and even reduced the amount of aggregate formation during hydration shifting the mean particle size peaks over to smaller values, Figures 4-9 to 4-11. Each crosslink agent condition with its respective hydrated mean diameter and percent change in size as calculated by Equation 4-2 is given in Table 4-4.

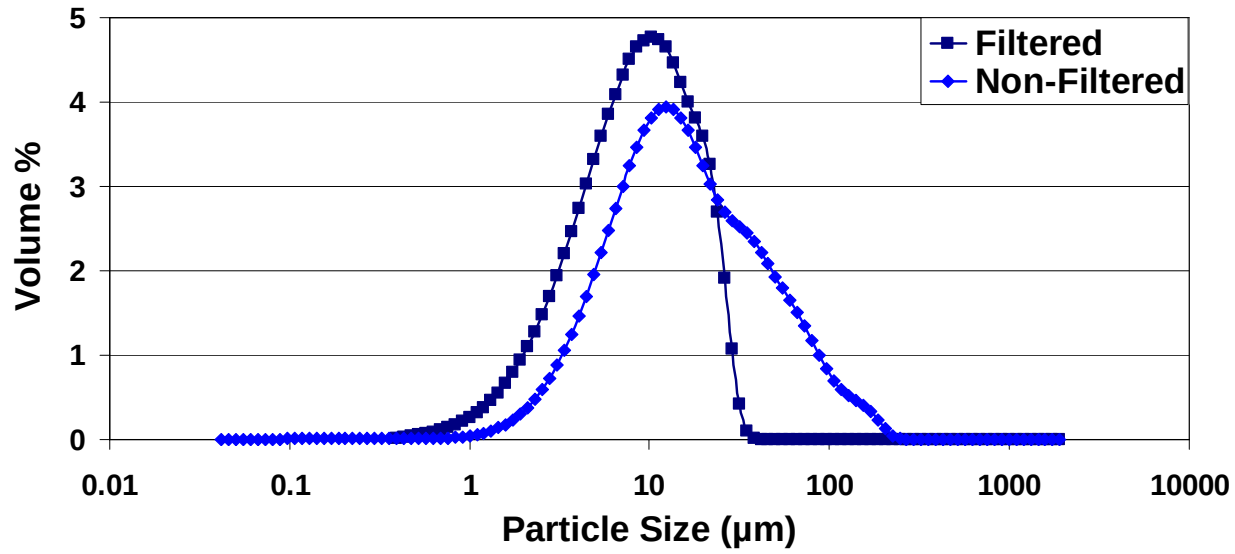

Figure 4-9. A particle size distribution comparison of 20µm-filtered and non-filtered chromium crosslinked DNA-MS under hydrated conditions.

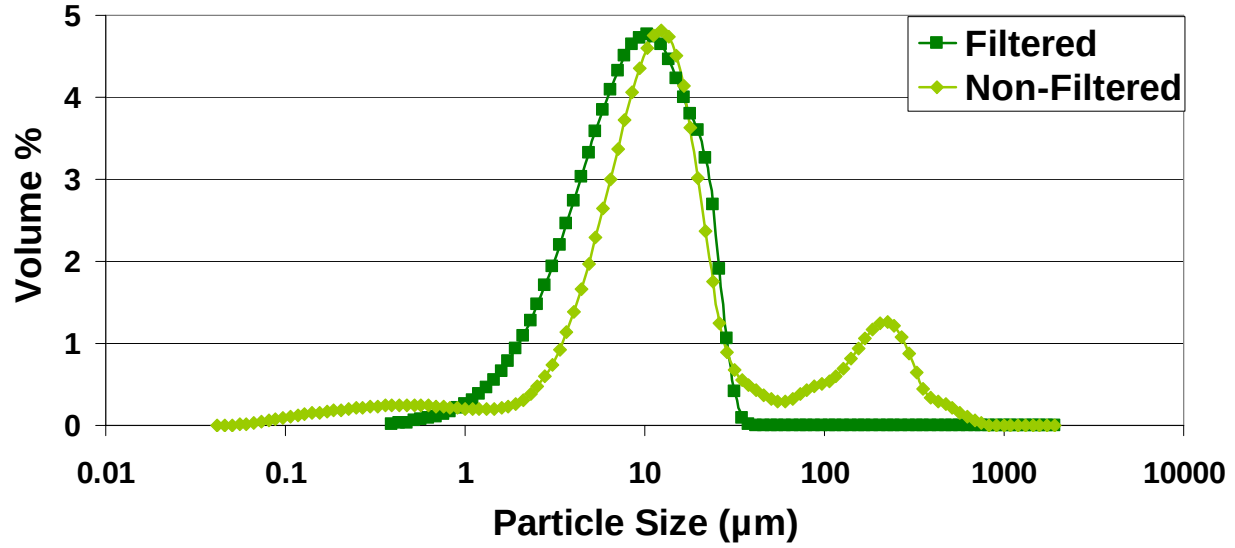

Figure 4-10. A particle size distribution comparison of 20µm-filtered and non-filtered gadolinium crosslinked DNA-MS under hydrated conditions.

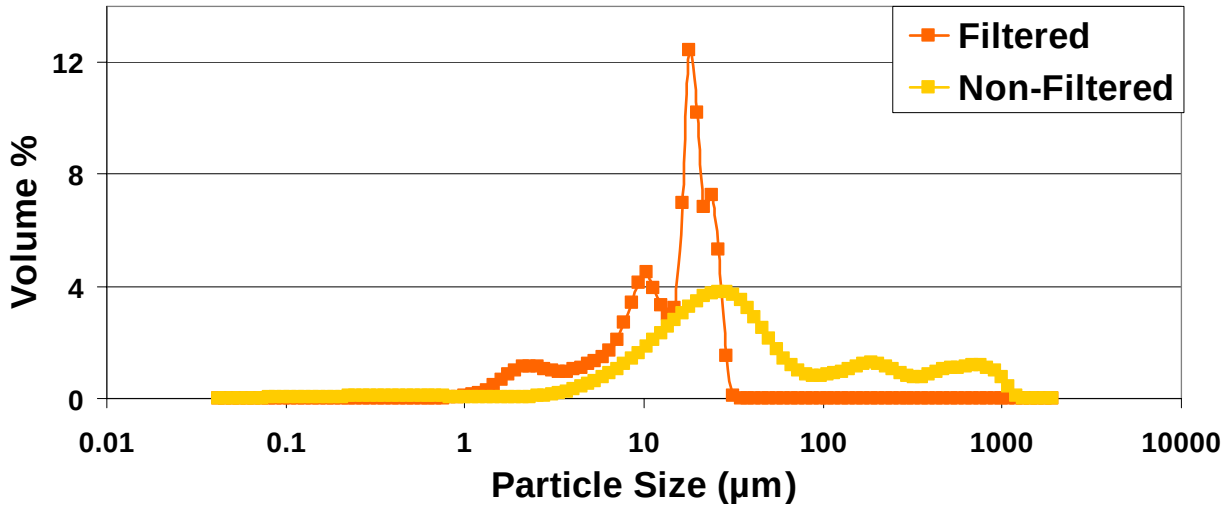

Figure 4-11. A particle size distribution comparison of 20µm-filtered and non-filtered glutaraldehyde crosslinked DNA-MS under hydrated conditions.

Table 4-4. The dry and hydrated mean particle diameters, percent change in size values, and crosslink concentrations for DNA-MS.

Crosslinking agent	Mean dry diameter (µm)	Mean hydrated diameter (µm)	Percent change in size (%)	Crosslink concentration (%M_{EQ})
Chromium	4.2 ± 6.0	12.6 ± 8.5	(+) 203	120
Gadolinium	3.3 ± 2.8	10.3 ± 7.0	(+) 211	120
Glutaraldehyde	5.5 ± 6.5	14.4 ± 7.4	(+) 125	540

Microscopy

Optical microscopy. Dried synthesized DNA-MS were observed under optical microscopy in order to evaluate the discreteness, morphology, and particle size of the MS after synthesis. DNA-MS ionically crosslinked with gadolinium and chromium, and covalently crosslinked with glutaraldehyde, produced discrete particles with small diameters and spherical morphologies, Figure 4-12. Optical images illustrated that the particle sizes were much smaller for the ionically crosslinked DNA-MS than the covalently crosslinked DNA-MS. This may be attributed to the amount of time it takes glutaraldehyde to crosslink with DNA. As mentioned from Chapter 3, glutaraldehyde reacts more slowly with the DNA molecule than chromium or gadolinium, and thus it would be expected that the glutaraldehyde condition with produce larger particles than the ionically crosslinked DNA-MS since the emulsion stir speed is much lower

after crosslinking (i.e. 600rpm instead of 1250rpm) leading to larger droplets in the emulsion which would lead to larger MS in the yield.

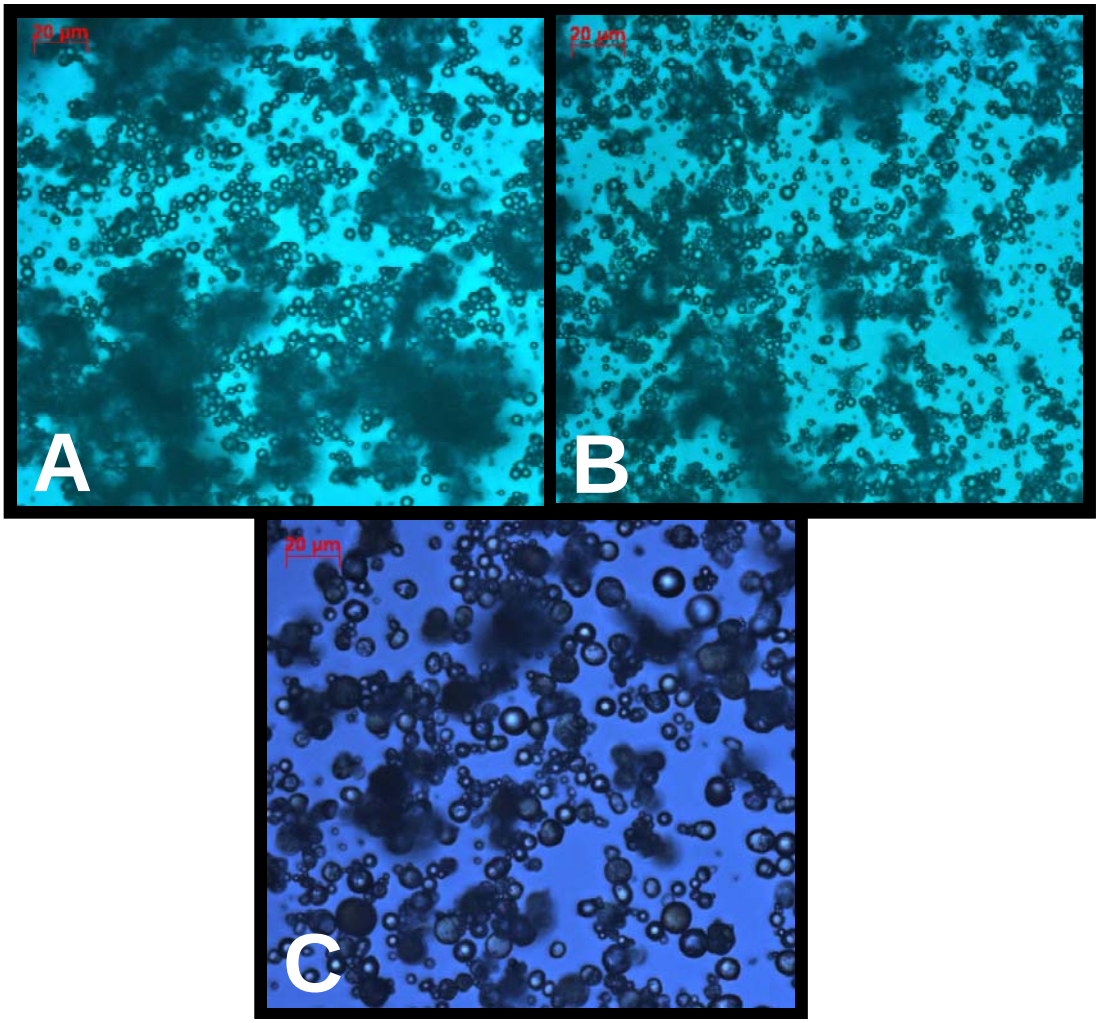

Figure 4-12. Optical images of the 20µm-filtered DNA-MS crosslinked with A) gadolinium, B) chromium, and C) glutaraldehyde (Magnification: 200x).

Scanning electron microscopy. SEM images were taken of the synthesized DNA-MS in order to characterize their morphology and surface topography. SEM images illustrated that the filtration step was successful in removing particles or aggregates with diameters greater than 20µm in size for both the ionically and covalently crosslinked DNA-MS, Figure 4-13. SEM images depicted discreet particles for conditions synthesized with the ionic crosslinking agents. SEM images of the glutaraldehyde crosslink agent condition displayed 1µm diameter particles

that aggregated together to form particles larger than 20μm in diameter, Figure 4-13. Since particles larger than 20μm in diameter were not capable of passing through the 20μm filter, these aggregates could have only been produced by liquid bridging or electrostatic interactions between particles upon drying.[107, 121, 122]

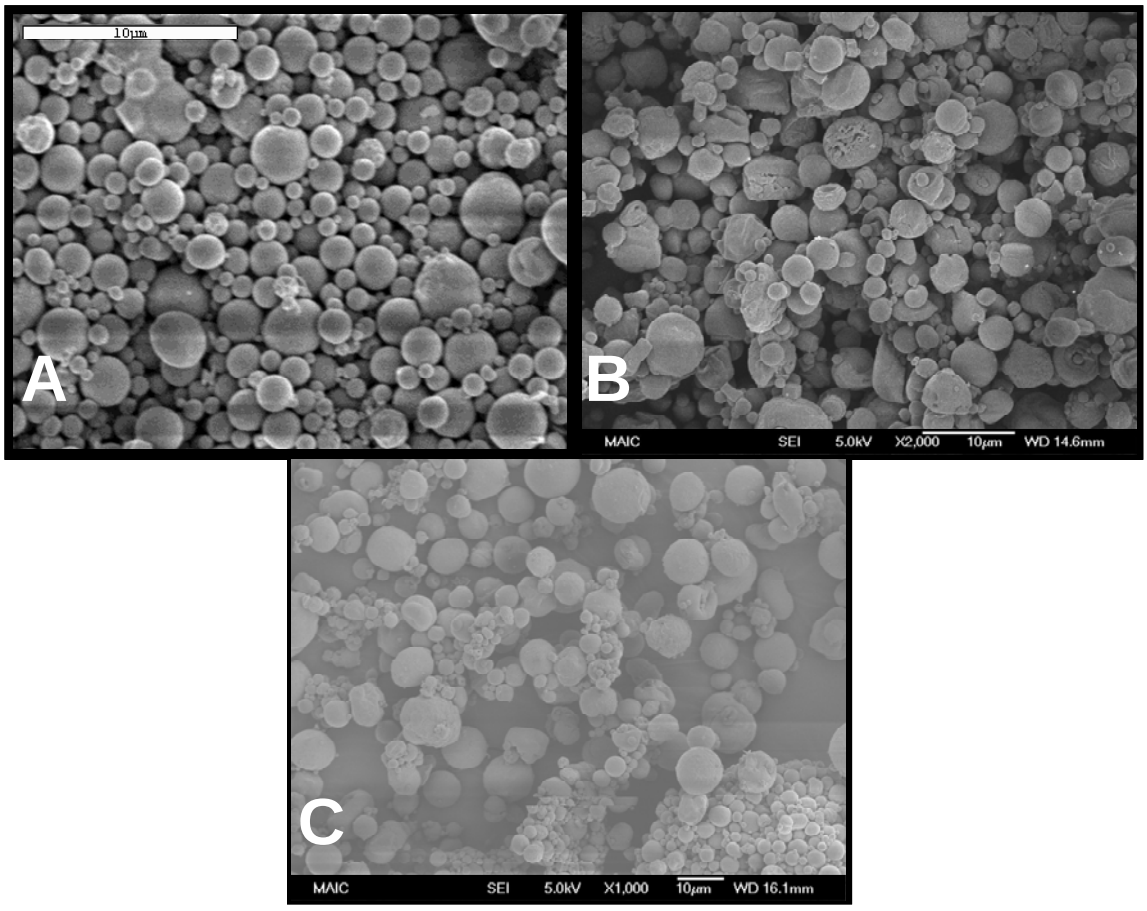

Figure 4-13. Scanning electron microscopy images of the 20μm-filtered DNA-MS crosslinked with A) chromium (Magnification: 4,500x), B) gadolinium (Magnification: 2,000x), and C) glutaraldehyde (Magnification: 1,000x).

The SEM images also displayed DNA-MS with spherical morphologies and smooth surface topographies for all conditions tested with the exception of the gadolinium crosslinked DNA-MS condition which produced some particles with irregular morphologies and rough surface topographies. Despite several morphological irregularities, DNA-MS at each crosslink

agent condition displayed particle sizes under 10μm further confirming results obtained from particle size analysis and optical microscopy observations.

Mixer Speed and Crosslink Concentration Study

Synopsis

The effects of mixer speed and crosslink concentration on DNA-MS particle diameters and size distributions were analyzed to determine optimum processing. Mixer speeds of 950rpm, 1250rpm, and 1550rpm along with crosslink concentrations of 20%M_{EQ}, 50%M_{EQ}, and 120%M_{EQ} were assessed in this study. Crosslink agent concentrations were obtained using 0.1M gadolinium crosslinking agent solution volumes of 0.3314mL for the 20%M_{EQ} condition, 0.8285mL for the 50%M_{EQ} condition, and 2mL for the 120%M_{EQ} condition during synthesis. The term M_{EQ} was used to denote the molar equivalence of gadolinium groups to phosphate groups and was calculated for each crosslink concentration condition. The gadolinium crosslink agent was the only crosslinking agent used for this study since it produced the highest yield with good particle size characteristics after filtration. The DNA-MS were synthesized, washed, and filtered with a 70μm nylon filter in order to not completely eliminate the possible size effects of the varying mixer speeds and gadolinium crosslink concentrations. Resulting DNA-MS were characterized by particle size, morphology, surface topography, and elemental analysis. All synthesis and characterization for this study was conducted with the assistance of Karly Jacobsen.

Particle analysis

Percent yield. The yield of each condition tested was calculated and expressed as a percent yield value after complete drying of the DNA-MS was achieved using Equation 4-1. Each synthesized condition generated yields over 60% with the exception of the 950rpm-20%M_{EQ} condition which produced a yield of 49% and the1250rpm-20%M_{EQ} condition which

produced a yield of 54%. The low yields obtained with these two conditions may have been attributed to the formation of aggregates with diameters larger than 70µm during synthesis. DNA-MS synthesized with a crosslink concentration of 20%M_{EQ} and/or mixer speeds of 950rpm performed the worst with low yields of less than 60%, whereas DNA-MS prepared with the 1250rpm-50%M_{EQ}, 1250rpm-120%M_{EQ}, and the 1550rpm-120%M_{EQ} conditions performed the best, with high yields of over 80%, Figure 4-14. Each DNA-MS condition with its respective yield is given in Table 4-5.

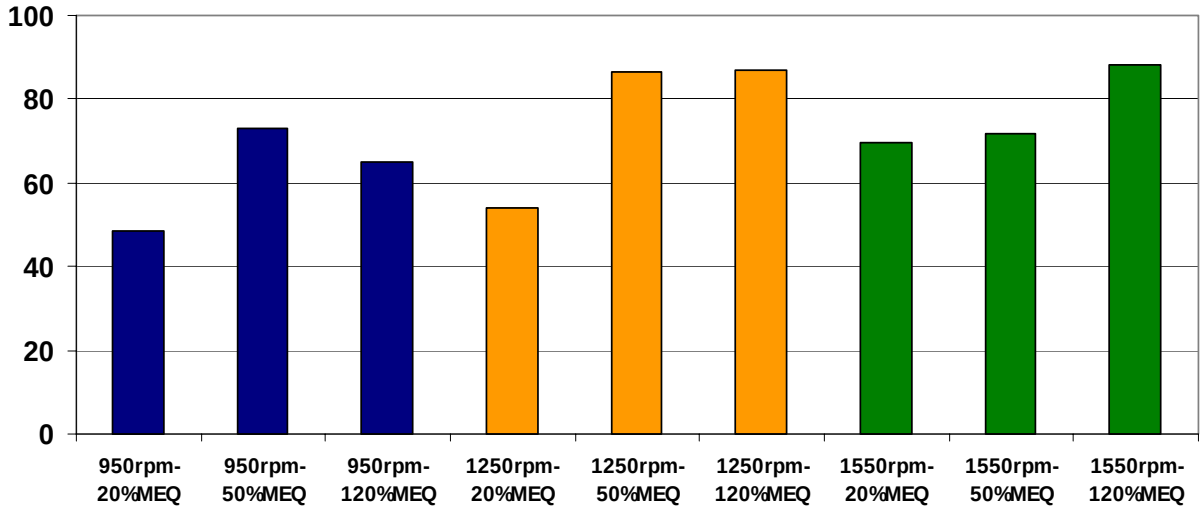

Figure 4-14. Graphical representation of yield values generated by each DNA-MS synthesis condition.

Table 4-5. Percent yield values for DNA-MS prepared at varying mixer speeds and gadolinium crosslink concentrations.

Synthesis condition	Percent yield (%)
950rpm-20%M_{EQ}	49
950rpm-50% M_{EQ}	73
950rpm-120% M_{EQ}	65
1250rpm-20% M_{EQ}	54
1250rpm-50% M_{EQ}	87
1250rpm-120% M_{EQ}	87
1550rpm-20% M_{EQ}	70
1550rpm-50% M_{EQ}	72
1550rpm-120% M_{EQ}	88

The production of these high yields may have been a result of the higher mixer speeds used during synthesis which not only reduced the formation of aggregates, but also produced particles with smaller diameters.[10, 107, 130, 131] DNA-MS with smaller particle sizes were created due to the decrease in the interfacial tension between the aqueous DNA phase and the continuous CAB phase by increasing the stir speeds during synthesis.[10, 107, 130, 131] Table 4-5 above lists each synthesis condition with its respective generated yield.

Dry particle size analysis. The dry particle size of ach DNA-MS condition prepared in this study was tested in methanol. Each synthesized condition produced particles with dry mean diameters of less than 20μm, Table 4-6.

Table 4-6. Mean dry particle size and size range values for DNA-MS prepared at varying mixer speeds and gadolinium crosslink concentrations.

Synthesis condition	Mean dry particle size (μm)	DNA-MS in 1μm to 10μm size range (%)	DNA-MS larger than 10μm (%)
950rpm-20%M_{EQ}	14.7 ± 28.5	46	19
950rpm-50%M_{EQ}	4.9 ± 6.9	48	14
950rpm-120%M_{EQ}	6.3 ± 9.5	54	18
1250rpm-20%M_{EQ}	3.7 ± 5.5	77	4
1250rpm-50%M_{EQ}	6.8 ± 14.4	59	14
1250rpm-120%M_{EQ}	5.7 ± 12.7	9	1
1550rpm-20%M_{EQ}	17.9 ± 21.9	57	31
1550rpm-50%M_{EQ}	3.3 ± 3.7	72	3
1550rpm-120%M_{EQ}	2.2 ± 2.1	68	1

Each DNA-MS condition at the 950rpm mixer speed produced particles with less than 60% of the diameters ranged in the mesosphere size range (i.e. 1μm to 10μm) and much greater than 5% were larger than 10μm. At the 1250rpm mixer speed, the 20%M_{EQ} condition produced favorable results; however, the 50%M_{EQ} condition produced many aggregates (i.e. 14% of all particles were larger than 10μm) and the 120%M_{EQ} condition produced many particles in the nanosphere size range (i.e. 90% of all particles were smaller than 1μm). At the 1550rpm mixer

speed, the 50%M_{EQ} and 120%M_{EQ} conditions produced particles that had greater than 60% of the diameters in the mesosphere size range and less than 5% of all diameters greater than 10µm.

DNA-MS prepared at the 950rpm and 1550rpm stir speeds and 20%M_{EQ} crosslink concentration, produced particles with mean diameters greater than 10µm and standard deviations greater than 20µm indicating that these conditions produced many large aggregates during synthesis, Figure 4-15. This may be a result of non-uniform crosslinking due to the low concentration of crosslink agent available in the system. With the exception of the 20%M_{EQ} crosslink concentration condition, no further particle size distribution trends were observed solely on crosslink concentration. These results are consistent with previous research and current literature which has cited that unlike emulsion stir speed, crosslink concentration does not have an effect on resulting microsphere sizes.[11, 57, 132, 133]

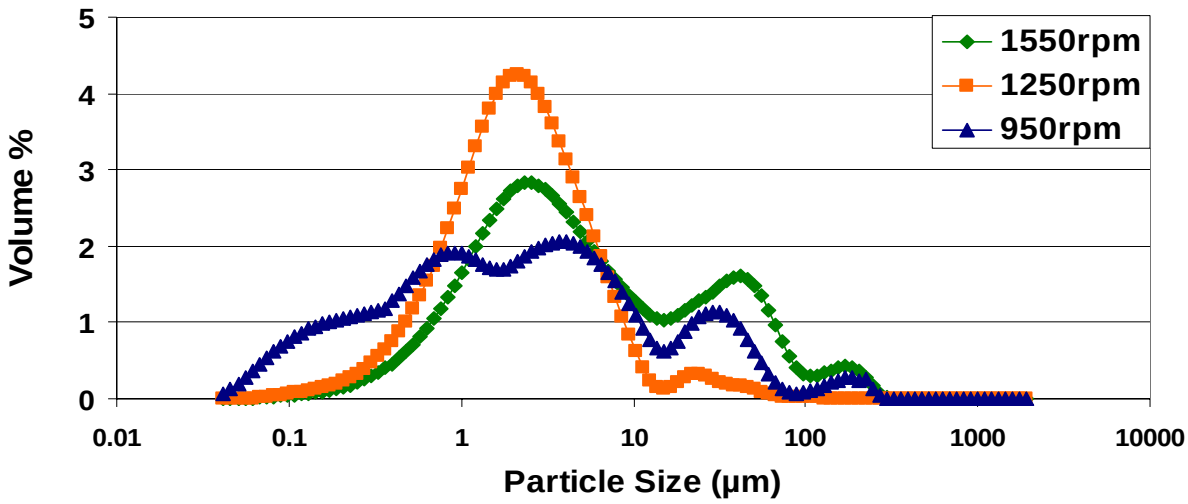

Figure 4-15. A dry particle size distribution comparison of DNA-MS synthesized at varying mixer speeds at the 20%M_{EQ} crosslink concentration condition.

Trends denoting the effects of mixer speed on particle diameter and size distribution were clearly observed. DNA-MS prepared at 950rpm produced particles with broad size ranges and multimodal distributions whereas DNA-MS synthesized at 1250rpm and 1550rpm displayed narrower and more normalized particle size distributions, Figures 4-16 to 4-18.

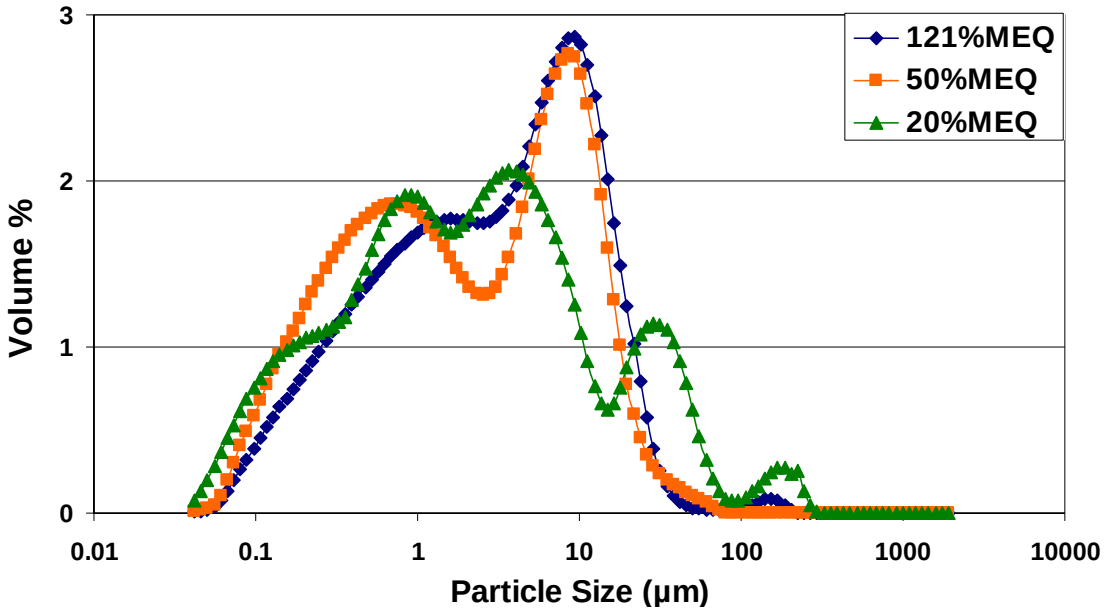

Figure 4-16. A dry particle size distribution comparison of DNA-MS synthesized at varying crosslink densities at the 950rpm mixer speed condition.

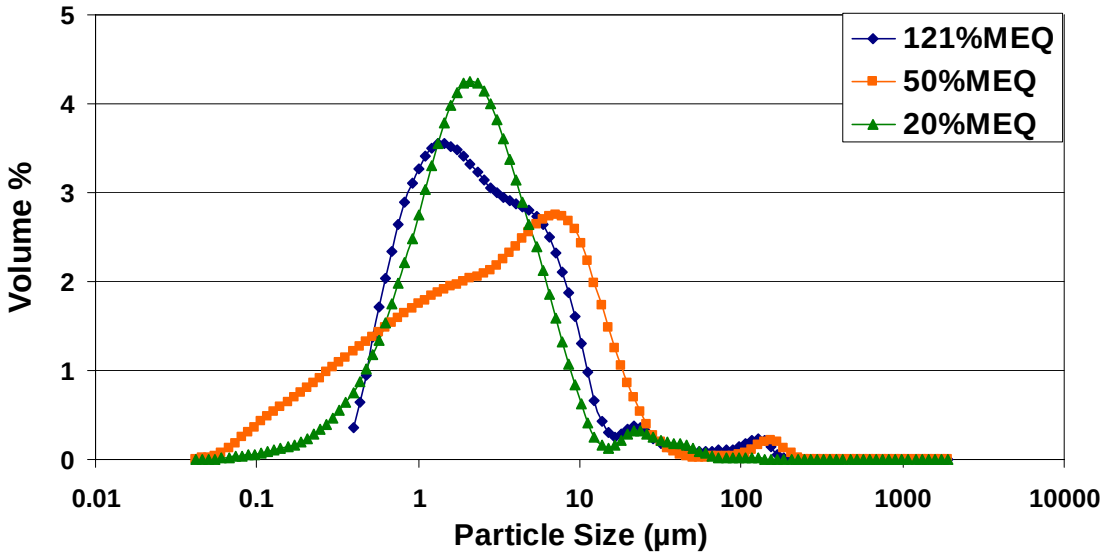

Figure 4-17. A dry particle size distribution comparison of DNA-MS synthesized at varying crosslink densities at the 1250rpm mixer speed condition.

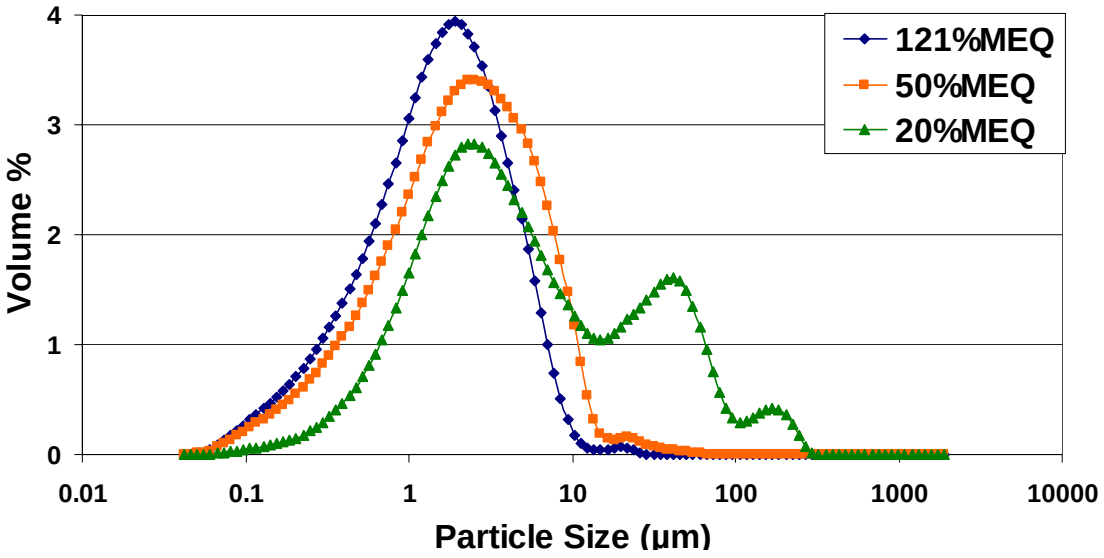

Figure 4-18. A dry particle size distribution comparison of DNA-MS synthesized at varying crosslink densities at the 1550rpm mixer speed condition.

This trend was to be expected since it has been well cited in the literature that by increasing the stir speed and in turn increasing the agitation in the system, the formation of aggregates during synthesis is prevented or reduced.[10, 125, 130, 131] DNA-MS prepared at the 1550rpm stir speed at crosslink concentrations greater than 50%M_{EQ} produced the smallest particles with the most narrow size distributions. This increase in the volume percent of smaller particles can be attributed to the higher stir speed used during synthesis which created a finer emulsion due to the increase in shear force exhibited on the system.[10, 57, 107, 130, 131, 134-136]

In order to quantify the effects of mixer speed and crosslink concentration on the particle sizes of the DNA-MS, a one way ANOVA test was conducted on all collected data. The test illustrated there to be no significant differences among all mean particle size values at each mixer speed and crosslink concentration condition. However, a strong trend was observed in that the particle size distributions for all crosslink concentration conditions at the 1550rpm mixer speed condition produced the best particle sizes and most normalized distributions, Figure 4-18. It is to be noted, however, that a 70µm filter was used in this study instead of a 20µm filter. If a

20µm filter had been used, aggregates seen past the 20µm mark would have been eliminated as seen in the results for the gadolinium condition in the Filter Study above.

Hydrated particle size analysis. DNA-MS synthesized at the 1550rpm mixer speed condition underwent particle size analysis under hydrated conditions in 0.05M PBS at a pH of 7.4. All other conditions were not tested due to their multimodal and broad particle size distributions. The DNA-MS prepared at the 1550rpm mixer speed condition each produced multimodal distributions upon hydration, Figures 4-19 to 4-21. These results are not consistent with observations made in the Filtration Study and may be attributed to the formation of aggregates during the DNA-MS drying process. However, it is assumed that the hydrated size distributions would be more normalized with fewer aggregates present if a 20µm filter had been used in place of the 70µm filter.

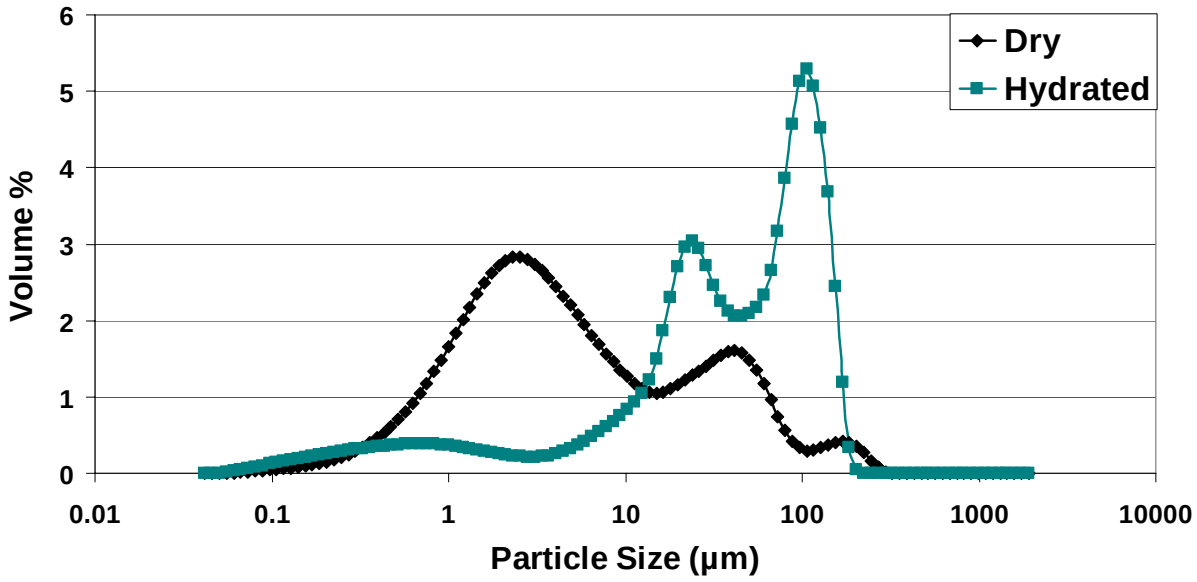

Figure 4-19. Dry and hydrated particle size distributions for DNA-MS prepared at 1550rpm and crosslinked with gadolinium to 20%M_{EQ}.

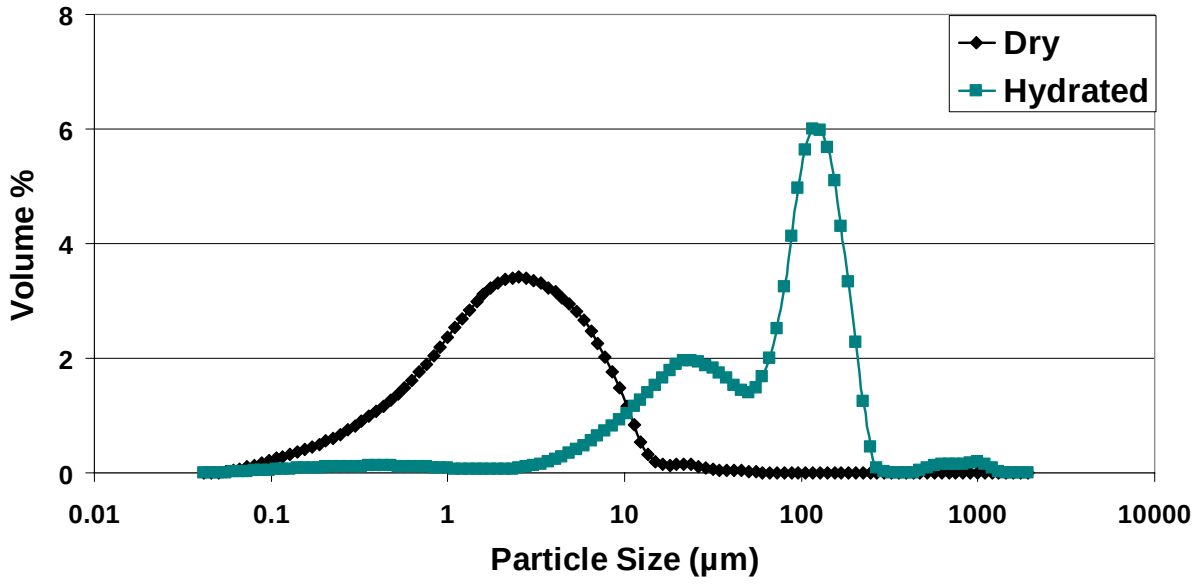

Figure 4-20. Dry and hydrated particle size distributions for DNA-MS prepared at 1550rpm and crosslinked with gadolinium to 50%M_{EQ}.

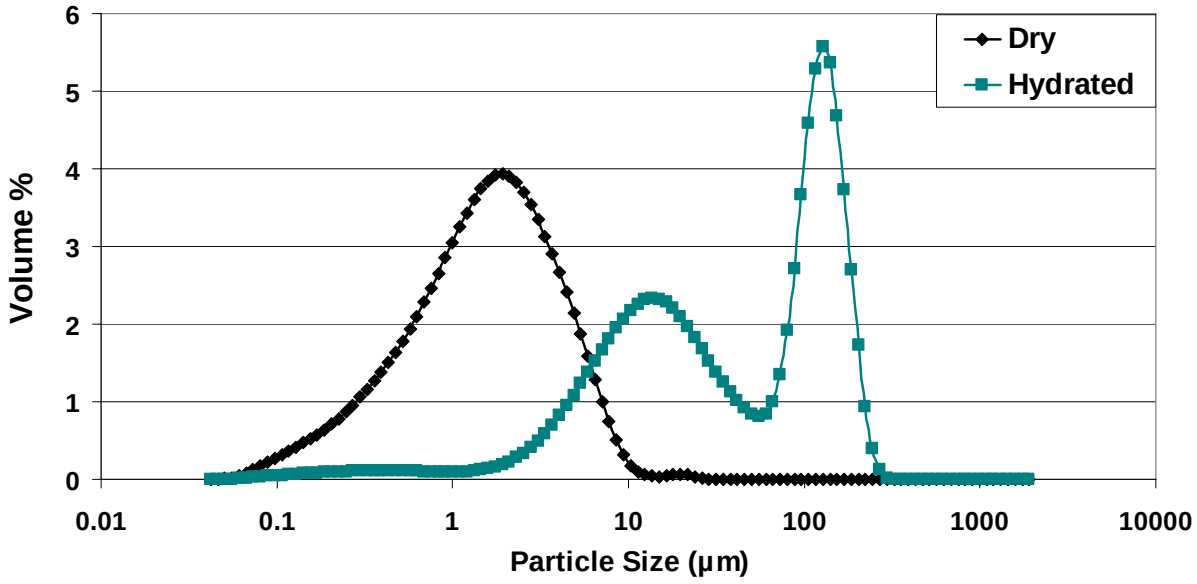

Figure 4-21. Dry and hydrated particle size distributions for DNA-MS prepared at 1550rpm and crosslinked with gadolinium to 120%M_{EQ}.

Each condition also produced hydrated mean diameters larger than 50µm; however, it was expected that these large diameter values better reflected the aggregates that formed during drying and then hydration more than the actual hydrated values of the individually swollen

particles. Upon closer analysis, it was assumed that the first peak better represented the distribution of the individually swollen DNA-MS as seen above in the Filtration Study. Therefore, the mean hydrated particle size and percent swelling values for those peaks were calculated and represented as the theorized mean particle size and percent swelling values for the DNA-MS.

In order to determine the effects of hydration on the particle size values of the DNA-MS at the 1550rpm mixer speed condition, a one way ANOVA was conducted on all dry, hydrated, and theorized hydrated diameter values at each crosslink concentration. The test illustrated no significant differences among each of the crosslink concentrations tested. The theorized mean particle size and percent swelling values as calculated by Equation 4-2 are reported along with the initial values in Table 4-7.

Table 4-7. Dry and hydrated mean particle size and percent swelling values for DNA-MS prepared at the 1550rpm mixer speed condition.

Condition	Mean dry particle size (μm)	Mean hydrated particle size (μm)	Percent swelling (%)	Theorized mean hydrated particle size (μm)	Theorized percent swelling (%)
20%M_{EQ}	17.9 ± 21.9	58.2 ± 47.4	225	23.8 ± 19.3	33
50%M_{EQ}	3.3 ± 3.7	94.9 ± 88.3	2780	23.8 ± 21.3	620
120%M_{EQ}	2.2 ± 2.1	69.2 ± 62.5	3050	13.6 ± 26.8	520

To further compare the crosslink concentration conditions at the 1550rpm mixer speed, the percent swelling for each condition was calculated. The 20%M_{EQ} crosslink concentration condition displayed the lowest amount of swelling upon hydration by swelling only to 225% of its original size. Surprisingly, the higher crosslink concentration conditions each produced swelling over 2000%; however, these larger values may rather reflect sizes of the aggregates that formed upon hydration and than the true swollen diameters of the DNA-MS. Thus a more realistic swollen value may be represented using the median values at each crosslink concentration condition. Using these values a 33% increase in size was reported for the 20%M_{EQ}

condition, a 620% increase in size was reported for the 50%M_{EQ} condition, and 520% increase in size was reported for the 120%M_{EQ} condition, Table 4-7. These values also illustrated that the 120%M_{EQ} crosslink concentration condition still produced significant swelling; however, the mean swollen diameter value was still lower than 20µm. The standard deviation of this value would be expected to decrease upon using a 20µm filter instead of 70µm filter at the end of the DNA-MS synthesis process since it would facilitate the break up of aggregates that form during washing and drying.

Surface charge analysis. The surface charge of the DNA-MS prepared at the 1550rpm mixer speed was measured in 0.01M PBS at a pH of 7.4 to determine the effects of crosslink concentration on yielding surface charge. Zeta potential measurements illustrated that DNA-MS values became more negative as the crosslink concentrations increased, Figure 4-22.

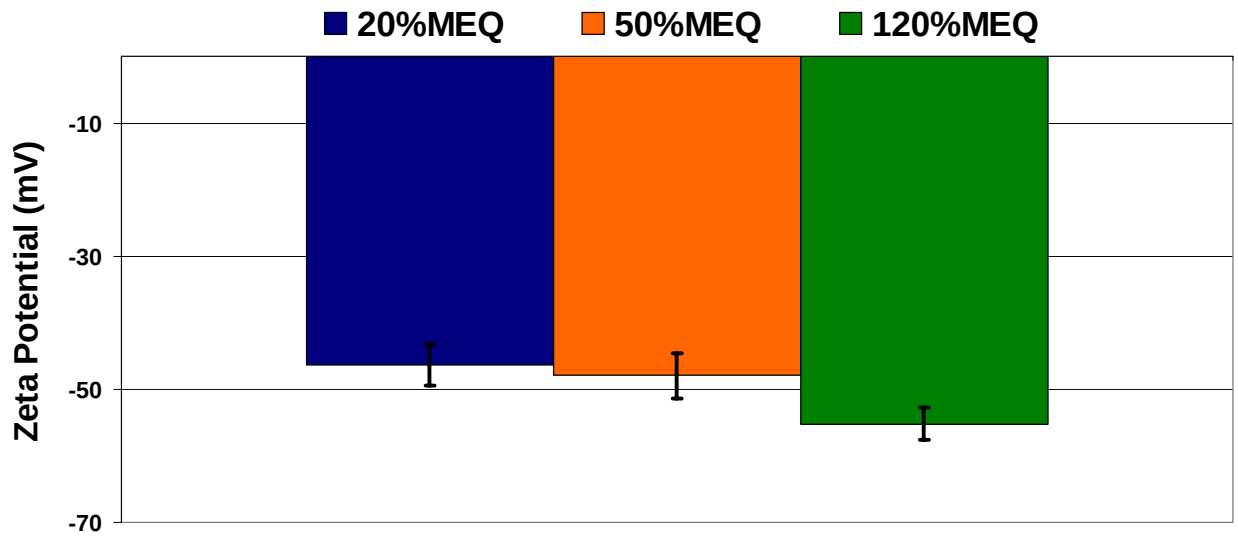

Figure 4-22. Zeta potential values for DNA-MS prepared with 20%M_{EQ}, 50%M_{EQ}, and 120%M_{EQ} crosslink concentrations (Note: Error bars represent standard error.).

DNA-MS prepared at the 120%M_{EQ} crosslink concentration produced the most negative zeta potential values of the three crosslink density values tested with a surface charge of -55.2mV,

Table 4-8. A one way ANOVA illustrated that this condition was significantly different from both the 20%M_{EQ} ($p = 0.001$) and 50%M_{EQ} ($p = 0.011$) crosslink concentration conditions.

Table 4-8. Zeta potential values for DNA-MS prepared with 20%M_{EQ}, 50%M_{EQ}, and 120%M_{EQ} crosslink concentrations.

Crosslink concentration condition	Zeta potential (mV)	Standard error (mV)
20%M_{EQ}	-55.2	3.0
50%M_{EQ}	-48.0	3.4
120%M_{EQ}	-46.3	2.4

Microscopy

Scanning electron microscopy. The morphology and topography of the synthesized DNA-MS was analyzed using SEM. SEM images illustrated that the particle size of the DNA-MS became more uniform as the mixer speed increased from 950rpm to 1550rpm, visually confirming results obtained through particle size analysis, Figures 4-23 to 4-25.

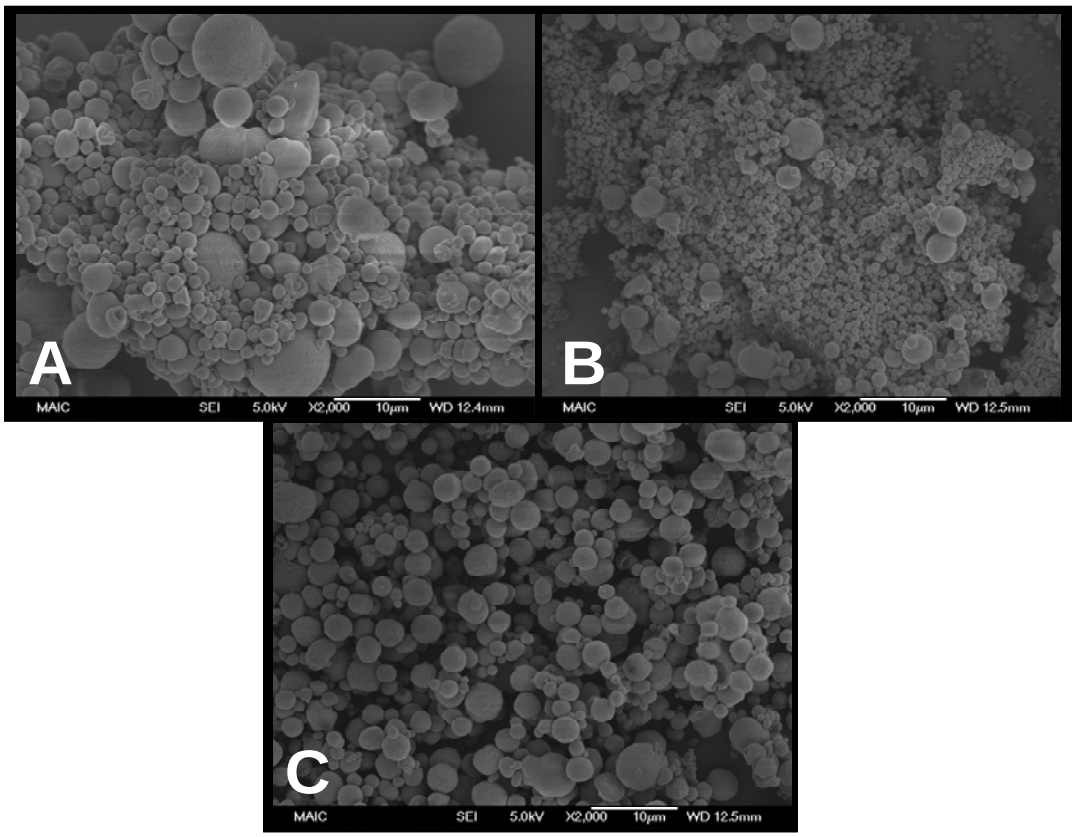

Figure 4-23. SEM images of DNA-MS crosslinked with 20%M_{EQ} gadolinium at the A) 950rpm, B) 1250rpm, and C) 1550rpm mixer speed conditions (Magnifications: 2,000x).

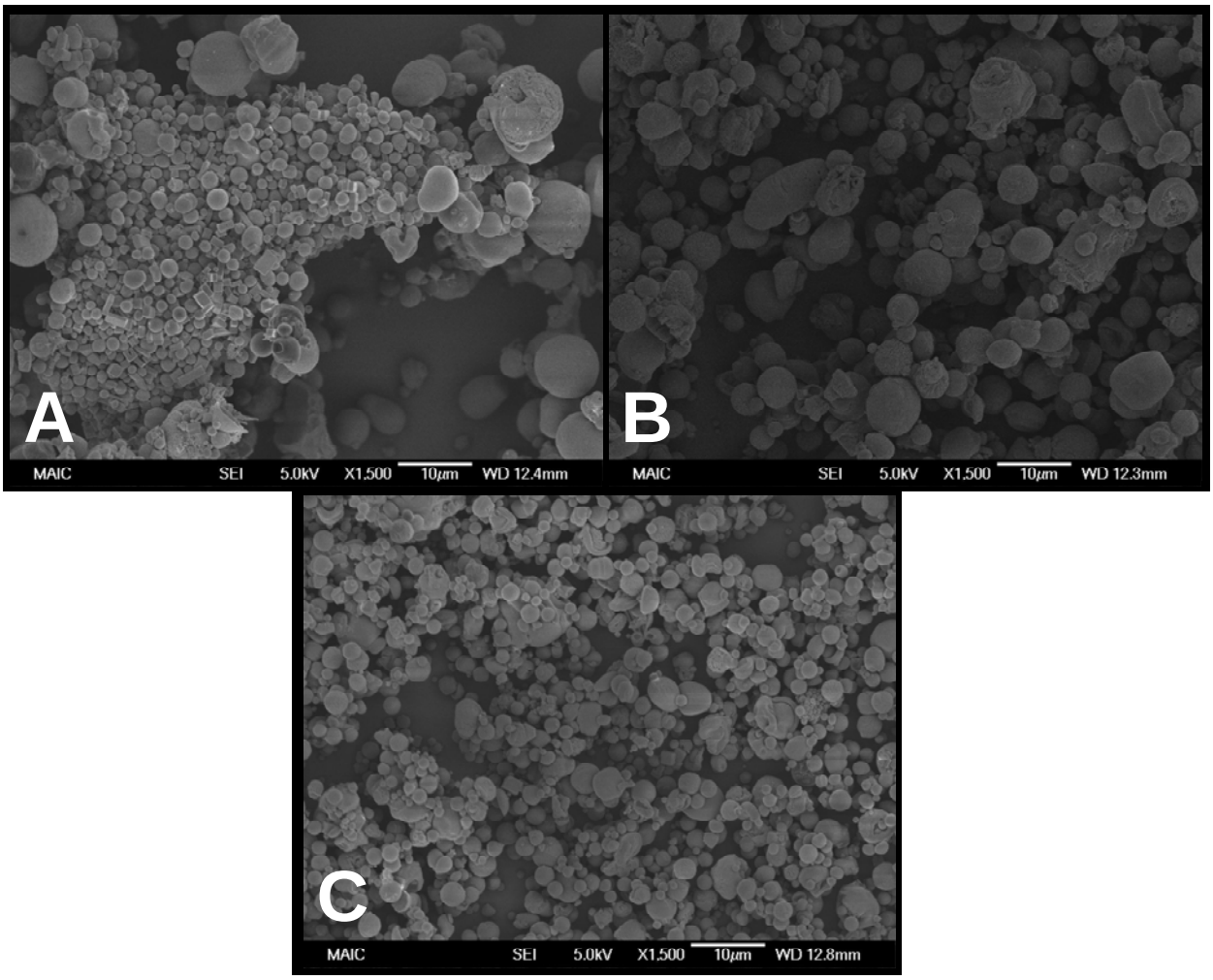

Figure 4-24. SEM images of DNA-MS crosslinked with 50%M_{EQ} gadolinium at the A) 950rpm, B) 1250rpm, and C) 1550rpm mixer speed conditions (Magnifications: 1,500x).

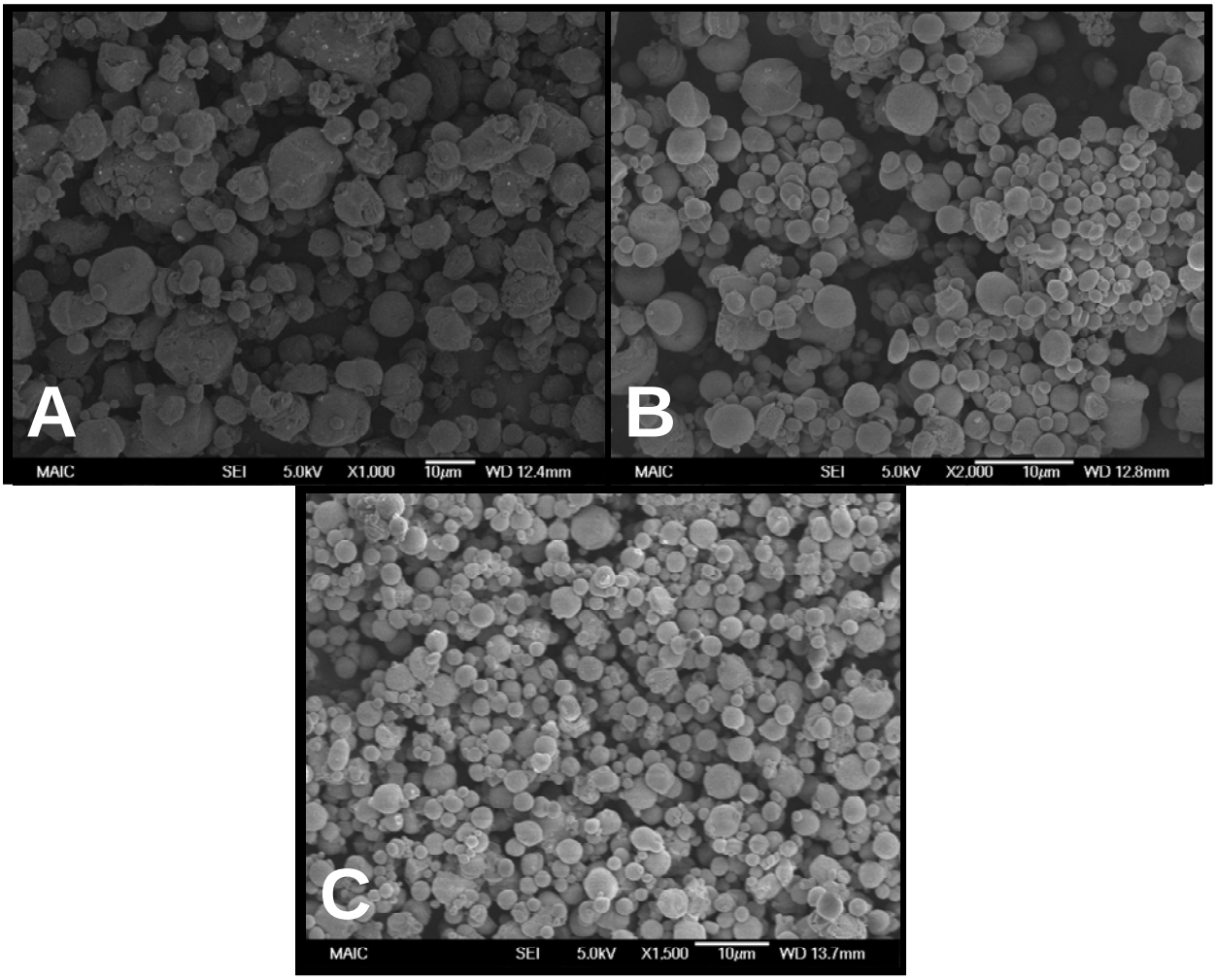

Figure 4-25. SEM images of DNA-MS crosslinked with 120%M_{EQ} gadolinium at the A) 950rpm, B) 1250rpm, and C) 1550rpm mixer speed conditions (Magnifications: 1,000x, 2,000x, and 1,500x, respectively).

The DNA-MS synthesized at the 1550rpm mixer speed conditions produced spherical morphologies and smooth topographies with normalized and mostly uniform particle size distributions; whereas the DNA-MS synthesized at the 950rpm and 1250rpm mixer speed conditions produced irregularly shaped particles with uneven surface topographies and heterogeneous particle size distributions. The SEM images illustrated that the DNA-MS synthesized at the 1550rpm mixer speed produced the most optimal particle morphologies, topographies, and size distributions.

Energy dispersive x-ray spectroscopy. Elemental analysis via EDS was conducted on the DNA-MS prepared at the 1550rpm mixer speed to confirm the presence of gadolinium. EDS measures the intensity of characteristic x-rays from different elements resulting from inner-shell excitations brought about by an electron beam.[110] The data is plotted in intensity versus energy where larger plotted intensities are indicative of a larger number of excitations received by the EDS detector.[110] EDS analysis illustrated that the DNA-MS synthesized at the 120%M_{EQ} condition produced spectra with higher x-ray counts of gadolinium than seen in the 50%M_{EQ} and 20%M_{EQ} conditions. These higher x-ray counts are to be expected due to the larger gadolinium crosslink concentration used.[110] The chlorine x-ray counts also increased from the 20%M_{EQ} condition to the 120%M_{EQ} condition further demonstrating an increase in the crosslinking agent concentration. The chlorine peaks were visible in the EDS spectra since the DNA-MS where crosslinked with a 0.1M gadolinium chloride solution, Figures 4-26 to 4-28.

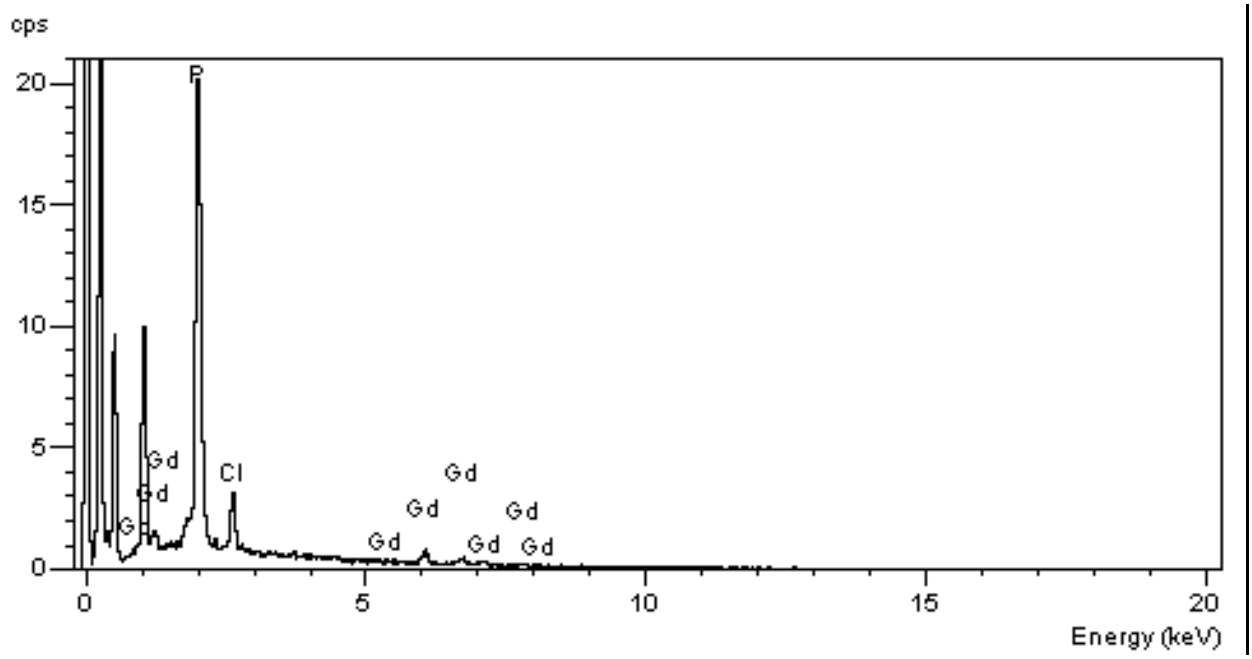

Figure 4-26. EDS spectra collected on DNA-MS prepared at the 1550rpm mixer speed and 20%M_{EQ} crosslink concentration condition.

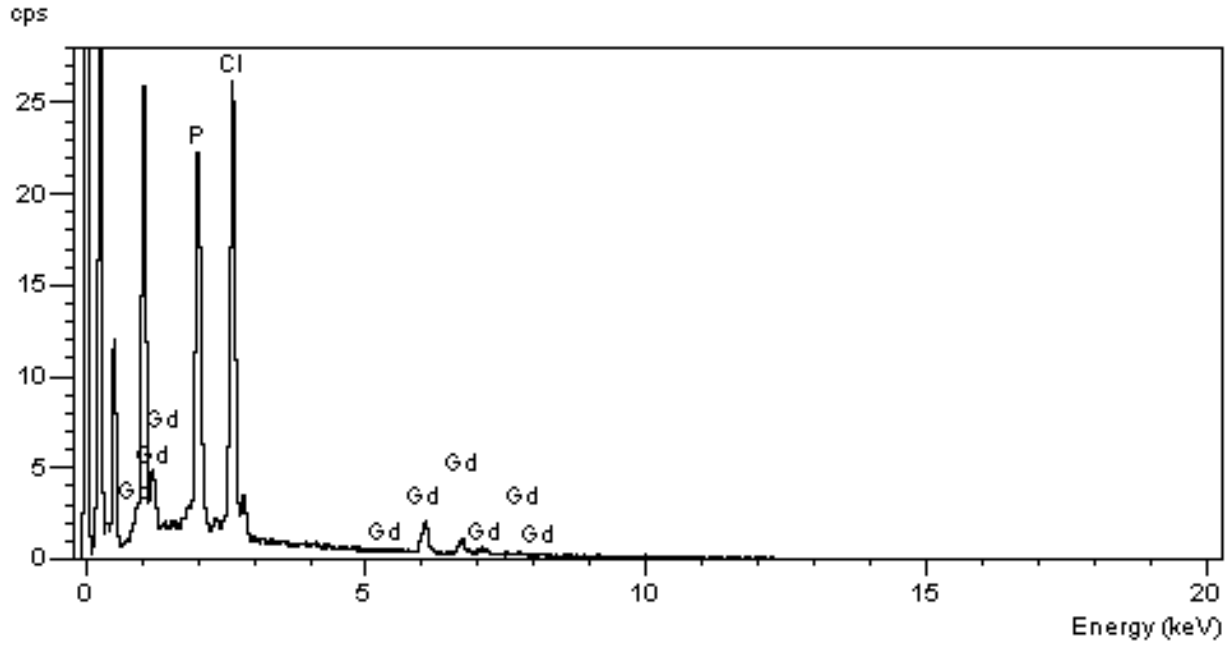

Figure 4-27. EDS spectra collected on DNA-MS prepared at the 1550rpm mixer speed and 50%M_{EQ} crosslink concentration condition.

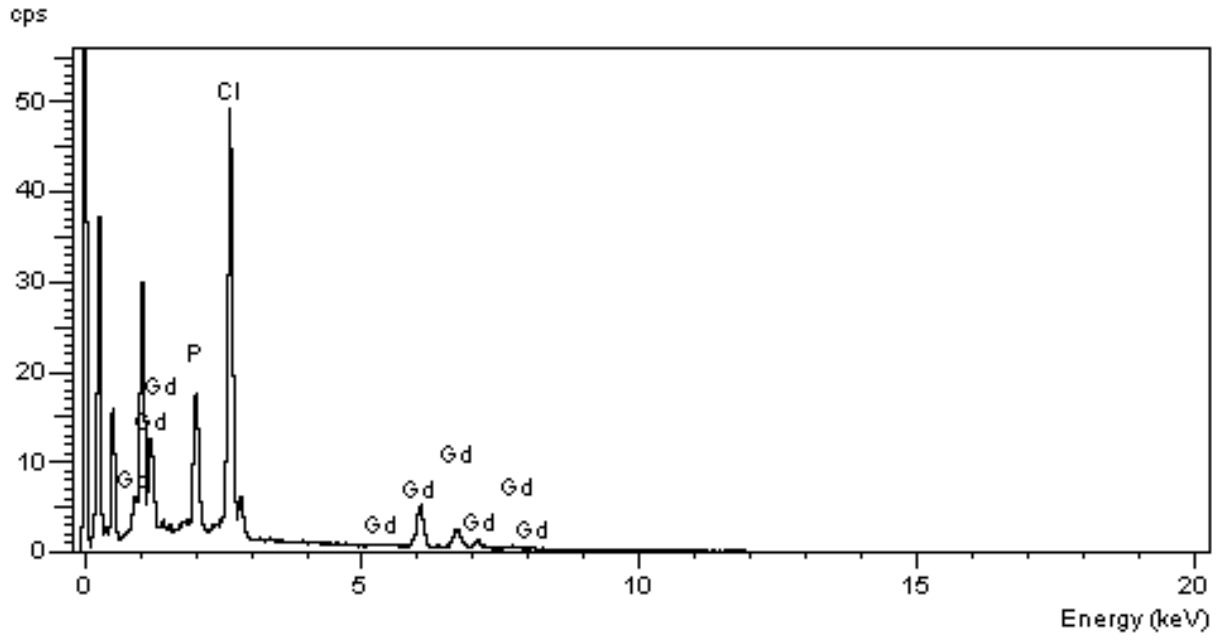

Figure 4-28. EDS spectra collected on the DNA-MS prepared at the 1550rpm mixer speed and 120%M_{EQ} crosslink concentration condition.

Conclusions

Filtration Study

The objectives of this study were to minimize or eliminate the presence of aggregates in the resulting DNA-MS yields and to produce controlled size distributions where at least 60% of all particles prepared fell within the mesosphere size range of 1μm to 10μm and less than 5% of all particles were greater than 10μm in size. Particles less than 1μm in diameter were also acceptable and DNA-MS were sought to obtain hydrated particle diameters of less than 25μm.

To achieve these goals the synthesis parameters for producing DNA-MS were altered by adding a filtration step to the end of the DNA-MS synthesis procedure using a nylon filter with a pore size of 20μm. A 20μm pore size was used for this study to better target the diameter range desired for optimal intratumoral chemotherapy.[69, 120] The resulting particle diameters and size distributions were then evaluated and compared to non-filtered controls. Data obtained in this study illustrated that the filtration step was successful in removing aggregates and particles over 20μm in diameter. The filtration step also normalized dry and hydrated particle size distributions by mechanically rupturing intermolecular bonds between the particles that formed during synthesis and drying for both ionically and covalently crosslinked DNA-MS. Data illustrated that the gadolinium crosslinked DNA-MS produced the best conditions after filtration with normalized dry and hydrated particle size distributions, dry diameters less than 5μm, 81% of all particles in the mesosphere size range, 2% greater than 10μm, hydrated diameters less than 20μm, and only an 18% decrease in yield as compared to the non-filtered yield.

Mixer Speed and Crosslink Concentration Study

The objective of this study was to optimize DNA-MS synthesis parameters to produce narrow and controlled size distributions where at least 60% of all particles prepared fell within the mesosphere size range of 1μm to 10μm and less than 5% of all particles were greater than

10μm in size. Particles less than 1μm in diameter were also acceptable and DNA-MS were sought to obtain hydrated particle diameters of less than 25μm.

The effects of mixer speed and crosslink concentration on particle diameter, swelling, morphology, and size distribution were analyzed. Mixer speeds of 950rpm, 1250rpm, and 1550rpm with gadolinium crosslink concentrations of 20%M_{EQ}, 50%M_{EQ}, and 120%M_{EQ} were assessed for these studies. The resulting DNA-MS were characterized by yield, particle size, elemental analysis, and surface topography and morphology.

Data obtained in this study revealed that the particle size distributions for all crosslink concentration conditions tested normalized as the stir speed increased. This study also revealed that the 20%M_{EQ} crosslink concentration condition produced the lowest yields at each of the three different mixer speeds tested indicating that this crosslink concentration was responsible for producing aggregates larger than 70μm in diameter. Data obtained in the study also illustrated that the 950rpm mixer speed produced DNA-MS with the largest percentage of particles with diameters greater than 10μm indicating that this speed produced many aggregates. Overall, the data obtained in this study illustrated that the 120%M_{EQ} crosslink concentration condition tested at the 1550rpm mixer speed produced the most optimal results with yields over 85%, dry particle diameters less than 5μm, 68% of all particles in the mesosphere size range, 1% of all particles greater than 10μm, hydrated particle diameters less than 25μm, and excellent stability in PBS.

CHAPTER 5
IN VITRO EVALUATIONS OF MITOXANTRONE LOADED DNA NANO-MESOSPHERES

Introduction

Mitoxantrone (MXN) *in situ* loaded DNA nano-mesospheres (DNA-MXN-MS) were prepared using optimized synthesis conditions from Chapter 4 to obtain particles with controlled size distributions where 60% of all particles prepared were within the mesosphere size range of 1μm to 10μm and < 5% of all particles were greater than 10μm in size. Particles less than 1μm in diameter were also acceptable and hydrated particle diameters were to be less than 25μm. In addition, MXN *in situ* loaded DNA-MS were sought to obtain loadings of ≥ 12% (w/w) MXN and release MXN for 24 hours or more in phosphate buffered saline under minimum sink conditions. DNA-MXN-MS were also sought to elicit a cytotoxic response ≥ to that of free drug on murine Lewis lung carcinoma (mLLC) cells in culture.

DNA-MXN-MS were prepared with a MXN concentration of 15% (w/w) and gadolinium crosslink concentrations of 20%, 50%, and 120% molar equivalence (M_{EQ}). The particle diameter, size distribution, morphology, drug loading, and percent drug release of the DNA-MXN-MS were evaluated with respect to the crosslink concentration. The particle diameters and size distributions were obtained using an LS Coulter 13 320 particle size analyzer. The morphology and presence of gadolinium trivalent cations were assessed using a scanning electron microscope with energy dispersive x-ray spectroscopy. Drug loading was determined by incubating the DNA-MXN-MS under stirred conditions in an enzymatic digestion buffer at 37ºC for 48 hours. The released drug concentrations were then analyzed using UV-visible spectroscopy against a MXN standard curve. The percent drug release was measured under minimum sink conditions in order to simulate the tumor environment. Drug release data was obtained by incubating the DNA-MXN-MS in phosphate buffered saline under constant agitation

at 37ºC for a minimum of fourteen days in triplicate. At specific times, aliquots were taken and measured using UV-visible spectroscopy against a MXN standard curve to determine drug concentration. The cytotoxicity of DNA-MXN-MS crosslinked with 120% M_{EQ} gadolinium was evaluated using a murine Lewis lung carcinoma (mLLC) cell line at MXN concentrations of 1μg/mL, 10μg/mL, and 25μg/mL and was compared to the same MXN concentrations of free drug. The cytotoxicity of blank DNA-MS were also evaluated. An MTS assay was used to measure the cellular viability of the mLLC cells at days 0 through 4.

Materials and Methods

Materials

Synthesis and characterization

DNA sodium salt derived from herring testes Type XIV (DNA), cellulose acetate butyrate, HPLC grade 1,2-dichloroethane, methanol, gadolinium (III) chloride hexahydrate, mitoxantrone dihydrochloride, L-cysteine hydrochloride hydrate, papain from papaya latex, deoxyribonuclease I from bovine pancreas, ethylenediaminetetraacetic acid disodium salt dihydrate (EDTA), and trichloroacetic acid were purchased from the Sigma-Aldrich Company. Sodium phosphate monobasic monohydrate, sodium phosphate dibasic anhydrous, and sodium chloride, each A.C.S. certified, acetone, 20μm and 70μm Spectra/Mesh Nylon filters, 16x125mm and 13x100mm borosilicate glass test tubes, Ultrafree-CL with Durapore Membrane Centrifugal Filter tubes (0.1μm pore, 2mL), Corning sterile 0.45μm pore filter bottles, Fisherbrand Semimicro methacrylate 1.5mL disposable cuvettes, and 15mL and 50mL polypropylene centrifuge tubes were purchased from Fisher Scientific International. Type I and Type II deionized ultrapure water was prepared with a resistivity of at least 16 $M\Omega\text{-}cm^{-1}$ using the Barnstead NANOpure Ultrapure Water System in the lab.

Cell culture

Corning 75cm^2 cell culture flasks, Fisherbrand clear polystyrene 96-well plates, MEM non-essential amino acid solution (NEAA), Cellgro heat inactivated fetal bovine serum (FBS), and 0.22μm Corning cellulose nitrate filters were each purchased from Fisher Scientific International. The CytoTox 96 Non-Radioactive Cytotoxicity Assay was purchased from the Promega Corporation. The mLLC cells, Dulbecco's Modified Eagle's Media with L-glutamine (DMEM), trypsin-EDTA solution, and penicillin-streptomycin were purchased from the American Type Culture Collection (ATCC, Manassas, VA).

Synthesis equipment

Solutions were washed or prepared on a Genie 2 vortex mixer. Centrifugation was conducted using a Dynac II bench top centrifuge. General DNA-MXN-MS syntheses were carried out using Caframo Model BDC6015 and Lightnin Model LIU08 mechanical lab mixers in 300mL Labconco lyophilization flasks.

Methods

Solution preparation

MXN *in situ* loaded DNA. MXN was *in situ* loaded into 5% (w/v) aqueous solutions of DNA at a concentration of 15% (w/w). Aqueous DNA solutions were prepared at room temperature by adding 0.5g of DNA to 5mL of ultrapure water in a 50mL polypropylene centrifuge tube. The solution was mixed on high on a vortex mixer for 30 seconds. Three milliliters of ultrapure water were then added to the DNA and placed on the rotary shaker for at least two hours until the DNA had completely dissolved. The volume was then brought up to 10mL and vortexed on high for 30 seconds. The DNA solution was then placed in the refrigerator over night to ensure the complete collapse of bubbles generated during vortex and rotary mixing. The percent solid concentration of the DNA solution was quantified using a

Metler LJ16 Moisture Analyzer at 130ºC for 60 minutes. Once the concentration was determined, 3.5mL of the DNA solution was placed into a 15mL polypropylene centrifuge tube. Using the true solid weight of the DNA in solution obtained during moisture analysis, the weight of the MXN, XgMXN, needed to obtain a 15% (w/w) loading was calculated by multiplying the true DNA solid weight in 3.5mL of DNA solution (W_{TDNA}) by 15 and then dividing the product by 100, Equation 5-1.

$$\text{Xg MXN} = \frac{15\text{g MXN} \times W_{TDNA}}{100\text{g DNA}} \tag{5-1}$$

The desired mass of MXN was weighed and added to the 3.5mL of the DNA solution. The DNA-MXN solution was then vortexed on high for 30 seconds and placed on the rotary mixer for 2 hours. The solution was then placed in the refrigerator until further use.

Cellulose acetate butyrate. Solutions of cellulose acetate butyrate in 1,2-dichloroethane (CAB) were used as the water-immiscible continuous phase for the emulsion stabilization process during DNA-MXN-MS synthesis. The CAB solutions were used at a concentration of 5% (w/v) and prepared by adding 25g of cellulose acetate butyrate to 500mL of 1,2-dichloroethane. The CAB solution was mixed at room temperature on a magnetic stir plate on high until the cellulose acetate butyrate had completely dissolved in the 1,2-dichloroethane. The resulting CAB solution was capped, parafilmed, and stored at room temperature.

Gadolinium (III) chloride. An aqueous solution of gadolinium (III) chloride was prepared to a concentration of 0.1M by adding 18.59g of gadolinium (III) chloride hexahydrate to 500mL of ultrapure water. The gadolinium (III) solution was mixed on a magnetic stir plate over night at room temperature until all the gadolinium had dissolved in the water. After complete mixing, the 0.1M gadolinium (III) crosslinking agent solution was parafilmed and stored at room temperature.

Phosphate buffered saline. Four liters of a 0.05M phosphate buffered saline (PBS) solution with a pH of 7.4 was prepared in the lab for measuring the swelling properties of the DNA-MXN-MS and for *in vitro* drug release analysis. The PBS solution was prepared by mixing 2.9L of a 0.05M sodium phosphate dibasic solution to 1L of a 0.05M sodium phosphate monobasic solution. The pH of the resulting solution was measured and the sodium phosphate monobasic solution was added until the target pH of 7.4 was reached. The PBS solution was then sterilized using a 0.45μm Corning 1L cellulose acetate filter system and left out at room temperature until needed.

A PBS solution with a concentration of 0.1M at a pH of 7.4 was used for determining the MXN loading efficiency of the DNA-MXN-MS. The 0.1M PBS solution was prepared by adding 2.9L of a 0.1M sodium phosphate dibasic solution into 1L of 0.1M sodium phosphate monobasic solution and the pH was adjusted by adding the monobasic to the solution until a pH of 7.4 was reached. The 0.1M PBS solution was then sterilized using a 0.45μm Corning 1L cellulose acetate filter system. A 0.01M PBS solution at a pH of 7.4 was used for zeta potential measurements and was prepared by diluting a 0.1M PBS solution and adjusting the pH back to 7.4. The solutions were left out at room temperature until needed.

Enzymatic digestion buffer. An enzymatic digestion buffer was used to digest the DNA-MXN-MS to determine their MXN loading efficiency. The enzymatic digestion buffer was prepared by adding 1,800mg of EDTA, 200mg of L-cysteine hydrochloride hydrate, 125mg of papain from papaya latex, and deoxyribonuclease I from bovine pancreas to 250mL of the 0.1M PBS solution (pH = 7.4). The enzymatic digestion buffer components were stirred at room temperature until completely dissolved and used immediately after preparation.

Cell culture media. Cell culture media was prepared by adding 50mL of FBS, 10mL of NEAA solution, and 10mL of penicillin-streptomycin to 500mL of DMEM to obtain a 10% FBS, 2% NEAA, and 2% penicillin-streptomycin treated media. This media mixture will be referred to as treated media throughout. The treated media solutions were mixed manually and placed in the refrigerator until further use.

Synthesis procedure

DNA-MXN-MS were prepared using a modified emulsion stabilization technique that was developed in this lab that sterically stabilizes the DNA molecule into spherical conformations and crosslinks them while in suspension. This emulsion stabilization process involved dispersing 3mL of the aqueous DNA-MXN solution (i.e. the aqueous phase) into 47mL of the organic CAB solution (i.e. the continuous phase) in a 300mL Labconco lyophilization flask. A DNA-MXN microemulsion was then created by vigorously mixing the two solutions at 1550rpm for 20 minutes at room temperature using a paddle mixer with a two inch, two blade propeller. The DNA-MXN microemulsion was then ionically crosslinked while in suspension by reducing the speed of the paddle mixer to 600rpm and adding 0.1M gadolinium (III) solution in volumes of 0.3314mL to obtain the 20%M_{EQ}, 0.8285mL to obtain the 50%M_{EQ}, or 2mL to obtain the 120%M_{EQ} crosslink concentration conditions. The DNA-MXN microemulsion then underwent crosslinking for 1 hour and 40 minutes at which time 50mL of acetone was added and any further reactions were allowed to reach completion for another hour. After synthesis was complete, the DNA-MXN-MS underwent four rinses in acetone to remove any residual organic phase, crosslinking agent, or non-loaded drug. The DNA-MXN-MS were rinsed by separating the resultant DNA-MXN-MS suspension into four separate 50mL polypropylene centrifuge tubes. Acetone was added to 40mL and the tubes were capped and vortexed on high for 30 seconds. The DNA-MXN-MS were then collected by centrifuging the tubes at 2600rpm for 10

minutes and decanting the acetone. Fresh acetone was added again to 40mL mark and the acetone rinse was repeated once more as mentioned above and then twice more by consolidating the contents of 4 tubes to 2 tubes and then 2 tubes to one tube. After the final acetone rinse, DNA-MXN-MS were resuspended in 30mL of acetone and vortexed on high for 30 seconds. The resuspended DNA-MXN-MS were then filtered using a stainless steel vacuum filtration device with a 70μm Spectra/Mesh Nylon filter. A 70μm Spectra/Mesh Nylon filter was used in place of the 20μm filter to not completely eliminate the possible size effects of the crosslink concentrations and the MXN drug loading on the DNA-MXN-MS. The device was then rinsed with 10mL of acetone to further filter any remaining DNA-MXN-MS under 70μm. The centrifuge tube was then capped, vortexed on high for 30 seconds, and centrifuged at 2600rpm for 5 minutes to collect the DNA-MXN-MS. The acetone was then decanted and a Kimwipe was secured over the mouth of tube using a rubber band to allow the DNA-MXN-MS to dry overnight at room temperature.

Particle characterization

Yield analysis. The yield and theoretical yield of each condition synthesized was calculated and expressed as a percent yield value. The percent yield was calculated by dividing the final weight of the DNA-MXN-MS by the amount of weight used to synthesize the DNA-MXN-MS, Equation 5-2. For the theoretical yield, the weight of the MXN that was *in situ* loaded into the DNA solution was added to the equation, Equation 5-3. The equations for the percent yield and percent theoretical yield are expressed below where W_F is the final weight of the DNA-MXN-MS, V_{DNA}, ρ_{DNA}, and C_{DNA} are the volume, density, and concentration of the aqueous DNA solution used respectively, W_X is the weight of the crosslinking agent added during synthesis, and W_Y is the theoretical weight of the *in situ* loaded MXN.

$$\%\ \text{Yield} = \left(\frac{W_F}{((V_{DNA} \times \rho_{DNA} \times C_{DNA}) + W_X)}\right) \times 100 \quad (5\text{-}2)$$

$$\%\ \text{Theoretical Yield} = \left(\frac{W_F}{((V_{DNA} \times \rho_{DNA} \times C_{DNA}) + W_X + W_Y)}\right) \times 100\ \% \quad (5\text{-}3)$$

Dry particle size analysis. Dry DNA-MXN-MS particle diameters and size distributions were obtained using a Coulter LS 13 320 particle size analyzer. DNA-MXN-MS were sonicated for 10 to 30 seconds to aerate and separate the particles prior to analysis and then approximately 2mg of the DNA-MXN-MS were suspended in 2mL of methanol. The suspension was then sonicated for 30 seconds to further break up any DNA-MXN-MS aggregates and tested. The Coulter LS 13 320 particle size analyzer was set to run at a pump speed of 73% using a protein/DNA particle diffraction model. Standards were tested in methanol before the first run to ensure that the instrument was performing adequately. Each condition was sampled three times in which each sample's particle size measurements consisted of two runs. This method of testing produced six independent particle diameters and size distributions. Data collected from these experiments were statistically analyzed using SigmaStat 3.0 software.

Hydrated particle size analysis. Swollen DNA-MXN-MS particle diameters and size distributions were obtained in 0.05M PBS at a pH of 7.4 using a Coulter LS 13 320 particle size analyzer. DNA-MXN-MS were sonicated for 10 to 30 seconds prior to analysis to aerate and separate the particles and then approximately 2mg of the DNA-MXN-MS were suspended in 2mL of PBS. The suspension was then sonicated for 30 seconds to further break up any DNA-MXN-MS aggregates. The DNA-MXN-MS were then allowed to swell in the PBS for an additional two minutes and thirty seconds. The DNA-MXN-MS were then tested in the Coulter LS 13 320 particle size analyzer using a pump speed of 73% and a protein/DNA particle diffraction model. Standards were tested in PBS before the first run to ensure that the instrument

was performing adequately. Each condition was sampled three times in which each sample's particle size measurements consisted of two runs. This method of testing produced six independent particle diameters and size distributions. The mean swollen particle diameters were then used to calculate the percent change in size by a using Equation 5-4 where D_H is the mean hydrated particle diameter and D_D is the mean dry particle diameter. A negative percent change in size depicted a decrease in particle size whereas a positive percent change in size depicted an increase in particle size, or swelling. Data collected from these experiments were statistically analyzed using SigmaStat 3.0 software.

$$\%\,\text{Change in Size} = \left(\frac{D_H - D_D}{D_D}\right) \times 100 \qquad (5\text{-}4)$$

Surface charge analysis. DNA-MXN-MS surface charge was measured to further characterize the *in situ* loading of MXN. DNA-MXN-MS surface charge was obtained in a 0.01M PBS solution at a pH of 7.4 using a Brookhaven ZetaPlus zeta potential analyzer with ZetaPALS software. Approximately 2mg of the DNA-MXN-MS were suspended in 1.5mL of the PBS solution. Each condition was sampled three times in which each sample underwent ten runs. This method of testing produced thirty independent zeta potential values. The data collected from the zeta potential analyzer was statistically analyzed using SigmaStat 3.0 software.

Scanning electron microscopy. The morphology and surface topography of the DNA-MXN-MS were observed using scanning electron microscopy (SEM). Approximately 1mg of dry DNA-MXN-MS were mounted onto a small piece of silicon wafer which in turn was mounted onto an aluminum SEM stub using double sided tape. The DNA-MSN-MS were then coated with gold-palladium for 2 minutes using a Technix Hummer V sputter coater. Images

were taken on a JEOL 6335F Field Emission SEM at an accelerating voltage of 5KeV and a working distance of 15mm.

Energy dispersive x-ray spectroscopy. The presence of trivalent cations in the DNA-MXN-MS after washing and drying was observed using energy dispersive x-ray spectroscopy (EDS). DNA-MXN-MS were mounted onto a piece of silicon wafer which was then secured to an aluminum SEM stub using carbon double sided tape. The DNA-MXN-MS were then coated with carbon for 2 minutes using a Technix Hummer V sputter coater. EDS spectra on the DNA-MXN-MS were collected using a JEOL 6400 SEM at an accelerating voltage of 15KeV and working distance of 15mm. A dead time of 20% to 40% was allowed for each condition tested.

***In vitro* DNA-MXN-MS characterization procedures**

MXN loading efficiency. The MXN loading efficiency of the DNA-MXN-MS was determined via enzymatic digestion followed by photometric analysis of the recovered entrapped drug. Approximately 5mg of the DNA-MXN-MS were weighed out into labeled 16x125mm glass test tubes and recorded. Ten milliliters of the enzymatic digestion buffer were added to the DNA-MXN-MS and the test tubes were capped, parafilmed, and incubated at 37˚C under stirred conditions for 48 hours. Control MXN solutions were also tested for drug degradation by adding 200µl of a 1,000µg/mL MXN solution into 10mL of the enzymatic digestion buffer. The control solutions were also incubated in 16x125mm glass test tubes at 37˚C under stirred conditions for 48 hours. The test tubes were then taken out of the incubator and the solutions were allowed to cool to room temperature. While the solutions were cooling, a 10% (w/v) solution of trichloroacetic acid (TCA) in ultrapure water was prepared. Two milliliters of each DNA-MXN-MS solution were placed into labeled 13x100mm glass test tubes. Two milliliters of the 10% (w/v) TCA solution was then added to each sample. The test tubes were capped and the two solutions were allowed to react for 30 minutes at room temperature. The samples were then

centrifuged at 2,600rpm for five minutes and the supernatants from each sample were collected into 1.5mL methacrylate disposable cuvettes for UV-Vis analysis. Each sample was analyzed on a Perkin Elmer Lambda 3 spectrophotometer at a wavelength of 610nm against a MXN in 5% (w/v) TCA standard curve with concentrations ranging from 1μg/mL to 50μg/mL and a correlation coefficient of 0.99966 to determine the MXN concentration. The MXN concentration was then used to determine the percent drug loading of MXN in the DNA-MXN-MS using Equation 5-5.[137, 138] The loading efficiency was then calculated using Equation 5-6.[137-139] Each condition was tested in triplicate and all collected data was statistically analyzed using SigmaStat 3.0 software.

$$\%\ \text{Drug Loading} = \left(\frac{\text{Mass of MXN in MS}}{\text{Mass of DNAMXNMS}}\right) \times 100 \qquad (5\text{-}5)$$

$$\text{Loading Efficiency} = \left(\frac{\text{Experimental Loading}}{\text{Theoretical Loading}}\right) \times 100 \qquad (5\text{-}6)$$

***In vitro* MXN release.** The *in vitro* release of MXN from DNA-MXN-MS under minimum sink conditions was tested in sterile filtered 0.05M PBS at a pH of 7.4. Approximately 2mg of each DNA-MXN-MS condition were weighed into labeled 2mL filter centrifuge tubes (0.1μm pore size) to which 1.25mL of the sterile filtered 0.05M PBS solution was added. The tubes were then capped, parafilmed, and incubated at 37˚C under stirred conditions. At specified time points, the filter centrifuge tubes were removed from the incubator and centrifuged for 10 minutes at 3,000rpm. Aliquots were then removed and placed into 1.5mL methacrylate disposable cuvettes for UV-Vis analysis. The cuvettes were capped, labeled, parafilmed, and stored in the refrigerator until analysis. Each centrifuge filter tube was then replenished with 1.25mL of fresh 0.05M PBS, capped, parafilmed, and placed back into the incubator at which time the incubation process was repeated until the next time point. The aliquots for each

condition were collected at hours 1-8, days 1-7, and days 10, 15, 20, 30, 40, 50, and 75. The aliquots for each condition were analyzed on a Perkin Elmer Lambda 3 spectrophotometer at a wavelength of 609nm against a MXN in 0.05M PBS standard curve with concentrations ranging from 1μg/mL to 50μg/mL and a correlation coefficient of 0.99669. Each condition was tested in triplicate and all collected data was statistically analyzed using SigmaStat 3.0 software.

Assessment of DNA-MXN-MS cytotoxicity

Synopsis. The cytotoxic effect of free MXN, DNA-MXN-MS, and blank DNA-MS on the cellular viability of mLLC cells was evaluated. Free MXN and DNA-MXN-MS were tested at MXN doses of 1μg/mL, 10μg/mL, and 25μg/mL and blank DNA-MS were tested at a concentration of 100μg. A colorimetric MTS assay which quantifies cell death by measuring the amount of lactate dehydrogenase (LDH) that is released upon cell lyses was used to assess the cellular viability of the mLLC.[140] The lactate from LDH that is released from dead cells reacts with the oxidized form of nicotinamide adenine dinucleotide (NAD^+) in the assay to produce pyruvate and the reduced form of nicotinamide adenine dinucleotide (NADH), Figure 5-1.[99, 140] NADH then reacts with a tetrazolium salt to form NAD^+ and a red formazan dye that is read photometrically at a wavelength of 490nm, Figure 5-2.[140] The mLLC cells were evaluated at hour 1, and days 1-4. A cytotoxic response was defined by an increase in absorbance at 490nm for any given treatment group.

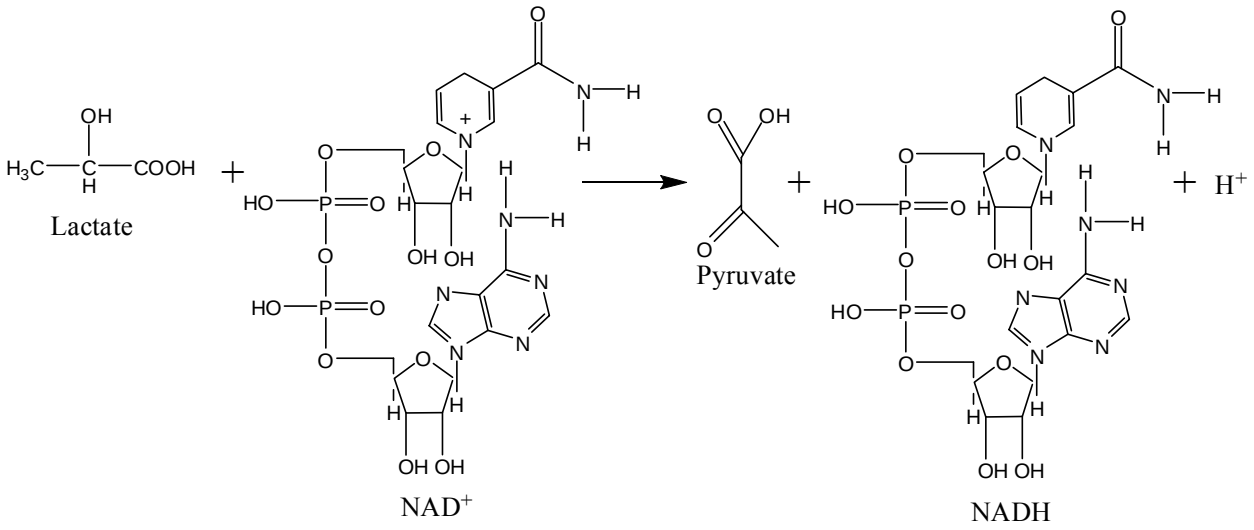

Figure 5-1. The first step in the reaction between lactate from the LDH enzyme and NAD^+ in the MTS cytotoxicity assay used for these studies.[99, 140]

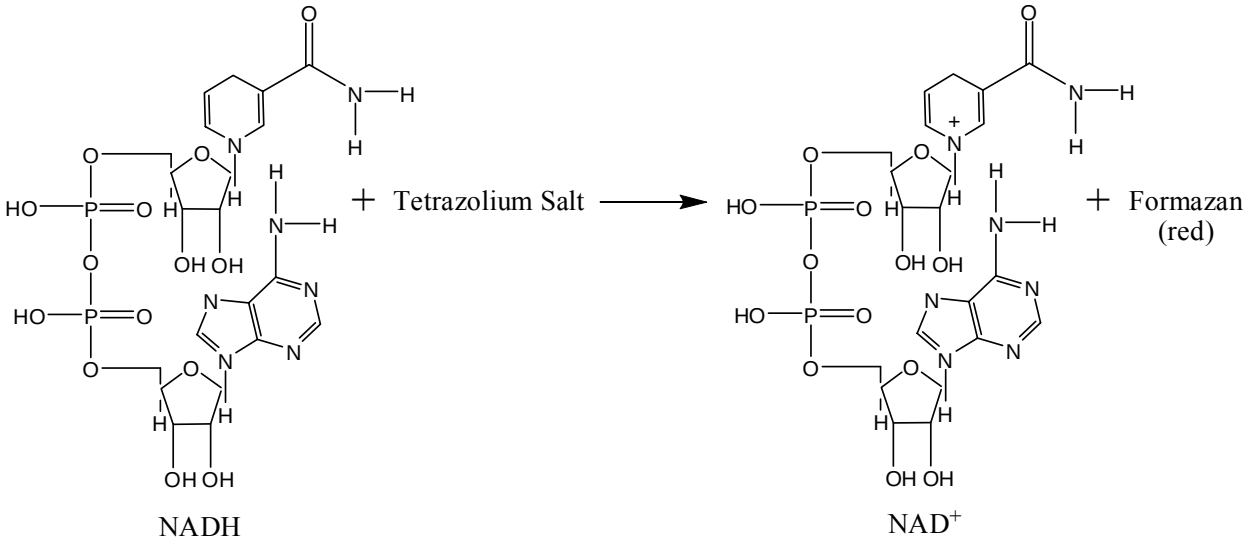

Figure 5-2. The second and final step in the MTS assay used for these studies where NADH reacts with the tetrazolium salt to produce NAD^+ and a red formazan dye.

Culture. The mLLC cells were cultured in 75cm^2 cell culture flasks with 20mL of treated media. The cells were incubated at 37ºC in humidified air with 5% carbon dioxide for at least 24 hours. After 24 hours, the cells were monitored daily until the cells reached 95% confluency. The cells were then trypsinized and counted to determine the cell density. If the cell density was below a concentration of 1 x 10^4 cells/mL, the cells were split and re-cultured until the cell

density was between 1 x 10^4 cells/mL and 1 x 10^5 cells/mL. The cell suspension was then used to seed the corresponding 96-well plates used for this study.

Cell seeding. A cell density of 9.3 x 10^4 cells/mL was obtained and 20µL of the acquired cell suspension were added to specified wells in five separate 96-well plates. The mLLC cells were seeded at a concentration of 1,860 cells/well which is consistent with cell seeding densities reported in the literature for the time frame used in this study.[141, 142] Six well plates were used for this study representing the one control plate used to measure the absorbance of treatment groups in the absence of cells and the five treatment plates for the following time points: hours 1, 2, and 6, and days 1 and 2. The five seeded well plates used to evaluate the cytotoxicity of the treatment groups were incubated at 37ºC in humidified air with 5% carbon dioxide in order to reach adequate attachment for at least 24 hours before adding the first treatment. The media was then removed from the wells and the treatments were added.

Treatment groups. The treatment groups for this study evaluated the cellular viability of mLLC cells exposed to free MXN and DNA-MXN-MS doses of 1µg/mL, 10µg/mL, and 25µg/mL and blank DNA-MS at a concentration of 100µg. Each treatment group was sterilized prior to cytotoxicity analysis. DNA-MXN-MS and blank DNA-MS were sterile rinsed with 70% ethanol, vortexed on high for 30 seconds, and centrifuged at 3,000rpm for 5 minutes. They were then collected by decanting the ethanol and allowed to air dry over night in a sterilized hood. The sterilized MS were then resuspended in treated media to a concentration of 2,000µg/mL and added to designated cells using appropriate volumes to reach desired treatment group concentrations. For the DNA-MXN-MS conditions, 4µL of the MS/media suspension were added for the1µg/mL treatment group, 39µL were added for the 10µg/mL treatment group, and 96µmL were added for the 25µg/mL treatment group. For the 100µg blank DNA-MS treatment

condition, 50μL of the MS/media suspension were added to specified wells. For the free MXN conditions, a stock 0.0001% MXN in treated media solution was prepared and sterilized using a 0.22μm sterile syringe filter. The sterile 0.0001% MXN stock solution was then added to specified wells. One microliter was added for the 1μg/mL treatment condition, 10μL were added for the 10μg/mL treatment condition, and 25μL were added for the 25μg/mL treatment condition. The treated wells were then filled with treated media to a total volume of 100μL.

There were three control groups used in this study which consisted of 1) treated media in the absence of cells, 2) treated media with cells, 3) treatment groups in treated media in the absence of cells. Absorbance values taken of the media and treatment groups in the absence of cells were used to correct cytotoxicity data obtained in the study. All control and treatment conditions were evaluated in replicates of six. All cellular viability data collected was statistically analyzed using SigmaStat 3.0 Software.

Results and Discussion

Particle Analysis

Percent yield

The percent yield and theoretical yield values for the DNA-MXN-MS prepared at the 20%M_{EQ}, 50% M_{EQ}, and 120%M_{EQ} crosslink concentrations were calculated using Equations 5-2 and 5-3. Each of the three crosslink conditions tested produced good yield and theoretical yield values of over 60%. Three batches were prepared for each condition to determine the batch-to-batch consistency at each condition. The 120%M_{EQ} crosslink concentration condition produced the smallest yield and theoretical yield standard deviations indicating that it generated the most consistent and reproducible processing condition, Table 5-1. It was also noted that the batch-to-batch consistency increased as the crosslink concentration increased suggesting that DNA-MXN-MS synthesis parameters become more stable and reproducible as the crosslink concentration is

increased. This may be attributed to more uniform or homogenous crosslinking of the DNA-MXN-MS.

Table 5-1. Yield and theoretical yield values for DNA-MXN-MS prepared at the 20%M_{EQ}, 50%M_{EQ}, and 120%M_{EQ} crosslink conditions.

Crosslink concentration condition	Yield (%)	Theoretical yield (%)
20%M_{EQ}	69 ± 12	61 ± 11
50%M_{EQ}	84 ± 9	76 ± 8
120%M_{EQ}	83 ± 3	75 ± 4

The 50% M_{EQ} and 120%M_{EQ} crosslink conditions produced the highest yield and theoretical yield values of over 80% and 75%, respectively; however, statistical analysis found no significant differences in yield values among all three crosslink conditions. The yield and theoretical yields values are depicted graphically in Figures 5-3 and 5-4.

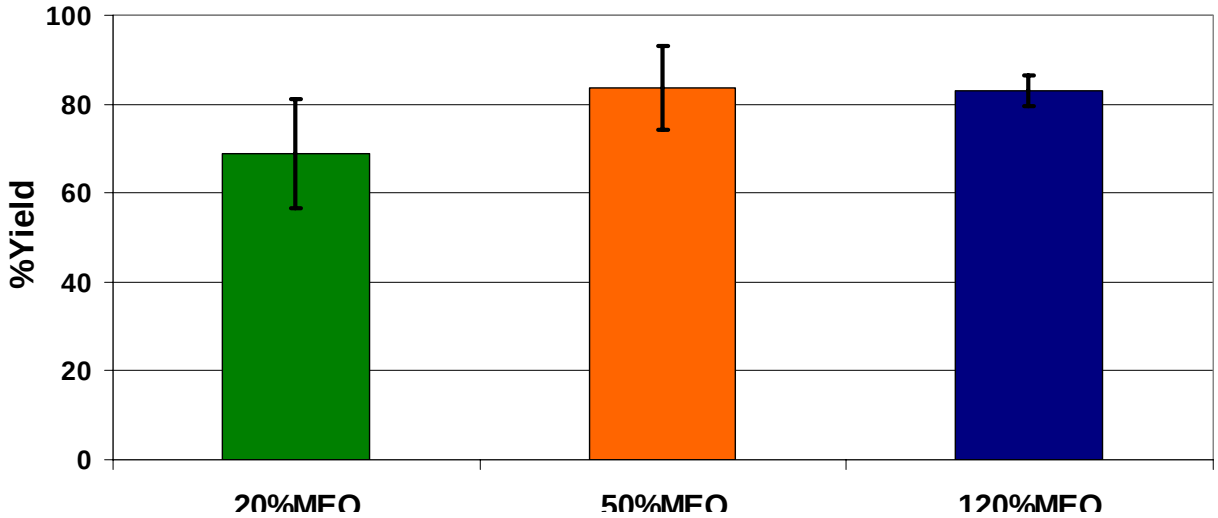

Figure 5-3. Yield values for DNA-MXN-MS prepared at the 20%M_{EQ}, 50%M_{EQ}, and 120%M_{EQ} crosslink conditions.

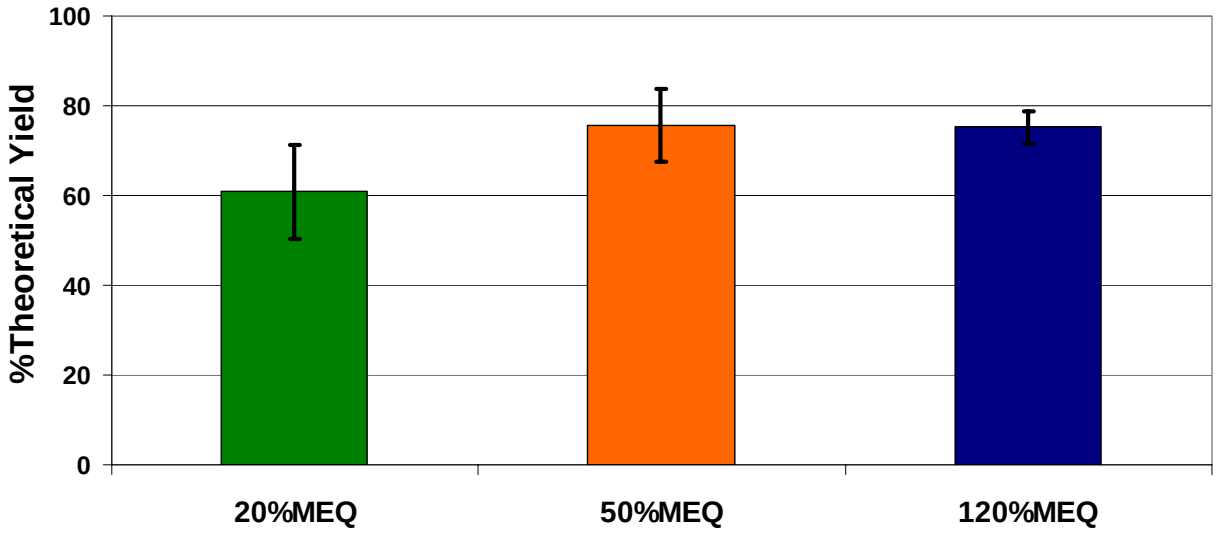

Figure 5-4. Theoretical yield values include the weight of the *in situ* loaded MXN for DNA-MXN-MS prepared at the 20%M_{EQ}, 50%M_{EQ}, and 120%M_{EQ} crosslink conditions.

The yield values of blank DNA-MS were compared to the theoretical yield values of DNA-MXN-MS for further comparisons, Figure 5-5. Graphical representation of the yields illustrated no significant differences between blank and MXN-loaded DNA-MS indicating that the *in situ* loading of MXN did not affect the yield values.

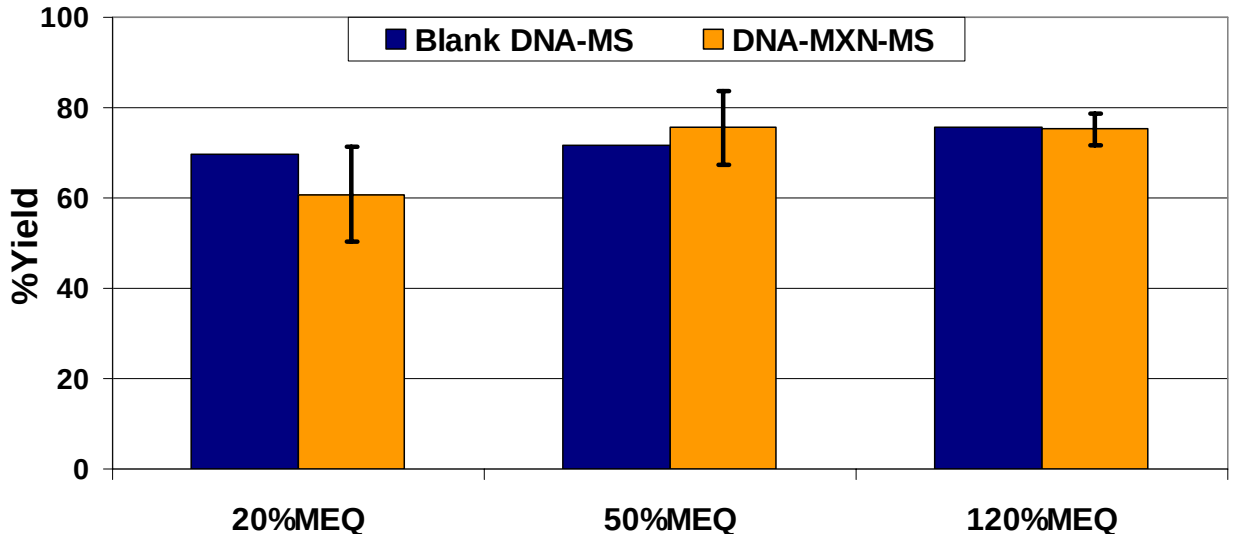

Figure 5-5. Graphical comparison of blank DNA-MS yield and DNA-MXN-MS theoretical yield values.

Dry particle size

The dry particle diameters and size distributions of the DNA-MXN-MS were obtained in methanol. DNA-MXN-MS prepared at the 120%M_{EQ} crosslink condition produced the most narrow size distributions with mean diameters of 2.1µm and standard deviations of 2.8µm, Figure 5-6. These findings are consistent with data obtained in the Mixer Study in Chapter 4 which demonstrated that the 120%M_{EQ} crosslink condition at the 1550rpm mixer speed produced the most narrow and normalized particle size distribution.

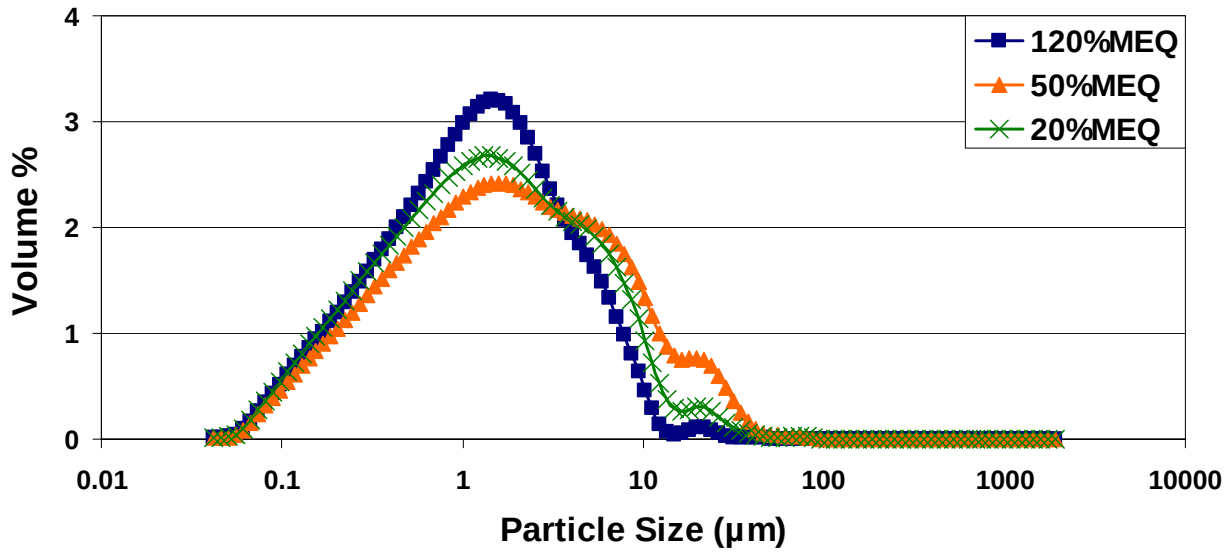

Figure 5-6. A dry particle size distribution comparison of DNA-MXN-MS synthesized at varying crosslink concentrations.

Each crosslink condition produced mean diameter values of less than 5µm with narrow and fairly normalized particle size distributions, Table 5-2. These findings are also consistent with previous data obtained in Chapter 4 which indicated that particle size distributions normalize as stir speed is increased due to the high shear forces that reduce aggregate formation during synthesis and produce smaller diameter particles.[11, 57, 107, 130, 135] A one way ANOVA illustrated no significant mean diameter size differences among each condition tested. This is also consistent with current literature which states that crosslink concentration or density does not

affect yielding particle size values.[11, 57, 132, 143, 144] The collected data also illustrated that the 120%M_{EQ} crosslink concentration produced the largest percentage of particles in the mesosphere size range and the lowest percentage of particles with diameters greater than 10μm.

Table 5-2. Dry mean particle diameter and size range values for DNA-MXN-MS.

Crosslink concentration condition	DNA-MXN-MS dry mean particle diameter (μm)	DNA-MXN-MS in 1μm to 10μm size range (%)	DNA-MXN-MS larger than 10μm (%)
20%M_{EQ}	2.9 ± 4.8	55	4
50%M_{EQ}	4.2 ± 6.4	55	10
120%M_{EQ}	2.1 ± 2.8	61	1

The dry mean diameter values for DNA-MXN-MS were compared to dry mean diameter values obtained in Chapter 4 for blank DNA-MS, to determine if MXN *in situ* loading affects MS particle diameter values or size distributions, Table 5-3. A one way ANOVA followed by a Tukey's test for multiple comparisons illustrated a significant difference between the mean dry diameter values of DNA-MXN-MS and blank DNA-MS at the 20%M_{EQ} crosslink condition ($p = 0.023$). This difference in size was mainly attributed to aggregates that formed during the synthesis of blank DNA-MS at the 20%M_{EQ} crosslink concentration condition. Thus the data obtained from the statistical analysis indicated that the *in situ* loading of MXN did not affect the particle diameter of resulting DNA-MXN-MS. This data reflects previous research and current literature which state that the incorporation of MXN does not affect resulting albumin, gelatin, chitosan, and gelatin-carboxymethyl cellulose blended MS diameter values.[11, 57, 143, 145] Mean dry particle diameter values for DNA-MXN-MS and blank DNA-MS for each crosslink condition are given in Table 5-3 and graphical comparisons are given in Figures 5-7 to 5-9.

Table 5-3. Dry mean particle diameter values for DNA-MXN-MS and blank DNA-MS.

Crosslink concentration condition	DNA-MXN-MS dry mean particle diameter (μm)	Blank DNA-MS dry mean particle diameter (μm)
20%M_{EQ}	2.9 ± 4.8	17.9 ± 21.9
50%M_{EQ}	4.2 ± 6.4	3.3 ± 3.7
120%M_{EQ}	2.1 ± 2.8	2.2 ± 2.1

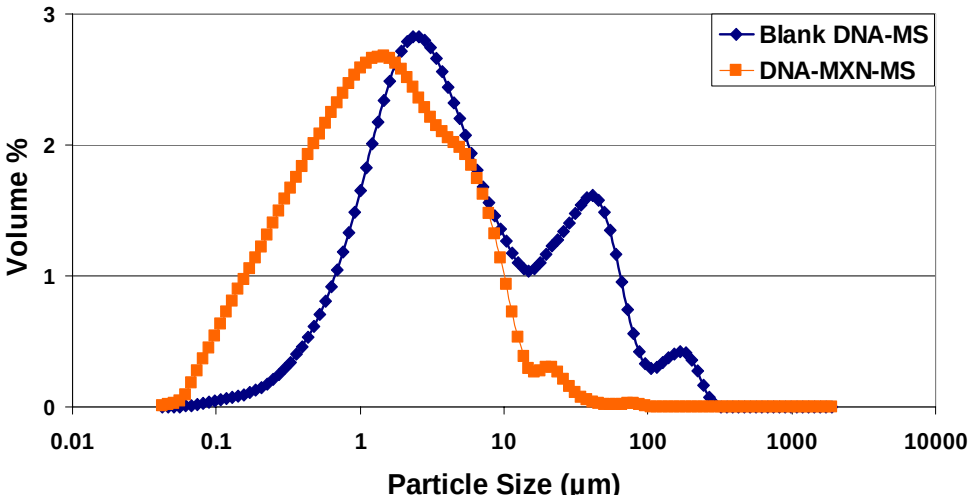

Figure 5-7. A comparison of DNA-MXN-MS and blank DNA-MS dry particle size distributions at the 20%M_{EQ} crosslink condition.

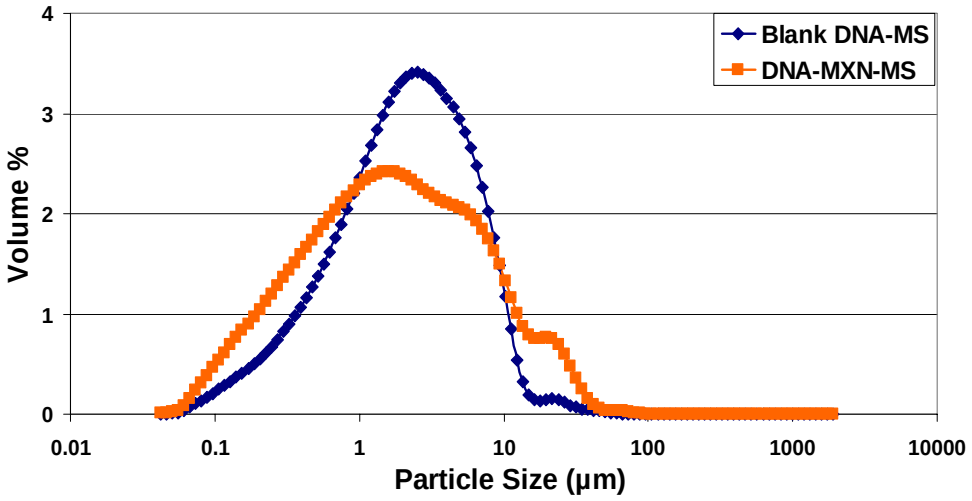

Figure 5-8. A comparison of DNA-MXN-MS and blank DNA-MS dry particle size distributions at the 50%M_{EQ} crosslink condition.

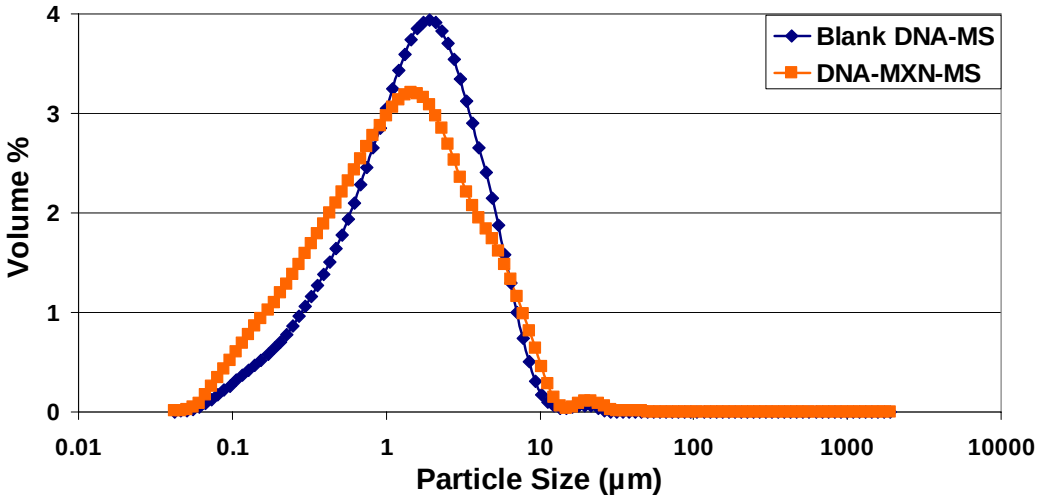

Figure 5-9. A comparison of DNA-MXN-MS and blank DNA-MS dry particle size distributions at the 120%M_{EQ} crosslink density condition.

Hydrated particle size

DNA-MXN-MS hydrated particle diameters and size distributions were obtained in 0.05M PBS at a pH of 7.4. DNA-MXN-MS prepared at the 50%M_{EQ} and 120%M_{EQ} crosslink concentration conditions displayed excellent dispersion behavior in PBS and exhibited hydrated diameters of less than 20µm. DNA-MXN-MS prepared at the 20%M_{EQ} condition gelled together and aggregated upon exposure to PBS and thus were unable to undergo hydrated particle size analysis. A t-test illustrated no significant differences between the hydrated diameter values for the 50%M_{EQ} and 120%M_{EQ} crosslink conditions, suggesting that the crosslink concentration did not influence particle swelling. This finding was supported by the narrow hydrated particle size distributions each condition produced with most of the swollen particle diameters falling within the 5µm to 20µm range, Figure 5-10. These results are contradictory to what is currently found in the literature which states that the swelling properties of particles and films are restricted by increasing the crosslink concentration or density.[57, 137, 146] Thus it would be expected that the DNA-MXN-MS prepared at the 120%M_{EQ} crosslink concentration would exhibit smaller

hydrated particle sizes than particles prepared at the lower crosslink concentrations. These findings suggest that maximum crosslinking occurs at 50%M_{EQ}.

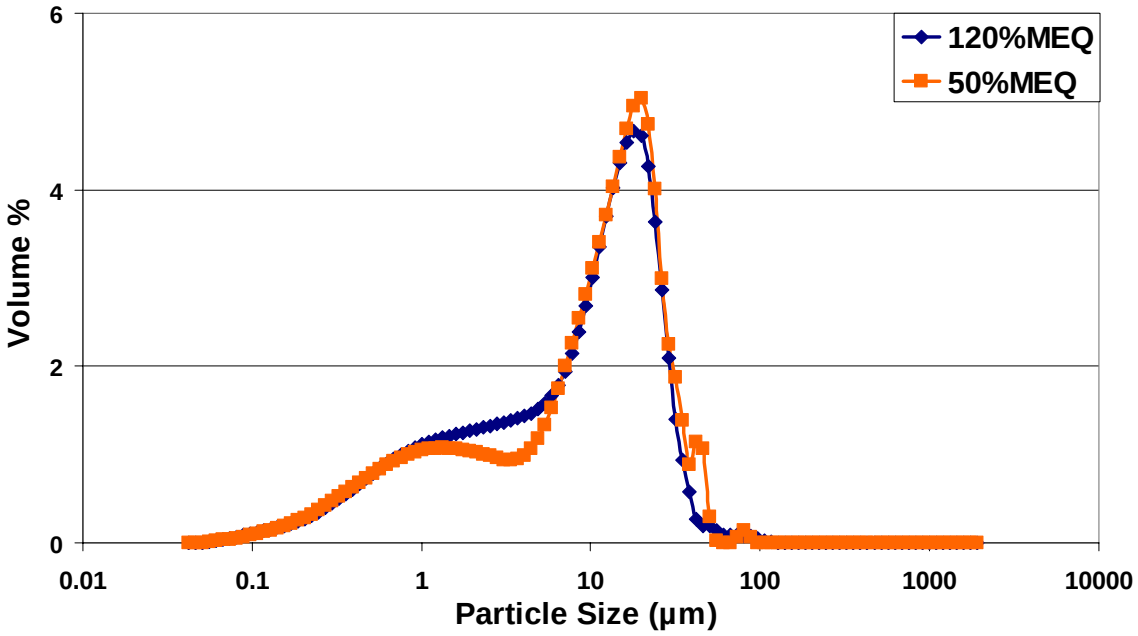

Figure 5-10. Hydrated particle size distributions for DNA-MXN-MS prepared at the 50%M_{EQ} and 120%M_{EQ} crosslink density conditions.

DNA-MXN-MS were further characterized by comparing the hydrated size distributions to the dry size distributions, Figures 5-11 and 5-12. Both conditions produced distributions that peaked at about the 20µm particle size. The swelling properties at each DNA-MXN-MS crosslink concentration were then measured by comparing the hydrated mean particle sizes to the dry mean particle sizes. These values were used to calculate the percent change in size using Equation 5-4. Calculated values illustrated that the DNA-MXN-MS prepared at the 50%M_{EQ} and 120%M_{EQ} crosslink conditions exhibited a 200% and 450% increase in size, Table 5-4.

Table 5-4. Mean dry and hydrated particle diameters with percent change in size due to swelling.

Crosslink concentration condition	Mean dry particle diameter µm)	Mean hydrated particle diameter (µm)	Percent change in size (%)
50%M_{EQ}	4.2 ± 6.4	12.8 ± 11.1	(+) 200
120%M_{EQ}	2.1 ± 2.8	11.5 ± 10.4	(+) 450

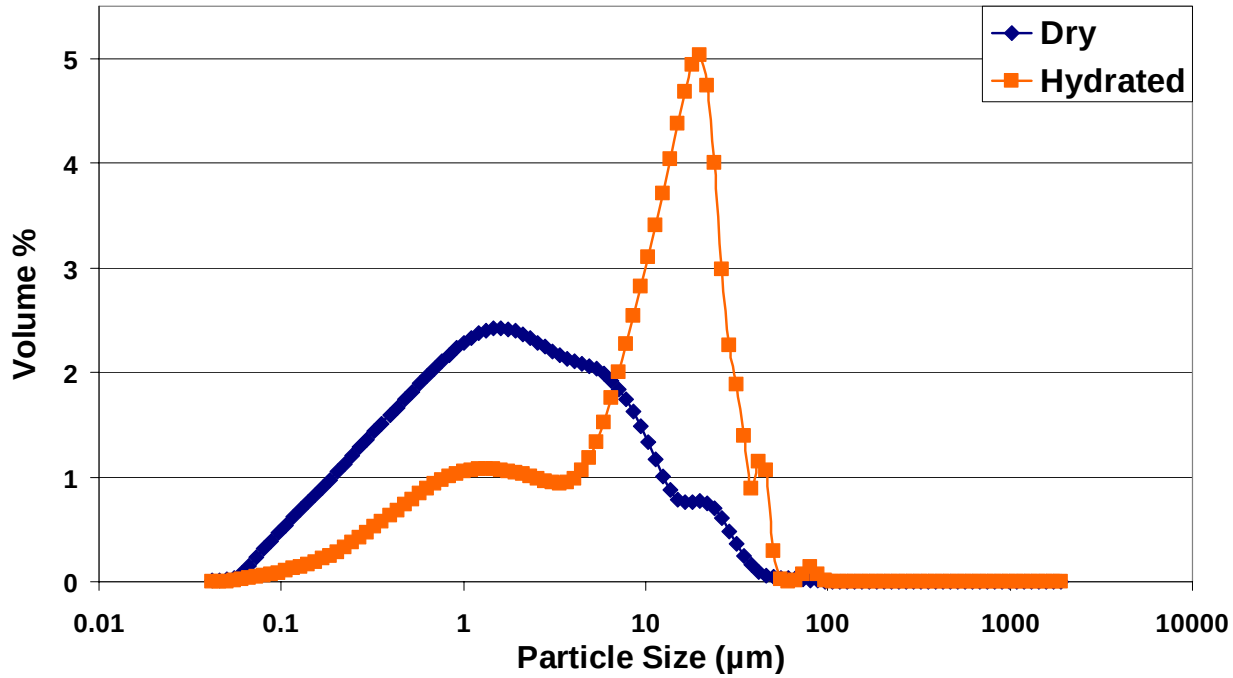

Figure 5-11. A dry and hydrated particle size distribution comparison of DNA-MXN-MS at the 50%M_{EQ} crosslink condition.

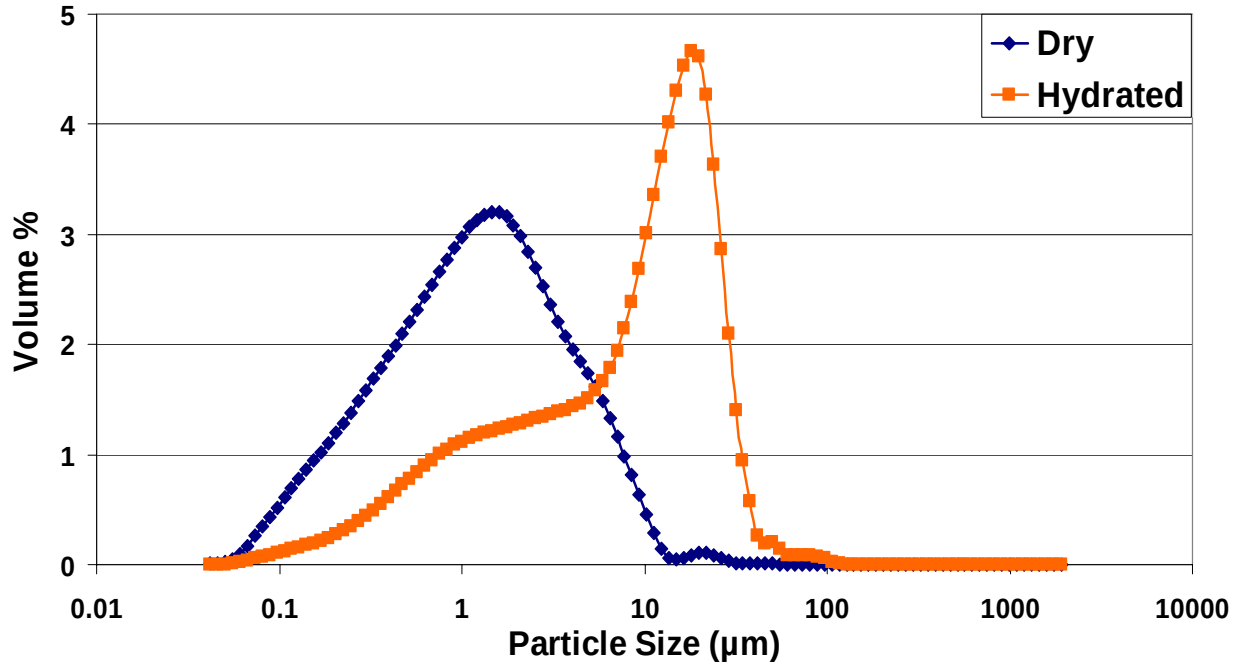

Figure 5-12. A dry and hydrated particle size distribution comparison of DNA-MXN-MS at the 120%M_{EQ} crosslink condition.

Surface charge analysis

The effect of *in situ* MXN loading on yielding DNA-MXN-MS surface charge was measured in 0.01M PBS at a pH of 7.4. Zeta potential values for DNA-MXN-MS illustrated over a 40% decrease indicating the successful loading of the cationic drug MXN, Table 5-5. Zeta potential values for DNA-MXN-MS ranged from -13.2mV to -28.3mV which was a decrease from the -46.3mV to -55.2mV values obtained for blank DNA-MS prepared with the same conditions. T-tests conducted on the zeta potential values obtained for DNA-MXN-MS and blank DNA-MS at each crosslink concentration illustrated that the incorporation of the cationic MXN significantly decreased the surface charge of the DNA-MS ($p < 0.001$), Figures 5-13 to 5-15. These findings are consistent to trends found in current literature which state that the charge of a particle will change upon the loading of a cationic or anionic drug.[10, 147, 148]

Table 5-5. Zeta potential values for DNA-MXN-MS and blank DNA-MS with their respective change in surface charge.

Crosslink concentration condition	Zeta potential for DNA-MXN-MS (mV)	Zeta potential for blank DNA-MS (mV)	Percent change in surface charge (%)
20%M_{EQ}	-13.2 ± 3.7	-46.3 ± 2.4	(-)71
50%M_{EQ}	-28.7 ± 2.1	-48.0 ± 3.4	(-) 40
120%M_{EQ}	-24.2 ± 4.0	-55.2 ± 3.0	(-) 56

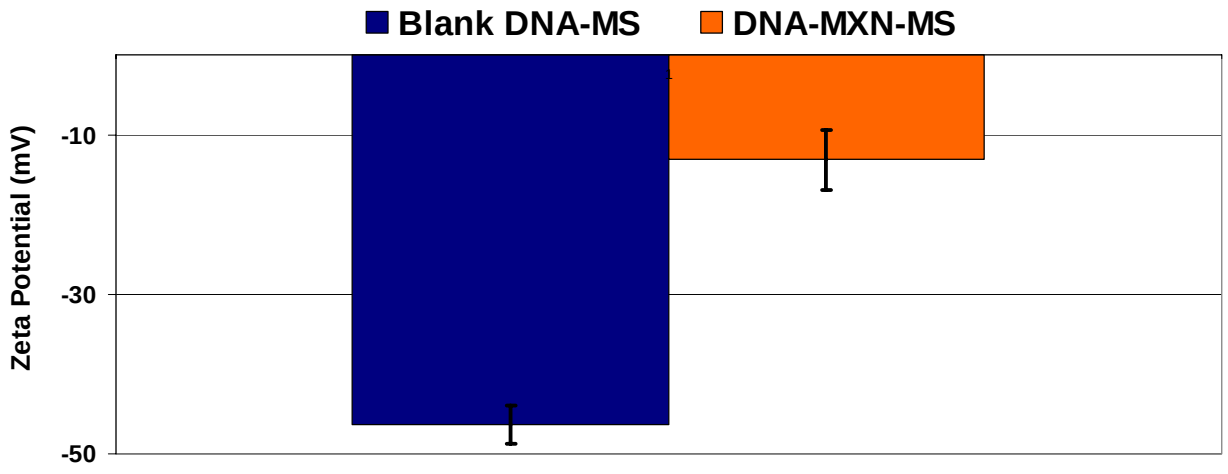

Figure 5-13. A zeta potential comparison of DNA-MXN-MS and blank DNA-MS prepared at the 20%M_{EQ} crosslink condition.

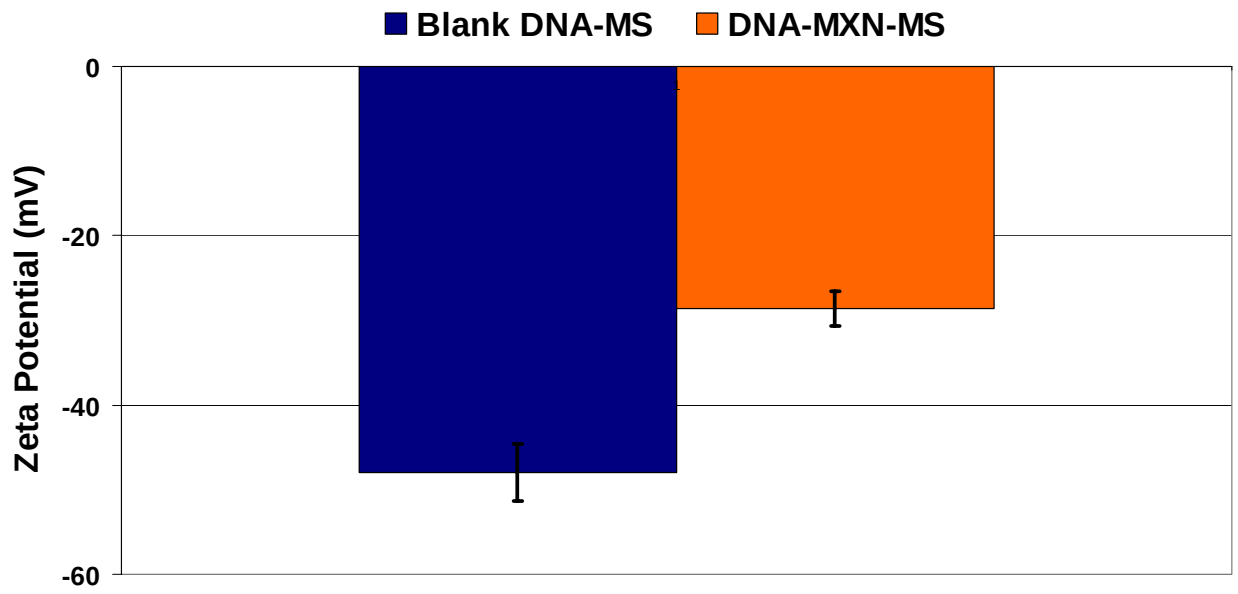

Figure 5-14. A zeta potential comparison of MXN loaded and blank DNA-MS prepared at the 50%M_{EQ} crosslink condition.

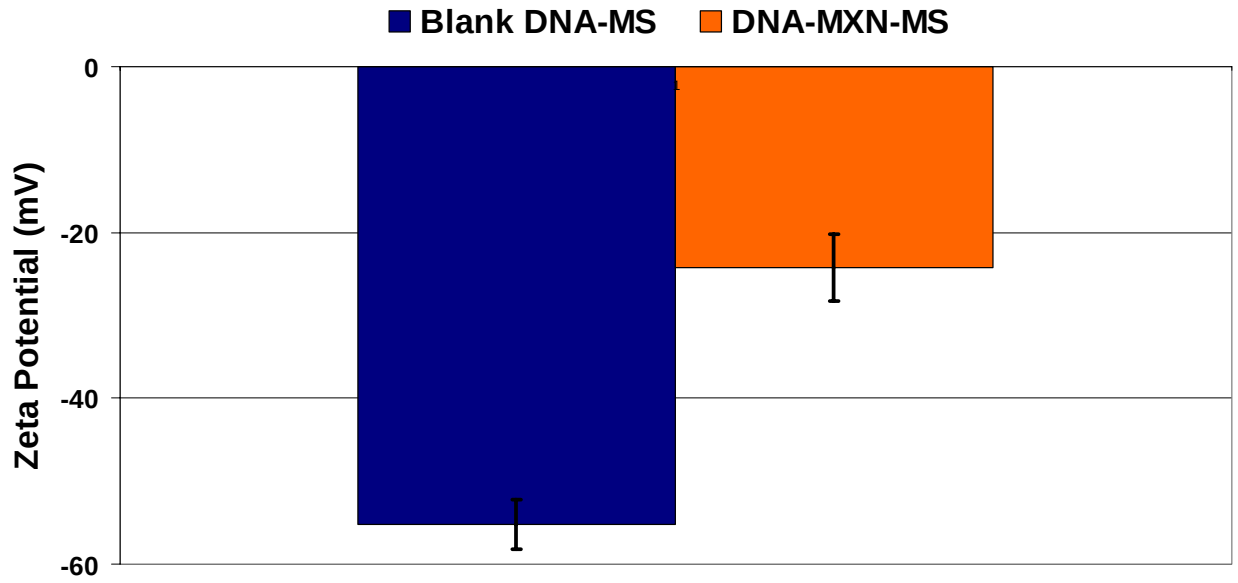

Figure 5-15. A zeta potential comparison of MXN loaded and blank DNA-MS prepared at the 120%M_{EQ} density condition.

A one way ANOVA followed by Tukey's test for multiple comparisons conducted on the zeta potential values obtained for the DNA-MXN-MS conditions illustrated that the zeta potential values for the 20%M_{EQ} crosslink condition were significantly lower than the 50%M_{EQ} and 120%M_{EQ} crosslink conditions ($p < 0.001$), Figure 5-16. A lower zeta potential value

explains why the 20%M_{EQ} condition coagulated once it was introduced to PBS during hydrated particle size analysis. The surface charge of a particle, as measured by zeta potential, determines its colloidal stability by determining its net interparticle forces while in an aqueous dispersion.[149] A particle with a large zeta potential value with have a high magnitude of interparticle repulsive forces leading to a stable dispersion.[107, 149] DNA-MXN-MS prepared at the 20%M_{EQ} condition had a zeta potential value of -13.2mV which was lower than the zeta potential values obtained with the 50%M_{EQ} and 120%M_{EQ} crosslink conditions. Therefore the 20%M_{EQ} crosslink condition was unable to produce sufficient interparticle repulsive forces to create a stable dispersion.

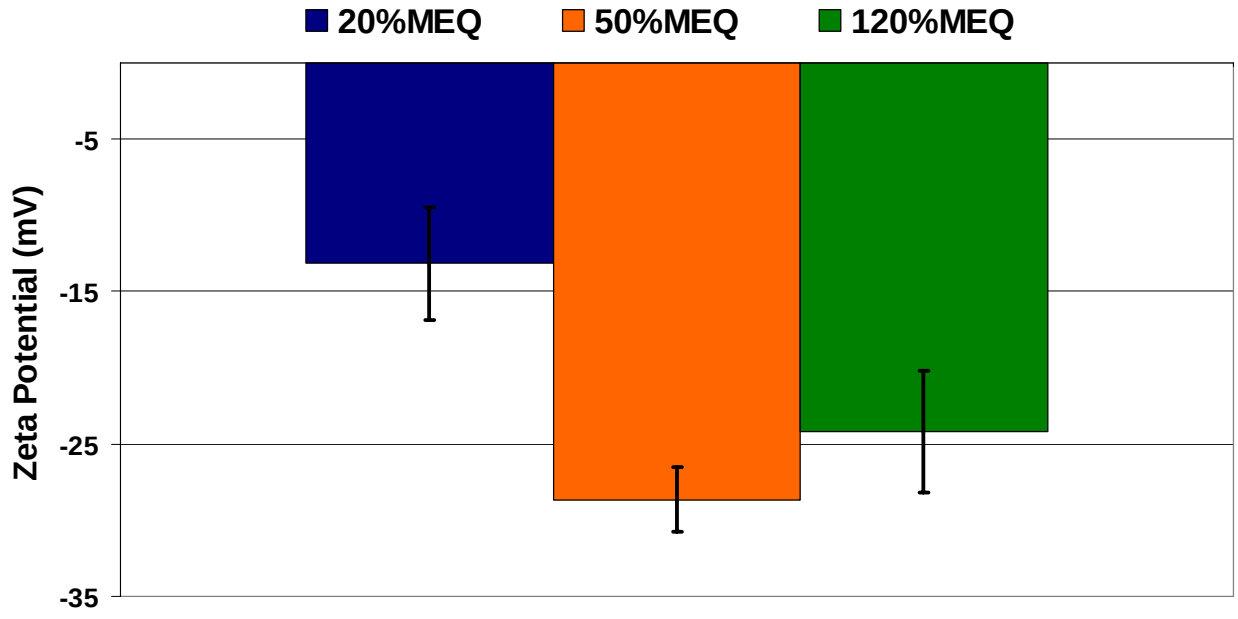

Figure 5-16. Zeta potential values for DNA-MXN-MS prepared at varying crosslink conditions.

Scanning electron microscopy

SEM images confirmed results obtained with dry particle size analysis and depicted particles that were under 5μm and had very narrow size distributions, Figure 5-17. SEM images

also illustrated that the DNA-MXN-MS produced discrete and spherical particles with smooth surface topographies.

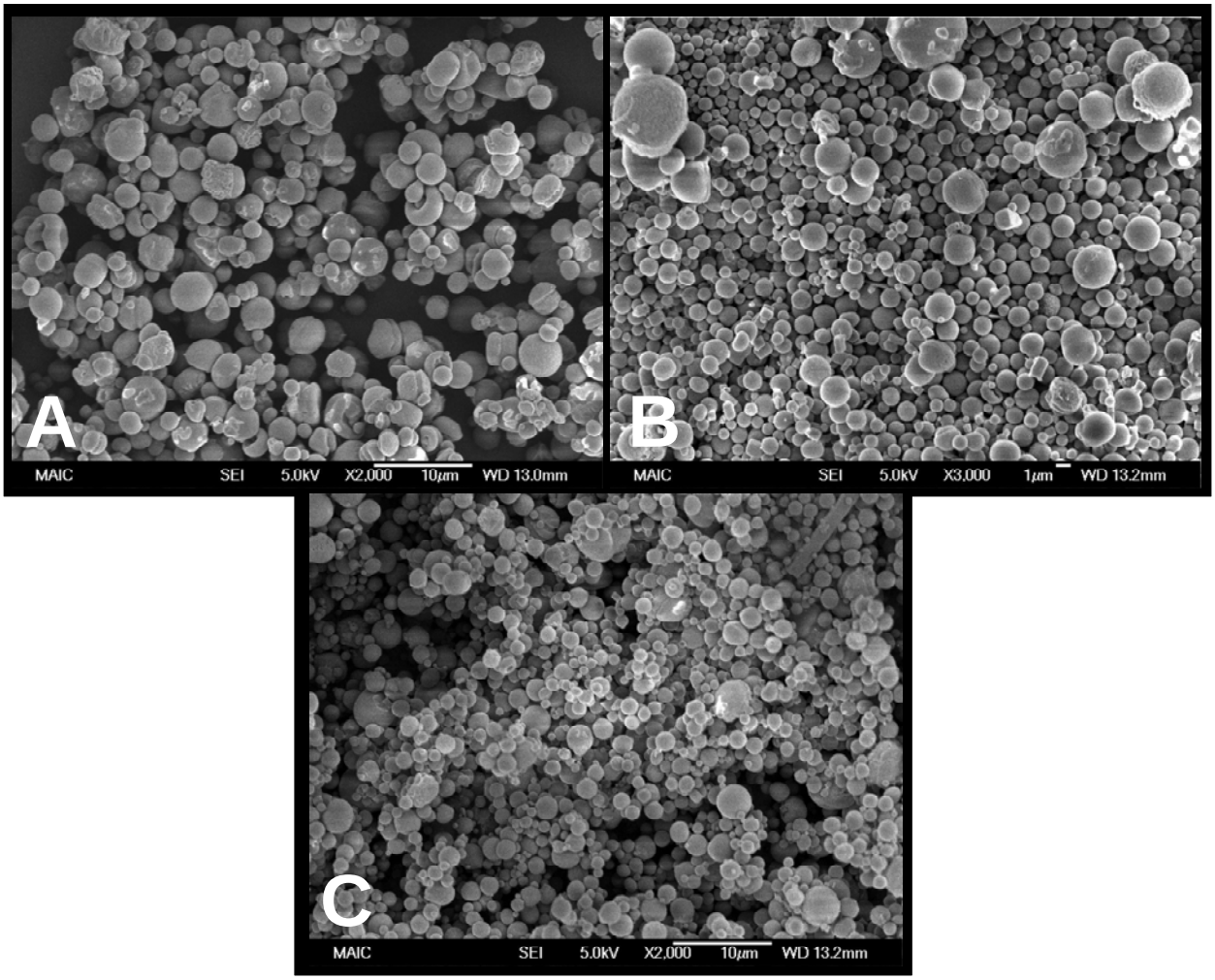

Figure 5-17. Scanning electron micrographs of DNA-MXN-MS prepared at the A) 20%M_{EQ} (Magnification: 2,000x), B) 50%M_{EQ} (Magnification: 3,000x), and C) 120%M_{EQ} crosslink conditions (Magnification: 2,000x).

Energy dispersive x-ray spectroscopy

Elemental analysis by EDS was conducted to confirm the presence of the gadolinium in the DNA-MXN-MS. EDS analysis illustrated that the DNA-MXN-MS followed the same increase in gadolinium peak trends as seen in the crosslink concentration study. DNA-MXN-MS prepared at the 120%M_{EQ} condition produced spectra with higher x-ray counts of gadolinium

and chlorine than seen in the 50%M_{EQ} and 20%M_{EQ} crosslink conditions demonstrating an increase in the crosslink agent concentration at the higher crosslink condition, Figures 5-18 to 5-20.[110]

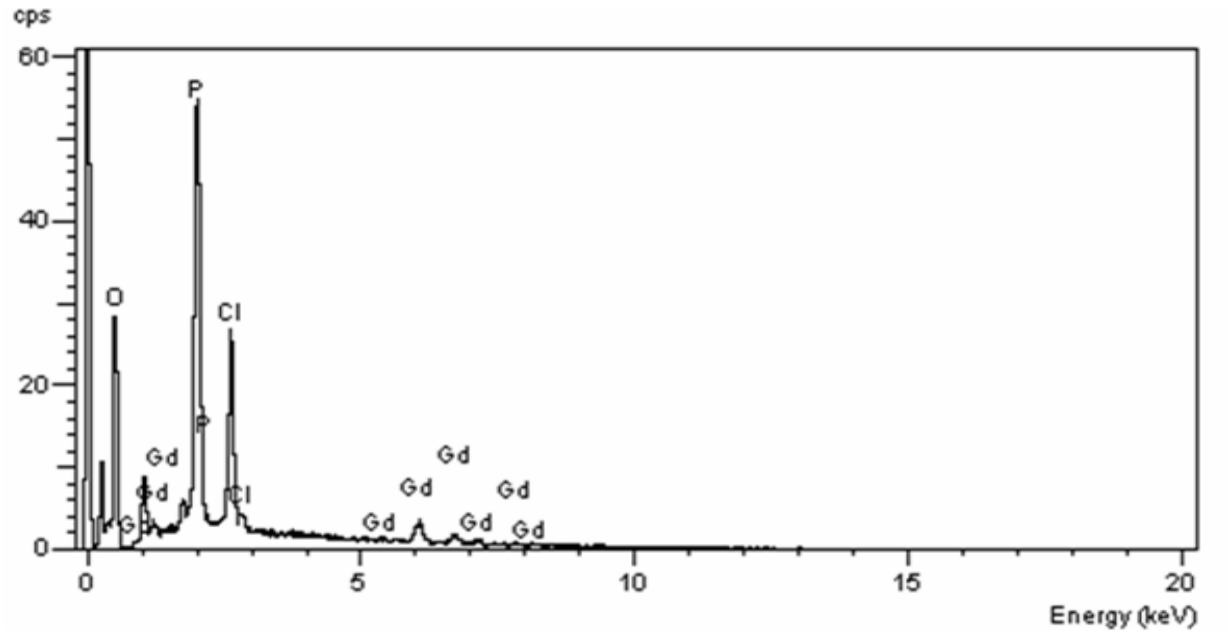

Figure 5-18. EDS spectra of DNA-MXN-MS prepared at the 20%M_{EQ} crosslink condition.

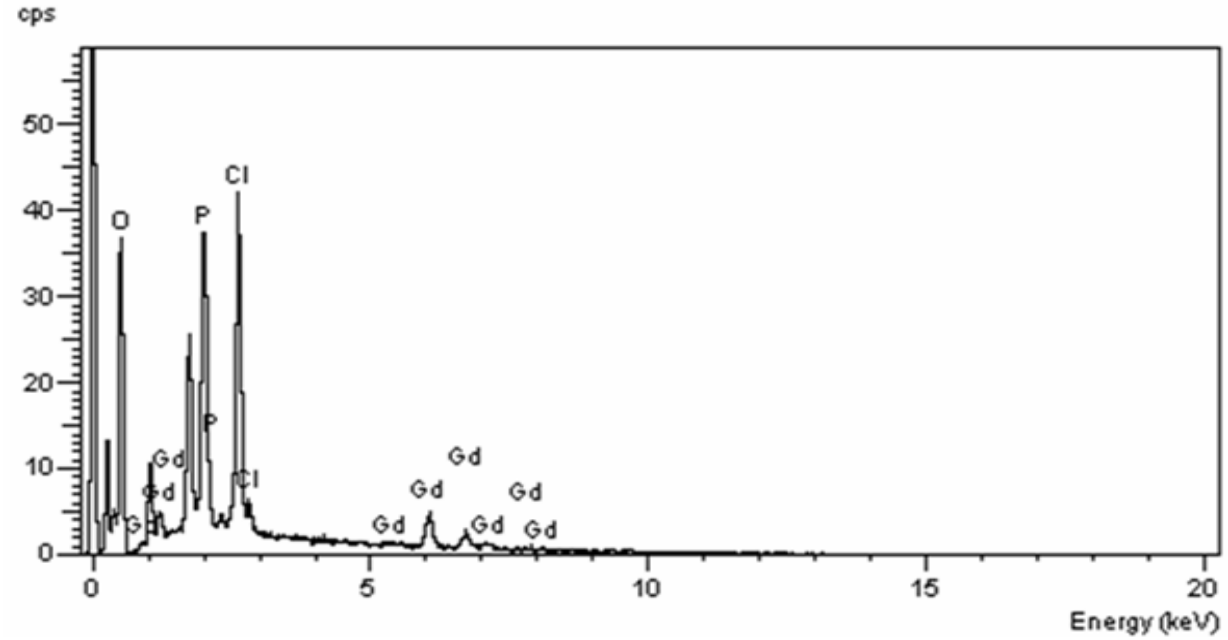

Figure 5-19. EDS spectra of DNA-MXN-MS prepared at the 50%M_{EQ} crosslink condition.

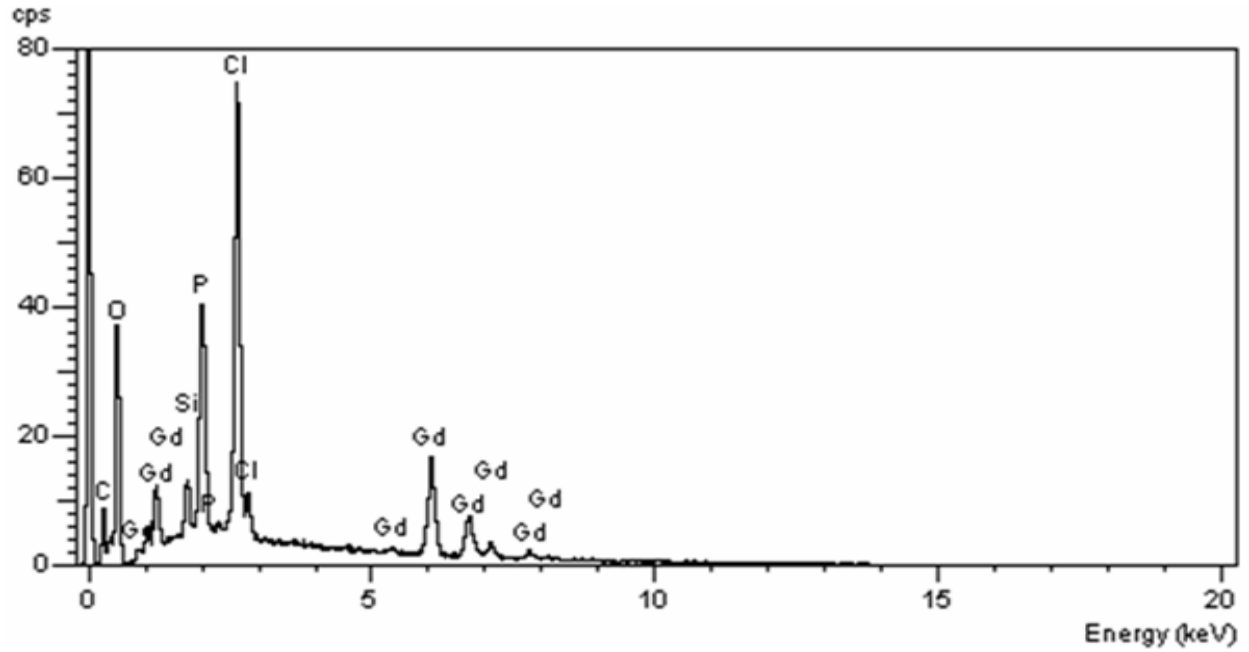

Figure 5-20. EDS spectra of DNA-MXN-MS prepared at the 120%M_{EQ} crosslink condition.

In Vitro DNA-MXN-MS Characterization

MXN loading efficiency

The MXN percent loadings and loading efficiencies of the DNA-MXN-MS crosslink condition were measured in triplicate by enzymatic digestion followed by photometric analysis. MXN loadings were calculated using Equation 5-5 and ranged from 10% (w/v) to 13.5% (w/v) for each of the DNA-MXN-MS crosslink conditions tested, Table 5-6. A one way ANOVA conducted on all DNA-MXN-MS data illustrated that the 50%M_{EQ} crosslink condition loaded a significantly lower amount of MXN than the 20%M_{EQ} condition ($p = 0.021$), but not the 120%M_{EQ} condition, Figure 5-21. MXN loadings for DNA-MXN-MS were also comparable to MXN loadings previously reported for albumin (BSA-MS) and gelatin (GEL-MS) MS.[11, 57] A one way ANOVA conducted on all collected DNA-MXN-MS data and data obtained from previous studies conducted on BSA-MS and GEL-MS showed no significant MXN loading

differences between the 20%M_{EQ} ($p = 0.055$), 50%M_{EQ} ($p = 0.076$), and 120%M_{EQ} ($p = 0.666$) DNA-MXN-MS conditions and the BSA-MS or GEL-MS conditions.

Table 5-6. MXN loading and loading efficiencies for DNA-MXN-MS, BSA-MS, and GEL-MS.

Crosslink concentration condition	MXN loading (%)	MXN loading efficiency (%)
20%M_{EQ}	13.5 ± 0.4	91.2 ± 2.6
50%M_{EQ}	10.4 ± 0.3	71.1 ± 2.3
120%M_{EQ}	12.4 ± 1.7	84.3 ± 11.2
Hadba albumin MS[11]	12.2 ± 0.2	81.3 ± 1.2
Cuevas gelatin MS[57]	11.5 ± 1.3	77 ± 9

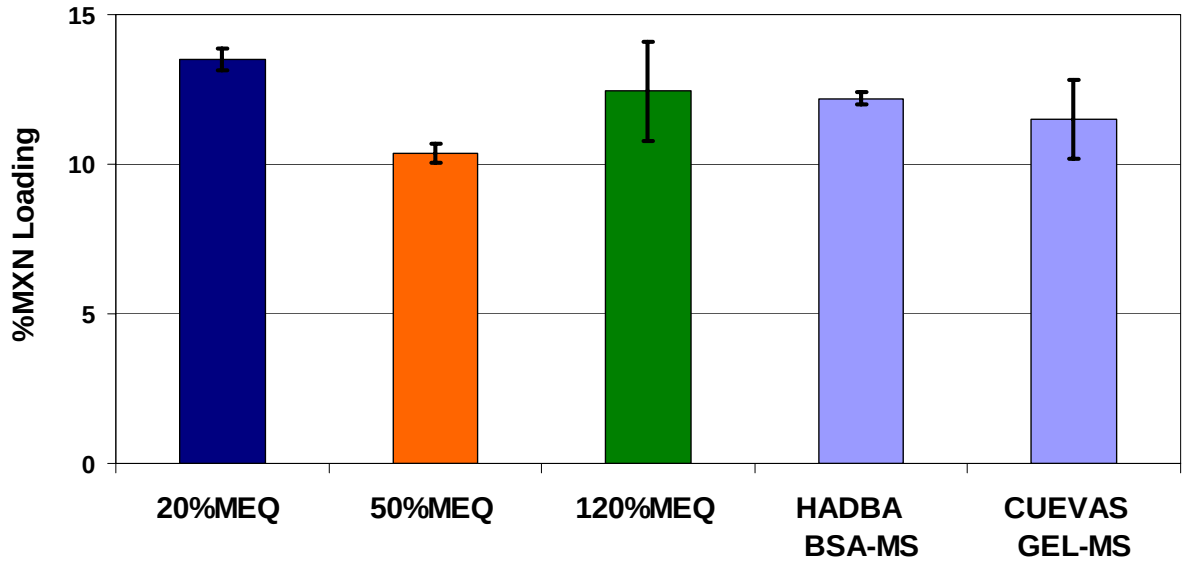

Figure 5-21. Percent MXN loading comparisons of DNA-MXN-MS, BSA-MS, and GEL-MS.

MXN loading efficiencies were calculated using Equation 5-6 and data collected demonstrated that the DNA-MXN-MS produced loading efficiencies of over 70% for all crosslink conditions tested with the 20%M_{EQ} crosslink condition producing the highest loading efficiency with a value of 91%, Table 5-6. This data is contradictory to certain citations in the literature which state that increasing the crosslink concentrations increases drug loading and therefore the loading efficiency in microspheres.[137, 144] Other sources and previous research in this lab have stated that crosslink concentration has no statistically significant effect on the drug loading efficiency of albumin and gelatin microspheres.[11, 57, 143] Results obtained from a one way

ANOVA followed by a Tukey's multiple comparisons test was supported by the latter claim and illustrated that the loading efficiency of the 50%M_{EQ} crosslink condition was significantly lower than the 20%M_{EQ} condition ($p = 0.008$), but not the 120%M_{EQ} condition, indicating no true correlation between crosslink concentration and loading efficiency, Figure 5-22. A one way ANOVA also showed no significant MXN loading efficiency differences between the DNA-MXN-MS and the BSA-MS or GEL-MS.

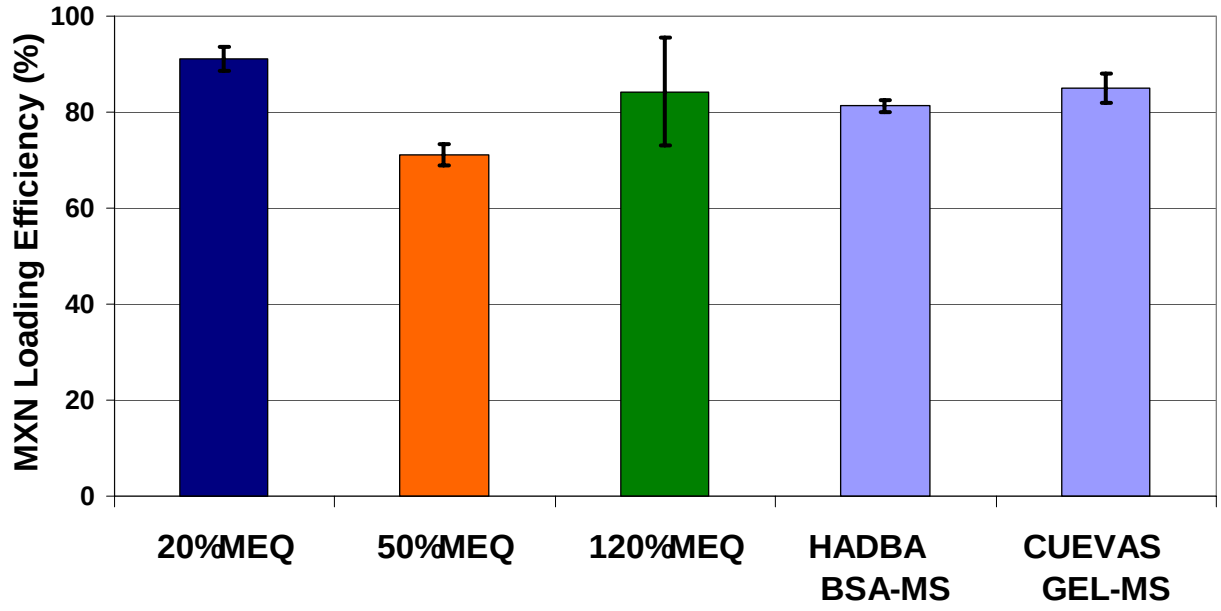

Figure 5-22. MXN loading efficiency comparisons for DNA-MXN-MS, BSA-MS, and GEL-MS.

***In vitro* MXN release**

The *in vitro* MXN release properties of DNA-MXN-MS were measured in 0.05M PBS at a pH of 7.4. The DNA-MXN-MS were tested in triplicate using minimum sink conditions and were incubated in 1.250mL of PBS at 37˚C to simulate the tumor environment. Each DNA-MXN-MS condition tested released over 30% of the entrapped MXN within the first 24 hours producing a "burst effect" as shown in Figure 5-23. DNA-MXN-MS at each crosslink condition continued to release MXN for the next 75 hours; however, a one way ANOVA followed by a

Tukey's multiple comparison test illustrated that the 120%M_{EQ} crosslink condition was the only condition to produce a significant increase in MXN release between Hour 1 and Day 1 ($p = 0.002$), Figure 5-24.

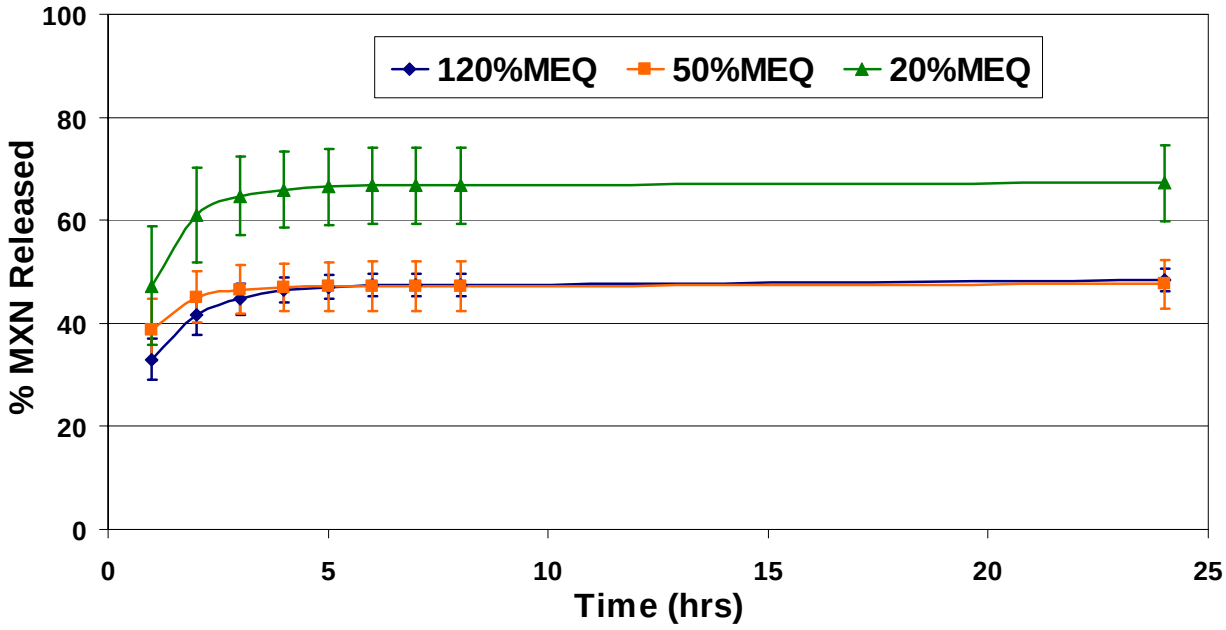

Figure 5-23. First 24 hour MXN release profile for DNA-MXN-MS at varying crosslink concentrations.

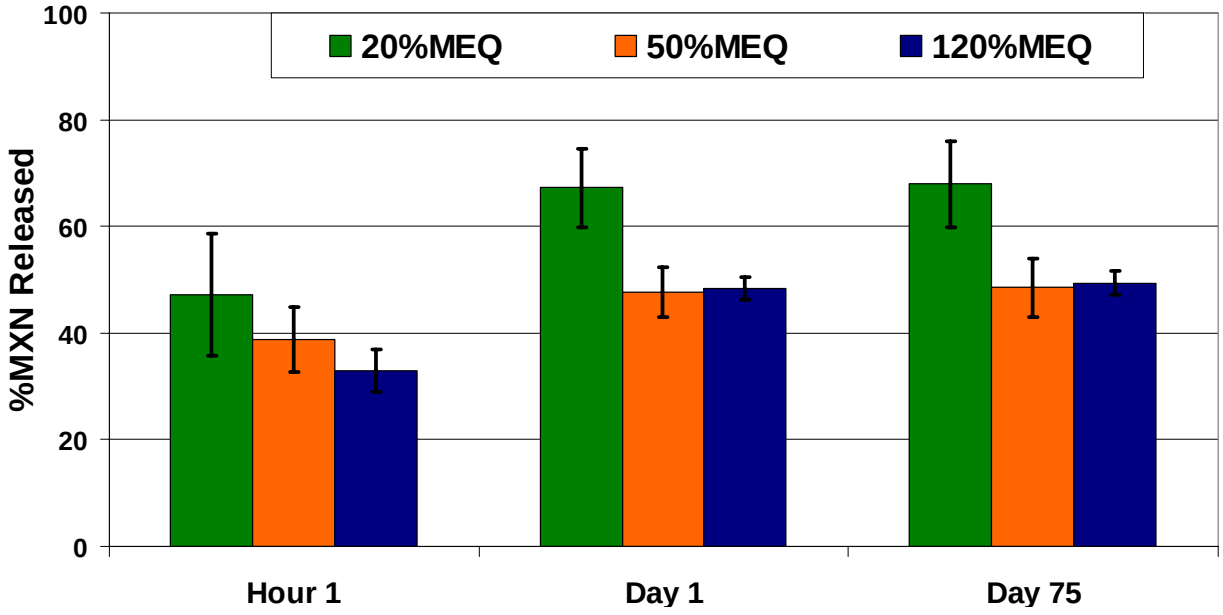

Figure 5-24. MXN release profiles for DNA-MXN-MS at Hour 1, Day 1, and Day 75.

There were no significant increases in MXN release between Day 1 and Day 75 for each DNA-MXN-MS crosslink condition tested suggesting that the loaded MXN is almost fully released within the first 24 hours, Figure 5-25. Previous research conducted on the release of MXN from BSA-MS and GEL-MS also found MXN release to cease within 24 hours.[11, 57] However, it should be noted that the DNA-MXN-MS were not fully degraded by Day 75 and were still blue in color suggesting that the MXN had not fully released. It is assumed that under *in vivo* conditions, the MXN release profiles would differ due to naturally occurring digestive enzymes in the body which may facilitate in the release of MXN past Day 1.

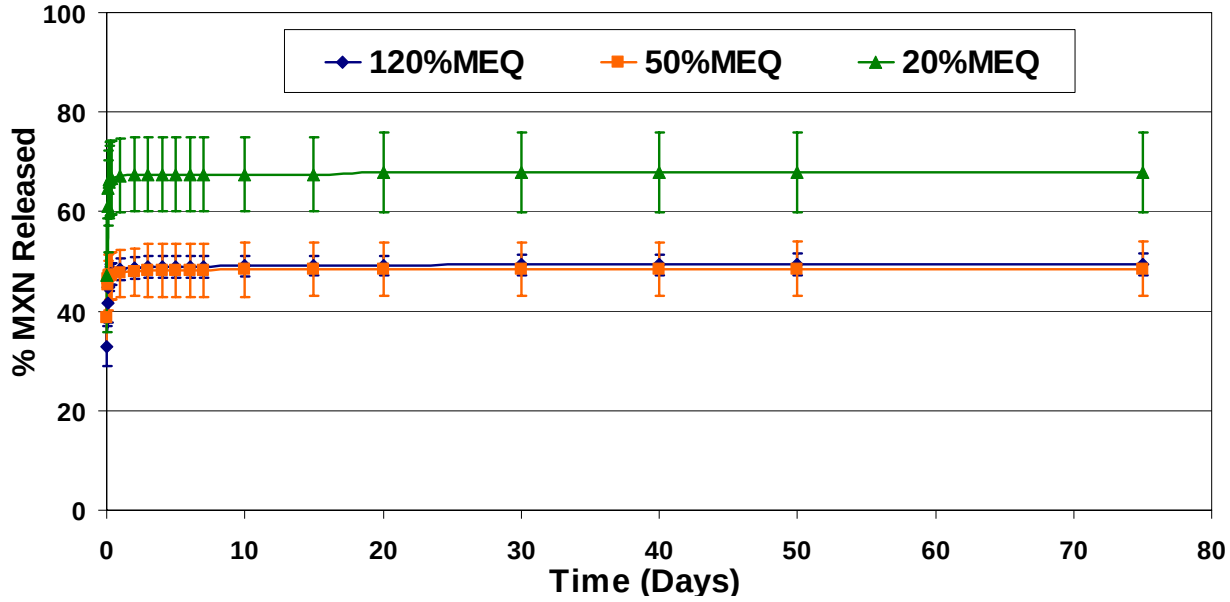

Figure 5-25. Total MXN release profile for varying crosslink DNA-MXN-MS conditions.

Further statistical analysis using a one way ANOVA followed by a Tukey's test for multiple comparisons illustrated that the 20%M_{EQ} crosslink condition released significantly more MXN than the 50%M_{EQ} ($p = 0.030$) and the 120%M_{EQ} ($p = 0.040$) crosslink conditions. These findings are also consistent with previous research and current literature which state that increasing the crosslink concentration or density of a drug carrier will decrease or decelerate its drug release.[10, 11, 57, 145, 146, 150-152] Drug release is diffusion driven and is dependent on the

swelling properties and biodegradation of the MS carrier.[67, 153] MS carriers with high swelling properties will allow the aqueous environment to penetrate the MS thus releasing the drug from the matrix quicker, Figure 5-26. Higher swelling properties also enable the MS carrier to solubilize or biodegrade more rapidly within the aqueous media. Therefore, swelling and biodegradation are reduced by increases in crosslink concentration, and thus it would be expected that the 20%M_{EQ} crosslink condition would release MXN faster than the 50%M_{EQ} and 120%M_{EQ} crosslink concentration conditions.[133, 144, 154]

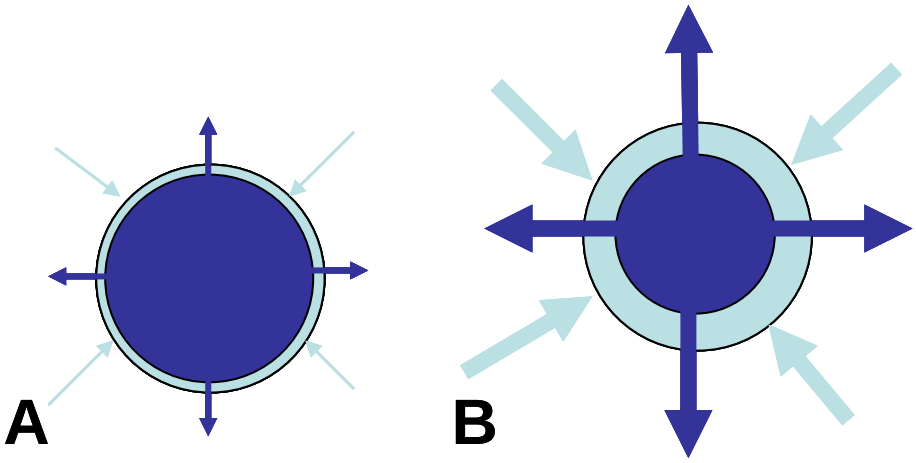

Figure 5-26. Schematic representation of crosslink concentration on drug release, A) high crosslink and B) low crosslink conditions.

Assessment of DNA-MXN-MS cytotoxicity

The cytotoxicity of DNA-MXN-MS on mLLC cells in culture was tested on Hour 1 and Days 1 through 4 using an MTS cytotoxicity assay. An increase in absorbance at 490nm indicated increased cell death. Each condition was tested in replicates of 6 at DNA-MXN-MS and free MXN doses of 1µg/mL, 10µg/mL, and 25µg/mL and DNA-MS concentration of 100µg. Data obtained from the MTS assay was statistically analyzed using a one way ANOVA followed by a Tukey's test for multiple comparisons. Cytotoxicity data obtained illustrated that the 25µg/mL DNA-MXN-MS condition produced the most cytotoxic response on the mLLC cells as

compared to the media with cells control by Day 4 ($p < 0.001$), Figure 5-27. Additionally, there were no significant differences in cytotoxicity responses among the 25µg/mL, 10µg/mL, and 1µg/mL conditions at Day 4.

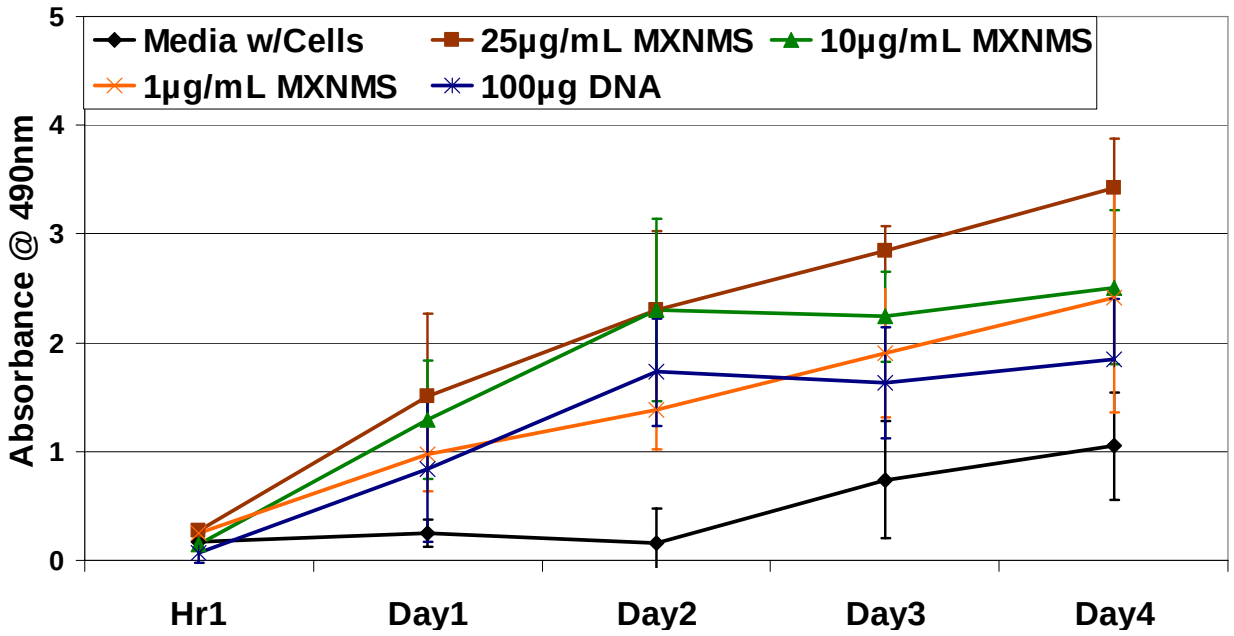

Figure 5-27. *In vitro* cytotoxicity profiles of DNA-MXN-MS and DNA-MS on mLLC cells.

There were no significant differences in cytotoxicity at Hour 1 between the control and DNA-MXN-MS dose conditions, however, by Day 1, cytotoxic responses were observed for the 10µg/mL ($p = 0.021$) and 25µg/mL ($p = 0.004$) DNA-MXN-MS dose conditions. The 1µg/mL DNA-MXN-MS dose did not elicit a cytotoxic response until Day 2 ($p < 0.001$) illustrating the cytotoxicity of the mLLC cells was dose dependent. Similar MXN dose responses on the *in vitro* viability of rat glioma, human myeloid leukemia, B-chronic lymphocytic leukemia and breast cancer cells have been reported in the literature.[13, 57, 155-157] The 100µg DNA-MS elicited similar cytotoxicity responses up to Day 2; however, by Day 3 and 4, there were no significant differences between this condition and the media with cells control. These results are consistent with fibroblast growth data obtained in the blank DNA-MS study which illustrated that cell

growth decreased upon addition of treatment, however, once the culture environment stabilized, cell growth increased and produced no significant growth differences as compared to the media with cells control.

Free MXN dose conditions exhibited similar trends as the DNA-MXN-MS dose conditions, however, by Day 4, a significant cytotoxicity response was found only for the 25µg/mL free MXN condition ($p = 0.023$) as compared to the media with cells control condition, Figure 5-28.

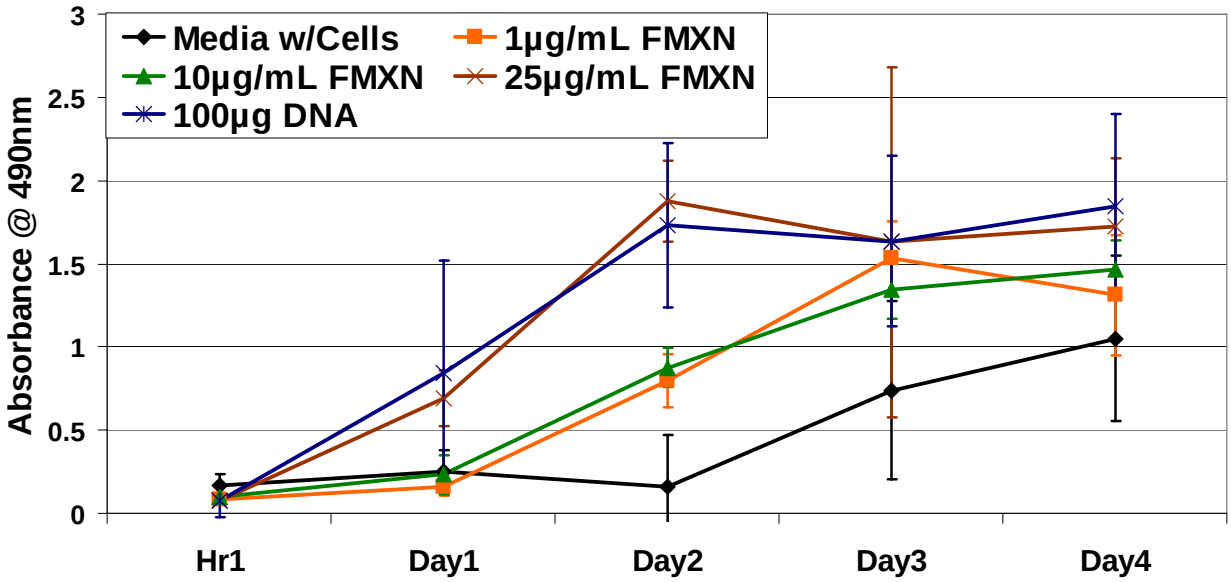

Figure 5-28. Cytotoxicity profiles for free MXN dose conditions.

Further data analysis also indicated that DNA-MXN-MS conditions elicited significantly higher cytotoxicities than the free MXN conditions at each dose tested ($p < 0.05$). This data suggested one of two things: 1) gadolinium crosslinked DNA contributes to the *in vitro* cytotoxicity of DNA-MXN-MS or 2) DNA-MXN-MS are more readily taken up by the mLLC cells than free MXN.

Conclusions

The objectives of these studies were to prepare MXN *in situ* loaded DNA-MS with narrow and controlled size distributions where 60% of all particles prepared were within the mesosphere size range of 1μm to 10μm and < 5% of all particles were greater than 10μm in size. Particles less than 1μm in diameter were also acceptable and hydrated particle diameters were to be less than 25μm. In addition, MXN *in situ* loaded DNA-MS were sought to obtain loadings of ≥ 12% (w/w) MXN and release MXN for 24 hours or more in phosphate buffered saline under minimum sink conditions. DNA-MXN-MS at MXN concentrations of 1μg/mL, 10μg/mL, and 25μg/mL were also sought to elicit a cytotoxic response ≥ to that of free drug at the same MXN concentrations on murine Lewis lung carcinoma (mLLC) cells in culture.

DNA-MXN-MS were prepared with three different crosslink concentrations to also determine the effect of crosslink concentration on MXN loading and release. The resulting DNA-MXN-MS were characterized by yield, particle size, elemental analysis, surface topography and morphology. DNA-MXN-MS also were evaluated *in vitro* for MXN loading, loading efficiency, release, and cytotoxicity on mLLC cells.

Particle Analysis

DNA-MXN-MS were prepared with good yields of over 60%, with narrow and controlled dry and hydrated size distributions. Resulting DNA-MXN-MS also produced discreet and spherical particles with smooth surface topographies. EDS analysis confirmed the presence of gadolinium in each of the DNA-MXN-MS crosslink concentration conditions tested, with the 120%M_{EQ} condition producing the largest counts of both gadolinium and chlorine.

DNA-MXN-MS prepared with the 120%M_{EQ} crosslink concentration produced the best dry and hydrated particle sizes with a dry mean diameter of 2.1μm, a hydrated mean diameter of 11.5μm, 61% of all particles within the mesosphere size range, 1% of all particles greater than

10μm, and were readily dispersible and stable in PBS. The 20%M_{EQ} crosslink concentration produced the least favorable DNA-MXN-MS conditions by coagulating immediately after being dispersed into PBS. A one way ANOVA illustrated no significant differences between the hydrated diameters for the 50%M_{EQ} and 120%M_{EQ} crosslink concentrations suggesting that maximum crosslinking may be achieved at the 50%M_{EQ} concentration.

***In Vitro* MXN Loading and Release**

Zeta potential analysis confirmed the loading of the cationic drug MXN into each of the three DNA-MXN-MS crosslink concentration conditions tested by producing a significant increase in DNA-MS surface charge ($p < 0.001$). MXN loadings ranging from 10.4% to 13.5% and loading efficiencies ranging from 70% to 91% at each of the DNA-MXN-MS crosslink conditions tested were found to be statistically comparable to those obtained with BSA-MS or GEL-MS. MXN release was measured up to 75 days for each DNA-MXN-MS crosslink concentration condition tested; however, each condition produced a "drug burst" release within the first 24 hours. The 20%M_{EQ} crosslink concentration condition produced the highest release of the three conditions tested; however, the 120%M_{EQ} crosslink concentration which was the only condition to produce a significant increase in release between Day 1 and Day 75.

***In Vitro* Cytotoxicity Analysis**

Data obtained from the cytotoxicity analysis concluded that the *in vitro* viability of mLLC cells was dose dependent. The 10μg/mL and 25μg/mL DNA-MXN-MS dose conditions exhibited cytotoxicity responses by Day 1; however, the 1μg/mL DNA-MXN-MS dose did not elicit a cytotoxic response until Day 2. Free MXN dose conditions exhibited similar trends as the DNA-MXN-MS dose conditions. Cytotoxicity data also concluded that by Day 4, a significant cytotoxicity response was found only for the 25μg/mL free MXN and DNA-MXN-MS conditions.

Additionally, the DNA-MXN-MS conditions elicited significantly higher cytotoxicities than the free MXN conditions at each dose tested suggesting one of two things: 1) gadolinium crosslinked DNA contributes to the *in vitro* cytotoxicity of DNA-MXN-MS or 2) DNA-MXN-MS are more readily taken up by the mLLC cells than free MXN.

CHAPTER 6
IN VITRO EVALUATIONS OF DRUG LOADED DNA AND BSA NANO-MESO-MICROSPHERES

Introduction

Deoxyribonucleic acid (DNA) and bovine serum albumin (BSA) nano-meso-microspheres (MS) were *in situ* loaded with methotrexate (MTX) and 5-fluorouracil (5-FU) using optimized DNA-MS synthesis conditions presented in Chapter 4 to further analyze the drug loading capabilities of DNA and BSA. MTX and 5-FU *in situ* loaded DNA-MS and BSA-MS were synthesized to produce particles with controlled size distributions where at least 60% of all particles prepared were within the mesosphere size range of 1μm to 10μm and < 5% of all particles were greater than 10μm in size. Particles less than 1μm in diameter were also acceptable and hydrated particle diameters were to be less than 25μm. In addition, DNA-MS and BSA-MS were sought to obtain drug loadings of ≥ 5% (w/w) MTX or 5-FU and release drug for more than 24 hours in phosphate buffered saline under minimum sink conditions. Drug loaded BSA-MS and DNA-MS were compared with respect to particle diameter, size distribution, morphology, topography, drug loading, and percent drug release.

Mitoxantrone (MXN) *in situ* loaded DNA-MS were also prepared to determine the maximum drug loading ability of DNA. DNA-MXN-MS were prepared with a 120%M_{EQ} gadolinium crosslink concentration and were loaded with 10% (w/w), 15% (w/w), and 25% (w/w) MXN. The particle diameter, size distribution, morphology, topography, drug loading, and percent drug release of the DNA-MXN-MS were evaluated with respect to MXN concentration. DNA-MXN-MS were also prepared with no gadolinium crosslinking to determine if MXN serves as a crosslinking agent to DNA-MS. DNA-MXN-MS were prepared to obtain *in situ* MXN loadings of ≥ 10% (w/w). The DNA-MXN-MS were characterized as mentioned above and compared with respect to crosslinking.

The particle diameters and size distributions were obtained using an LS Coulter 13 320 particle size analyzer. The particle morphologies and topographies were assessed using a field emission scanning electron microscope. Drug loading was determined by incubating the drug loaded MS under stirred conditions in an enzymatic digestion buffer at 37ºC for 48 hours. The released drug concentrations were then analyzed using UV-visible spectroscopy against a MTX, 5-FU, or MXN standard curve. The percent drug release was measured under minimum sink conditions in order to simulate the tumor environment. Drug release data was obtained by incubating the drug loaded MS in phosphate buffered saline under constant agitation at 37ºC for a minimum of fourteen days in triplicate. At specific time points, aliquots were taken and measured using UV-visible spectroscopy against a MTX, 5-FU, or MXN standard curve to determine drug concentration.

Materials and Methods

Materials

DNA sodium salt derived from herring testes Type XIV, albumin from bovine serum (BSA), cellulose acetate butyrate, HPLC grade 1,2-dichloroethane, methanol, gadolinium (III) chloride hexahydrate, 25% (w/w) Grade II aqueous glutaraldehyde solution, mitoxantrone dihydrochloride, methotrexate hydrate, 5-fluorouracil, L-cysteine hydrochloride hydrate, papain from papaya latex, deoxyribonuclease I from bovine pancreas, proteinase from Bacillus licheniformis, ethylenediaminetetraacetic acid disodium salt dihydrate (EDTA), and trichloroacetic acid were purchased from the Sigma-Aldrich Company. Sodium phosphate monobasic monohydrate, sodium phosphate dibasic anhydrous, and sodium chloride, each A.C.S. certified, acetone, 70µm Spectra/Mesh Nylon filters, 16x125mm and 13x100mm borosilicate glass test tubes, Ultrafree-CL with Durapore Membrane Centrifugal Filter tubes (0.1µm pore, 2mL), Corning sterile 0.45µm pore filter bottles, Fisherbrand Semimicro

methacrylate 1.5mL disposable cuvettes, and 15mL and 50mL polypropylene centrifuge tubes were purchased from Fisher Scientific International. Type I and Type II deionized ultrapure water was prepared with a resistivity of at least 16 MΩ-cm^{-1} using the Barnstead NANOpure Ultrapure Water System in the lab.

Methods

Solution preparation

MTX and 5-FU *in situ* loaded DNA and BSA. MTX and 5-FU were *in situ* loaded into 5% (w/v) aqueous solutions of DNA or BSA at concentrations of 15% (w/w) and 30% (w/w). Aqueous DNA and BSA solutions were prepared at room temperature by adding 0.5g of DNA or 0.5g of BSA to 5mL of ultrapure water in a 50mL polypropylene centrifuge tube. The solutions were then mixed on a vortex for 30 seconds. Three milliliters of ultrapure water were then added to the DNA or BSA solutions and placed on the rotary shaker for at least two hours until the DNA or BSA had completely dissolved. The volume was then brought up to 10mL and vortexed on high for 30 seconds. The DNA or BSA solution was then placed in the refrigerator over night to ensure the complete collapse of bubbles generated during vortex and rotary mixing. The percent solid concentration of the DNA or BSA solution was quantified using a Metler LJ16 Moisture Analyzer at 130ºC for 60 minutes. Once the concentration was determined, 3.5mL of the DNA or BSA solution was placed into a 15mL polypropylene centrifuge tube. Using the true solid weight of DNA or BSA in solution obtained during moisture analysis, the weight of the MTX or 5-FU, XgDrug, needed to obtain 15% (w/w) or 30% (w/w) loadings was calculated by multiplying the true solid DNA or BSA weight in 3.5mL of solution (W_{TSOLID}) by 15 or 30. The product was then divided by 100, Equations 6-1 and 6-2.

$$\text{Xg Drug} = \frac{15\text{g Drug} \times W_{TSOLID}}{100\text{g DNAorBSA}} \qquad (6\text{-}1)$$

$$\text{Xg Drug} = \frac{30\text{g Drug} \times W_{TSOLID}}{100\text{g DNAorBSA}} \quad (6\text{-}2)$$

The desired mass of MTX or 5-FU was weighed and added to the 3.5mL of the DNA or BSA solution. The solutions were then vortexed on high for 30 seconds, placed on the rotary mixer for 2 hours and then placed in the refrigerator until further use.

MXN *in situ* loaded DNA. Based on data obtained in Chapter 5, 15% (w/w) MXN *in situ* loaded DNA solutions were prepared to determine if MXN serves as a crosslinking agent for DNA-MXN-MS. Aqueous DNA solutions were *in situ* loaded as outlined in the Methods Section of Chapter 5.

Aqueous DNA solutions were also *in situ* loaded with 10% (w/w) and 25% (w/w) MXN to determine the maximum drug loading ability of DNA. Aqueous DNA solutions were prepared and the percent solid concentrations were determined as mentioned above. Three and a half milliliters of the DNA solution was then placed into a 15mL polypropylene centrifuge tube and the weight of the MXN, XgMXN, needed to obtain 10% (w/w) or 25% (w/w) loadings was calculated by multiplying the true solid DNA weight, W_{TDNA}, in 3.5mL of solution by 10 or 25, Equations 6-3 and 6-4.

$$\text{Xg MXN} = \frac{10\text{g MXN} \times W_{TDNA}}{100\text{g DNA}} \quad (6\text{-}3)$$

$$\text{Xg MXN} = \frac{25\text{g MXN} \times W_{TDNA}}{100\text{g DNA}} \quad (6\text{-}4)$$

Enzymatic digestion buffers. Enzymatic digestion buffers were used to digest the drug loaded DNA-MS and BSA-MS to determine their drug loadings and loading efficiencies. The DNA enzymatic digestion buffer was prepared by adding 1,800mg of EDTA, 200mg of L-cysteine hydrochloride hydrate, 125mg of papain from papaya latex, and 125mg of

deoxyribonuclease I from bovine pancreas to 250mL of the 0.05M PBS solution (pH = 7.4). The BSA enzymatic digestion buffer was prepared the same way; however, 125mg of proteinase from Bacillus licheniformis was added to the buffer in place of the deoxyribonuclease. The enzymatic digestion buffer components were stirred at room temperature until completely dissolved and used immediately after preparation.

Additional synthesis and characterization solutions. Solutions of cellulose acetate butyrate in 1,2-dichloroethane (CAB) were used as the water-immiscible continuous phase during DNA-MXN-MS synthesis. The CAB solutions were used at a concentration of 5% (w/v). Aqueous solutions of 0.1M gadolinium (III) chloride were used as the ionic crosslinking agent for all DNA-MS syntheses. All BSA-MS syntheses were conducted with covalent crosslinking using aqueous 4% (w/v) glutaraldehyde solutions. Phosphate buffered saline (PBS) solution at a pH of 7.4 and a concentration of 0.05M was used for all *in vitro* drug release analysis. Solutions mentioned here were prepared using the same methods as outlined in Chapter 5.

Synthesis procedure

Drug loaded DNA- MS and BSA-MS were prepared using optimized synthesis conditions from Chapter 4 to obtain particles with particle diameters in the range of 50nm to 10μm and normal and narrow size distributions. A modified emulsion stabilization technique was used that sterically stabilizes the DNA or BSA molecule into spherical conformations and crosslinks them while in suspension. The synthesis process involved dispersing 3mL of the aqueous drug loaded DNA or BSA solutions (i.e. the aqueous phase) into 47mL of the organic CAB solution (i.e. the continuous phase) in a 300mL Labconco lyophilization flask. A DNA-MS or BSA-MS microemulsion was then created by vigorously mixing the two solutions at 1550rpm for 20 minutes at room temperature using a paddle mixer with a two inch, two blade propeller. The DNA-MS microemulsions were then ionically crosslinked while in suspension by

reducing the speed of the paddle mixer to 600rpm and adding 2mL of the 0.1M gadolinium (III) solution to obtain a 120%M_{EQ} crosslink concentration. The BSA-MS were similarly crosslinked, however, 2mL of the 4% (w/v) aqueous glutaraldehyde solution was added. The MS microemulsions then underwent crosslinking for 1 hour and 40 minutes at which time 50mL of acetone was added and any further reactions were allowed to reach completion for another hour. After synthesis was complete, the drug loaded DNA- MS or BSA-MS underwent four rinses in acetone to remove any residual organic phase, crosslinking agent, or non-loaded drug. The MS were rinsed by separating the resultant DNA- MS or BSA-MS suspension into four separate 50mL polypropylene centrifuge tubes. Acetone was added to 40mL and the tubes were capped and vortexed on high for 30 seconds. The MS were then collected by centrifuging the tubes at 2600rpm for 10 minutes and decanting the acetone. Fresh acetone was added again to 40mL mark and the acetone rinse was repeated once more as mentioned above and then twice more by consolidating the contents of 4 tubes to 2 tubes and then 2 tubes to one tube. After the final acetone rinse, the drug loaded DNA-MS were resuspended in 30mL of acetone, vortexed on high for 30 seconds, and filtered using a stainless steel vacuum filtration device with a 70μm Spectra/Mesh Nylon filter. A 70μm Spectra/Mesh Nylon filter was used in place of the 20μm filter to not completely eliminate the possible size effects of drug loadings on the DNA-MS. The device was then rinsed with 10mL of acetone to further filter any remaining DNA-MS under 70μm. The centrifuge tube was then capped, vortexed on high for 30 seconds, and centrifuged at 2600rpm for 5 minutes to collect the drug loaded DNA-MS. The acetone was then decanted and a Kimwipe was secured over the mouth of tube using a rubber band to allow the drug loaded DNA-MS to dry overnight at room temperature. DNA-MXN-MS prepared without crosslinking agent and drug loaded BSA-MS were not filtered. After the final acetone rinse, the acetone was

decanted and a Kimwipe was secured over the mouth of tubes using a rubber band, and the MS were allowed to dry overnight at room temperature.

Particle characterization

Yield analysis. The yields of the resulting drug loaded DNA-MS and BSA-MS were calculated and expressed as percent yield values. The percent yields were calculated by dividing the final weight of the drug loaded DNA- MS and BSA-MS by the amount of weight used to synthesize them, Equation 6-5. The weight of the *in situ* loaded drugs was also added to the equation and expressed as the percent theoretical yield, Equation 6-6. The equations for the percent yield and percent theoretical yield are expressed below where W_F is the final weight of the MS, V, ρ, and C are the volume, density, and concentration of the aqueous DNA or BSA solutions used respectively, W_X is the weight of the crosslinking agent added during synthesis, and W_Y is the theoretical weight of the *in situ* loaded drug.

$$\%\ \text{Yield} = \left(\frac{W_F}{((V \times \rho \times C) + W_X)}\right) \times 100 \qquad (6\text{-}5)$$

$$\%\ \text{Theoretical Yield} = \left(\frac{W_F}{((V \times \rho \times C) + W_X + W_Y)}\right) \times 100 \qquad (6\text{-}6)$$

Dry particle size analysis. Dry drug loaded DNA-MS and BSA-MS particle diameters and size distributions were obtained using a Coulter LS 13 320 particle size analyzer. MS were sonicated for 10 to 30 seconds to aerate and separate the particles prior to analysis and then approximately 2mg of the MS were suspended in 2mL of methanol. The suspension was then sonicated for 30 seconds to further break up any MS aggregates and tested. The Coulter LS 13 320 particle size analyzer was set to run at a pump speed of 73% using a protein/DNA particle diffraction model. Standards were tested in methanol before the first run to ensure that the instrument was performing adequately. Each condition was sampled three times in which each

sample's particle size measurements consisted of two runs. This method of testing produced six independent particle diameters and size distributions. Data collected from these experiments were statistically analyzed using SigmaStat 3.0 software.

Scanning electron microscopy. The morphology and surface topography of the drug loaded DNA-MS and BSA-MS were observed using scanning electron microscopy (SEM). Approximately 1mg of dry MS were mounted onto a small piece of silicon wafer which in turn was mounted onto an aluminum SEM stub using double sided tape. The MS were then coated with gold-palladium for 2 minutes using a Technix Hummer V sputter coater. Images were taken on a JEOL 6335F Field Emission SEM at an accelerating voltage of 5KeV and a working distance of 15mm.

***In vitro* drug evaluation procedures**

MTX, 5-FU, and MXN loading efficiency. The loading efficiencies of the drug loaded DNA-MS and BSA-MS were determined by enzymatic digestion followed by photometric analysis of the recovered entrapped drug. Approximately 5mg of the drug loaded MS were weighed out into labeled 16x125mm glass test tubes and recorded. Ten milliliters of the enzymatic digestion buffer were then added to the MS and the test tubes were capped, parafilmed, and incubated at 37˚C under stirred conditions for 48 hours. The test tubes were then taken out of the incubator and the solutions were allowed to cool to room temperature. While the solutions were cooling, a 10% (w/v) solution of trichloroacetic acid (TCA) in ultrapure water was prepared. Two milliliters of each drug loaded DNA-MS or BSA-MS solution were then placed into labeled 13x100mm glass test tubes. Two milliliters of the 10% (w/v) TCA solution was then added to each sample. The test tubes were capped and the two solutions were allowed to react for 30 minutes at room temperature. The samples were then centrifuged at 2,600rpm for five minutes and the supernatants from each sample were collected into 1.5mL methacrylate

disposable cuvettes for UV-Vis analysis. Each sample was analyzed on a Perkin Elmer Lambda 3 spectrophotometer to determine the concentration of the entrapped drug. MTX samples were analyzed at a wavelength of 308nm against a MTX in 5% (w/v) TCA standard curve with a correlation coefficient of 0.99955. 5-FU samples were analyzed at a wavelength of 269nm against a 5-FU in 5% (w/v) TCA standard curve with a correlation coefficient of 0.99979 and MXN samples were analyzed at a wavelength of 610nm against a MXN in 5% (w/v) TCA standard curve with a correlation coefficient of 0.99966. Concentrations for each of the standard curves ranged from 1μg/mL to 50μg/mL.

The drug concentrations were then used to determine the percent drug loadings in each of the DNA- MS and BSA-MS using Equation 6-7.[137, 138] The loading efficiencies were also calculated using Equation 6-8.[137-139] Each condition was tested in triplicate and all collected data was statistically analyzed using SigmaStat 3.0 software.

$$\%\ \text{Drug Loading} = \left(\frac{\text{Mass of Drug in MS}}{\text{Mass of DNA - MS or BSA - MS}}\right) \times 100 \qquad (6\text{-}7)$$

$$\%\ \text{Loading Efficiency} = \left(\frac{\text{Experimental Loading}}{\text{Theoretical Loading}}\right) \times 100 \qquad (6\text{-}8)$$

***In vitro* MTX, 5-FU, and MXN release.** The *in vitro* release of MTX, 5-FU, and MXN from DNA-MS and BSA-MS under minimum sink conditions was tested in sterile filtered 0.05M PBS at a pH of 7.4. Approximately 2mg of each drug loaded DNA-MS and BSA-MS condition were weighed into labeled 2mL filter centrifuge tubes (0.1μm pore size) to which 1.25mL of the sterile filtered 0.05M PBS solution was added. The tubes were then capped, parafilmed, and incubated at 37˚C under stirred conditions. At specified time points, the filter centrifuge tubes were removed from the incubator and centrifuged for 10 minutes at 3,000rpm. Aliquots were then removed and placed into 1.5mL methacrylate disposable cuvettes for UV-Vis analysis. The

cuvettes were capped, labeled, parafilmed, and stored in the refrigerator until analysis. Each centrifuge filter tube was then replenished with 1.25mL of fresh 0.05M PBS, capped, parafilmed, and placed back into the incubator at which time the incubation process was repeated until the next time point. The aliquots were collected at hours 1-8, days 1-7, and days 10, 15, 20, 30, 40, 50, and 75 for the 10% (w/w), 15% (w/w), and 25% (w/w) DNA-MXN-MS and the 15% (w/w) DNA-MXN-MS prepared without gadolinium crosslinking. Aliquots were also collected at hours 1-8 and days 1, 2, 7, 14, 21, and 35 for the MTX and 5-FU loaded DNA-MS and BSA-MS. The aliquots for each condition were analyzed on a Perkin Elmer Lambda 3 spectrophotometer to determine the drug concentrations at each time point. MTX samples were analyzed at a wavelength of 306nm against a MTX in 0.05M PBS standard curve with a correlation coefficient of 0.9948. 5-FU samples were analyzed at a wavelength of 260nm against a 5-FU in 0.05M PBS standard curve with a correlation coefficient of 0.99110 and MXN samples were analyzed at a wavelength of 609nm against a MXN in 0.05M PBS standard curve with a correlation coefficient of 0.99669. Concentrations for each standard curve ranged from 1μg/mL to 50μg/mL. Each condition was tested in triplicate and all collected data was statistically analyzed using SigmaStat.

Results and Discussion

MTX and 5-FU *In Situ* Loaded DNA-MS and BSA-MS

Particle analysis

Percent yield. The percent yield and theoretical yield values for all MTX and 5-FU *in situ* loaded BSA-MS and DNA-MS were calculated using Equations 6-5 and 6-6. BSA-MS that were *in situ* loaded with 15% (w/w) MTX were initially prepared with an emulsion speed of 1250rpm and a 8% (w/w) glutaraldehyde concentration based on the excellent MXN release properties obtained in past studies with BSA-MS prepared with those conditions.[11] MTX loaded BSA-MS

produced over an 80% yield and over a 70% theoretical yield. MTX *in situ* loaded DNA-MS were prepared with optimized synthesis conditions from Chapter 4 and produced excellent yields of over 80%. Based on these results, BSA-MS were re-synthesized with the same conditions used to prepare the DNA-MS to determine if increasing the mixer speed would increase the yields. Re-synthesized BSA-MS produced yields similar to those obtained at the 1250rpm mixer speed. These results were consistent with data obtained in Chapter 4 which illustrated that mixer speeds past 1250rpm do not influence MS yields. BSA-MS were also *in situ* loaded with 30% (w/w) MTX to determine the maximum loading capabilities of BSA. BSA-MS with 30% (w/w) MTX loadings produced lower yield and theoretical yield values than the 15% (w/w) MTX loaded BSA-MS prepared at both the 1250rpm and 1550rpm mixer speeds, Table 6-1.

Table 6-1. Percent yield and theoretical yield values for drug loaded DNA-MS and BSA-MS.

Condition	Percent yield (%)	Percent theoretical yield (%)
15% (w/w) BSA-MTX-MS (1250rpm)	84	75
15% (w/w) BSA-MTX-MS (1550rpm)	81	71
15% (w/w) DNA-MTX-MS	93	83
30% (w/w) BSA-MTX-MS	71	58
30% (w/w) BSA-5FU-MS	50	41
30% (w/w) DNA-5FU-MS	59	50

BSA-MS and DNA-MS were *in situ* loaded with 30% (w/w) 5-FU to further analyze the drug loading capabilities of BSA and DNA. BSA-MS produced yield and theoretical yield values of over 40% whereas the DNA-MS produced yield and theoretical yield values of over 50%, Table 6-1. It was noted that the DNA-MS produced higher yield and theoretical yield values than the BSA-MS for both *in situ* loaded drug conditions. The percent yield values for the DNA-MS were approximately 10% higher than the BSA-MS, Figures 6-1 and 6-2.

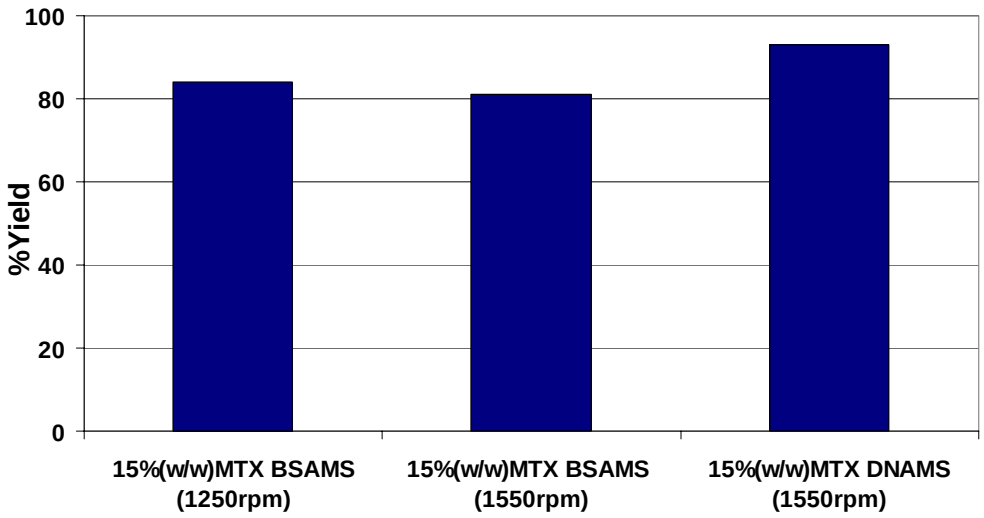

Figure 6-1. Percent yield values for 15% (w/w) MTX *in situ* loaded BSA-MS and DNA-MS.

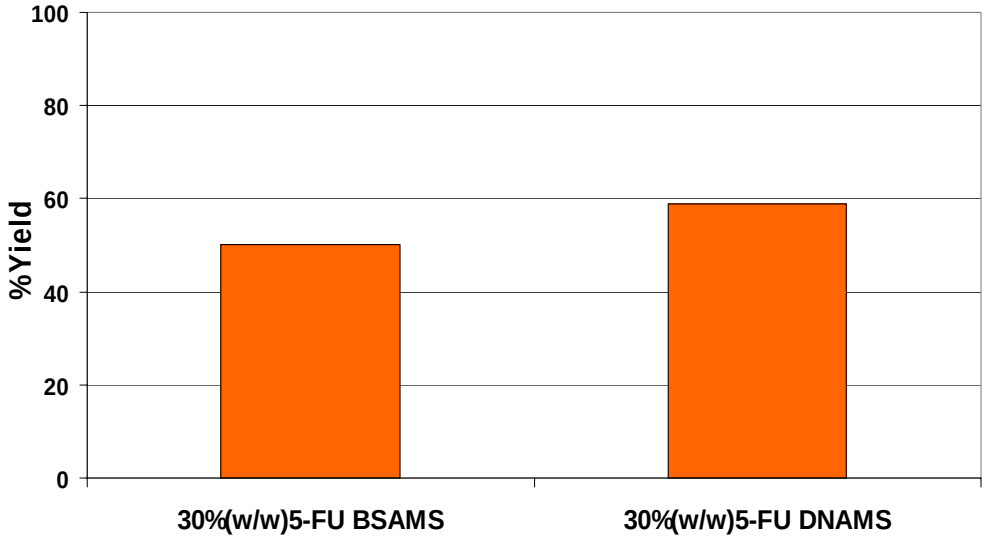

Figure 6-2. Percent yield values for 30% (w/w) 5-FU *in situ* loaded BSA-MS and DNA-MS.

Dry particle size. Each MTX *in situ* loaded condition produced over 60% of all particles with diameters within the 1μm to 10μm size range, Table 6-2. The BSA-MS produced smaller particles than the DNA-MS. The MTX *in situ* loaded DNA-MS displayed evidence of the production of aggregates with 8% of all particles produced displaying diameters of greater than 10μm.

Table 6-2. Dry mean particle diameter and size range values for MTX *in situ* loaded BSA-MS and DNA-MS.

Condition	Dry mean particle diameter (µm)	MS in 1µm to 10µm size range (%)	MS larger than 10µm (%)
15% (w/w) MTX BSA-MS (1250rpm)	2.9 ± 2.7	67	1
15% (w/w) MTX BSA-MS (1550rpm)	2.8 ± 1.4	95	0
15% (w/w) MTX DNA-MS	4.8 ± 5.9	72	8
30% (w/w) MTX BSA-MS	3.0 ± 1.9	96	0

MTX *in situ* loaded BSA-MS prepared at 1250rpm produced particles with a slightly bimodal distribution and a mean diameter of 2.9µm, Table 6-2. It was noted that the size distributions were narrow with particle diameters that ranged from 55nm to 14µm, Figure 6-3. This is important to note since DNA-MS require filtering at the end of synthesis to obtain particles with narrow diameter ranges.

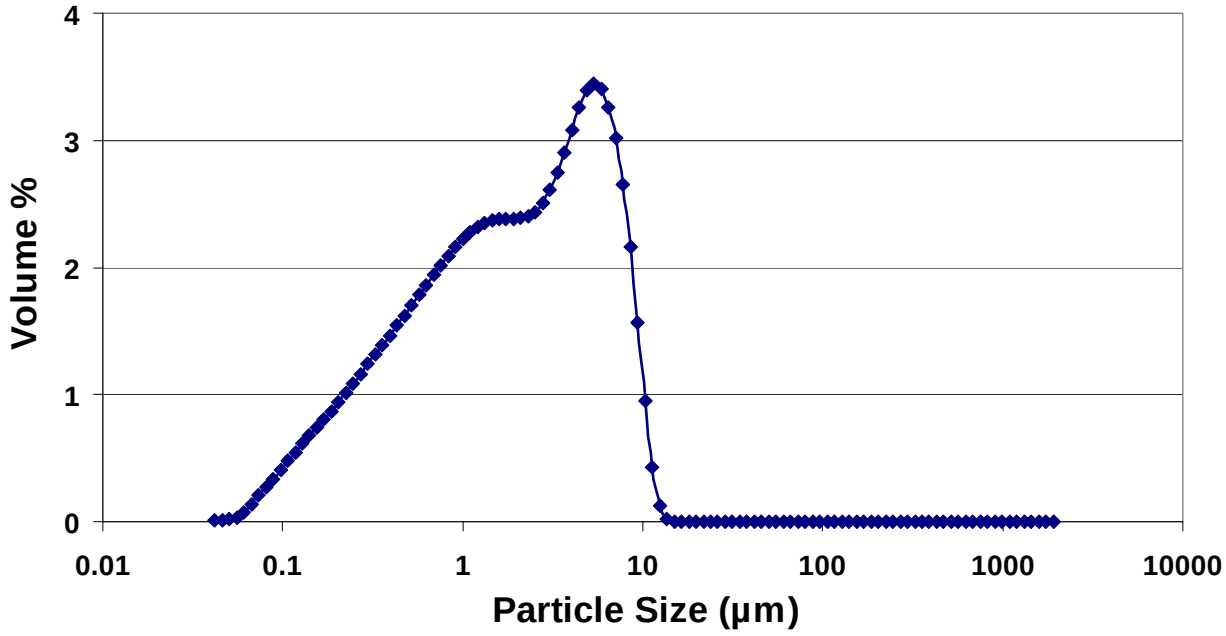

Figure 6-3. Dry particle size distribution for 15% (w/w) MTX *in situ* loaded BSA-MS prepared at 1250rpm with 8% (w/w) GTA.

BSA-MS *in situ* loaded 15% (w/w) MTX that were re-synthesized at the 1550rpm mixer speed produced a more normalized size distribution with particles ranging from 470nm to 8.5µm,

Figure 6-4. This was consistent with data obtained in Chapter 4 which illustrated that particle size distributions normalized as mixer speed increased. The normalization of the particle size distribution can be attributed to an increase in finer particles created due to the larger shear forces exerted on the MS during synthesis.[10, 57, 107, 130, 131, 134-136]

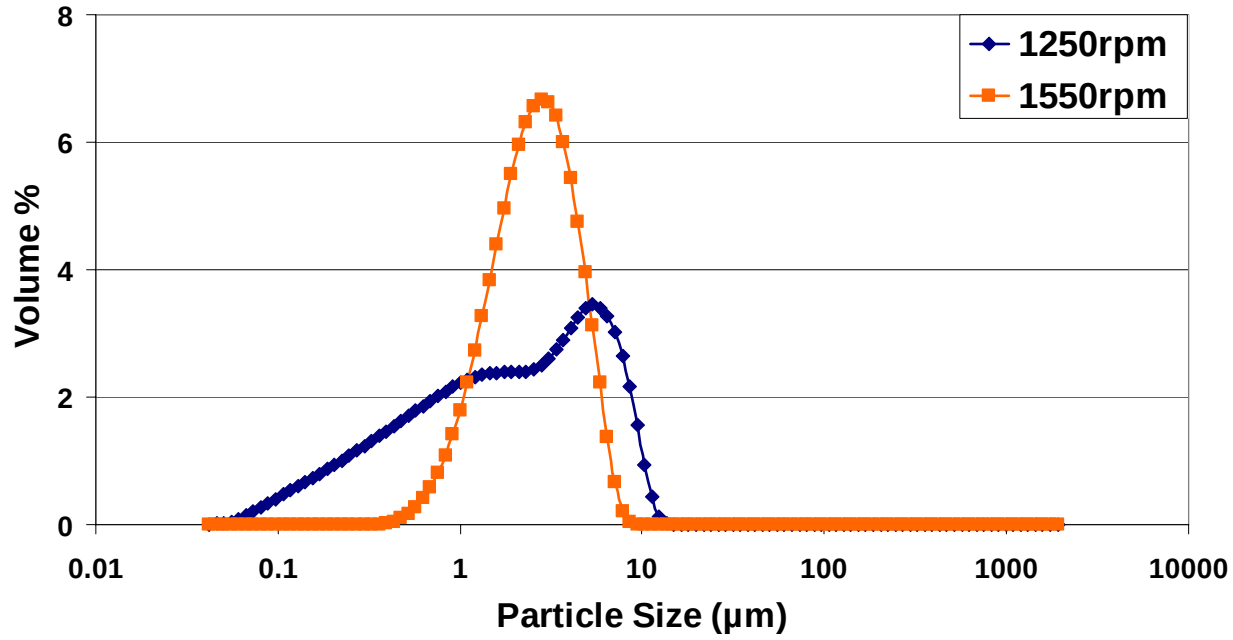

Figure 6-4. Dry particle size distributions of 15% (w/w) MTX *in situ* loaded BSA-MS prepared at 1250rpm and 1550rpm.

MTX *in situ* loaded DNA-MS produced particles with fairly normalized size distributions and mean dry diameters of 4.8µm, Figure 6-5. Particle diameters ranged from 60nm to 60µm; however, it is assumed that if a 20µm filter would have been used in place of the 70µm filter, particles ranging past 20µm in diameter would have been eliminated from the yield and the size distribution would have become more normalized as seen in results obtained in Chapter 4.

BSA-MS prepared at the 30% (w/w) MTX loading also produced a normalized size distribution with a mean diameter of 3.0µm. The size distribution obtained for the 30% (w/w) MTX loaded BSA-MS was almost identical to that obtained for the 15% (w/w) MTX conditions, Figure 6-6. A one way analysis of variance (ANOVA) further supported these results and

indicated that there were no significant size differences between the 15% (w/w) and 30% (w/w) *in situ* loaded BSA-MS. These findings are consistent with current literature which state that resulting particle size values are not affected by drug loading at high concentrations as those seen in these studies.[11, 57, 143, 145, 158] The one way ANOVA also illustrated no significant particle size differences among all MTX *in situ* loaded BSA-MS and DNA-MS conditions.

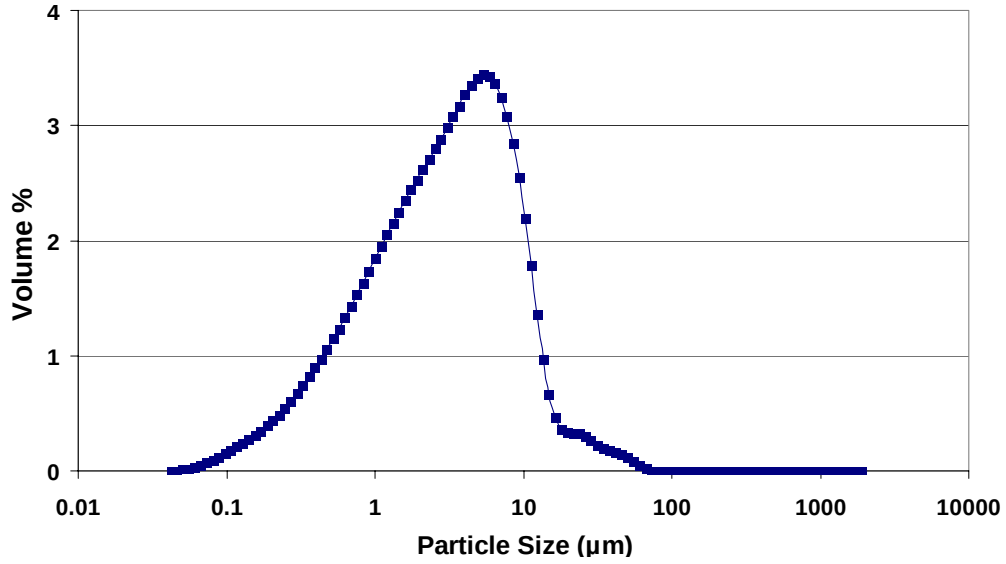

Figure 6-5. Dry particle size distribution of 15% (w/w) *in situ* loaded DNA-MS.

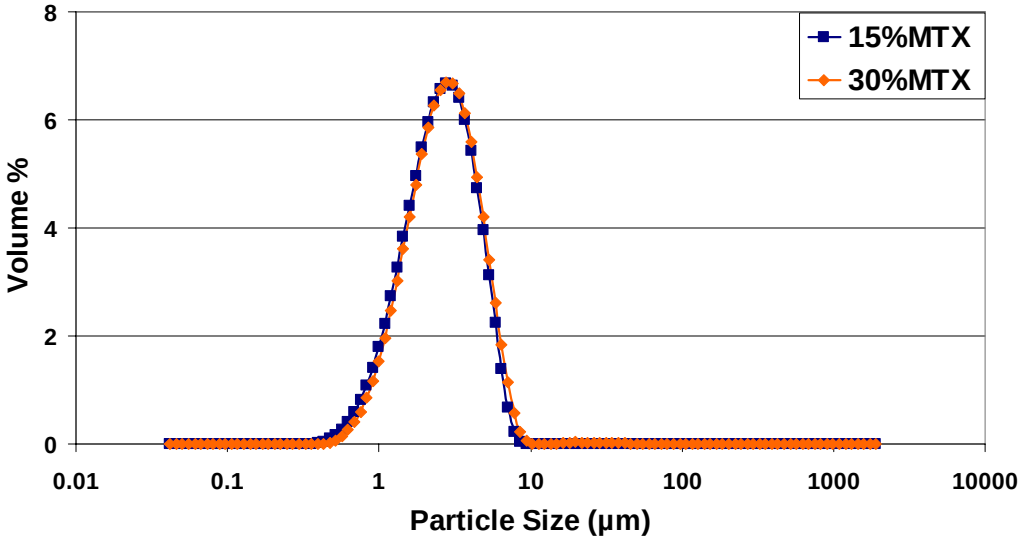

Figure 6-6. Dry particle size distribution for BSA-MS prepared at 1550rpm and *in situ* loaded with 15% (w/w) or 30% (w/w) MTX.

BSA-MS *in situ* loaded with 30% (w/w) 5-FU produced normalized size distributions with particle diameters ranging from 200nm to 8.5µm, Figure 6-7. There was some evidence of slight aggregate formation past the 8.5µm size; however, this may be due to the formation of van der Waals interparticle attractions which occur during drying or upon dispersion in methanol.[90, 107, 125, 128, 129, 159]

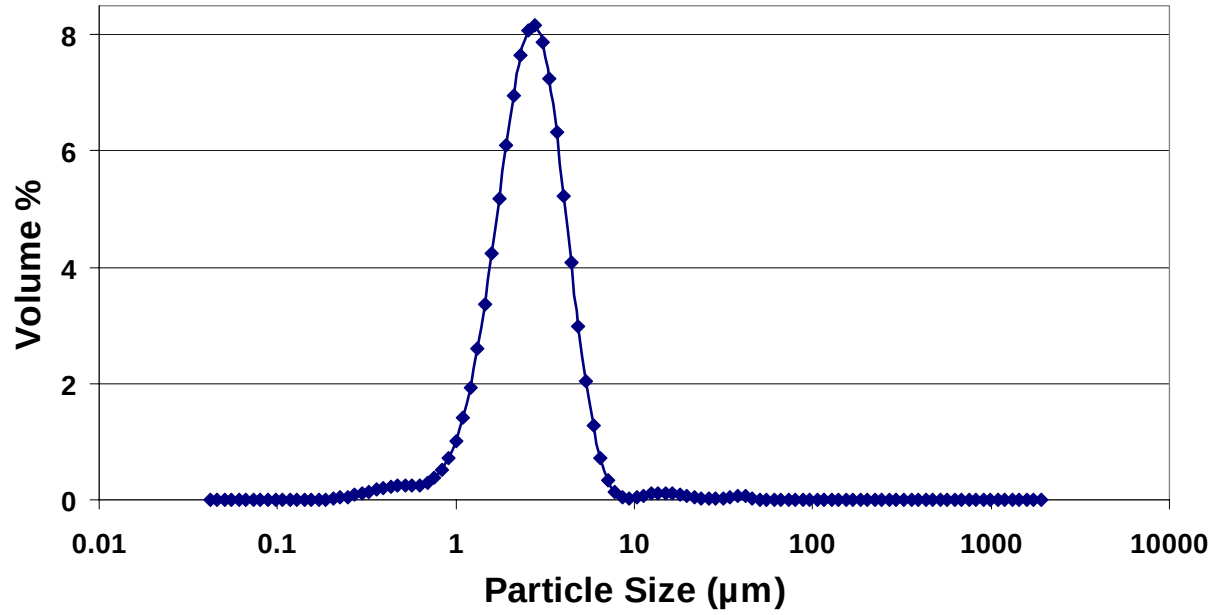

Figure 6-7. Dry particle size distribution for 30% (w/w) 5-FU *in situ* loaded BSA-MS.

5-FU loaded BSA-MS and DNA-MS produced mean diameters that were very similar in size to one another with greater than 60% of all particles produced falling within the mesosphere size range and less than 5% of all particles produced larger than 10µm, Table 6-3. A t-test conducted on the 5-FU data collected found no significant size differences between the BSA-MS and DNA-MS.

Table 6-3. Dry mean particle diameter values for 5-FU *in situ* loaded BSA-MS and DNA-MS.

Condition	Dry mean particle diameter (µm)	MS in 1µm to 10µm size range (%)	MS larger than 10µm in size (%)
30% (w/w) 5-FU BSA-MS	2.9 ± 2.1	95	1
30% (w/w) 5-FU DNA-MS	3.3 ± 4.7	68	4

DNA-MS prepared with *in situ* loadings of 30% (w/w) 5-FU also produced normalized size distributions with particles ranging from 60nm to 50µm, Figure 6-8. As noted with the DNA-MTX-MS conditions, it is assumed that particles past 20µm in diameter would be eliminated from the yield if a 20µm filter is used in place of a 70µm filter.

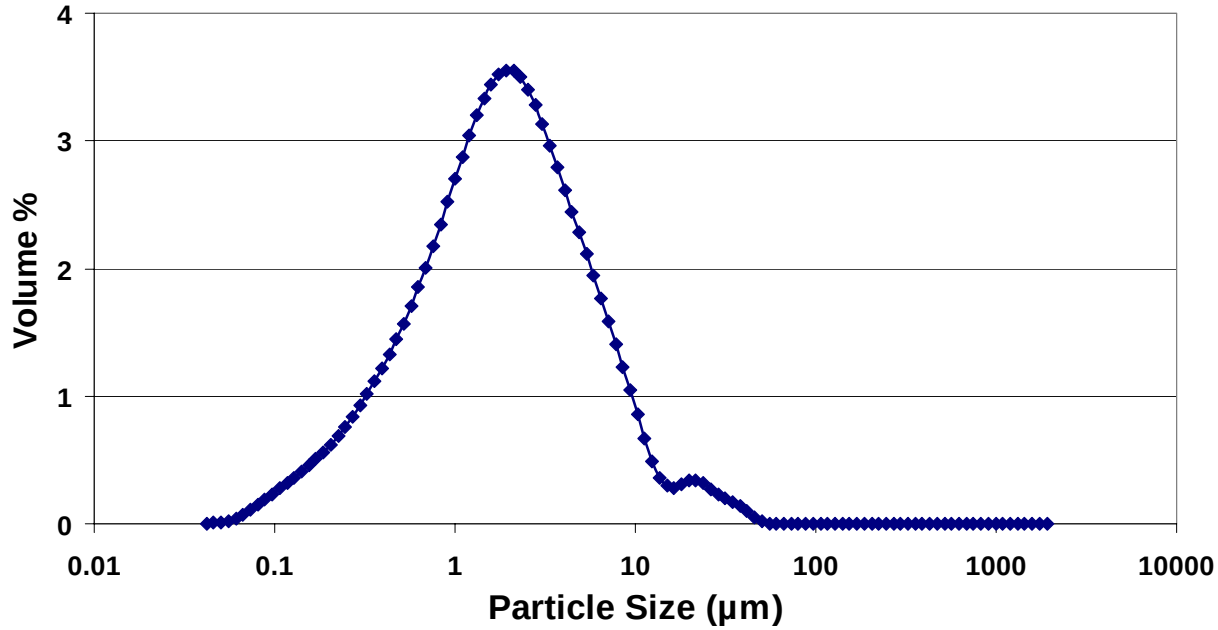

Figure 6-8. Dry particle size distribution for 30% (w/w) 5-FU *in situ* loaded DNA-MS.

Scanning electron microscopy. SEM micrographs of the BSA-MS that were *in situ* loaded with 15% (w/w) MTX depicted particles with spherical morphologies. The BSA-MS that were synthesized at the 1550rpm mixer speed produced particles that were more discreet and uniform than those obtained at the 1250rpm mixer speed, Figure 6-9. SEM micrographs also illustrated that both BSA-MS conditions produced particles with wrinkled or textured topographies. It was further noted that the BSA-MS prepared at the 1550rpm mixer speed, which were also prepared at a higher crosslink concentration (2mL of GTA vs. 0.382mL of GTA) produced particles with more surface texture than those prepared at the 1250rpm, Figure 6-10. The wrinkled topographies of the BSA-MS prepared at the 1550rpm mixer speed may be attributed to the GTA crosslink agent used during synthesis. Since the early 1980s, BSA-MS

have been prepared in this lab using GTA crosslinking introduced through the organic phase.[4, 11, 57-59, 94] This method of crosslinking yields BSA-MS with smooth surface topographies due to GTA crosslinking the BSA-MS at the stabilizing agent/BSA interface.[59] The BSA-MS prepared in this study were crosslinked with GTA through the aqueous phase. This form of crosslinking results in GTA interacting with the BSA from within the MS core to the outer layer yielding BSA-MS that are crosslinked more uniformly within. The BSA-MS become wrinkled due to dehydration from within the MS core that results from acetone washing and MS drying.[160] Thus it would be expected for BSA-MS with higher GTA concentrations to have more surface texture.

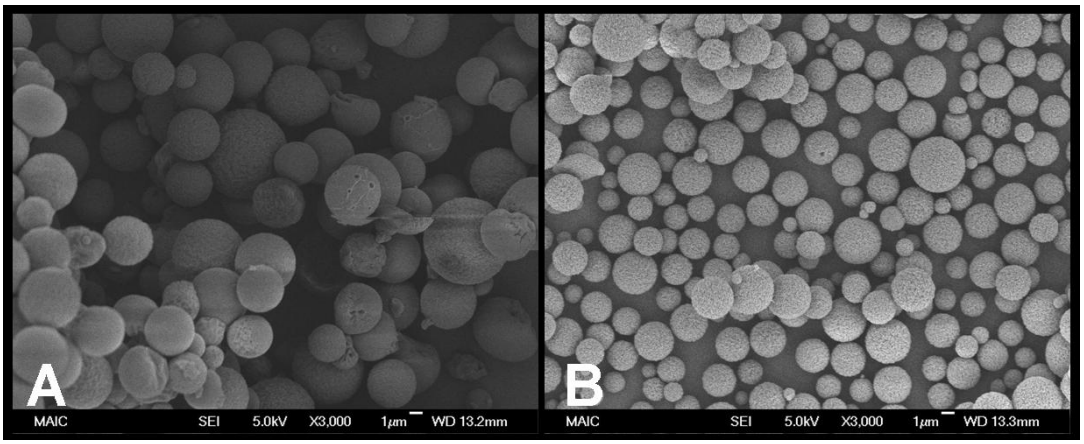

Figure 6-9. SEM micrograph of 15% (w/w) MTX *in situ* loaded BSA-MS prepared at the A) 1250rpm mixer speed and B) 1550rpm mixer speed (Magnifications: 3,000x).

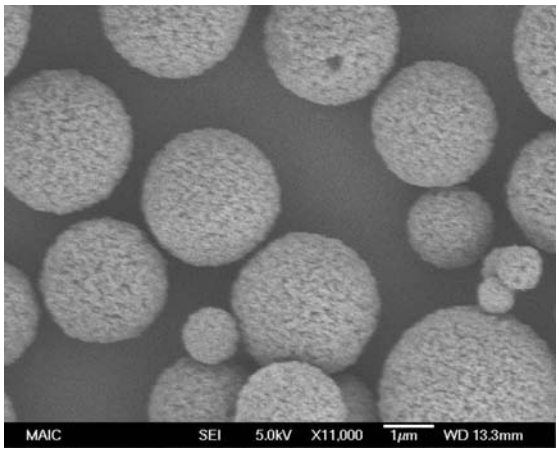

Figure 6-10. SEM micrograph of 15% (w/w) MTX *in situ* loaded BSA-MS prepared at the 1550rpm mixer speed with 2mL of GTA (Magnification: 11,000x).

SEM micrographs of the 30% (w/w) MTX *in situ* loaded BSA-MS depicted discreet and uniform particles that were consistent with data obtained during dry particle size analysis, Figure 6-11. The micrographs also displayed that the 30% (w/w) MTX loaded BSA-MS produced particles with wrinkled surface topographies that were similar to those seen with the 15% (w/w) MTX BSA-MS. The formation of the wrinkled topographies observed on the BSA-MS was a result of the GTA crosslink agent used during synthesis.

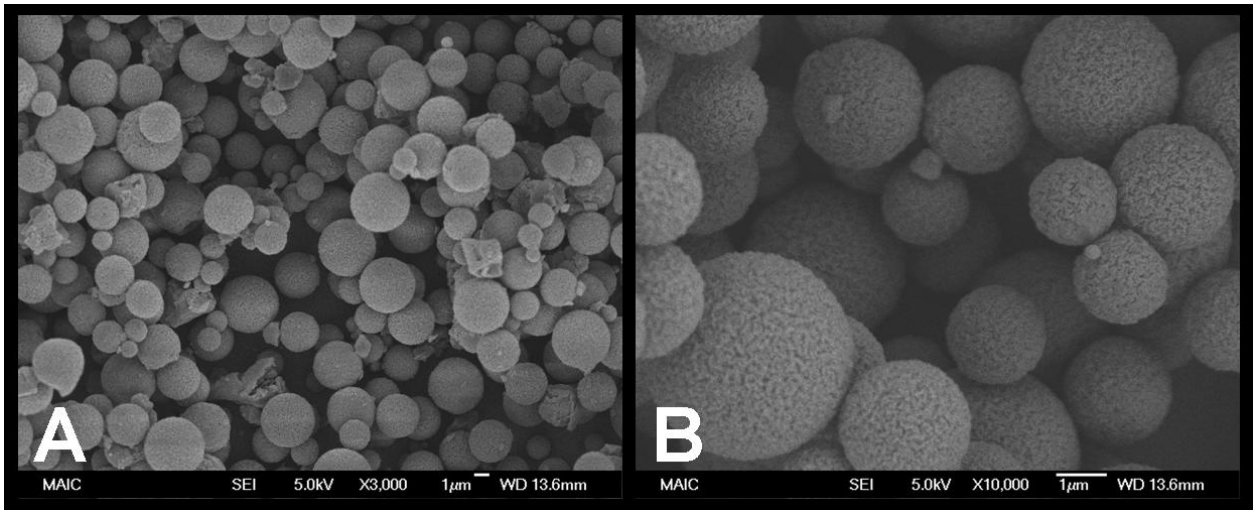

Figure 6-11. SEM micrographs of the 30% (w/w) MTX *in situ* loaded BSA-MS at magnifications of A) 3,000x and B) 10,000x.

SEM micrographs taken of the 15% (w/w) MTX *in situ* loaded DNA-MS displayed aggregated particles with irregular morphologies, Figure 6-12. These images were consistent with data obtained during particle size analysis which illustrated the presence of aggregates past the 10μm size. The SEM micrographs also illustrated that the MTX loaded DNA-MS were fused together which lead to particle aggregation. The amount of particle aggregation may have been a result of unloaded MTX since unloaded DNA-MS prepared with these conditions produce discreet and uniform particles with smooth topographies and spherical morphologies (Chapter 4).

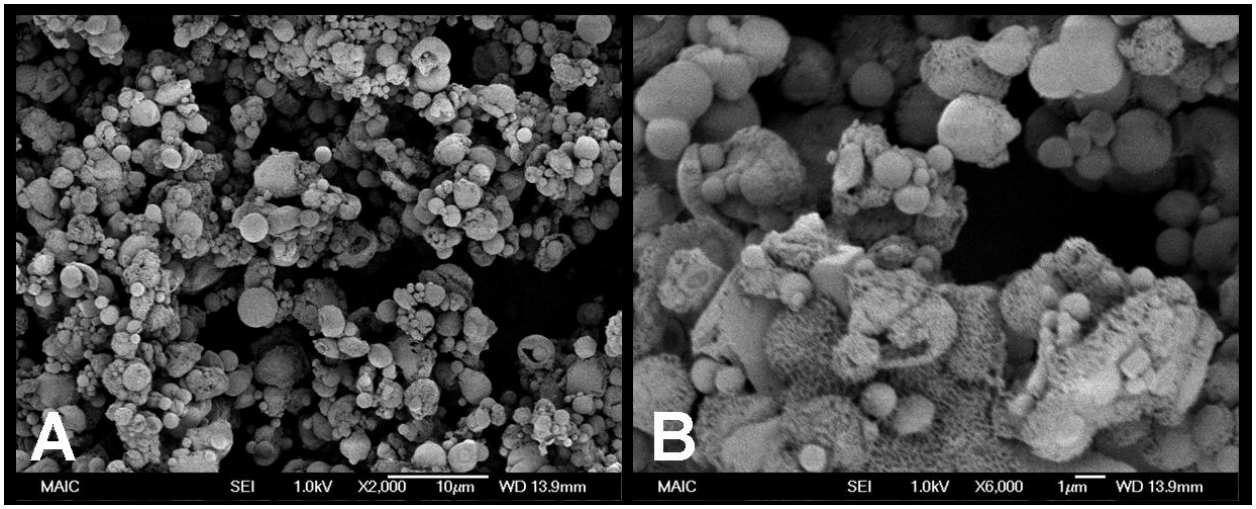

Figure 6-12. SEM micrographs of 15% (w/w) MTX *in situ* loaded DNA-MS at magnifications of A) 2,000x and B) 6,000x.

BSA-MS and DNA-MS that were *in situ* loaded with 30% (w/w) 5-FU produced discreet particles with spherical morphologies, Figure 6-13. SEM micrographs taken of the 5-FU loaded BSA-MS depicted particles with wrinkled surface topographies, Figure 6-14. The increase in surface texture noted with the BSA-MS is attributed to the large concentration of GTA used during synthesis. Further comparisons of the 30% (w/w) 5-FU loaded MS also suggested that the BSA-MS produced larger particles than the DNA-MS.

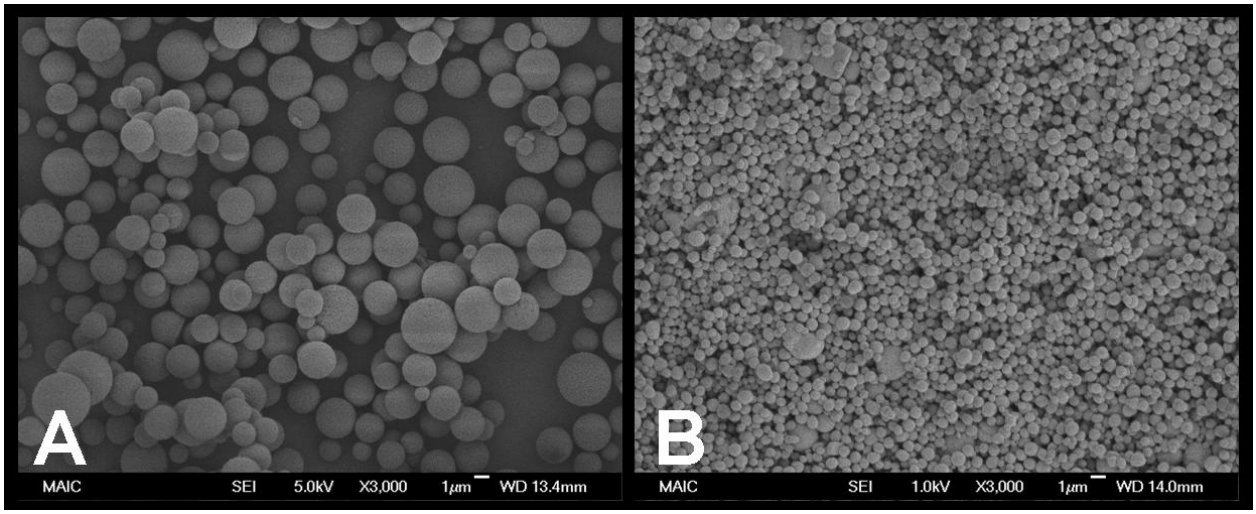

Figure 6-13. SEM micrographs of 30% 5-FU *in situ* loaded A) BSA-MS and B) DNA-MS (Magnifications: 3,000x).

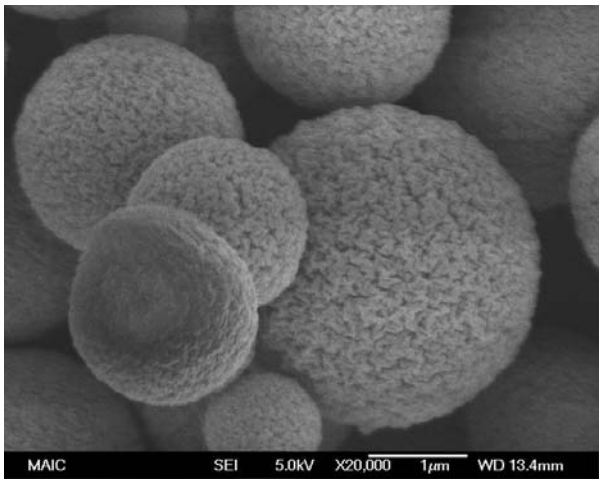

Figure 6-14. SEM micrograph of 30% (w/w) 5-FU loaded BSA-MS (Magnification: 20,000x).

SEM micrographs of the 5-FU loaded DNA-MS depicted particles with smooth surface topographies. The 5-FU loaded DNA-MS were also very uniform in size suggesting that the particle diameters obtained past the 2μm size during particle size analysis were more representative of MS aggregates rather than the individual DNA-MS, Figure 6-15. The formation of DNA-MS aggregates may have been a result of attractive electrostatic or van der Waals interactions between the particles during the drying process or upon dispersion into methanol since these interactions play a dominant role in systems where the particles are less than 10μm in size. [124, 125]

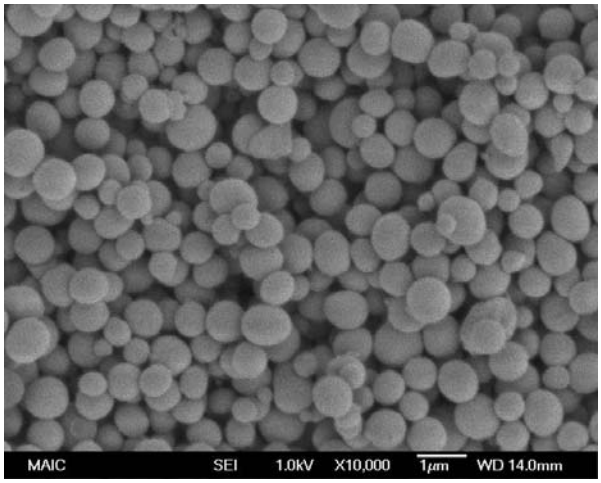

Figure 6-15. SEM micrograph of 30% 5-FU *in situ* loaded DNA-MS (Magnification: 10,000x).

In vitro MTX and 5-FU loading efficiency

The MTX and 5-FU percent loadings and loading efficiencies of the BSA-MS and DNA-MS were measured in triplicate by enzymatic digestion followed by photometric analysis. MTX and 5-FU percent loadings were calculated using Equation 6-7 to in order to obtain the loading efficiencies for the conditions tested which were calculated using Equation 6-8. The loading efficiencies for the conditions loaded with 15% (w/w) MTX ranged from 61% to 94%, Table 6-4. The 30% (w/w) MTX BSA-MS condition produced a loading efficiency of 87%. The 30% (w/w) 5-FU conditions produced poor loading efficiencies of approximately 20% for both BSA-MS and DNA-MS conditions.

Table 6-4. Loading efficiency values for MTX and 5-FU *in situ* loaded BSA-MS and DNA-MS.

Condition	Experimental loading (%)	Theoretical loading (%)	Loading efficiency (%)
15% (w/w) MTX BSA-MS (1250rpm)	10.6 ± 2.2	13.9	76.1 ± 15.8
15% (w/w) MTX BSA-MS (1550rpm)	16.0 ± 0.6	17.0	94.3 ± 3.8
15% (w/w) MTX DNA-MS	9.2 ± 1.1	15.0	61.2 ± 7.4
30% (w/w) MTX BSA-MS	24.4 ± 5.0	28.0	87.2 ± 17.8
30% (w/w) 5-FU BSA-MS	5.5 ± 0.6	27.0	20.3 ± 2.1
30% (w/w) 5-FU DNA-MS	5.0 ± 0.7	23.2	21.3 ± 3.0

T-tests were conducted on the MTX conditions to determine if mixer speed, amount of drug loaded, or drug loading material effected MTX loading. The t-tests illustrated no significant loading efficiency differences as a result of mixer speed or percent drug loaded; however the t-tests did find that the BSA-MS entrapped significantly more MTX than the DNA-MS ($p = 0.002$), Figures 6-16 to 6-18. These findings are consistent with current literature which cite that loading efficiencies are independent of mixer speed and amount of drug loaded.[134, 139] However, it has also been cited in the literature that increases in GTA concentration increase MTX loading which was somewhat observed with these data.[161]

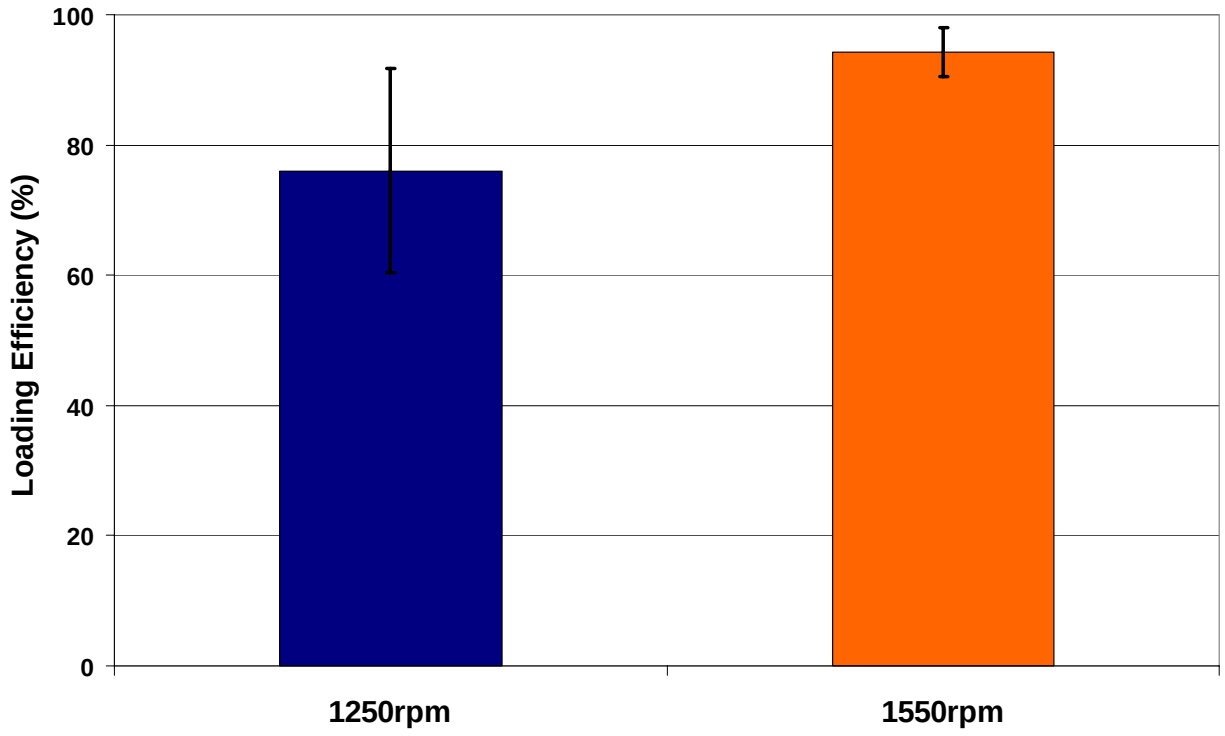

Figure 6-16. Loading efficiency comparison chart for 15% (w/w) MTX *in situ* loaded BSA-MS prepared at different mixer speeds.

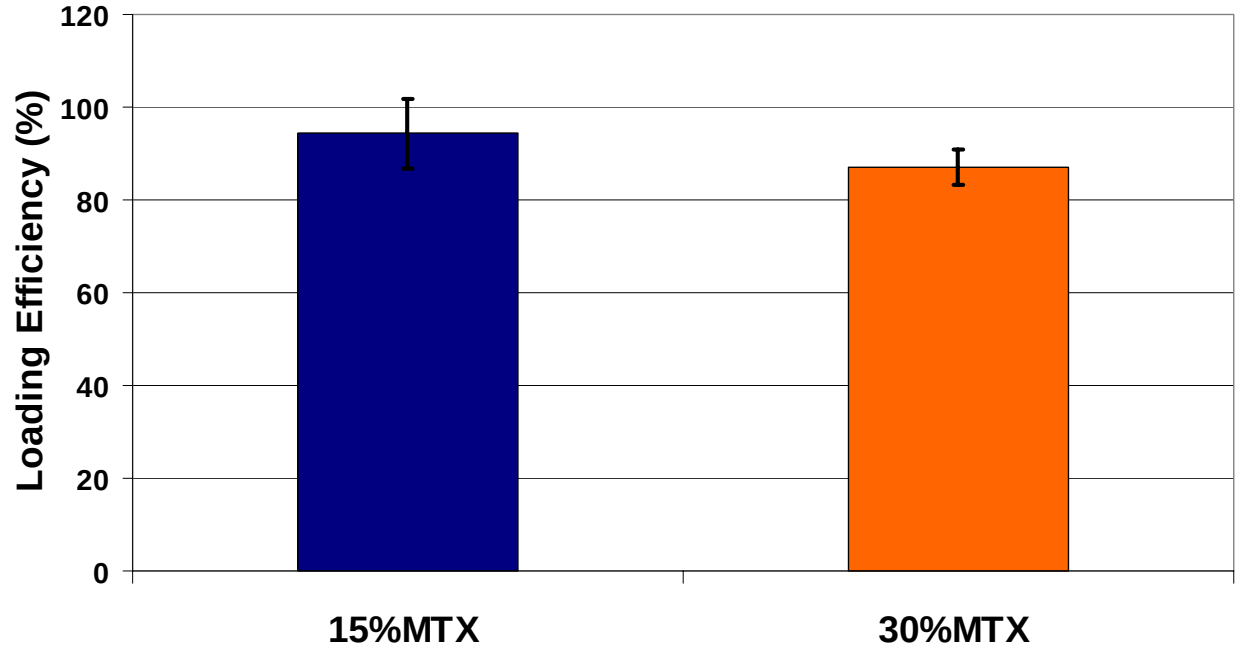

Figure 6-17. Loading efficiency comparison chart for BSA-MS loaded with different MTX concentrations prepared at the 1550rpm mixer speed.

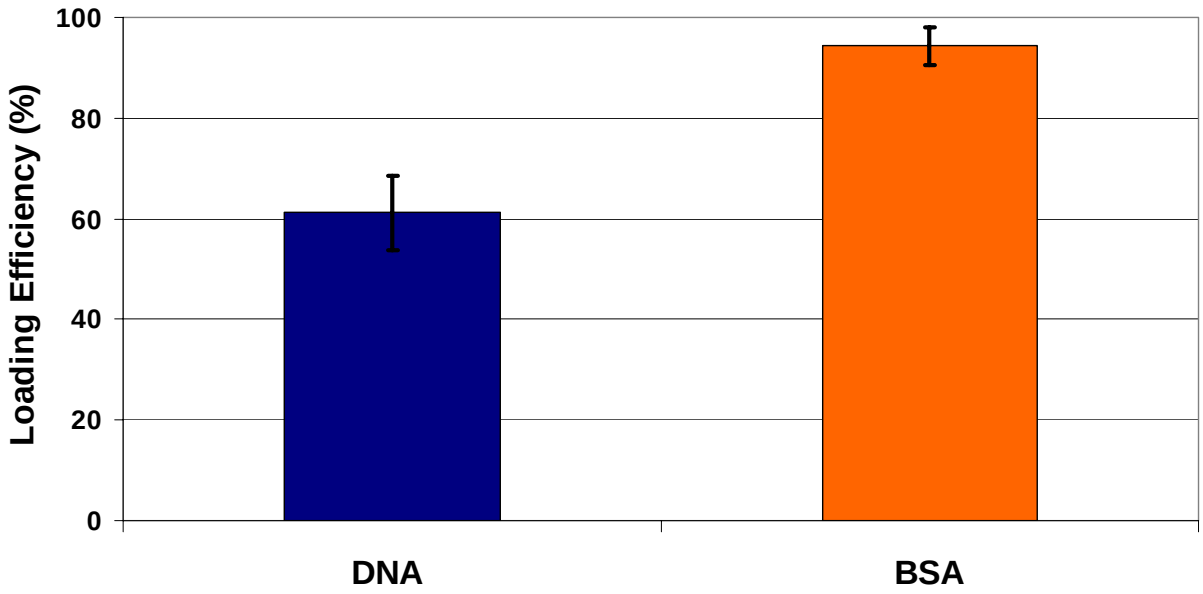

Figure 6-18. Loading efficiency comparison chart of the 15% (w/w) MTX *in situ* loaded DNA-MS and BSA-MS prepared at the 1550rpm mixer speed.

A t-test was also conducted on the 5-FU conditions to determine if the drug loading material effected 5-FU loading. The t-test illustrated no significant loading efficiency differences between the BSA-MS and DNA-MS conditions, Figure 6-19.

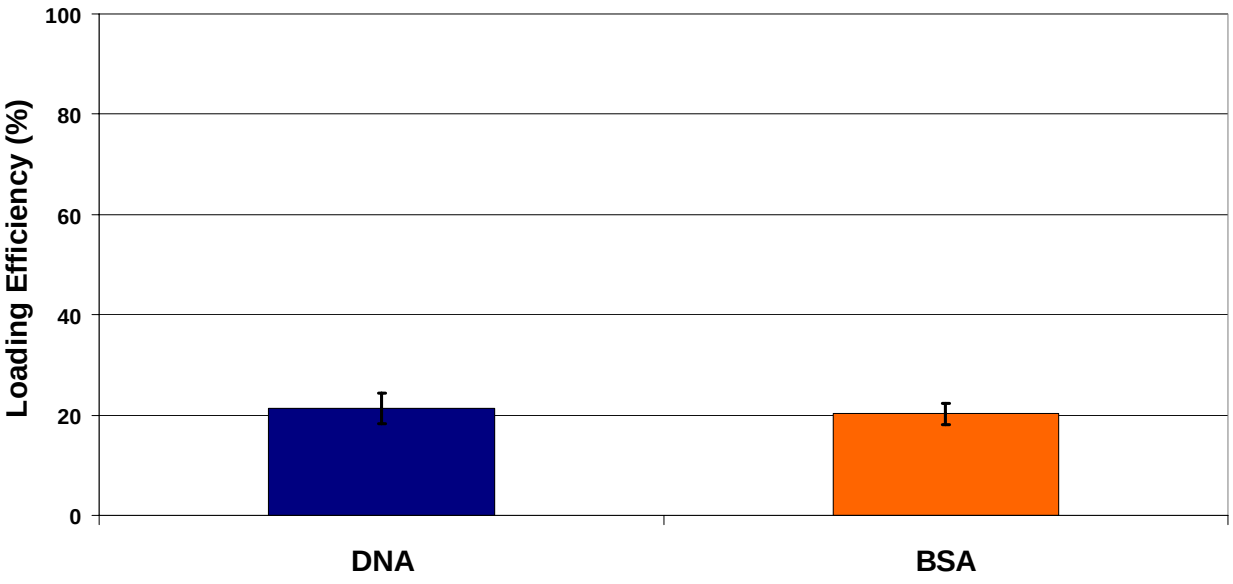

Figure 6-19. Loading efficiency comparison chart of the 30% 5-FU *in situ* loaded DNA-MS and BSA-MS.

In vitro MTX and 5-FU release

The *in vitro* MTX and 5-FU release properties of BSA-MS and DNA-MS were measured in 0.05M PBS at a pH of 7.4. Each drug loaded MS condition was tested in triplicate using minimum sink conditions and incubated in 1.250mL of PBS at 37˚C to simulate the tumor environment. Each MTX condition tested displayed an initial "burst" release within the first three hours, Figure 6-20 and had ceased releasing by Day 2, Figure 6-21.

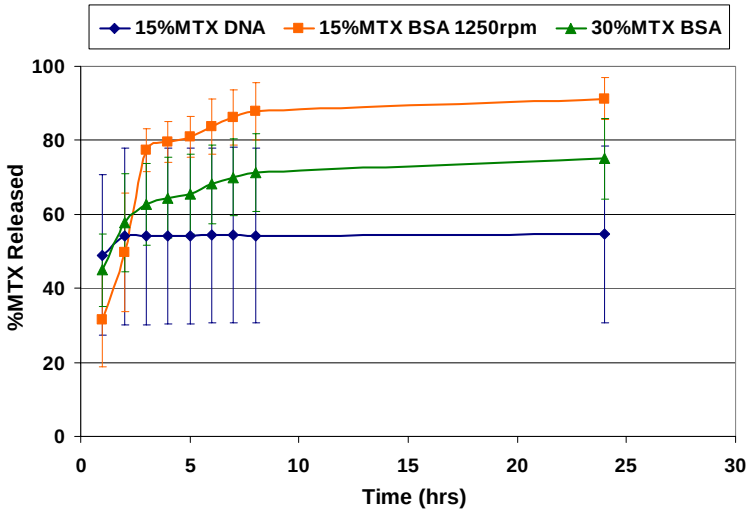

Figure 6-20. MTX release profiles for *in situ* loaded DNA-MS and BSA-MS for the first 24 hours.

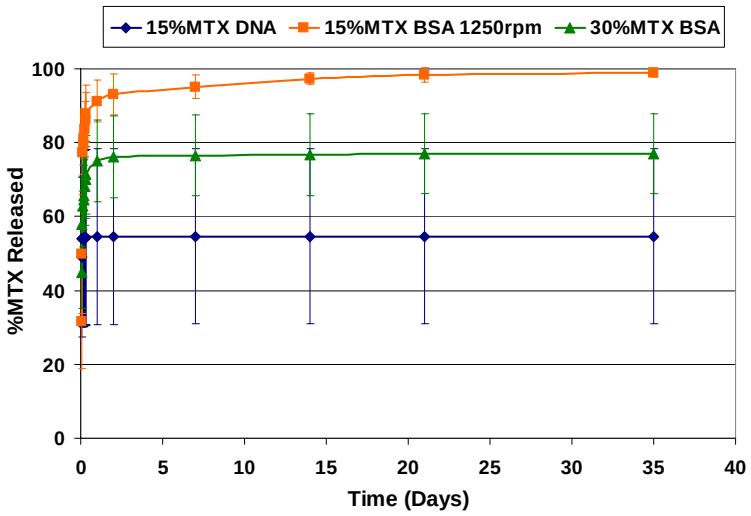

Figure 6-21. MTX release profiles for *in situ* loaded DNA-MS and BSA-MS for duration of study.

These *in vitro* release results are consistent with studies that have been presented in the literature that site that MTX produces an initial 30% to 50% "burst" release from nano- and microparticles and then finishes releasing within 24 hours.[58, 162] MTX release analyzed from both 15% (w/w) *in situ* loaded conditions were diffusion controlled and followed first-order release kinetics where the amount of drug released from the MS decreased over time after it's initial burst release.[67, 70] The MTX release from the 30% (w/w) *in situ* loaded condition was also diffusion controlled and exhibited a biphasic release pattern in which the first eight hours followed the Higuchi square root time kinetics model and the MTX release after hour 8 followed first-order release kinetics, Figure 6-22.[158]

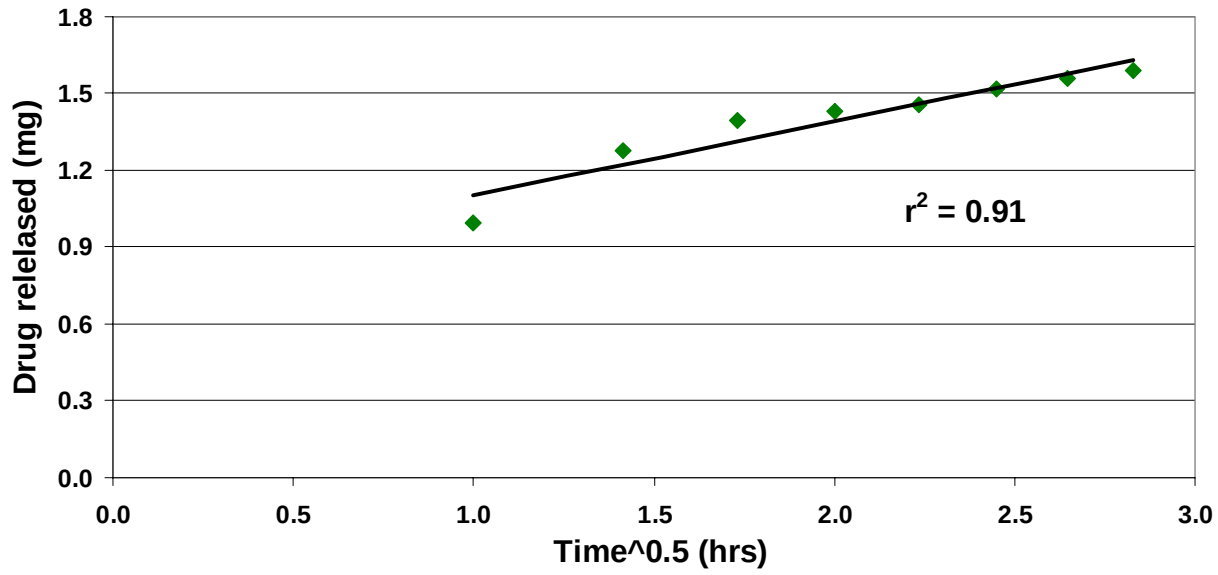

Figure 6-22. Higuchi square root time kinetics MTX *in vitro* release for the 30% (w/w) MTX *in situ* loaded BSA-MS condition (Hours 1 through 8).

The 5-FU *in situ* loaded DNA-MS released a larger concentration of drug at a quicker rate than the BSA-MS condition, Figure 6-23. The *in vitro* release of 5-FU from DNA-MS appeared to be diffusion controlled and followed the Higuchi square root time kinetics model for release during the first eight hours and first-order kinetics for the duration of release, Figure 6-24. The 5-FU *in situ* loaded BSA-MS however, exhibited erosion controlled release and followed the

Higuchi square root time kinetics model for release throughout the duration of the study, Figure 6-25.

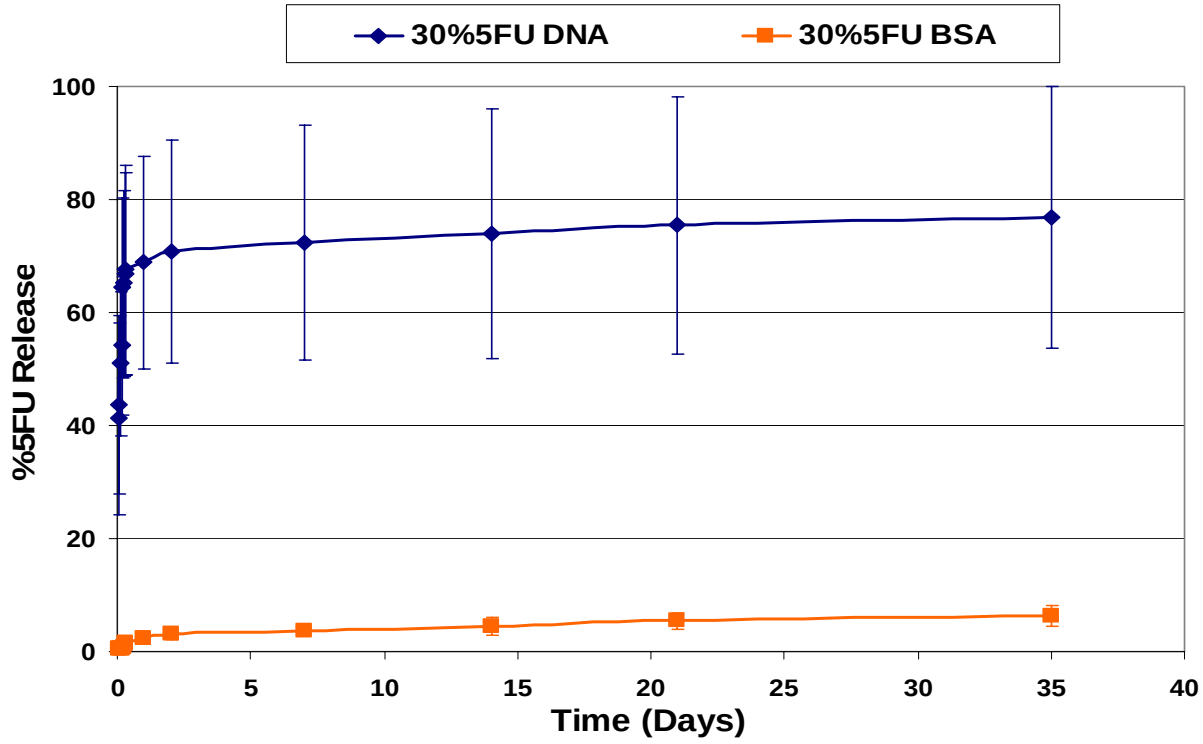

Figure 6-23. 5-FU release profiles for *in situ* loaded DNA-MS and BSA-MS.

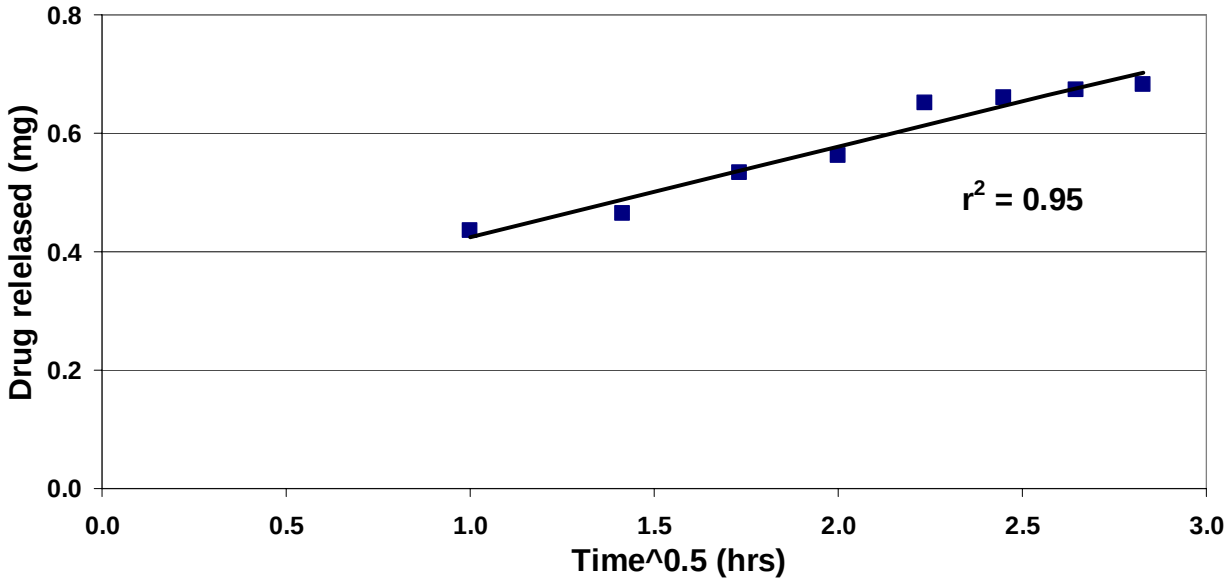

Figure 6-24. Higuchi square root time kinetics 5-FU *in vitro* release for the 23% (w/w) 5-FU *in situ* loaded DNA-MS condition (Hours 1 through 8).

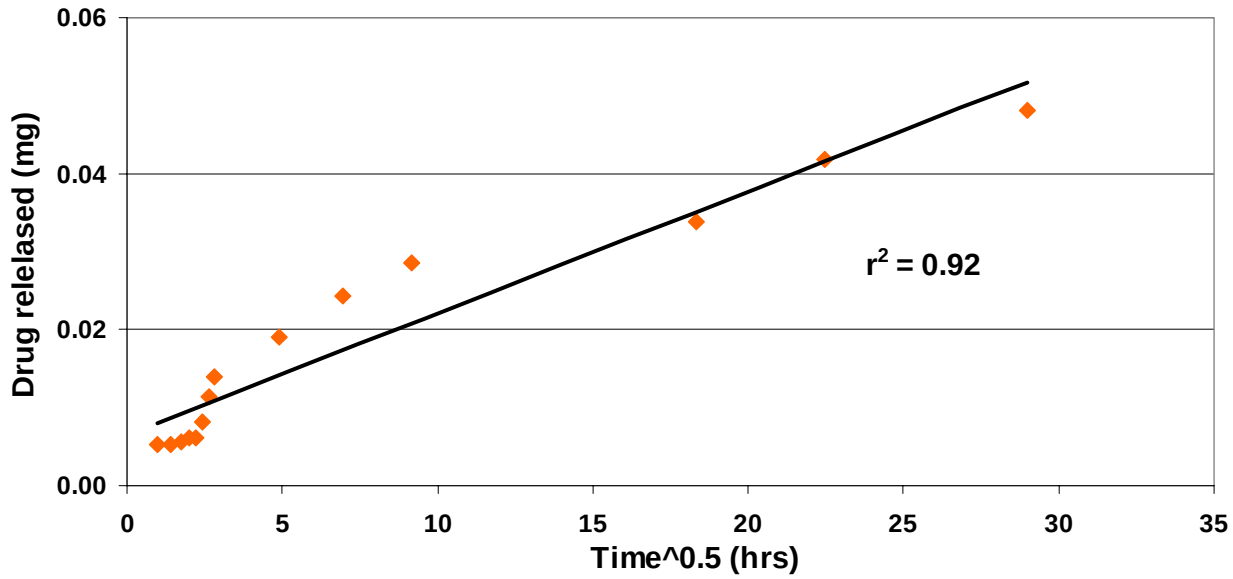

Figure 6-25. Higuchi square root time kinetics 5-FU *in vitro* release for the 27% (w/w) 5-FU *in situ* loaded BSA-MS condition (Hour 1 through Day 35).

The data collected from the 5-FU *in situ* loaded DNA-MS is consistent to research presented in current literature which site that 5-FU tends to exhibit a biphasic release profile *in vitro* from various biomaterials such as gelatin, albumin, chitosan, and poly(lactic acid)[163, 158, 161, 164] Release trends as those seen with the 5-FU *in situ* loaded BSA-MS have also been presented in the literature where the 5-FU is initially released slowly and then exhibits an increase in release due to the degradation of the highly crosslinked MS.[165]

DNA-MXN-MS Studies

Particle analysis

Percent yield. The percent yield and theoretical yield values for all MXN *in situ* loaded DNA-MS were calculated using Equations 6-5 and 6-6. Each DNA-MXN-MS condition produced yields and theoretical yields of over 65%, Table 6-5. There were no clear yield trends observed with regard to MXN concentration, Figure 6-26.

The MXN *in situ* loaded DNA-MS produced larger percent yields values than the non-loaded (i.e. blank) DNA-MS, Figure 6-27. In addition, the crosslinked blank DNA-MS produced

larger yields than the blank non-crosslinked DNA-MS, Figure 6-27. The larger yields observed for the MXN *in situ* loaded DNA-MS may have resulted from the formation of a tighter DNA-MS network due to the intercalation interactions between MXN and the DNA matrix.[166-168] MXN intercalates DNA through interactions between MXN's aminoalkylamino side chains and the DNA base pairs.[166, 168] MXN is also capable of binding with DNA through electrostatic interactions between the aminoalkylamino side chains of MXN and the phosphate groups of DNA.[166, 167] The electrostatic interactions begin to arise at pH's $\geq$ 7.4 due to the deprotonation of the NH_3^+ groups in the aminoalkylamino chains.[167] In addition, the larger yields observed with the crosslinked blank DNA-MS may have been attributed to formation of crosslinks in the DNA-MS which resulted in a larger retention of DNA in the yield.

Table 6-5. Percent yield and theoretical yield values for DNA-MXN-MS.

Condition	Percent yield (%)	Percent theoretical yield (%)
10% (w/w) MXN	75	69
15% (w/w) MXN	83	75
25% (w/w) MXN	80	67
15% (w/w) MXN (no Gd crosslinking)	96	80
Blank DNA-MS	76	NA
Blank DNA-MS (no Gd crosslinking)	63	NA

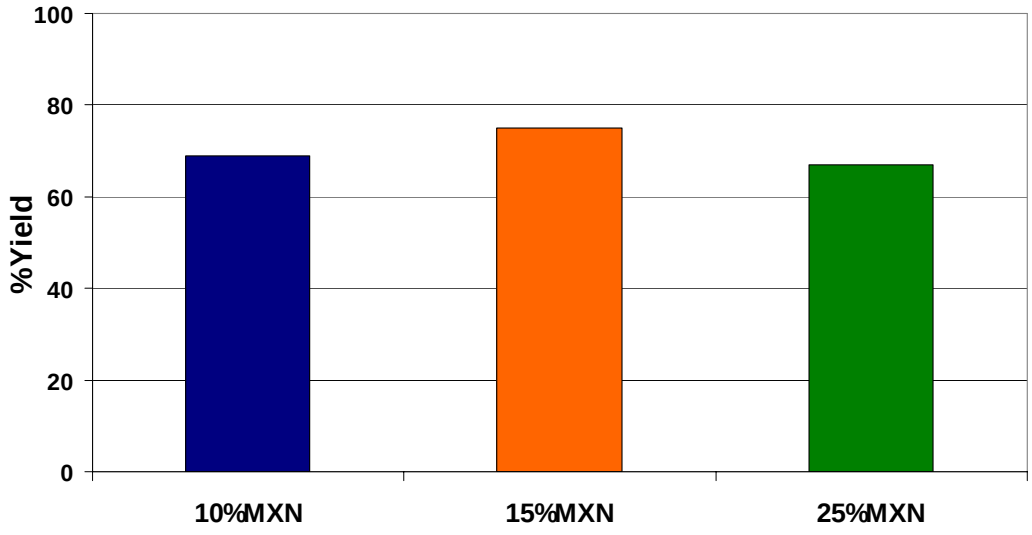

Figure 6-26. Theoretical yield values for DNA-MXN-MS prepared at varying MXN concentrations.

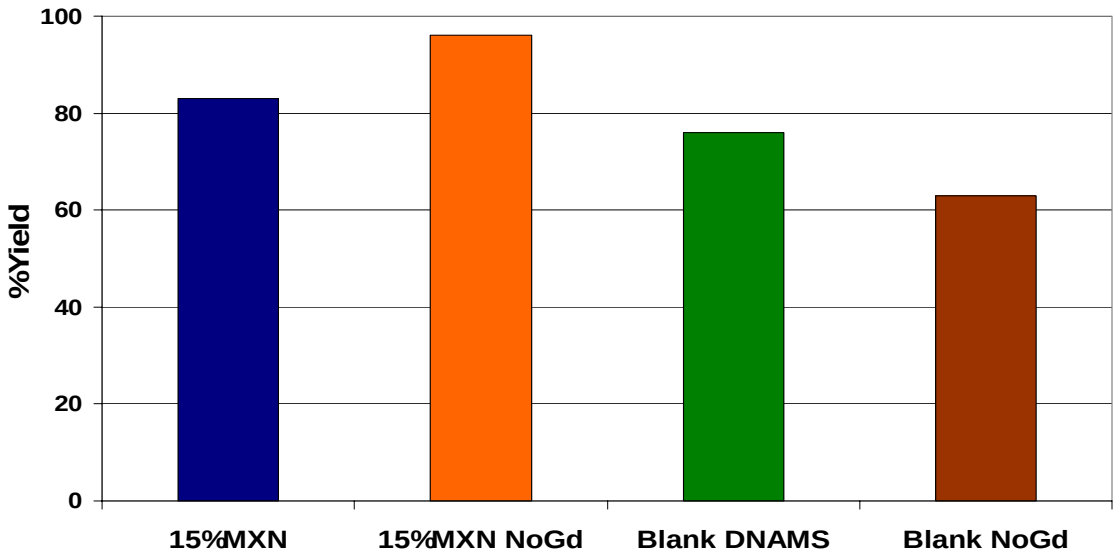

Figure 6-27. Percent yield values for MXN *in situ* loaded and non-loaded DNA-MS.

Dry particle size. Each DNA-MXN-MS and blank DNA-MS produced particles with mean dry diameters of less than 10μm in diameter, Table 6-6. DNA-MNX-MS prepared at the 10% (w/w), 15% (w/w), and 25% (w/w) MXN concentrations produced narrow and normalized particle size distributions, Figure 6-28. The 10% (w/w) MXN condition produced a small volume percent of aggregates between the 15μm and 30μm diameter range which may have arisen due to interparticle bonding. The presence of aggregates was reflected in standard deviation of the 10% (w/w) MXN condition, however, a one way ANOVA illustrated no significant size differences among the DNA-MXN-MS prepared at the varying MXN concentrations.

Table 6-6. Dry mean particle diameter values for crosslinked and non-crosslinked DNA-MXN-MS and DNA-MS.

Condition	Dry mean particle diameter (μm)
10% (w/w) DNA-MXN-MS	2.7 ± 4.5
15% (w/w) DNA-MXN-MS	2.1 ± 2.8
25% (w/w) DNA-MXN-MS	1.8 ± 1.9
15% (w/w) DNA-MXN-MS (no Gd crosslinking)	2.8 ± 4.1
DNA-MS	2.2 ± 2.1
DNA-MS (no Gd crosslinking)	5.5 ± 8.7

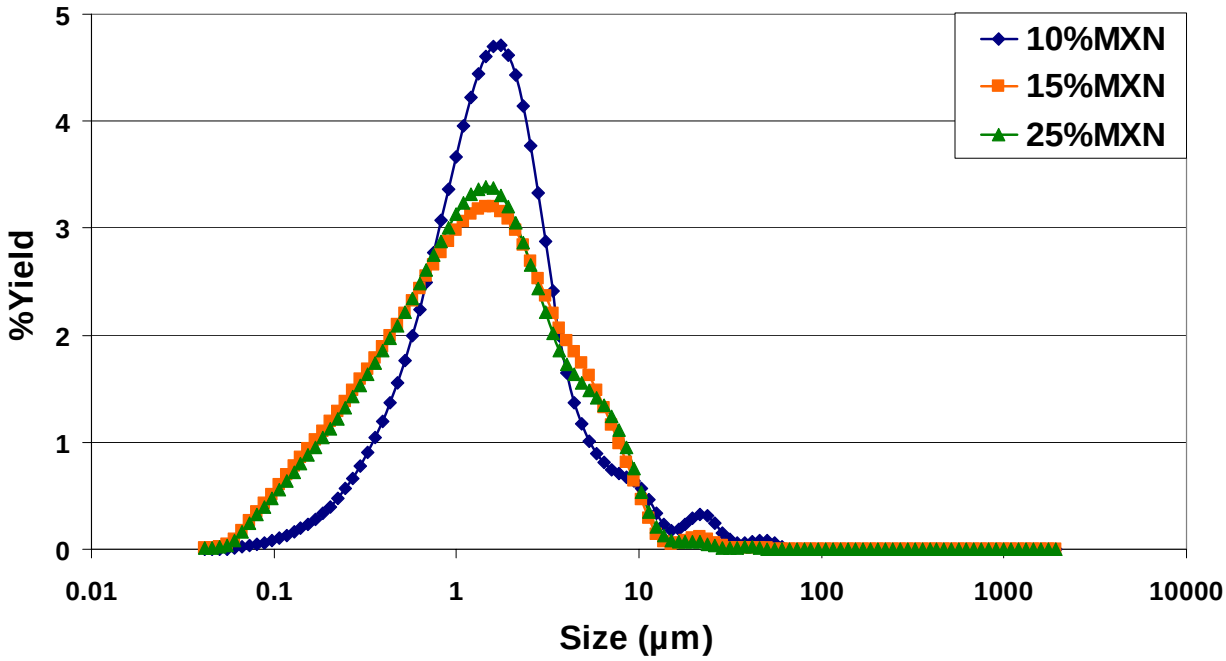

Figure 6-28. Dry particle size distribution for DNA-MXN-MS prepared at varying MXN concentrations.

Particle size distributions for non-crosslinked conditions were normalized; however, they exhibited aggregate formation within the 13µm to 55µm diameter range, Figure 6-29. The aggregates present may have been a result of non-crosslinked DNA material in the yield. A larger degree of aggregates were present in the non-crosslinked blank DNA-MS size distributions as compared to the non-crosslinked DNA-MXN-MS, Figure 6-30. This data suggests that MXN may help to bind the DNA-MS together and thus reduce the amount of aggregates formed in the yield.

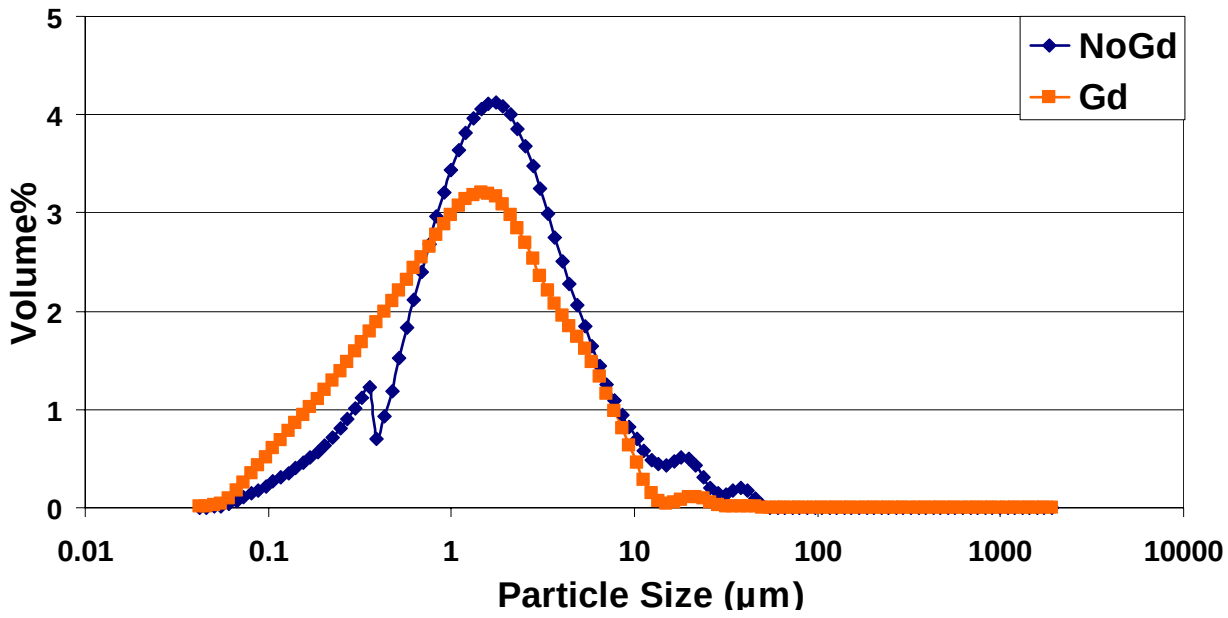

Figure 6-29. Dry particle size distribution comparison of DNA-MXN-MS prepared with and without gadolinium crosslinking.

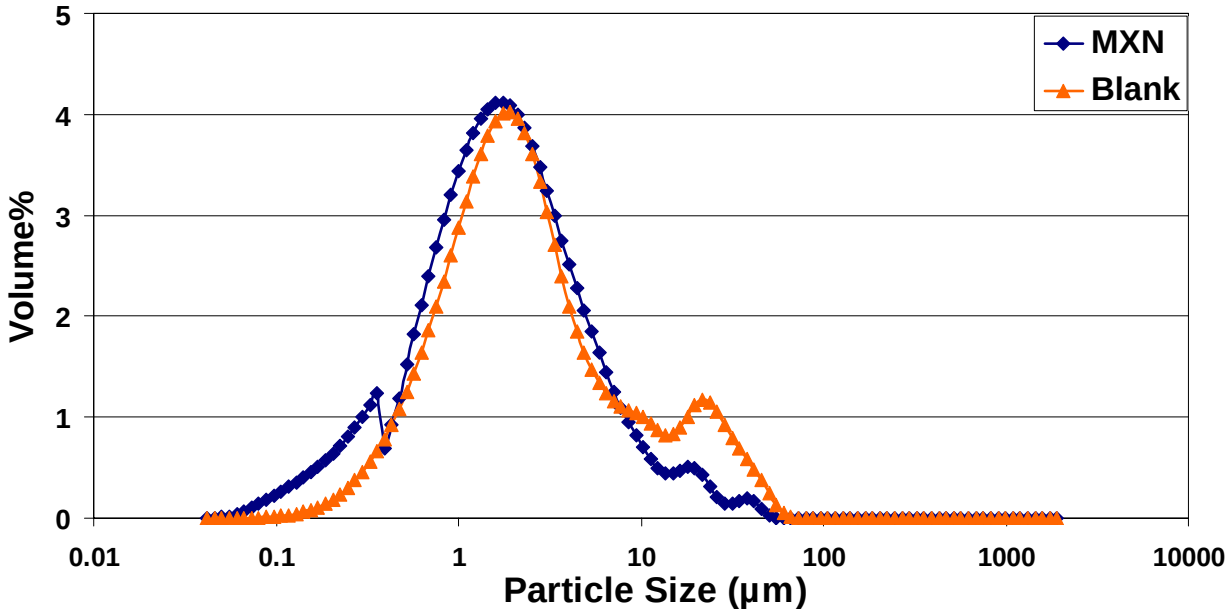

Figure 6-30. Dry particle size distribution comparison of non-crosslinked DNA-MXN-MS and blank DNA-MS.

Scanning electron microscopy. SEM micrographs of the DNA-MXN-MS prepared at varying MXN concentrations depicted particles with spherical morphologies and smooth topographies, Figure 6-31. These results are consistent with data obtain in Chapter 5 for DNA-

MXN-MS prepared at the 1550rpm mixer speed with 120%M_{EQ} gadolinium crosslinking. SEM micrographs of the DNA-MXN-MS also illustrated that the DNA-MXN-MS produced at the 25% (w/w) MXN concentration produced smaller particles than those obtained at the 10% (w/w) and 15% (w/w) MXN concentrations confirming results obtained during particle size analysis. In addition, particles produced at the 25% (w/w) MXN concentration appear to be more uniform in size. These findings are inconsistent with current literature which cite that increasing the drug concentration increases the MS particle diameters.[144, 169]

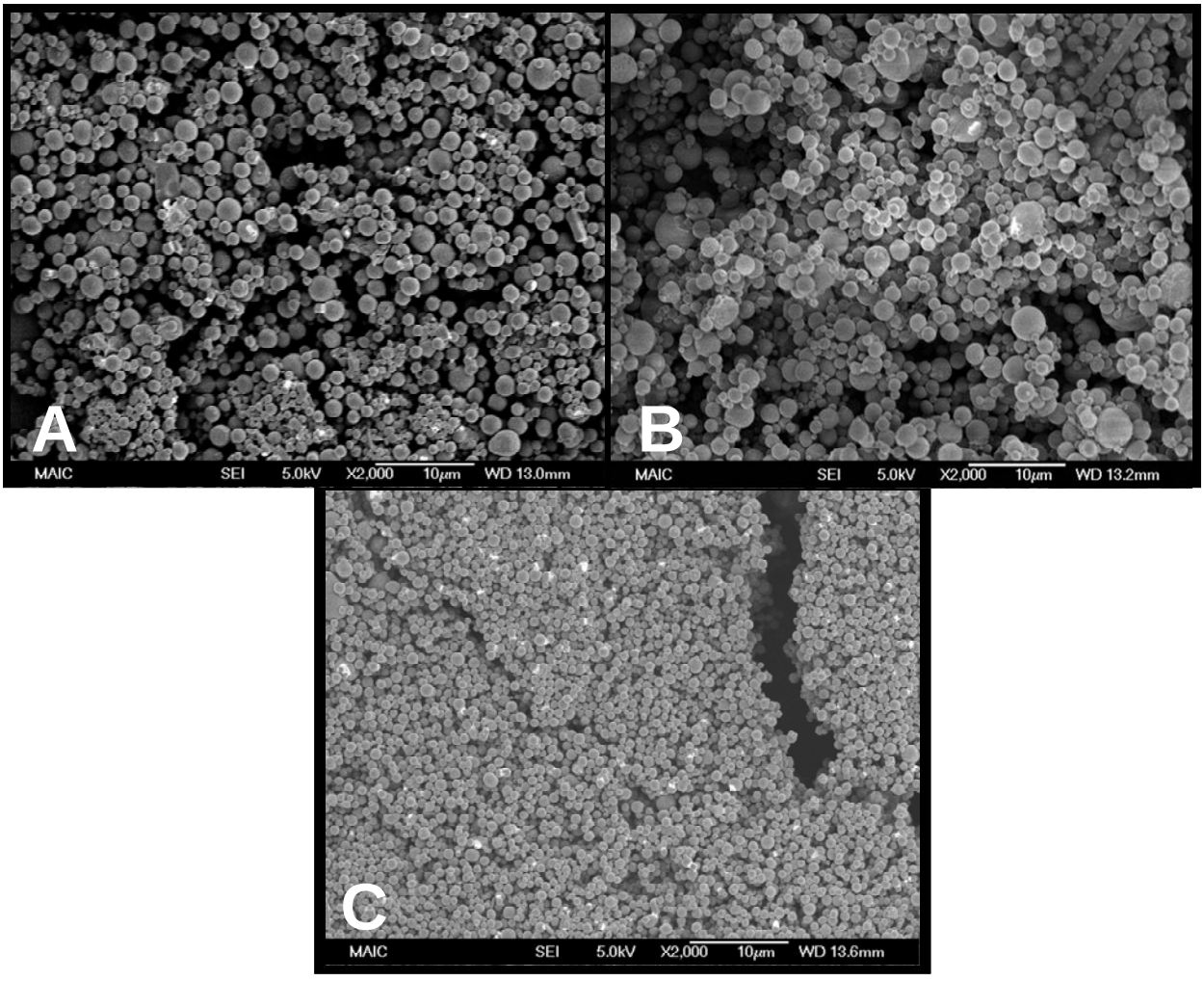

Figure 6-31. SEM micrographs of DNA-MXN-MS prepared at the A) 10% (w/w), B) 15% (w/w), and C) 25% (w/w) MXN concentrations (Magnifications: 2,000x).

DNA-MXN-MS prepared with no gadolinium crosslinking produced particles with smooth surface topographies; however, some particles displayed irregular morphologies as compared to DNA-MXN-MS prepared with gadolinium crosslinking, Figure 6-32. In addition, DNA-MXN-MS prepared with no crosslinking displayed particles that were less uniform in size. The same trends were seen for DNA-MS prepared without gadolinium crosslinking, Figure 6-33.

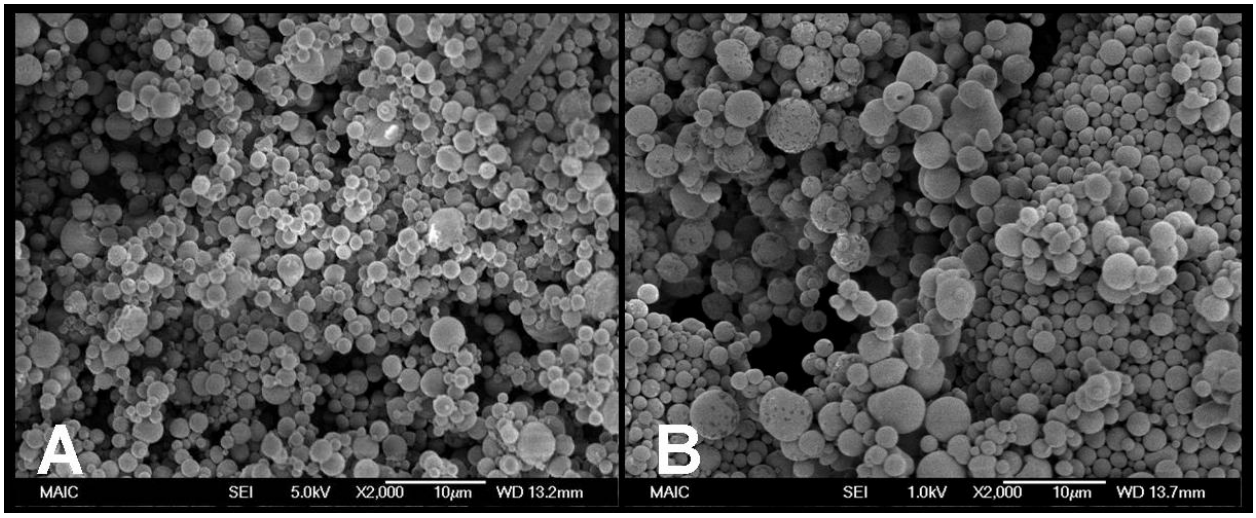

Figure 6-32. SEM micrographs of DNA-MXN-MS prepared with A) gadolinium crosslinking and B) no gadolinium crosslinking (Magnifications: 2,000x).

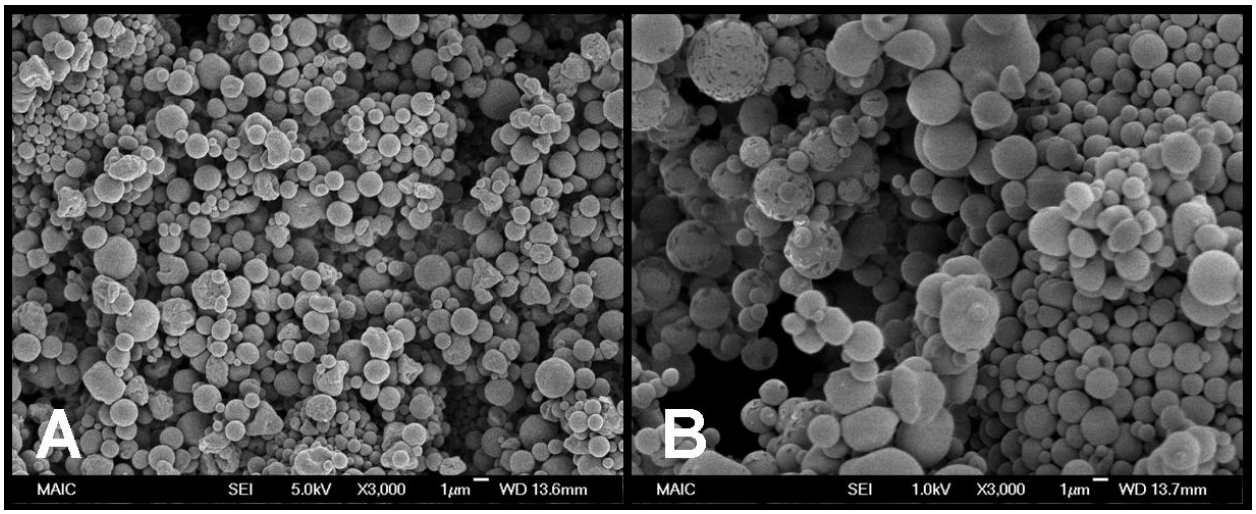

Figure 6-33. SEM micrographs of DNA-MS prepared with no gadolinium crosslinking, A) blank DNA-MS and B) MXN *in situ* loaded DNA-MS (Magnifications: 3,000x).

In vitro MXN loading efficiency

The MXN percent loadings and loading efficiencies of the DNA-MXN-MS were measured in triplicate by enzymatic digestion followed by photometric analysis. MXN percent loadings were calculated using Equation 6-7 and the loading efficiencies were calculated using Equation 6-8. The 10% (w/w) and 15% (w/w) MXN conditions produced loading efficiencies of over 80% whereas the 25% (w/w) MXN condition only produced loading efficiencies of over 30%, Figure 6-34. It was noted, however, that the 25% (w/w) MXN samples were still blue on the final day of the digestion study suggesting that the entrapped MXN may not have fully released due to incomplete digestion of the MS. This may explain the low loading efficiency of the 25% (w/w) MXN condition, however, it has been cited in the literature that the drug loading efficiencies are decreased when the drug payloads are increased.[135, 144, 170]

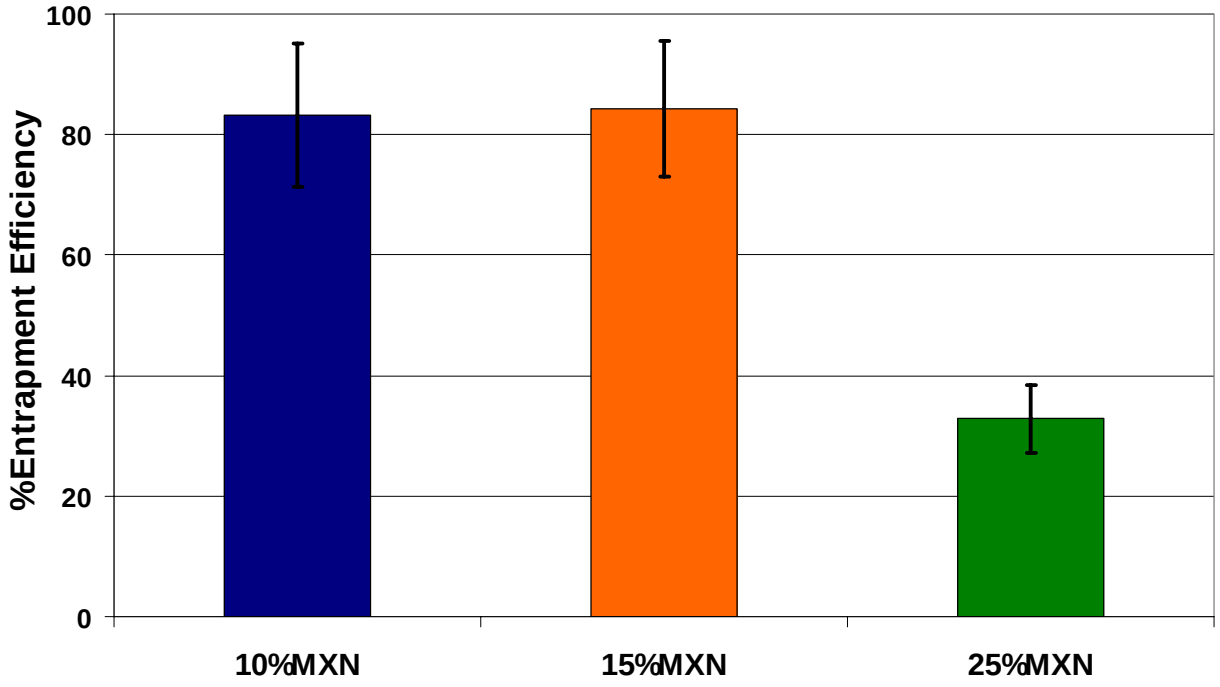

Figure 6-34. Loading efficiency comparison chart for DNA-MXN-MS prepared at varying MXN concentrations.

DNA-MXN-MS prepared with no gadolinium crosslinking produced loading efficiencies of over 95% which were slightly larger than those obtained for DNA-MXN-MS prepared with gadolinium crosslinking, Figure 6-35. Non-crosslinked DNA-MXN-MS were fully digested by the end of the digestion study suggesting that incomplete digestion of the crosslinked DNA-MXN-MS may have resulted in lower loading efficiency values. Table 6-7 lists the percent drug loading and loading efficiency values for each DN-MXN-MS condition tested.

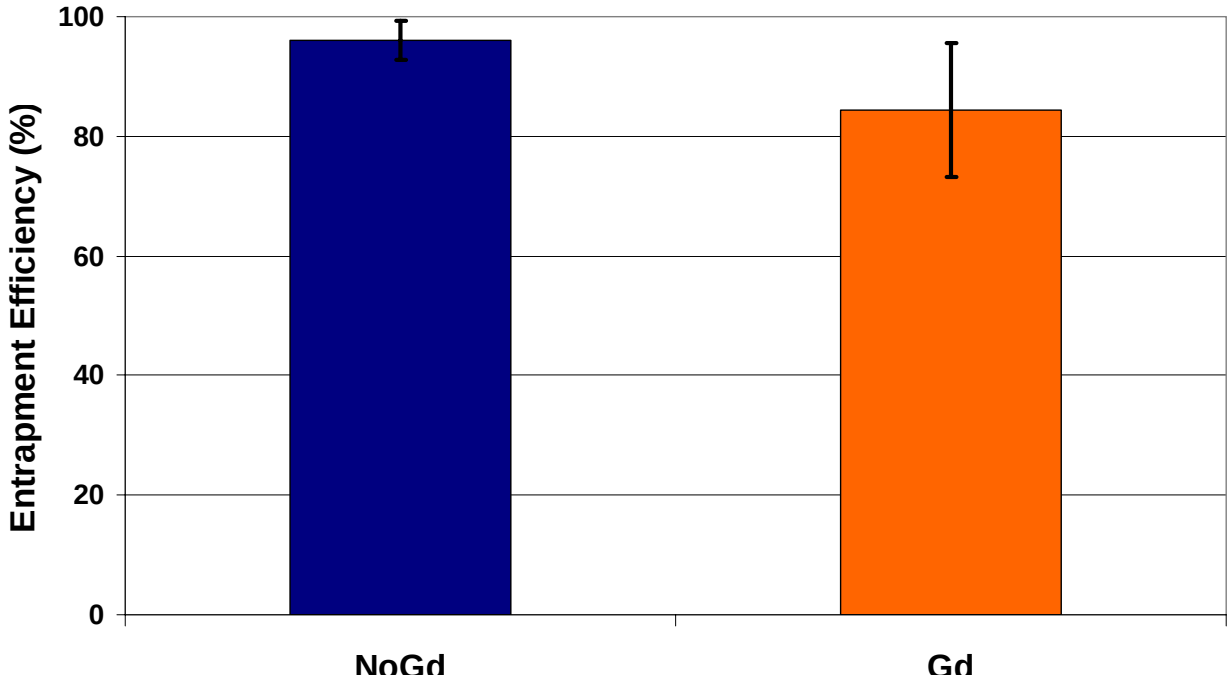

Figure 6-35. Loading efficiency comparison chart for DNA-MXN-MS prepared at with and without gadolinium crosslinking.

Table 6-7. Percent loading and loading efficiency values for DNA-MXN-MS.

Condition	Experimental loading (%)	Theoretical loading (%)	Loading efficiency (%)
10% (w/w) MXN	9.3 ± 1.3	11.1	83.3 ± 11.9
15% (w/w) MXN	12.4 ± 1.7	14.8	84.3 ± 11.2
25% (w/w) MXN	8.2 ± 1.4	25.0	32.8 ± 5.6
15% (w/w) MXN (no gadolinium crosslinking)	17.9 ± 0.6	18.7	96.0 ± 3.3

A one way ANOVA followed by a Tukey's test for multiple comparisons was conducted on all DNA-MXN-MS collected data and illustrated that the 25% (w/w) MXN condition

produced significantly lower loading efficiencies than the 10% (w/w) and the 15% (w/w) MXN conditions ($p = 0.002$). There were no significant loading efficiency differences between the 10% (w/w) and 15% (w/w) MXN conditions. A t-test also illustrated no significant loading efficiency differences between the non-crosslinked and crosslinked DNA-MXN-MS.

***In vitro* MXN release**

The *in vitro* MXN release properties of the DNA-MXN-MS were measured in 0.05M PBS at a pH of 7.4. Each DNA-MXN-MS condition was tested in triplicate using minimum sink conditions (i.e. low volume) and incubated in 1.250mL of PBS at 37˚C to simulate the tumor environment. DNA-MXN-MS prepared with varying MXN concentrations each released an initial "burst" of MXN within the first two hours with the 10% (w/w) MXN condition producing the largest and quickest MXN release, Figure 6-36. The 25% (w/w) MXN condition displayed the slowest sustained release within the first 24 hours followed by the 15% (w/w) and 10% (w/w) MXN conditions. The slower release of MXN from the 25% (w/w) condition suggests that the intercalation of MXN within the DNA matrix helps to control the release of MXN *in vitro*. MXN ceased to release for the 10% (w/w) and 15% (w/w) MXN conditions after 24 hours; however, the 25% (w/w) MXN condition exhibited an increase in release between days 3 and 4 and ceased releasing after day 4, Figure 6-37. This increase in release may have been a result of the degradation of the DNA-MXN-MS. These findings are inconsistent with current literature which site that release rates are increased when drug payload is increased due to a decrease in the integrity of the MS due to the larger drug payload.[170] This citing further validates our assumptions that the MXN is helping to hold the DNA-MS matrix together *in vitro*. The *in vitro* release of MXN from the 10% (w/w) and 15% (w/w) MXN conditions appeared to be diffusion controlled and follow first-order release kinetics. The *in vitro* release of MXN from the 25%

(w/w) MXN condition appeared to be controlled by both, diffusion and erosion, and followed first-order release kinetics.

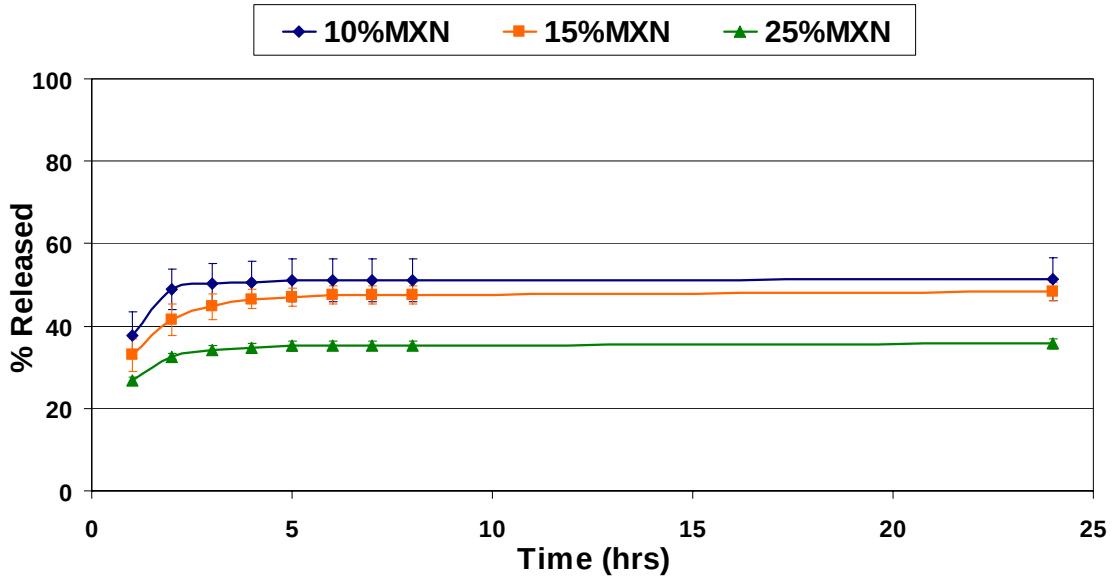

Figure 6-36. The first 24 hour MXN release profiles for DNA-MXN-MS prepared at varying MXN concentrations.

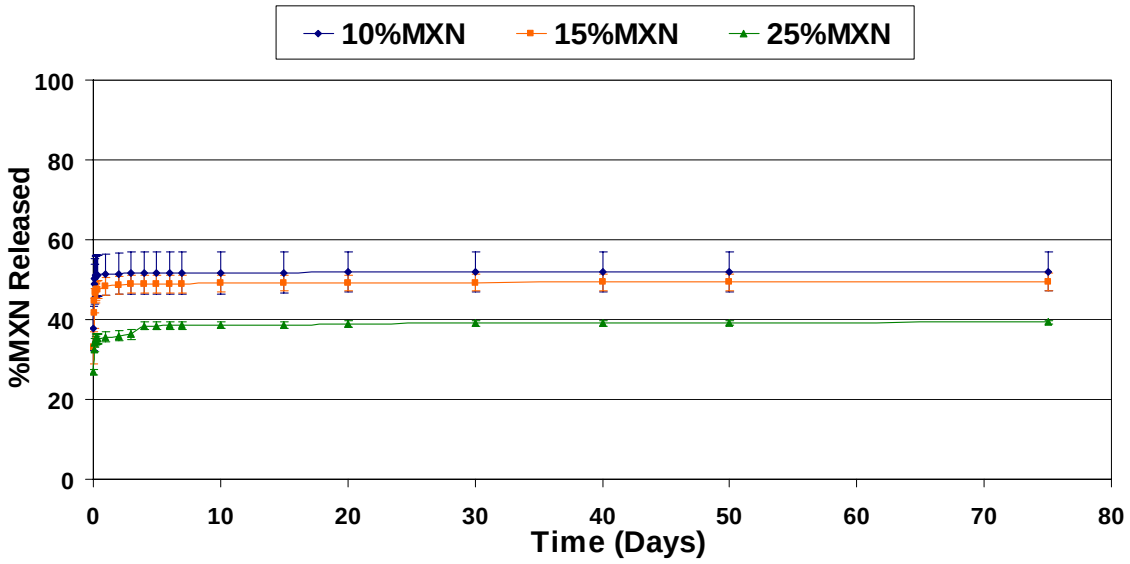

Figure 6-37. MXN release profiles for DNA-MXN-MS prepared at varying MXN concentrations.

DNA-MXN-MS prepared with out gadolinium crosslinked also produced an initial "burst" release within the first three hours and ceased releasing after 24 hours, Figures 6-38 and 6-39.

As expected, the non-crosslinked DNA-MXN-MS released MXN quicker than the crosslinked DNA-MXN-MS which exhibited a more sustained release. The *in vitro* release of MXN from the non-crosslinked and crosslinked DNA-MXN-MS appeared to be diffusion controlled and follow first-order release kinetics.

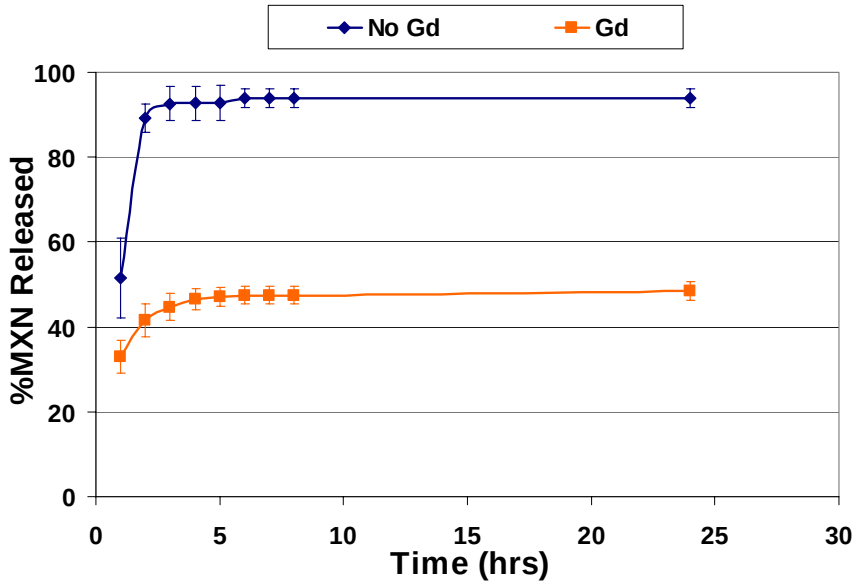

Figure 6-38. The first 24 hour MXN release profiles for DNA-MXN-MS prepared with and without gadolinium crosslinking.

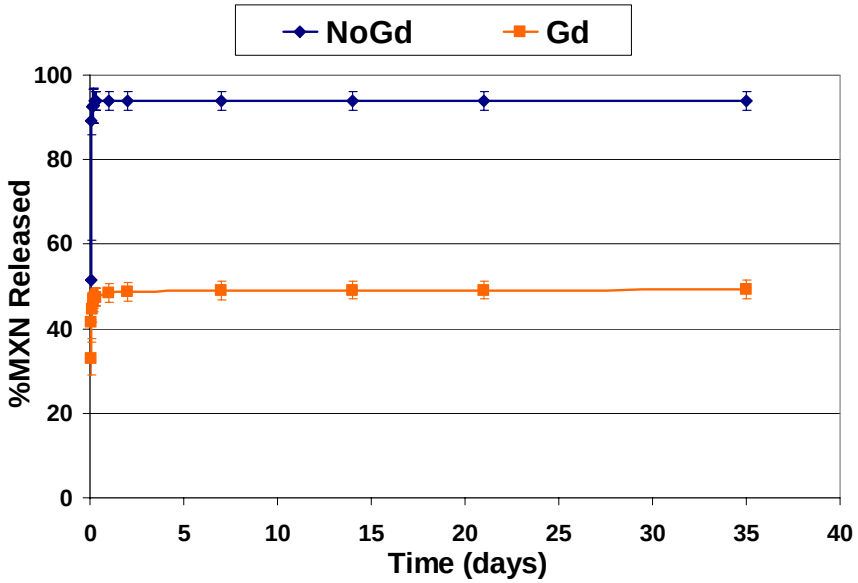

Figure 6-39. MXN release profiles for DNA-MXN-MS prepared with and without gadolinium crosslinking.

Conclusions

MTX and 5-FU *In Situ* Loaded DNA-MS and BSA-MS

The objective of these studies was to further analyze the drug loading capabilities of DNA and BSA. MTX and 5-FU *in situ* loaded BSA-MS and DNA-MS were prepared to produce particles with controlled size distributions where at least 60% of all particles prepared were within the mesosphere size range of 1μm to 10μm and < 5% of all particles were greater than 10μm in size. Particles less than 1μm in diameter were also acceptable and hydrated particle diameters were to be less than 25μm. In addition, DNA-MS and BSA-MS were sought to obtain drug loadings of ≥ 5% (w/w) MTX or 5-FU and release drug for more than 24 hours in phosphate buffered saline under minimum sink conditions. Drug loaded BSA-MS and DNA-MS were compared with respect to particle diameter, size distribution, morphology, topography, drug loading, and percent drug release.

Particle analysis

MTX and 5-FU *in situ* loaded BSA-MS and DNA-MS produced discreet particles with yields that ranged from 40% to 81%. Drug loaded particles displayed narrow and normal size distributions with mean diameters of less than 10μm. Each MTX and 5-FU loaded MS condition produced particles where greater than 60% of all the particles prepared fell within the 1μm to 10μm size range and less than 5% of all the particles were larger than 10μm with the exception of the MTX loaded DNA-MS. Drug load concentration did not affect the particle diameters and size distributions of MTX loaded BSA-MS, however, increasing the mixer speed from 1250rpm to 1550rpm did narrow and normalize size distributions. There were no significant size differences between MTX loaded BSA-MS and DNA-MS; however, BSA was the only material to produce MTX loaded MS with spherical morphologies. MTX did not readily load into DNA. In addition, 5-FU loaded BSA-MS and DNA-MS produced discreet particles with spherical

morphologies with no significant size differences between them. 5-FU loaded DNA-MS produced particles with smooth topographies, however, BSA-MS loaded with MTX and 5-FU exhibited wrinkled surface topographies. The yielding surface topography was a result of the dehydration of the BSA-MS during acetone washing and drying due to the large concentration of aqueous glutaraldehyde used during synthesis. It is expected that using a lower concentration of glutaraldehyde would result in smoother BSA-MS topographies.

***In vitro* MTX and 5-FU loading efficiency and release**

The loading efficiencies for the MTX loaded conditions ranged from 61% to 94%. A maximum loading of 24% (w/w) MTX was obtained for the BSA-MS and 10% (w/w) for the DNA-MS. The 5-FU loaded conditions produced poor loading efficiencies of approximately 20% for both BSA-MS and DNA-MS. A maximum loading of 6% (w/w) 5-FU was obtained for BSA-MS and 5% (w/w) for DNA-MS.

T-tests were conducted on BSA-MS to determine if mixer speed or drug payload effected MTX loading. These t-tests illustrated no significant loading efficiency differences as a result of mixer speed or percent drug loaded; however the t-tests did find that the BSA-MS entrapped significantly more MTX than the DNA-MS ($p = 0.002$). A t-test was also conducted on the 5-FU conditions to determine if the drug loading material effected 5-FU loading. The t-test illustrated no significant loading efficiency differences between the BSA-MS and DNA-MS conditions.

MTX loaded BSA-MS released higher concentrations of MTX at a quicker rate than those obtained with the MTX loaded DNA-MS. Each MTX condition tested displayed an initial "burst" release within the first three hours, and had ceased releasing by Day 2. MTX release analyzed from both BSA-MS and DNA-MS 15% (w/w) *in situ* loaded conditions were found to be diffusion controlled and follow first-order release kinetics. MTX concentrations released from the BSA-MS and DNA-MS were found to decrease over time after the initial burst release.

The MTX release from the 30% (w/w) *in situ* loaded BSA-MS condition was also diffusion controlled and exhibited a biphasic release pattern. The first eight hours of MTX release were governed by the Higuchi square root time release kinetics model and the MTX release after hour 8 followed first-order release kinetics.[158]

The 5-FU *in situ* loaded DNA-MS released a larger concentration of drug at a quicker rate than the BSA-MS condition. The *in vitro* release of 5-FU from DNA-MS appeared to be diffusion controlled and followed the Higuchi square root time kinetics model for release during the first eight hours and first-order kinetics for the duration of release. The 5-FU *in situ* loaded BSA-MS however; exhibited erosion controlled release and followed the Higuchi square root time kinetics model for release throughout the duration of the study. The sustained release of 5-FU achieved with the BSA-MS may have been attributed to the slow degradation of the highly crosslinked BSA-MS.

Overall conclusions

Overall, BSA-MS produced optimal particle properties for intratumoral chemotherapy and were able to load MTX more efficiently than DNA-MS. BSA-MS entrapped 14% (w/w) more MTX than DNA-MS and released MTX at larger concentrations at a faster rate. MTX release analyzed from both BSA-MS and DNA-MS were found to be diffusion controlled and follow first-order release kinetics. MTX release from BSA-MS was found to be diffusion controlled and exhibit a biphasic release pattern by increasing the MTX release from 15% (w/w) to 30% (w/w). Release from 30% (w/w) MTX loaded BSA-MS were governed by the Higuchi square root time release kinetics model during the first eight hours and first-order release kinetics after hour 8.

DNA-MS and BSA-MS produced equivalent 5-FU loadings with optimal MS properties; however, DNA-MS released 5-FU at larger concentrations and at a faster rate than BSA-MS. 5-

FU release from DNA-MS was diffusion controlled and followed Higuchi and first-order release kinetics, whereas 5-FU release from BSA-MS was erosion controlled and followed the Higuchi model throughout the release study duration.

DNA-MXN-MS Studies

MXN *in situ* loaded DNA-MS were prepared to determine the maximum drug loading ability of DNA. DNA-MXN-MS were prepared with a 120%M_{EQ} gadolinium crosslink concentration and were loaded with 10% (w/w), 15% (w/w), and 25% (w/w) MXN. The particle diameter, size distribution, morphology, topography, drug loading, and percent drug release of the DNA-MXN-MS were evaluated with respect to MXN concentration. DNA-MXN-MS were also prepared with no gadolinium crosslinking to determine if MXN serves as a crosslinking agent to DNA-MS. DNA-MXN-MS were prepared with 15% (w/w) *in situ* loaded MXN and were compared with respect to crosslinking.

Particle analysis

DNA-MXN-MS produced discreet particles with yields of over 65%. Each DNA-MXN-MS and blank DNA-MS produced particles with mean dry diameters of less than 10μm in diameter. A one way ANOVA conducted on the DNA-MXN-MS prepared at the 10% (w/w), 15% (w/w), and 25% (w/w) MXN concentrations illustrated no significant size differences among the DNA-MXN-MS with regard to MXN concentration. A t-test conducted on the crosslinked and non-crosslinked DNA-MXN-MS illustrated that size was not dependent on gadolinium crosslinking; however, particle morphologies were less spherical for the non-crosslinked DNA-MXN-MS than for the crosslinked DNA-MXN-MS.

DNA-MXN-MS prepared at varying MXN concentrations produced particles with narrow and normalized particle size distributions, spherical morphologies, and smooth topographies. Particle size distributions for non-crosslinked conditions were normalized; however, they

exhibited aggregate formation within the 13μm to 55μm diameter range. A larger degree of aggregates were present in the non-crosslinked blank DNA-MS size distributions as compared to the non-crosslinked DNA-MXN-MS which may have been a result of non-crosslinked DNA material in the yield. This data suggests that MXN may help to bind the DNA-MS together through intercalation thus reducing the amount of aggregates formed in the yield.

***In vitro* MXN loading efficiency and release**

A maximum MXN loading concentration of 18% (w/w) was obtained for DNA-MS and MXN loading efficiencies ranged from 33% to 96%. The 10% (w/w) and 15% (w/w) MXN conditions produced loading efficiencies of over 80% whereas the 25% (w/w) MXN condition only produced a significantly lower loading efficiency of just over 30%. However, DNA-MXN-MS prepared at the 25% (w/w) MXN condition were not fully digested at the end of the digestion study and the low loading efficiency values obtained at this condition may have been a result of their incomplete digestion suggesting that MXN may further stabilize the DNA-MS matrix through intercalation.

DNA-MXN-MS prepared with no gadolinium ion crosslinking produced loading efficiencies of over 95% which were slightly larger than those obtained for DNA-MXN-MS prepared with gadolinium crosslinking; however, a t-test found no significant loading efficiency differences between the non-crosslinked and crosslinked DNA-MXN-MS.

The 10% (w/w), 15% (w/w), and 25% (w/w) DNA-MXN-MS conditions exhibited first-order release kinetics and each released an initial "burst" of MXN of over 30% within the first two hours with the 10% (w/w) MXN condition producing the largest and quickest MXN release. The 25% (w/w) MXN condition displayed the slowest sustained release within the first 24 hours followed by the 15% (w/w) and 10% (w/w) MXN conditions. The slower release of MXN from the 25% (w/w) condition further suggests that the intercalation of MXN within the DNA matrix

helps to control the release of MXN *in vitro*. MXN ceased to release for the 10% (w/w) and 15% (w/w) MXN conditions after 24 hours; however, the 25% (w/w) MXN condition exhibited an increase in release between Days 3 and 4 and ceased releasing after Day 4 suggesting that MXN release from the 25% (w/w) condition is erosion controlled whereas MXN release for the 10% (w/w) and the 15% (w/w) MXN conditions are diffusion controlled.

Overall conclusions

Overall, DNA-MS produced a maximum MXN loading of 18% (w/w). Resulting DNA-MXN-MS mean diameters were found to not be dependent on gadolinium crosslinking nor MXN payload; however, gadolinium ion crosslinked DNA-MXN-MS produced MS with more spherical morphologies and more narrow and normal size distributions. The *in vitro* release of MXN from DNA-MS was diffusion controlled and followed first-order release kinetics. The 10% (w/w) MXN condition produced the largest and quickest MXN release followed by the 15% (w/w) and 25% (w/w) MXN conditions. The incomplete digestion and the slow release of MXN from the 25% (w/w) MXN condition suggest that MXN may stabilize the DNA-MS matrix through intercalation and help control the release of MXN *in vitro*.

CHAPTER 7
CONCLUSIONS

Overview

DNA nano-mesospheres (DNA-MS) were prepared for the first time using a modified steric stabilization method that was developed in this lab for the preparation of albumin meso-microspheres. The steric stabilization method was modified for DNA-MS synthesis by increasing the initial mixer speed to 1550rpm and by adding a filtration step to the end of the process. These two modifications resulted in discreet DNA-MS with yields of over 70% and optimal particle diameters that ranged from 50nm to 10μm with normal and narrow size distributions.

DNA-MS were prepared with gadolinium crosslinking through ionic interactions with DNA phosphate groups. Gadolinium crosslinking was confirmed by DNA-MS stability in Grey's balanced salt solution (BSS) and phosphate buffered saline (PBS). Evidence of gadolinium bonding with DNA was determined via energy dispersive x-ray spectroscopy (EDS) which suggest that these mesospheres may have imaging capabilities.

The chemotherapy drug mitoxantrone (MXN) was readily incorporated into the DNA-MS during synthesis with MXN entrapments of over 70%. 5-fluorouracil (5-FU) was also loaded into DNA-MS suggesting the significant potential for the use of these DNA-MS as biodegradable carriers for intratumoral chemotherapy. MXN and 5-FU release profiles extending over 30 days demonstrated a controlled and prolonged release of the chemotherapy drugs from the DNA-MS. The efficacy of MXN loaded DNA-MS was demonstrated *in vitro* using a murine Lewis lung carcinoma (mLLC) cell line. The *in vitro* cell study illustrated that MXN loaded DNA-MS produce a cytotoxic response on the mLLC cells at doses as low as 1ppm. The controlled and sustained release properties and *in vitro* cytotoxicity of drug loaded

DNA-MS suggests that their clinical use may provide less frequent chemotherapy visits, which may substantially improve the quality of life for patients suffering from various solid tumor cancers.

Overall, these DNA nano-mesospheres may offer a possible alternative to conventional oral or intravenous therapies by providing localized, controlled, and prolonged chemotherapy.

DNA Nano-Meso-Microspheres Synthesis

1. A stabilizing agent concentration of 5% (w/v) CAB (cellulose acetate butyrate in 1,2-dichloroethane) was found to produce spherical and discreet DNA-MS the most efficiently.

2. Chromium, gadolinium, and iron trivalent cationic crosslinking agents were found to react instantaneously with DNA, whereas reactions with glutaraldehyde take 2 hours and reactions with genipin take over 72 hours.

3. DNA-MS synthesized with ionic and covalent crosslinking agents produced dry mean diameters of less than 20μm; however, genipin was unable to crosslink DNA (i.e. DNA-MS did not turn blue) and chromium, iron, and glutaraldehyde crosslinked DNA-MS displayed multimodal dry particle size distributions suggesting that they may not be optimal crosslinking agents for DNA-MS.

4. Gadolinium crosslinked DNA-MS produced the smallest dry (2.6μm) and hydrated (12.1μm) particles, with the largest zeta potential values (-45.3mV), and the most narrow and normal size distributions of all the crosslinking agents tested. In addition, the gadolinium crosslinked DNA-MS displayed the most stable dispersability in Grey's BSS with dispersion times exceeding 48 hours.

5. EDS analysis of DNA-MS confirmed the presence of the chromium, gadolinium, and iron cationic crosslinking agents strongly suggesting that the trivalent cations are indeed chemically bonding with the DNA.

6. Filtration removed aggregates and particles over 20μm in diameter, normalized dry and hydrated particle size distributions, and produced only an18% decrease in yield, as compared to the non-filtered yield, for gadolinium crosslinked DNA-MS.

7. Increasing the stir speed from 950rpm to 1550rpm produced particles with mean diameters of less than 10μm and normalized particle size distributions for all non-drug loaded and drug loaded DNA-MS and BSA-MS (i.e. MXN, MTX, 5-FU).

8. Drug pay load did not affect the particle diameters and size distributions of MXN, MTX, and 5-FU loaded DNA-MS and BSA-MS.

9. Increasing the gadolinium crosslink concentration from 20%M_{EQ} to 120%M_{EQ} did not affect the mean dry particle diameters or the particle size distributions for DNA-MXN-MS.

10. Gadolinium crosslinked DNA-MS and DNA-MXN-MS produce less aggregates than non-crosslinked DNA-MS and DNA-MXN-MS.

11. DNA-MXN-MS prepared at the 1550rpm mixer speed with a gadolinium concentration of 120%M_{EQ} produced the most optimal MS results with yields over 85%, dry particle diameters less than 5μm, hydrated particle diameters less than 20μm, normalized and narrow size distributions, and excellent stability in PBS.

12. EDS analysis confirmed the presence of gadolinium in DNA-MXN-MS prepared with gadolinium concentrations in the range of 20%M_{EQ} to 120%M_{EQ} with the 120%M_{EQ} condition producing the largest counts of both gadolinium and chlorine.

13. Zeta potential analysis confirmed the *in situ* loading of the cationic drug MXN into the DNA-MXN-MS through a significant increase in DNA-MS surface charge (i.e. -45.3mV to -22.4mV).

14. BSA-MS *in situ* loaded with MTX produced discreet particles with spherical morphologies and wrinkled topographies. DNA-MS *in situ* loaded with MTX produced discreet particles with irregular morphologies and topographies.

15. BSA-MS *in situ* loaded with 5-FU produced discreet particles with spherical morphologies and wrinkled topographies. DNA-MS *in situ* loaded with 5-FU produced discreet particles with spherical morphologies and smooth topographies.

Drug Loading and Release

1. Increasing the gadolinium concentration from 20%M_{EQ} to 120%M_{EQ} for DNA-MXN-MS decreased MXN loading efficiencies from 91% to 84% and decreased MXN loadings from 13.5% to 12.4%; however, conditions were statistically comparable. Increasing the gadolinium concentration also decreased the *in vitro* release of MXN into phosphate buffered saline.

2. MXN loading and loading efficiencies for gadolinium crosslinked DNA-MXN-MS were found to be statistically comparable to those obtained with MXN *in situ* loaded albumin and gelatin microspheres.

3. Non-crosslinked DNA-MXN-MS loaded 6% (w/w) more MXN than gadolinium crosslinked DNA-MXN-MS (i.e. Non-crosslinked max loading was 18% (w/w) MXN where gadolinium crosslinked max loading was 12.4% (w/w) MXN).

4. DNA-MXN-MS prepared with gadolinium concentrations that ranged from 20%M_{EQ} to 120%M_{EQ} each produced a “drug burst” release within the first 24 hours; however, a sustained MXN release was measured up to 75 days.

5. DNA-MXN-MS prepared at the 120%M_{EQ} gadolinium crosslink concentration were found to release MXN most efficiently (i.e. a significant increase in MXN release was found between Day 1 and Day 75).

6. Increasing the MXN payload from 10% (w/w) to 25% (w/w) decreased MXN loading efficiencies from 83% to 33% with a maximum MXN loading of 18% (w/w) obtained. In addition, increasing the MXN payload from 10% (w/w) to 25% (w/w) decreased the *in vitro* release of MXN into phosphate buffered saline; however, low MXN loading efficiency and *in vitro* release values obtained for the 25% (w/w) MXN condition may have been a result of incomplete digestion which was observed during analysis.

7. The sustained release of MXN was measured for up to 35 days for the 10% (w/w), 15% (w/w), and 25% (w/w) DNA-MXN-MS conditions. Each MXN condition exhibited diffusion controlled first-order release kinetics after releasing an initial "burst" of over 30% MXN within the first two hours.

8. BSA-MS entrapped 14% (w/w) more MTX than DNA-MS and released larger concentrations of MTX at a faster rate (i.e. BSA max loading was 24% (w/w) MTX and DNA max loading was 10% (w/w) MTX).

9. MTX release from both BSA-MS and DNA-MS were measured up to 35 days and were found to be diffusion controlled and follow first-order release kinetics after the initial burst exhibited during the first three hours.

10. Increasing MTX loading from 15% (w/w) to 30% (w/w) resulted in a diffusion controlled biphasic release pattern where MTX release was governed by the Higuchi square root time release kinetics model during the first eight hours and first-order release kinetics after hour 8.

11. 5-FU loaded conditions produced poor loading efficiencies of approximately 20% for both BSA-MS and DNA-MS. A maximum loading of 6% (w/w) 5-FU was obtained for BSA-MS and 5% (w/w) for DNA-MS.

12. DNA-MS released 5-FU at larger concentrations and at a faster rate than BSA-MS. 5-FU release from DNA-MS was diffusion controlled and followed Higuchi and first-order release kinetics, whereas 5-FU release from BSA-MS was erosion controlled and followed the Higuchi model throughout the release study duration.

In vitro Cell Growth and Cytotoxicity

1. Human dermal fibroblast growth data and optical microscopy images illustrated that DNA derived from herring testes does not elicit an anti-proliferative response or a cytotoxic response *in vitro*.

2. DNA-MS crosslinked with chromium and gadolinium produced the best *in vitro* fibroblast growth results with proliferation rates that either exceeded or were comparable

to the media with cells control condition at both the 25μg and 100μg DNA-MS concentrations.

3. Iron crosslinked DNA-MS produced significantly lower proliferation rates than the media with cells control group for both 25μg and 100μg DNA-MS concentrations indicating that iron at DNA-MS concentrations as low as 25μg elicit negative fibroblast growth responses *in vitro*.

4. Glutaraldehyde crosslinked DNA-MS elicited a negative fibroblast growth response at the 100μg DNA-MS concentration and not at the 25μg DNA-MS concentration indicating that glutaraldehyde crosslinked DNA-MS elicit negative fibroblast growth responses at DNA-MS concentrations greater than 25μg.

5. The effect of MXN on the *in vitro* viability of murine Lewis lung carcinoma cells was found to be dose dependent. The 1μg/mL DNA-MXN-MS dose did not elicit a cytotoxic response until Day 2; however, the 10μg/mL and 25μg/mL DNA-MXN-MS dose conditions exhibited cytotoxicity responses by Day 1.

6. DNA-MXN-MS conditions elicited significantly higher murine Lewis lung carcinoma cytotoxicities than the free MXN conditions at each dose suggesting that the gadolinium in the DNA-MXN-MS contributes to the *in vitro* cytotoxicity or that DNA-MXN-MS are more readily taken up by the murine Lewis lung carcinoma cells than free MXN.

CHAPTER 8
FUTURE STUDIES

The research presented in this dissertation was devoted to the synthesis and properties of drug loaded DNA nano-meso-microspheres (DNA-MS) for intratumoral chemotherapy applications. This section highlights research topics that may be of interest to pursue for future studies.

1. **Synthesis and characterization of DNA-MS crosslinked with genipin.** Crosslink reaction studies presented in Chapter 3 illustrated that DNA did interact with genipin after 24 hours as indicated from the change of color of the DNA solution from white to a purplish-yellow. DNA-MS synthesis studies should be repeated to include longer reaction times for genipin crosslinking. DNA-MS studies should look at 2, 12, 24, and 48 hour time points to determine if genipin can be used as a crosslinking agent for DNA-MS. Crosslinking should be confirmed in phosphate buffered saline at a pH of 7.4 using hydrated particle sizing methods outlined in Chapters 3 through 6.

2. ***In vivo* efficacy and imaging studies with mitoxantrone loaded DNA-MS crosslinked with gadolinium.** *In vivo* studies should be conducted using our 16/C murine mammary adenocarcinoma cell model to determine the *in vivo* efficacy of mitoxantrone loaded DNA-MS. Studies should be conducted using similar methods as those presented in Dr. Brett Almond's dissertation.[4] Data obtained with DNA-MS should be compared to BSA-MS data. *In vivo* studies should also be conducted to determine the imaging potential of gadolinium crosslinked DNA-MS. Studies should be carried out with the assistance of faculty at the Brain Institute. It would also be interesting to determine if gadolinium crosslinked DNA-MS could be used for magnetically guided therapy.

3. ***In vivo* distribution testing of mitoxantrone loaded DNA-MS.** *In vivo* studies should be conducted to determine the distribution of DNA-MS within the tumor interstitium and throughout the body using the 16/C murine mammary adenocarcinoma cell model.

4. **Synthesis, characterization, and *in vitro* evaluations of mitoxantrone loaded DNA-MS crosslinked with glutaraldehyde and gadolinium.** Glutaraldehyde is assumed to crosslink DNA through the base pairs whereas gadolinium crosslinks DNA through the phosphate groups. DNA-MS synthesis should be repeated using both crosslinking agents simultaneously to determine their effect on MS morphology, topography, particle size, and mitoxantrone *in vitro* entrapment and release.

5. ***In vitro* evaluations of folic acid delivery from folic acid and mitoxantrone loaded DNA-MS.** Many human tumor cells are known to have overexpressed folic acid receptors on their surfaces such as breast, ovarian, lung, renal, and colon cancers.[171] Folic acid has been conjugated to various therapeutic particles to enhance their uptake into tumor cells.[171, 172] Folic acid conjugation has shown to increase the therapeutic efficacy of chemotherapy agents while also decreasing their systemic toxicity *in vivo*

using mice bearing human cancer cell lines due to an increase in tumor uptake.[172] *In vitro* studies should be conducted using folic acid loaded DNA-MS and BSA-MS to determine if the same outcome could be achieved through delivery of folic acid from a MS instead of through surface conjugation. DNA-MS and BSA-MS loaded with 15% (w/w) mitoxantrone and 0.5% (w/w) and 1% (w/w) folic acid were prepared and have been partially characterized with the assistance of Karly Jacobsen. Preliminary results are given in Appendix B. *In vitro* studies should be conducted to further characterize folic acid and mitoxantrone loaded DNA-MS and BSA-MS using a murine Lewis Lung Carcinoma cell line to determine if the delivery of folic acid increases mitoxantrone uptake. The cell study should look at the 1, 2, 4, 8, 12, 24, and 48 hour time points. The cell study should include free mitoxantrone, mitoxantrone loaded DNA-MS and BSA-MS (DNA-MXN-MS and BSA-MXN-MS), and folic acid loaded DNA-MXN-MS and BSA-MXN-MS. *In vitro* entrapment and release studies should also be conducted to determine if folic acid effects the entrapment and release of mitoxantrone.

6. ***In vitro* evaluations of mitoxantrone, methotrexate, or 5-fluorouracil loaded DNA-BSA blended MS.** Studies should be conducted to look at the *in vitro* entrapment and release properties of mitoxantrone, methotrexate, or 5-fluorouracil loaded DNA-BSA blended MS. MS should be prepared with 30% (w/w) drug loadings and compared at the 80:20 and 50:50 DNA to BSA ratios. Drug entrapment and loadings should be compared to DNA-MS and BSA-MS controls. MS should also be characterized by particle size, morphology, and topography.

7. **Delivery of Tumor Killing Bacteria.** Non-toxic systemic bacteria cocktails containing bacterium such as Clostridium novyi-NT have shown great potential in eradicating non-operable solid tumors in mice.[173] Their tumor killing potential may be maximized by delivering them intratumorally via MS prepared with biodegradable materials such as DNA or BSA. Bacteria loaded DNA-MS and BSA-MS should be prepared and tested *in vitro* for efficacy. DNA-MS and BSA-MS should be characterized by particle size, morphology, and surface topography. The tumor killing properties of the bacteria should be analyzed *in vitro* with murine Lewis Lung Carcinoma cells and compared to mitoxantrone releasing DNA-MS and BSA-MS.

8. **Synthesis of fruit or vegetable DNA-MS.** Now that DNA-MS synthesis and characterization protocols have been established, studies should be conducted on the synthesis of DNA-MS from fruit or vegetable DNA sources such as banana, onion, and tomato. DNA extraction protocols have been modified to produce optimal extraction yields and are presented in Appendix C. The next steps for these studies should include DNA purification followed by DNA-MS synthesis, DNA-MS characterization, and drug entrapment and release studies.

9. **Synthesis, characterization, and *in vitro* evaluations of 2-methacryloyloxyethyl phosphorylcholine (MPC), phosphorylcholine, or phosphatidylcholine modified DNA-MS and BSA-MS.** MPC phospholipid polymer surfaces have shown excellent *in vivo* blood compatibility due to high fractions of free water that can be bound to their surface.[174] Surfaces containing MPC or phosphorylcholine groups help to suppress blood

cell adhesion even in the absence of anticoagulants.[174] Furthermore, liposomes that have been sterically stabilized or modified with MPC, phosphorylcholine, phosphatidylcholine phospholipid polymers have prolonged the half-life, enhanced the cellular permeability of solid tumor cells, provided an "anti-burst" sustained release, and increased the uptake of chemotherapy agents *in vivo*. [175-179] These phospholipid modified liposomes have also shown multiple imaging or therapeutic agent loading capabilities.[175-178] Therefore, DNA-MS and BSA-MS should be prepared following general MS synthesis procedures and modified with the aforementioned phospholipid polymers. DNA-MS may be modified through electrostatic interactions found with the phosphate groups found in the phospholipid polymers. BSA-MS may be modified with covalent interactions between the amino groups of the phospholipid polymers and the free aldehyde groups of the BSA-MS. For BSA-MS modifications, BSA-MS should be prepared by crosslinking the organic phase, rather than the aqueous phase since organic phase crosslinking yields many free aldehyde groups at the surface of the BSA-MS.[11] DNA-MS and BSA-MS should be characterized by particle size, morphology, and surface topography. The effects of phospholipid modification on drug entrapment, release, and uptake by tumor cells should also be analyzed.

10. **Synthesis, Characterization, and *In Vitro/Vivo* Evaluations of DNA-MS and BSA-MS Loaded with Antiangiogenic Drugs.** Angiogenesis, which is the formation of new vascular networks in tumors, is thought to be the lead contributor to tumor metastasis.[35, 180, 181] Angiogenic vessels develop rapidly in vessels due to vascular endothelial growth factor (VEGF).[181] Bevacizumab is an antiangiogenic drug recently approved by the FDA for its use against renal and colon cancers. [180] Bevacizumab is a monoclonal antibody that functions against VEGF and helps to inhibit capillary and vessel growth.[180] Bevacizumab is typically given in combination with other chemotherapy drugs such as 5-Fluorouracil (5-FU) intravenously and has shown statistically significant survival improvements in human colorectal cancer clinical trials.[182] Studies should be conducted to evaluate the *in vitro* and *in vivo* efficacy of bevacizumab loaded DNA-MS and BSA-MS. Study should compare the *in vitro* efficacy of bevacizumab, bevacizumab and 5-FU, and 5-FU loaded DNA-MS and BSA-MS against blank MS using murine Lewis Lung Carcinoma cells. The study should then be repeated *in vivo* using the murine mammary adenocarcinoma model. Loading with respect to particle size and morphology should also be evaluated.

APPENDIX A
EDS CHARACTERISTIC X-RAY DESIGNATIONS AND ENERGIES FOR DNA NANO-MESO-MICROSPHERES

Table A-1. Characteristic x-ray designations and energies for elements analyzed via energy dispersive x-ray spectroscopy.[106]

Element	Designation	Energy (keV)
Silicon	$K\alpha_{1,2}$	1.739
Carbon	$K\alpha$	0.277
Sodium	$K\alpha_{1,2}$	1.041
	$K\beta$	1.071
Phosphorous	$K\alpha_{2}$	2.012
	$K\alpha_{1}$	2.013
Gadolinium	$M\varsigma$	0.914
	$M\alpha$	1.185
	$M\beta$	1.209
	$L\iota$	5.362
	$L\alpha_{2}$	6.025
	$L\alpha_{1}$	6.057
	$L\beta_{6}$	6.867
	$L\beta_{2,15}$	7.102
	$L\beta_{7}$	7.207
	$L\gamma_{1}$	7.785
Chlorine	$K\alpha_{2}$	2.620
	$K\alpha_{1}$	2.622
	$K\beta$	2.815
Chromium	$L\iota$	0.500
	$L\beta_{1}$	0.582
	$K\alpha_{2}$	5.405
	$K\alpha_{1}$	5.414
	$K\beta_{1,3}$	5.946
Potassium	$K\alpha_{1}$	3.313
	$K\beta_{1,3}$	3.589
Iron	$L\beta_{3,4}$	0.792
	$K\alpha_{2}$	6.390
	$K\alpha_{1}$	6.403

APPENDIX B
FOLIC ACID MODIFICATION OF MITOXANTRONE LOADED DNA-MS AND BSA-MS PRELIMINARY RESULTS

Introduction

Many human tumor cells are known to have overexpressed folic acid receptors on their surfaces such as breast, ovarian, lung, renal, and colon cancers.[171, 183] Folic acid has been conjugated to various therapeutic particles to enhance their uptake into tumor cells.[171, 172] Folic acid conjugation has shown to increase the therapeutic efficacy of chemotherapy agents while also decreasing their systemic toxicity *in vivo* using mice bearing human cancer cell lines due to an increase in tumor uptake.[172] Therefore, folic acid modification of DNA-MS and BSA-MS was prepared as a possible enhancement for tumor cell uptake. DNA-MS and BSA-MS *in situ* loaded with 15% (w/w) mitoxantrone (DNA-MXN-MS or BSA-MXN-MS) were modified with 0.5% (w/w) and 1% (w/w) folic acid (FA) to initiate these studies. The particle diameter, size distribution, and morphology of the folic acid modified DNA-MXN-MS and BSA-MXN-MS were evaluated with respect to the folic acid incorporation. The particle diameters and size distributions were obtained using an LS Coulter 13 320 particle size analyzer and the morphology was assessed using a field emission scanning electron microscope. The preliminary data presented here was conducted with the assistance of Karly Jacobsen and summarizes the particle and morphological analysis of the FA modified DNA-MXN-MS and BSA-MXN-MS.

Materials and Methods

Materials

DNA sodium salt derived from herring testes Type XIV (DNA), albumin from bovine serum (BSA), cellulose acetate butyrate, HPLC grade 1,2-dichloroethane, methanol, gadolinium (III) chloride hexahydrate, 25% (w/w) Grade II aqueous glutaraldehyde solution, mitoxantrone dihydrochloride, and trichloroacetic acid were purchased from the Sigma-Aldrich Company.

Acetone, 70µm Spectra/Mesh® Nylon filters, and 15mL and 50mL polypropylene centrifuge tubes were purchased from Fisher Scientific International. Type I and Type II deionized ultrapure water was prepared with a resistivity of at least 16 MΩ-cm^{-1} using the Barnstead NANOpure™ Ultrapure Water System in the lab.

Methods

All solutions, synthesis, and characterization methods were performed as outlined in Chapters 4 through 6. Folic acid was loaded into MXN loaded aqueous DNA and BSA solutions using the same protocol for MXN loading.

Results

Preliminary particle size analysis illustrated that FA did not affect the particle size of the DNA-MS or DNA-MXN-MS. Each FA modified DNA-MS and DNA-MXN-MS condition produced an average dry mean particle size of 2.7µm ± 3.2µm, Figure B-1. FA modification did not affect BSA-MS particle size as well; however, a 2µm increase in mean dry particle sizes was observed with respect to MXN loading, Figure B-2. Table B-1 gives the dry mean particle diameters for each MS condition tested.

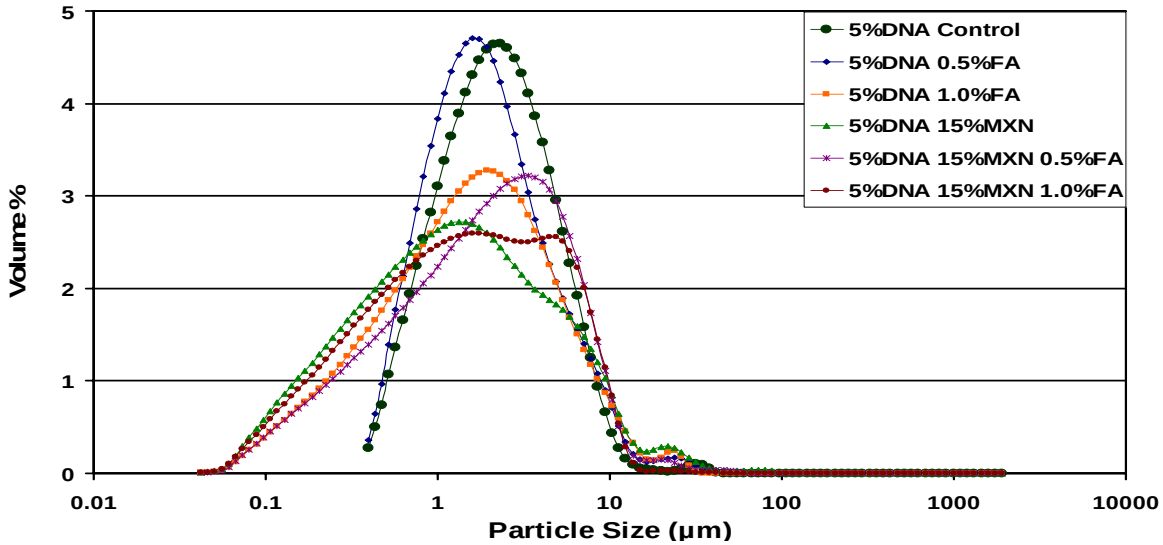

Figure B-1. Particle size distribution comparison of FA and MXN loaded DNA-MS conditions.

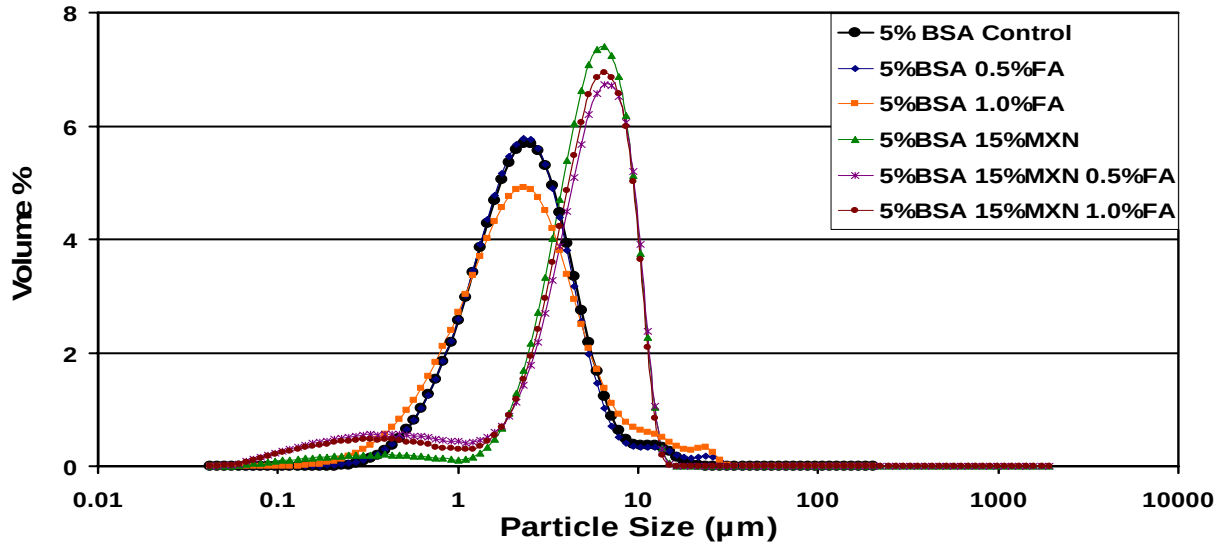

Figure B-2. Particle size distribution comparison of FA and MXN loaded BSA-MS conditions.

Table B-1. Dry mean particle diameters for FA and MXN loaded DNA-MS and BSA-MS.

Condition	Dry mean particle size (µm)
5%DNA Control	2.9 ± 2.7
5%DNA 15%MXN	2.7 ± 4.6
5%DNA 0.5%FA	2.8 ± 3.0
5%DNA 0.5%FA 15%MXN	2.9 ± 3.3
5%DNA 1%FA	2.6 ± 3.3
5%DNA 1%FA 15%MXN	2.5 ± 2.7
5%BSA Control	2.8 ± 2.2
5%BSA 15%MXN	6.1 ± 2.6
5%BSA 0.5%FA	2.9 ± 2.6
5%BSA 0.5%FA 15%MXN	5.3 ± 3.4
5%BSA 1%FA	3.2 ± 3.5
5%BSA 1%FA 15%MXN	5.3 ± 2.9

FA modified DNA-MS and DNA-MXN-MS produced discreet spherical particles with smooth surface topographies, Figures B-3 and B-4. FA modified BSA-MS also produced spherical particles with smooth topographies, Figure B-5, however, FA modified BSA-MXN-MS produced smooth and discreet particles with dish shaped morphologies, Figure B-6.

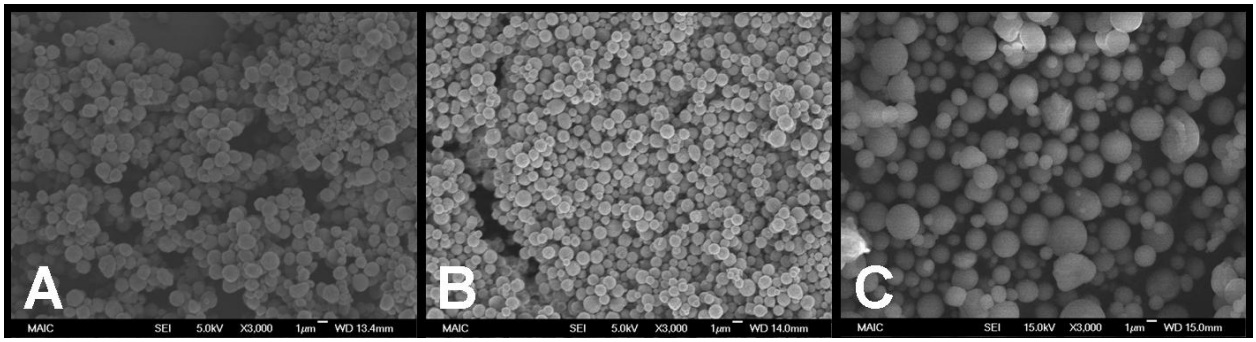

Figure B-3. SEM micrographs of DNA-MS with A) 0.5% FA, B) 1% FA, and C) no FA (Magnifications: 3,000x).

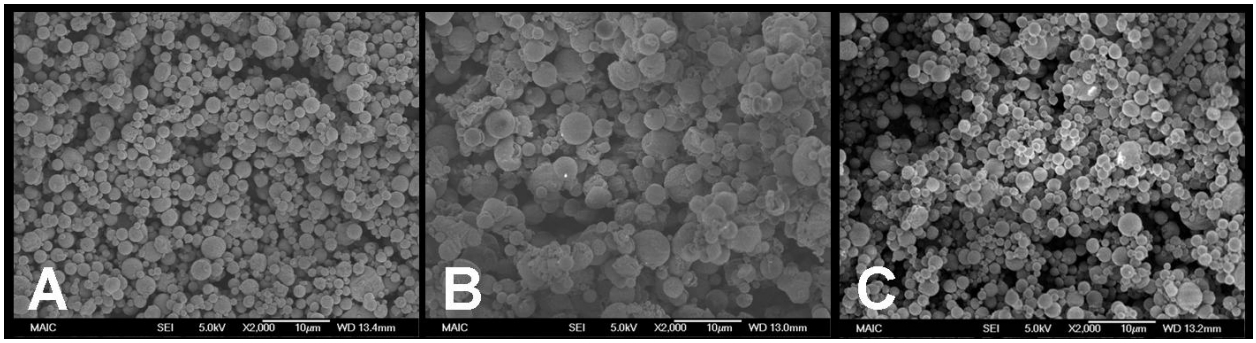

Figure B-4. SEM micrographs of DNA-MXN-MS with A) 0.5% FA, B) 1% FA, and C) no FA (Magnifications: 2,000x).

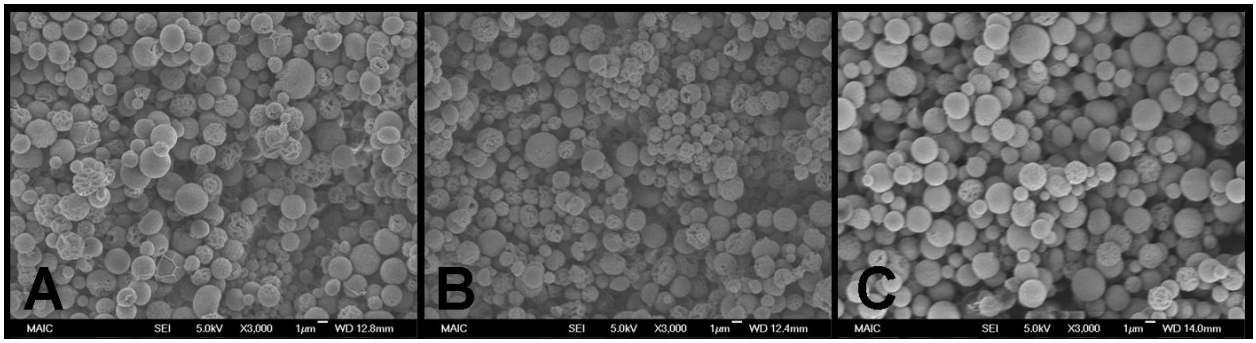

Figure B-5. SEM micrographs of BSA-MS with A) 0.5% FA, B) 1% FA, and C) no FA (Magnifications: 3,000x).

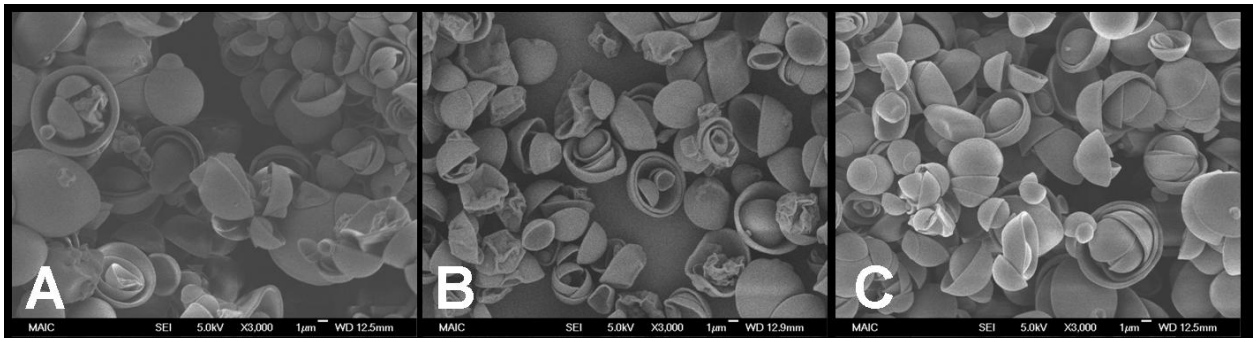

Figure B-6. SEM micrographs of BSA-MXN-MS with A) 0.5% FA, B) 1% FA, and C) no FA (Magnifications: 3,000x).

Preliminary Conclusions

The data presented in this appendix illustrates that FA may be *in situ* loaded into DNA-MS, BSA-MS, DNA-MXN-MS, and BSA-MXN-MS. The *in situ* loading of FA into DNA-MS and BSA-MS was visually noted by the light orange color of the resulting MS yields. FA modified MS produced optimal particle size properties with normal and narrow size distributions and dry diameters in the range of 50nm to15μm. Theoretical FA loadings were attempted up to 1.0% (w/w) and should be quantified in the future using a combination of FTIR, to confirm FA binding or loading, and a microbiological assay, to quantify FA uptake into DNA-MS and BSA-MS.[184] In addition, *in vitro* cell uptake tests using murine Lewis lung carcinoma cells were inconclusive (not presented here) in the FA theoretical range tested and should be retested to determine if FA modification increases DNA-MXN-MS and BSA-MXN-MS uptake.

APPENDIX C
FRUIT AND VEGETABLE DNA EXTRACTION PROTOCOLS

Overview

Based on the success obtained with DNA nano-meso-microsphere (DNA-MS) synthesis using DNA derived from herring testes, experiments were set forth to prepare DNA-MS from DNA extracted from fruit and vegetables. DNA extraction protocols were acquired and modified to produce optimal extraction yields. DNA-MS syntheses were attempted; however, discreet particles were not obtained due to the contamination of polysaccharides in the extracted DNA yields. DNA extraction protocols are described below for the extraction of DNA from bananas, onions, and tomatoes. The most efficient extraction process with the highest DNA yields is obtained using the banana DNA extraction protocol; however, each individual protocol will produce good extracted DNA yields. These protocols may also be modified to extract DNA from other living sources. Future studies should include the purification of the extracted DNA using DNA purification kits such as those that may be purchased from Promega (i.e. the solution-based Wizard® Genomic DNA purification kit). DNA-MS should then be prepared using methods described in Chapters 4 through 6 using DNA extracted from bananas, onions, or tomatoes.

Materials

6 Bananas, or bag of yellow Spanish onions, or 8 Plum Tomatoes or 4 Regular Sized Tomatoes
Ethanol squirt bottle
Refrigerator
Test tube rack
12 – 15 50mL polypropylene centrifuge tubes
3 – 6 spatulas
200mL glass bottle with lid
1L plastic bottle with lid
2 magnetic stir bars
Sodium lauryl sulfate (or sodium dodecyl sulfate)
Sodium citrate
Deionized salt (sodium chloride)

Adolf's meat tenderizer
Ethylenediamine tetraacetic acid (EDTA)
1L glass beaker
2 ½ #6 Coffee filters
Metal strainer
Parafilm strips
Sharpie marker
Blender
Thermometer
1 Round 2L bowl dish
Cutting board
Knife
Tape
1 stir plate
1 heat plate
1 25mL pipette
1 10mL pipette
2 pipette bulbs

Protocols

Homogenization Medium

1. Place large magnetic stir bar into the 1L plastic bottle.
2. Weigh out 50g of the sodium lauryl sulfate and add to the bottle.
3. Weigh out 8.770g of the deionized sodium chloride and add to the bottle.
4. Weigh out 4.410g of the sodium citrate and add to the bottle.
5. Weigh out 0.292g of the ethylenediamine tetraacetic acid (EDTA) and add to the bottle.
6. Add 1L of ultrapure water to the bottle.
7. Cap the bottle and parafilm.
8. Place bottle on stir plate and allow to stir for an hour.

Enzyme Solution

1. Place a magnetic stir bar into the 250mL glass bottle.
2. Weigh out 10g of the Adolf's meat tenderizer and add to the bottle.
3. Add 190mL of ultrapure water to the bottle.
4. Cap the bottle and parafilm.
5. Place bottle on stir plate and allow to stir at low speed throughout the extraction experiment.

Banana DNA Extraction

1. Place ethanol squirt bottle in the refrigerator and allow to chill during experiment (best if placed in the refrigerator the night before – keep ethanol in refrigerator at all times).
2. Prepare 1L of the homogenization medium and 200mL of the enzyme solution (Note: Homogenization medium may already be prepared from previous extraction. Medium

should not be used if it has been more than 7 days since last prepared. Enzyme solution will need to be prepared fresh for each extraction).[185, 186]

3. Cut up two bananas into ¼ inch pieces and place pieces into the 500mL beaker.
4. Pour the homogenization medium over the bananas until all the bananas are covered in medium (~200mL to 300mL).
5. Using one of the spatulas, mash the bananas in the medium. Continue to mash the bananas until the bananas/medium mixture looks syrupy.
6. Place the strainer over the 2L glass bowl dish and place the 2 ½ #6 coffee filters into the strainer making sure not to leave any open sections.
7. Pour the banana/medium mixture into the strainer and allow the mixture to filter.
8. During this time, repeat steps 3 to 7 for the remaining 4 bananas.
9. While the banana/medium solutions are filtering, label your centrifuge tubes with the following:

   Banana DNA
   Your Name
   Date

   Place a piece of invisible tape over the label to prevent the label from erasing.
10. Once straining is complete, pipette 20mL of the banana DNA solution into a 50mL PP centrifuge tube (Note: can do up to 6 tubes at a time).
11. Pipette 10mL of the enzyme solution into the centrifuge tube. Cap the tube and shake vigorously for 10 to 20 seconds in order to get a nice foam in the tube.
12. Set the tube down and slowly add very cold ethanol to the side of the tube in order to get an ethanol layer on top of the banana DNA solution. (Note: You should immediately see the banana DNA precipitate into the ethanol layer. Extracted DNA resembles the appearance and consistency of clear mucus.)
13. Cap and parafilm the tube.
14. Place into the refrigerator.
15. Repeat steps 10 through 14 until all the banana DNA solution has been used.
16. Once all the banana DNA solution has been used, place dishes in the sink.
17. Label an unused 50mL PP centrifuge tube using format from step 9. This will be your banana DNA collection tube.
18. Add 5mL of cold ethanol to the bottom of the centrifuge tube.
19. Using a new spatula, collect the extracted banana DNA from all the tubes in the refrigerator by scooping out the banana DNA and placing it into the collection tube.
20. After all the banana DNA has been collected, add 5mL of cold ethanol to the tube and cap.
21. Centrifuge the tube for 5 minutes at ~2600rpm.
22. After centrifuging, dump out ethanol into waste container being careful to not dump out extracted DNA.
23. Once all the ethanol has been removed from the extracted banana DNA, cap and parafilm the tube and place in freezer over night.
24. The next day, remove the frozen banana DNA from the freezer and place in the lyophilizer over night. (Note: Settings should be -45˚C>T>-41˚C and $10x10^{-3}$Mbar>P>$11x10^{-3}$Mbar)

Onion DNA Extraction

1. Place top part of blender in freezer and allow to chill through experiment (best if place blender in freezer night before).
2. Place ethanol squirt bottle in the refrigerator and allow to chill during experiment (also best if placed in the refrigerator the night before – keep ethanol in refrigerator at all times).
3. Prepare 1L of the homogenization medium and 200mL of the enzyme solution (Note: Medium may already be prepared from previous extraction. Enzyme solution will need to be prepared fresh for each extraction).[185, 186]
4. Cut the ends and the sides off of an onion. Dice the remaining onion into half inch squares.
5. Place the diced onions into the round 2L bowl dish.
6. Repeat steps 4 and 5 for four to six onions.
7. Pour approximately 200mL to 300mL of the homogenization medium[185] over the onion in the bowl.
8. Tape the thermometer to the inside of the bowl and turn the heat plate on to setting 6.
9. Allow onion mixture to homogenize for 12 minutes at a temperature between 55°C and 60°C[1]. (Note: Do not allow mixture to get warmer than 60°C)
10. After 12 minutes, remove the thermometer and place the onion mixture into the freezer and allow to cool for 8 minutes.
11. During this time, label your centrifuge tubes with the following:
    Onion DNA
    Your Name
    Date
    Place a piece of invisible tape over to prevent the label from erasing.
12. After 8 minutes, remove the onion DNA mixture and the top part of the blender from the freezer.
13. Assemble the blender and plug in.
14. Pour the onion DNA mixture into the blender and blend on low (Low button pressed with the Chop button at the same time) for 30 seconds and on high (High button pressed with the Chop button at the same time) for an additional 30 seconds. Allow to settle.
15. Place the strainer over the 1L glass beaker and place the 2 ½ #6 coffee filters into the strainer making sure not to leave any open sections.
16. Pour the blended onion DNA solution into the strainer. Allow complete straining.
17. Once straining is complete, pipette 20mL of the onion DNA solution into a 50mL PP centrifuge tube (Note: can do up to 6 tubes at a time).
18. Pipette 10mL of the enzyme solution into the centrifuge tube. Cap the tube and shake vigorously for 10 to 20 seconds in order to get a nice foam in the tube.
19. Set the tube down and slowly add very cold ethanol to the side of the tube in order to get an ethanol layer on top of the onion DNA solution.
20. Cap the tube and parafilm.
21. The onion DNA will precipitate into the ethanol.
22. Place into the refrigerator.
23. Repeat steps 17 through 22 until all the onion DNA solution has been used.

Tomato DNA Extraction

1. Place ethanol squirt bottle in the refrigerator and allow to chill during experiment (best if placed in the refrigerator the night before – keep ethanol in refrigerator at all times).
2. Prepare 1L of the homogenization medium and 200mL of the enzyme solution (Note: Homogenization medium[185] may already be prepared from previous extraction. Medium should not be used if it has been more than 7 days since last prepared. Enzyme solution will need to be prepared fresh for each extraction).[185, 186]
3. Dice up four plum tomatoes (or two regular sized tomatoes) and place pieces into the blender.
4. Pour the homogenization medium over the tomatoes until all the tomatoes are covered in medium (~200mL to 400mL).
5. Blend the tomatoes and the homogenization medium for 20 seconds on the lowest setting.
6. Allow the foam to settle for 5 minutes.
7. Place the strainer over the 2L glass bowl dish and place the 2 ½ #6 coffee filters into the strainer making sure not to leave any open sections.
8. Pour the tomato/medium mixture into the strainer and allow the solution to filter.
9. During this time, repeat steps 3 to 8 for the remaining 4 plum tomatoes (or 2 regular sized tomatoes).
10. While the tomato/medium solutions are filtering, label your centrifuge tubes with the following:

    Tomato DNA
    Your Name
    Date

    Place a piece of invisible tape over the label to prevent the label from erasing.
11. Once straining is complete, pipette 20mL of the tomato DNA solution into a 50mL PP centrifuge tube (Note: can do up to 6 tubes at a time).
12. Pipette 10mL of the enzyme solution into the centrifuge tube. Cap the tube and shake vigorously for 10 to 20 seconds in order to get a nice foam in the tube.
13. Set the tube down and slowly add very cold ethanol down the side of the tube in order to get an ethanol layer on top of the tomato DNA solution. (Note: You should immediately see the tomato DNA precipitate into the ethanol layer. Extracted DNA resembles the appearance and consistency of clear slime. Extracted tomato DNA will be reddish in color.)
14. Cap and parafilm the tube.
15. Place into the refrigerator.
16. Repeat steps 11 through 15 until all of the tomato DNA solution has been used.
17. Once all the tomato DNA solution has been used, place dishes in the sink.
18. Label an unused 50mL PP centrifuge tube using format from step 10. This will be your tomato DNA collection tube.
19. Add 5mL of cold ethanol to the bottom of the centrifuge tube.
20. Using a new spatula, collect the extracted tomato DNA from all the tubes in the refrigerator by scooping out the tomato DNA and placing it into the collection tube.
21. After all of the tomato DNA has been collected, add 5mL of cold ethanol to the tube and cap.
22. Centrifuge the tube for 5 minutes at ~2600rpm.

23. After centrifuging, dump out ethanol into waste container being careful not to dump out the extracted DNA.
24. Once all the ethanol has been removed from the extracted tomato DNA, cap and parafilm the tube and place in freezer over night.
25. The next day, remove the frozen tomato DNA from the freezer and place in the lyophilizer over night. (Note: Settings should be -45˚C>T>-41˚C and $10x10^{-3}$Mbar>P>$11x10^{-3}$Mbar)

LIST OF REFERENCES

1. Jemal A, Murray T, Ward E, Samuels A, Tiwari RC, Ghafoor A, Feuer EJ, Thun MJ. Cancer statistics, 2005. CA Cancer J Clin 2005;55(1):10-30.

2. American Cancer Society. Cancer facts and figures 2006. Atlanta: American Cancer Society; 2006.

3. Cukier D, Gingerelli F, Makari-Judson G, McCullough VE. Coping with chemotherapy and radiation. New York, NY: The McGraw-Hill Companies, Inc.; 2005.

4. Goldberg EP, Hadba AR, Almond BA, Marotta JS. Intratumoral cancer chemotherapy and immunotherapy: Opportunities for nonsystemic preoperative drug delivery. J Pharm Pharmacol 2002;54:159-80.

5. Cheung RY, Rauth AM, Wu XY. In vivo efficacy and toxicity of intratumorally delivered mitomycin c and its combination with doxorubicin using microsphere formulations. Anti-Cancer Drug 2005;16(4):423-33.

6. Jain RK. Delivery of novel therapeutic agents in tumors: Physiological barriers and strategies. J Natl Cancer I 1989;81:570-6.

7. Emerich DF, Snodgrass P, Lafreniere D, Dean RL, Salzberg H, Marsh J, Perdomo B, Arastu M, Winn SR, Bartus RT. Sustained release chemotherapeutic microspheres provide superior efficacy over systemic therapy and local bolus infusions. Pharm Res 2002;19(7):1052-60.

8. CreechJr. O, Krementz ET, Ryan RF, Winblad JN. Chemotherapy of cancer: Regional perfusion utilizing an extracorporeal circuit. Ann Surg 1958;148(4):616-32.

9. Anderson JH, McArdle CS, Cooke TG. Microparticulate carriers as a therapeutic option in regional cancer therapy: Clinical consideration. In: N Willmott, JM Daly, eds. Microspheres and regional cancer therapy. Boca Raton, FL: CRC Press, Inc.; 1994.

10. Chen Y, Burton MA, Gray BN. Pharmaceutical and methodological aspects of microparticles. In: N Willmott, J Daly, eds. Microspheres and regional cancer therapy. Boca Raton, FL: CRC Press, Inc.; 1994.

11. Hadba AR. Synthesis, properties, and in vivo evaluation of sustained release albumin-mitoxantrone microsphere formulations for nonsystemic treatment of breast cancer and other high mortality cancers [Doctoral Dissertation]. Gainesville, FL: University of Florida; 2001.

12. Almond BA, Hadba AR, Freeman ST, Cuevas BJ, York AM, Detrisac CJ, Goldberg EP. Efficacy of mitoxantrone-loaded albumin microspheres for intratumoral chemotherapy of breast cancer. J Control Release 2003;91:147-55.

13. York AM. Synthesis, properties, and in vivo evaluations of protein meso/microsphere compositions for intratumoral chemotherapy [Doctoral Dissertation]. Gainesville, FL: University of Florida; 2006.

14. Segura T, Shea LD. Surface-tethered DNA complexes for enhanced gene delivery. Bioconjugate Chem 2002;13:621-9.

15. Breaker RR. Natural and engineered nucleic acids as tools to explore biology. Nature 2004;432:838-45.

16. Luo D, Saltzman WM. Synthetic DNA delivery systems. Nat Biotechnol 2000;18(1):33-7.

17. Iwata K, Sawadaishi T, Nishimura S-I, Tokura S, Nishi N. Utilization of DNA as functional materials: Preparation of filters containing DNA insolubilized with alginic acid gel. Int J Biol Macromol 1996;18:149-50.

18. Zhao C, Liu X, Nomizu M, Nishi N. Blood compatible aspects of DNA-modified polysulfone membrane-protein adsorption and platelet adhesion. Biomaterials 2003;24:3747-55.

19. Tanaka K, Okahata Y. A DNA-lipid complex in organic media and formation of an aligned cast film. J Am Chem Soc 1996;118(44):10679-83.

20. Yamada M, Kato K, Shindo K, Nomizu M, Sakairi N, Yamamoto H, Nishi N. Immobilization of DNA by uv irradiation and its utilization as functional materials. Nucleic Acids Symp Ser 1999;42:103-4.

21. Stopek JB. Biopolymer-microglia cell compositions for neural tissue repair [Doctoral Dissertation]. Gainesville, FL: University of Florida; 2003.

22. Jaenke RS, Campeneere DD-D, Trouet A. Cadiotoxicity and comparative pharmacokinetics of six anthracyclines in the rabbit. Cancer Res 1980;40:3530-6.

23. Campeneere DD-D, Trouet A. DNA-anthracycline complexes. I. Toxicity in mice and chemotherapeutic activity against l1210 leukemia of daunorubicin-DNA and adriamycin-DNA. Eur J Cancer 1980;16(8):981-6.

24. York AM, Stopek JB, Enriquez IV, Martin PJ, Goldberg EP. Albumin-DNA mesosphere synthesis and characterization for local delivery of chemotherapy agents. In: 7th World Biomaterials Congress Transactions; 2004; Sydney, Australia: Society for Biomaterials; 2004.

25. Hanahan D, Weinberg RA. The hallmarks of cancer. Cell 2000;100:57–70.

26. Kaufman D, Chabner BA. Clinical strategies for cancer treatment: The role of drugs. In: BA Chabner, DL Longo, eds. Cancer chemotherapy and biotherapy: Principles and practice. 2nd ed. Philadelphia, PA: Lippincott-Raven Publishers; 1996.

27. Society AC. Cancer facts and figures 2007. Atlanta, GA: American Cancer Society, Inc.; 2007.

28. Hartwell LH, Lander ES. Report to national cancer advisory board: Ncab working group on biomedical technology. In: National Cancer Advisory Board, ed.: National Cancer Advisory Board; 2005.

29. World Cancer Research Fund, AICR. Food, nutrition and the prevention of cancer: A global perspective. In. London, UK: WCRF, AICR; 1997.

30. Cancer trends progress report - 2005 update. National Cancer Institute, NIH, DHHS, December 2005. (Accessed October 16, 2006, 2006, at http://progressreport.cancer.gov.)

31. Trouet A, Baurain R, Campeneere DD-D, Layton D, Masquelier M. DNA, liposomes, and proteins as carriers for antitumoral drugs. Recent Results Canc Res 1980;75:229-35.

32. Campeneere DD-D, Jaenke R, Trouet A, Baudon H, Maldague P. DNA-anthracycline complexes. II. Comparative study of the acute lesions induced in mice after intravenous administration of free and DNA bound adriamycin. Eur J Cancer 1980;16(8):987-98.

33. Trouet A, Sokal G. Clinical studies with daunorubicin-DNA and adriamycin-DNA complexes: A review. Canc Treat Rep 1979;63(5895-898).

34. Weinberg RA. The biology of cancer. New York, NY: Garland Science, Taylor & Francis Group, LLC; 2007.

35. Harrington L, Bristow RG, Hill RP, Tannock IF. Introduction to cancer biology. In: IF Tannock, RP Hill, RG Bristow, L Harrington, eds. The basic science of oncology. Fourth ed. Toronto, Canada: McGraw-Hill Medical Publishing Division; 2005.

36. Scott RE, Wille JJJ, Wier ML, Hoerl BJ, Maercklein PB. Carcinogenesis and defects in the integrated control of cell proliferation and differentiation. In: CM Veneziale, ed. Control of cell growth and proliferation. Rochester, MN: Van Nostrand Reinhold Company Inc.; 1985.

37. Bertram JS. The molecular biology of cancer. Mol Aspect Med 2001;21:167-223.

38. Pledger WJ. Regulation of cell proliferation: Serum growth factors control an ordered series of g_1 events. In: CM Veneziale, ed. Control of cell growth and proliferation. New York, NY: Van Nostrand Reinhold Company Inc.; 1985.

39. Potten C, Wilson J. Apoptosis: The life and death of cells. New York, NY: Cambridge University Press; 2004.

40. Rode H-J, Eisel D, Frost I, eds. Apoptosis, cell death, and cell proliferation. 3rd ed: Roche Diagnostics Corporation; 2004-2005

41. Heath JK. Principles of cell proliferation. Birmingham, United Kingdom: Blackwell Science Ltd.; 2001.

42. Bowen ID, Bowen SM, Jones AH. Mitosis and apoptosis: Matters of life and death. London, United Kingdom: Chapman & Hall; 1998.

43. Nurse PM. Cyclin dependent kinases and cell cycle control. Bioscience Rep 2002;22:487-99.

44. Hartwell LH. Yeast and cancer. Bioscience Rep 2002;22:373-94.

45. Pratt WB, Ruddon RW, Ensminger WD, Maybaum J. Principles of cancer chemotherapy. In: The anticancer drugs. 2nd ed. New York, NY: Oxford University Press, Inc.; 1994.

46. Corrie PG. Cytotoxic chemotherapy: Clinical aspects. Medicine 2004;32:25-9

47. Ingwersen KC. Cell cycle kinetics and antineoplastic agents. In: M Barton-Burke, GM Wilkes, KC Ingwersen, eds. Cancer chemotherapy: A nursing process approach 3rd ed. Sudbury, Massachusetts: Jones and Bartlett Publishers, Inc.; 2001.

48. Sörgel F. The return of ehrlich's 'therapia magna sterilisans' and other ehrlich concepts?: Series of papers honoring paul ehrlich on the occasion of his 150th birthday. Chemotherapy 2004;50:6-10.

49. Wilkes GM. Potential toxicities and nursing management. In: M Barton-Burke, GM Wilkes, KC Ingwersen, eds. Cancer chemotherapy: A nursing process approach. 3rd ed. Sudbury, MA: Jones and Bartlett Publishers, Inc.; 2001.

50. Rabussay D, Dev NB, Fewell J, Smith LC, Widera G, Zhang L. Enhancement of therapeutic drug and DNA delivery into cells by electroporation. J Phys D 2003;36:348-63.

51. Markman M. Principles of regional antineoplastic drug delivery. In: M Markman, ed. Regional chemotherapy: Clinical research and practice. Totowa, New Jersey: Humana Press Inc.; 2000.

52. Sinko P, Kohn J. Polymeric drug delivey systems. In: MA El-Nokaly, DM Piatt, BA Charpentier, eds. Polymeric delivery systems: Properties and applications. Washington, D.C.: American Chemical Society; 1993.

53. Kerr DJ. Introduction: Pharmacokinetic basis of regional chemotherapy. In: DJ Kerr, CS McArdle, eds. Regional chemotherapy: Theory and practice. Amersterdam, The Netherlands: Overseas Publishers Association; 2000.

54. Heller J, Hoffman AS. Drug delivery systems. In: BD Ratner, AS Hoffman, FJ Schoen, JE Lemmons, eds. Biomaterials science: An intoduction to materials in medicine. London, UK: Elsevier Academic Press; 2004.

55. Denkbas EB, Ottenbrite RM. Perspectives on: Chitosan drug delivery systems based on their geometries. J Bioact Compat Pol 2006;21:351-68.

56. Almond BA. Mitoxantrone-loaded albumin microspheres for localized intratumoral chemotherapy of breast cancer [Doctoral Dissertation]. Gainesville, FL: University of Florida; 2002.

57. Cuevas BJ. Synthesis and properties of protein micro/mesosphere-drug compositions designed for intratumoral cancer therapy [Doctoral Dissertation]. Gainesville, FL: University of Florida; 2003.

58. Kirk JF. Protein microspheres for controlled drug delivery and related analysis of biopolymers [Doctoral Dissertation]. Gainesville, FL: University of Florida; 1997.

59. Longo WE. Albumin microspheres for the controlled release of therapeutic agents [Doctoral Dissertation]. Gainesville, FL: University of Florida; 1983.

60. McArdle CS. Regional chemotherapy for colorectal liver metastases. In: DJ Kerr, CS McArdle, eds. Regional chemotherapy: Theory and practice. Amsterdam, The Netherlands: Overseas Publishers Association; 2000.

61. Walter KA, Tamargo RJ, Olivi A, Burger PC, Brem H. Intratumoral chemotherapy. Neurosurgery 1995;37:1129-45.

62. Cavalheiro S, Sparapani FVDC, Franco JOB, Silva MCD, Braga FM. Use of bleomycin in intratumoral chemotherapy for cystic craniopharyngioma. J Neurosurg 1996;84:124-6.

63. Nakamura Y, Hamabe Y, Ikuta H, Hyon S-H, Kuroda Y. An experimental study of regional chemotherapy using CDDP-loaded microspheres for esophageal cancer. Surg Today 2002;32:335-42.

64. Boiardi A, Eoli M, Salmaggi A, Zappacosta B, Fariselli L, Milanesi I, Broggi G, Silvani A. Efficacy of intratumoral delivery of mitoxantrone in recurrent malignant glial tumours. J Neuro-Oncol 2001;54:39-47.

65. Fournier E, Passirani C, Montero-Menei C, Colin N, Breton P, Sagodira S, Menei P, Benoit J-P. Therapeutic effectiveness of novel 5-fluorouracil-loaded poly(methylidene malonate 2.1.2)-based microspheres on f98 glioma-bearing rats. Cancer 2003;97:2822-9.

66. Yoo GH, Subramanian G, Boinpally RR, Iskander A, Shehadeh N, Oliver J, Ezzat W, Piechocki MP, Ensley JF, Lin H-S, Shibuya TY, Polin L, Parchment RE. An in vivo evaluation of docetaxel delivered intratumorally in head and neck squamous cell carcinoma. Arch Otolaryngol 2005;131:418-29.

67. Heller J, Hoffman AS. Drug delivery systems. In: BD Ratner, AS Hoffman, FJ Schoen, JE Lemons, eds. Biomaterials science: An introduction to materials in medicine. 2nd ed. San Diego, CL: Elsevier Academic Press; 2004.

68. Matsumura Y, Maeda H. A new concept for macromolecular therapeutics in cancer chemotherapy: Mechanism of tumoritropic accumulation of proteins and the antitumor agent smancs. Cancer Res 1986;46:6387-92.

69. Hirst DG. Blood flow and its modulation in malignant tumors. In: N Willmott, JM Daly, eds. Microspheres and regional cancer therapy. Boca Raton, FL: CRC Press, Inc.; 1994.

70. Murty SB, Wei Q, Thanoo BC, DeLuca PP. In vivo release kinetics of octreotide acetate from experimental polymeric microsphere formulations using oil/water and oil/oil processes. AAPS Pharm Sci Tech 2004;5:Article 49.

71. Jacobs IC, Mason NS. Polymer delivery systems concepts. In: MA El-Nokaly, DM Piatt, BA Charpentier, eds. Polymeric delivery systems: Properties and applications. Washington D.C.: American Chemical Society; 1993.

72. Schwartz JB, Simonelli AP, Higuchi WI. Drug release from wax matrices I. J Pharm Sci-US 1968;57:274-7.

73. Benita S, Hoffman A, Donbrow M. Microencapsulation of paracetamol using polyacrylate resins (eudragit retard), kinetics of drug release and evaluation of kinetic model. J Pharm Pharmacol 1985;37:391-5.

74. Ehtezazi T, Washington C, Melia CD. First order release rate from porous PLA microspheres with limited exit holes on the exterior surface. J Control Release 2000;66:27-38.

75. Higuchi T. Mechanism of sustained-action medication: Theoretical analysis of rate of release of solid drugs dispersed in solid matrices. J Pharm Sci-US 1963;52:1145-9.

76. Gohel MC, Panchal MK, Jogani VV. Novel mathematical method for quantitative expression of deviation from the Higuchi model. AAPS Pharm Sci Tech 2000;1:Article 31.

77. Higuchi T. Rate of release of medicaments from ointment bases containing drugs in suspension. J Pharm Sci-US 1961;50:874-5.

78. Pratt WB, Ruddon RW, Ensminger WD, Maybaum J. The anticancer drugs. In: The anticancer drugs. 2nd ed. New York, NY: Oxford University Press, Inc.; 1994.

79. Doroshow JH. Anthracyclines. In: BA Chabner, DL Longo, eds. Cancer chemotherapy and biotherapy: Principles and practice. 2nd ed. Philadelphia, PA: Lipincott-Raven Publishers; 1996.

80. Wilkes GM. Chemotherapeutic agents: Standardized nursing care plans to minimize toxicity. In: M Barton-Burke, GM Wilkes, KC Ingwersen, eds. Cancer chemotherapy: A nursing approach. 3rd ed. Sudbury, MA: Jones and Bartlett Publishers, Inc.; 2001.

81. Dorr RT, Hoff DDV. Drug monographs. In: RT Dorr, DDV Hoff, eds. Cancer chemotherapy handbook. 2nd ed. Norwalk, CT: Appleton & Lange; 1994.

82. Chu E, Allegra CJ. Antifolates. In: BA Chabner, DL Longo, eds. Cancer chemotherapy and biotherapy: Principles and practice. 2nd ed. Philadelphia, PA: Lippincott-Raven Publishers; 1996.

83. Grem JL. 5-fluoropyrimidines. In: BA Chabner, DL Longo, eds. Cancer chemotherapy and biotherapy: Principles and practice. 2nd ed. Philadelphia, PA: Lippincott-Raven Publishers; 1996.

84. Campbell NA. Biology. Fourth ed. Menlo Park, CA: The Benjamin/Cummings Publishing Company, Inc.; 1996.

85. Bonadio J. Tissue engineering via local gene delivery: Update and future prospects for enhancing the technology. Adv Drug Deliver Rev 2000;44:185-94.

86. Lehninger AL, Nelson DL, Cox MM. Principles of biochemistry. Second ed. New York, NY: Worth Publishers, Inc.; 1993.

87. Watson JD, Crick FHC. Molecular structure of nucleic acids: A structure for deoxyribose nucleic acid. Nature 1953;171:737-8.

88. Trouet A. Carriers for bioactive materials. In: RJ Kostelnik, ed. Polymeric delivery systems. New York, NY: Gordon and Breach Science Publishers, Inc.; 1978.

89. von der Beucken JJJP, Vos MRJ, Thüne PC, Hayakawa T, Fukushima T, Okahata Y, Walboomers XF, Sommerdijk NAJM, Nolte RJM, Jansen JA. Fabrication, characterization, and biological assessment of multilayered DNA-coatings for biomaterial purposes. Biomaterials 2006;27:691–701.

90. Morrison ID, Ross S. Colloidal dispersions: Suspensions, emulsions, and foams. New York, NY: John Wiley and Sons, Inc.; 2002.

91. Eichhorn GL, Shin YA. Interaction of metal ions with polynucleotides and related compounds. Xii. The relative effect of various metal ions on DNA helicity. J Am Chem Soc 1968;90:7323-8.

92. Kazakov SA. Nucleic acid binding and catalysis by metal ions. In: SM Hecht, ed. Bioorganic chemistry: Nucleic acids. New York, NY: Oxford University Press, Inc.; 1996:244-87.

93. Labiuk SL, Delbaere LTJ, Lee JS. Gamma and ultraviolet radiation cause DNA crosslinking in the presence of metal ions at high ph. Photochem Photobiol 2001;73(6):579-84.

94. McCluskey RA. Synthesis and properties of submicron albumin spheres [Doctoral Dissertation]. Gainesville, FL: University of Florida; 1987.

95. Sung H-W, Huang R-N, Huang LLH, Tsai C-C, C-T. Feasibility study of a natural crosslinking reagent for biological tissue fixation. J Biomed Mater Res 1998;42:560-7.

96. Sung H-W, Chang Y, Liang I-L, Chang W-H, Chen Y-C. Fixation of biological tissues with a naturally occurring crosslinking agent: Fixation rate and effects of pH, temperature, and initial fixative concentration. J Biomed Mater Res 2000;52(1):77-87.

97. Owen TC, inventor University of South Florida, assignee. Tetrazolium compounds for cell viability assays. US patent 5,185,450. February 9, 1993.

98. Berridge MV, Tan AS. Characterization of the cellular reduction of 3-(4,5-dimethylthiazol-2-yl)-2,3-diphenyltetrazolium bromide (MTT): Subcellular localization, substrate dependence, and involvement of mitochondrial electron transport in MTT reduction. Arch Biochem Biophys 1993;303:474-82.

99. Lehninger AJ. Biochemistry. 2nd ed. New York, NY: Worth Publishers, Inc.; 1975.

100. Raspaud E, Cruz MO, Sikorav JL, Livolant F. Precipitation of DNA by polyamines: A polyelectrolyte behavior. Biophys J 1998;74(1):381-93.

101. Touyama R, K. InoueK, Y. Takeda Y, M. Yatsuzuka M, T. Ikumoto T, N. Moritome N, Shingu T, Yokoi T, Inouye H. Studies on the blue pigments produced from genipin and methylamine. II: On the formation mechanisms of brownish-red intermediates leading to the blue pigment formation. Chem Pharm Bull 1994;42:1571-8.

102. Long EC. Fundamentals of nucleic acids. In: SM Hecht, ed. Bioorganic chemistry: Nucleic acids. New York, NY: Oxford University Press, Inc.; 1996:3-35.

103. Barton JK, Lippard SJ. Heavy metal interactions with nucleic acids. In: TG Spiro, ed. Nucleic acid-metal ion interactions. New York, NY: John Wiley & Sons, Inc.; 1980.

104. Marzilli LG, Kistenmacher TJ, Eichhorn GL. Structural principles of metal ion-nucleotide and metal ion-nucleic acid interactions. In: TG Spiro, ed. Nucleic acid-metal ion interactions. New York, NY: John Wiley & Sons, Inc.; 1980.

105. Bloomfield VA, Crothers DM, TinocoJr. I. Nucleic acids: Structures, properties, and functions. Sausalito, CA: University Science Books; 2000.

106. Weast RC, Astle MJ, eds. CRC handbook of chemisty and physics. 63rd ed. Boca Raton, FL: CRC Press, Inc.; 1982-1983.

107. Meyers D. Surfaces, interfaces, and colloids: Principles and applications. 2nd ed. New York, NY: John Wiley & Sons; 1999.

108. Arakawa H, Ahmad R, Naoui M, Tajmir-Riahi H-A. A comparative study of calf thymus DNA binding to Cr(III) and Cr(VI) ions: Evidence for the guanine N-7-chromium-phosphate chelate formation. J Biol Chem 2000;275:10150–3.

109. Ouameur AA, Arakawa H, Ahmad R, Naoui M, Tajmir-Riahi HA. A comparative study of Fe(II) and Fe(III) interactions with DNA duplex: Major and minor grooves bindings. DNA Cell Biol 2005;24:394–401.

110. Shindo D, Oikawa T. Analytical electron microscopy for materials science. Tokyo, Japan: Springer-Verlag; 2002.

111. Hu G-F. Copper stimulates proliferation of human endothelial cells under culture. J Cell Biochem 1998;69:326-35.

112. Liu R, Liu W, Doctrow SR, Baudry M. Iron toxicity in organotypic cultures of hippocampal slices: Role of reactive oxygen species. J Neurochem 2003;85:492–502.

113. Kehrer JP. The Haber–Weiss reaction and mechanisms of toxicity. Toxicology 2000;149:43–50.

114. Cornett CR, Markesbery WR, Ehmann WD. Imbalances of trace elements related to oxidative damage in Alzheimer's disease brain. Neurotoxicology 1998;19:339-45.

115. Jenner P. Oxidative stress in Parkinson's disease. Ann Neurol 2003;53:S26–S38.

116. Shrivastava HY, Ravikumar T, Shanmugasundaram N, Babu M, Nair BU. Cytotoxicity studies of chromium(III) complexes on human dermal fibroblasts. Free Radical Bio Med 2005;38:58– 69.

117. Heckl S, Debus J, Jenne J, Pipkorn R, Waldeck W, Spring H, Rastert R, von der Lieth CW, Braun K. CNN-Gd^{3+} enables cell nucleus molecular imaging of prostate cancer cells: The last 600 nm. Cancer Res 2002;62:7018–24.

118. Pathak AP. Magnetic resonance imaging of tumor physiology. In: PV Prasad, ed. Magnetic resonance imaging: Methods and biologic applications. Totowa, New Jersey: Humana Press, Inc.; 2006.

119. Zhitkovich A, Voitkun V, Costa M. Formation of the amino acid-DNA complexes by hexavalent and trivalent chromium in vitro: Importance of trivalent chromium and the phosphate group. Biochemistry 1996;35:7275-82.

120. Meade VM, Burton MA, Gray BN, Self GW. Distribution of different sized microspheres in experimental hepatic tumors. Eur J Cancer Clin Oncol 1987;23:37-41.

121. Teipel U, Bremser JK. Particle characterization. In: U Teipel, ed. Energetic materials: Particle processing and characterization. Weinheim, Germany: WILEY-VCH Verlag GmbH & Co. KGaA; 2005.

122. Barbosa-Canovas GV, Ortega-Rivas E, Juliano P, Yan H. Food powders: Physical properties, processing, and functionality. New York, NY: Kluwer Academic/Plenum Publishers 2005.

123. Cazabat AM, Chatenay D, Guering P, Urbach W, Langevin D, Meunier J. Dynamic processes in water/oil microemulsions. In: HL Rosano, M Clausse, eds. Microemulsion systems. New York, NY: Marcel Dekker, Inc.; 1987.

124. Feng JQ, Hays DA. Relative importance of electrostatic forces on powder particles. Powder Technol 2003;135-136:65– 75.

125. Saltiel C, Chen Q, Manickavasagam S, Schadler LS, Siegel RW, Menguc MP. Identification of the dispersion behavior of surface treated nanoscale powders. J Nanopart Res 2004;6:35–46.

126. Klokova TP, Volodin YA, Glagoleva OF. Effect of ultrasound on the colloidal-disperse properties of petroleum systems. Chem Tech Fuel Oil 2006;42:43-6.

127. Yong V, Hahn HT. Processing and properties of sic/vinyl ester nanocomposites. Nanotechnology 2004;15:1338–43.

128. Martinez CJ, Liu J, Rhode SK, Luijten E, Weeks ER, Lewis JA. Interparticle interactions and direct imaging of colloidal phases assembled from microsphere-nanoparticle mixtures. Langmuir 2005;21:9978-89.

129. Zhu X, Jiang D, Tan S, Zhang Z. Dispersion properties of alumina powders in silica sol. J Eur Ceram Soc 2001;21:2879–85.

130. Mateovic T, Kriznar B, Bogataj M, Mrhar A. The influence of stirring rate on biopharmaceutical properties of Eudragit RS microspheres. J Microencapsul 2002;19:29 - 36.

131. Benoit JP, Puisieux F. Microcapsules and microspheres for embolization and chemoembolization. In: P Guiot, P Couvreur, eds. Polymeric nanoparticles and microspheres. Boca Raton, FL: CRC Press, Inc.; 1986.

132. Kawaguchi Y, Oishi T. Synthesis and properties of thermoplastic expandable microspheres: The relation between crosslinking density and expandable property. J Appl Polym Sci 2004;93:505–12.

133. Jameela SR, Jayakrishnan A. Glutaraldehyde cross-linked chitosan microspheres as a long acting biodegradable drug delivery vehicle: Studies on the in vitro release of mitoxantrone and in vivo degradation of microspheres in rat muscle. Biomaterials 1995;15:769-75.

134. Yang Q, Owusu-Ababio G. Biodegradable progesterone microsphere delivery system for osteoporosis therapy. Drug Dev Ind Pharm 2000;26:61–70.

135. Gabor F, Ertl B, Wirth M, Mallinger R. Ketoprofen-poly(d,l-lactic-co-glycolic acid) microspheres: Influence of manufacturing parameters and type of polymer on the release characteristics. J Microencapsul 1999;16:1-12.

136. Yang Q, Williams D, Owusu-Ababio G, Ebube NK. Controlled release tacrine delivery system for the treatment of alzheimer's disease. Drug Deliv 2001;8:93–8.

137. Muvaffak A, Gurhan I, Hasirci N. Cytotoxicity of 5-fluorouracil entrapped in gelatin microspheres. J Microencapsul 2004;21(3):293-306.

138. Tong W, Wang L, D'Souza MJ. Evaluation of PLGA microspheres as delivery system for antitumor agent-camptothecin. Drug Dev Ind Pharm 2003;29(7):745-56.

139. Yang Q, Williams D, Owusu-Ababio G, Ebube NK. Controlled release tacrine delivery system for the treatment of Alzheimer's disease. Drug Deliv 2001;8:93-8.

140. Dobson J. Gene therapy progress and prospects: Magnetic nanoparticle-based gene delivery. Gene Therapy 2006;13:283-7.

141. Holden SA, Lan Y, Pardo AM, Wesolowski JS, Gillies SD. Augmentation of antitumor activity of an antibody-interleukin 2 immunocytokine with chemotherapeutic agents. Clin Cancer Res 2001;7:2862-9.

142. Lee SJ, Sakurai H, Koizumi K, Song GY, Bae YS, Kim H-M, Kang K-S, Surh Y-J, Saiki I, Kim SH. MAPK regulation and caspase activation are required in DMNQ S-52 induced apoptosis in lewis lung carcinoma cells. Cancer Lett 2006;233:57-67.

143. Bozdağ S, Çapan Y, Vural I, Dalkara T, Dogan AL, Guc D, Hincal AA, Deluca PP. In vitro cytotoxicity of mitoxantrone-incorporated albumin microspheres on acute promyelocytic leukaemia cells. J Microencapsul 2004;21:751-60.

144. Luftensteiner CP, Viernstein H. Statistical experimental design based studies on placebo and mitoxantrone-loaded albumin microspheres. Int J Pharm 1998;171:87-99.

145. Jameela SR, Jayakrishnan A. Glutaraldehyde cross-linked chitosan microspheres as a long acting biodegradable drug delivery vehicle: Studies on the *in vitro* release of mitoxantrone and *in vivo* degradation of microspheres in rat muscle. Biomaterials 1995;16:769-75.

146. Muvaffak A, Gurhan I, Hasirci N. Prolonged cytotoxic effect of colchicine released from biodegradable microspheres. J Biomed Mater Res B 2004;71B:295-304.

147. Memisoglu-Bilensoy E, Vural I, Bochot A, Renoir JM, Duchene D, Hincal AA. Tamoxifen citrate loaded amphiphilic β-cyclodextrin nanoparticles: In vitro characterization and cytotoxicity. J Control Release 2005;104:489–96.

148. Han HD, Lee A, Song CK, Hwang T, Seong H, Lee CO, Shin BC. In vivo distribution and antitumor activity of heparin-stabilized doxorubicin-loaded liposomes. Int J Pharm 2006;313:181–8.

149. Morrison ID, Ross S. Colloidal dispersions: Suspensions, emulsions, and foams. New York, NY: John Wiley and Sons, Inc.; 2002.

150. Bayomi MA. Aqueous preparation and evaluation of albumin-chitosan microspheres containing indomethacin. Drug Dev Ind Pharm 2004;30:329–39.

151. Oppenheim RC. Nanoparticulate drug delivery systems based on gelatin and albumin. In: P Guiot, P Couvreur, eds. Polymeric nanoparticles and microspheres. Boca Raton, FL: CRC Press, Inc.; 1986.

152. Jin J, Song M. Chitosan and chitosan–peo blend membranes crosslinked by genipin for drug release. J Appl Polym Sci 2006;102:436–44.

153. Mathiowitz E, Kreitz MR, Brannon-Peppas L. Microencapsulation. Encyc Control Drug Deliv 1999;2:493-546.

154. S. Bozdağ, Y. Çapan, I. Vural, T. Dalkara, A.L. Dogan, D. Guc, A.A. Hincal, Deluca aPP. In vitro cytotoxicity of mitoxantrone-incorporated albumin microspheres on acute promyelocytic leukaemia cells. J Microencapsul 2004;21:751-60.

155. Bellosillo B, Colomer D, Pons G, Gil J. Mitoxantrone, a topoisomerase II inhibitor, induces apoptosis of B-chronic lymphocytic leukaemia cells. Brit J Haematol 1998;100:142-6.

156. Bhalla K, Ibrado AM, Tourkina E, Tang C, Grant S, Bullock G, Huang Y, Ponnathpur V, Mahoney ME. High-dose mitoxantrone induces programmed cell death or apoptosis in human myeloid leukemia cells. Blood 1993;82:3133-40.

157. Vibet S, Mahéo K, Goré J, Dubois P, Bougnoux P, Chourpa I. Differential subcellular distribution of mitoxantrone in relation to chemosensitization in two human breast cancer cell lines. Drug Metab Dispos 2007;35:822-8.

158. Dubey RR, Parikh RH. Two-stage optimization process for formulation of chitosan microspheres. AAPS Pharm Sci Tech 2004;5:Article 5.

159. von Oss CJ. Interfacial forces in aqueous media. 2nd ed. Boca Raton, FL: Taylor & Francis Group, LLC; 2006.

160. Bahukudumbi P, Carson KH, Rice-Ficht AC, Andrews MJ. On the diameter and size distributions of bovine serum albumin (BSA)-based microspberes. J Microencapsul 2004;21:787-803.

161. Muvaffak A, Gurhan I, Gunduz U, Hasirci N. Preparation and characterization of a biodegradable drug targeting system for anticancer drug delivery: Microsphere-antibody conjugate. J Drug Target 2005;13:151–9.

162. Santhi K, Dhanaraj SA, Koshy M, Ponnusankar S, Suresh B. Study of biodistribution of methotrexate-loaded bovine serum albumin nanospheres in mice. Drug Dev Ind Pharm 2000;26:1293–6.

163. Chandy T, Das GS, Rao GHR. 5-fluorouracil-loaded chitosan coated polylactic acid microspheres as biodegradable drug carriers for cerebral tumours. J Microencapsul 2000;17:625 - 38.

164. Jia WJ, Liu JG, Zhang YD, Wang JW, Wang J, Sun CY, Pan YF, Yu C, Li GZ, Zhang H, Guo ML, Tu MJ, Qian ZY. Preparation, characterization, and optimization of pancreas-targeted 5-FU loaded magnetic bovine serum albumin microspheres. J Drug Target 2007;15:14-145.

165. Muvaffak A, Gürhan I, Hasirci N. Cytotoxicity of 5-fluorouracil entrapped in gelatin microspheres. J Microencapsul 2004;21:293-306.

166. Wang S, Peng T, Yang CF. Investigation on the interaction of DNA and electroactive ligands using a rapid electrochemical method. J Biochem Bioph Meth 2003;55:191–204.

167. Feofanov A, Sharonov S, Kudelina I, Fleury F, Nabiev I. Localization and molecular interactions of mitoxantrone within living K562 cells as probed by confocal spectral imaging analysis. Biophys J 1997;73:3317-27.

168. Panousis C, R.Phillips D. DNA sequence specificity of mitoxantrone. Nucleic Acid Res 1994;22:1342-5.

169. Bhardwaj SB, Shukla AJ, Collins CC. Effect of varying drug loading on particle size distribution and drug release kinetics of verapamil hydrochloride microspheres prepared with cellulose esters. J Microencapsul 1995;12:71-81.

170. Yang Q, Williams D, Owusu-Ababio G, Ebube NK. Controlled release of tacrine delivery system for the treatment of Alzheimer's disease. Drug Deliv 2001;8:93-8.

171. Sun C, Sze R, Zhang M. Folic acid-PEG conjugated superparamagnetic nanoparticles for targeted cellular uptake and detection by MRI. J Biomed Mater Res A 2006;78A:550-7.

172. Kukowska-Latallo JF, Candido KA, Cao Z, Nigavekar SS, Majoros IJ, Thomas TP, Balogh LP, Khan MK, BakerJr. JR. Nanoparticle targeting of anticancer drug improves therapeutic response in animal model of human epithelial cancer. Cancer Res 2005;65(12):5317-24.

173. Forbes NS. Profile of a bacterial tumor killer. Nat Biotechnol 2006;24:1484-5.

174. Ishihara K, Nomura H, Mihara T, Kurita K, Iwasaki Y, Nakabayashi N. Why do phospholipid polymers reduce protein adsorption? J Biomed Mater Res 1998;39:323-30.

175. Yuan F, Leunig M, Huang SK, Berk DA, Papahadjopoulos D, Jam RK. Microvascular permeability and interstitial penetration of sterically stabilized (stealth) liposomes in a human tumor xenograft. Cancer Res 1994;54:3352-6.

176. Huang SK, Lee K-D, Hong K, Friend DS, Papahadjopoulos D. Microscopic localization of sterically stabilized liposomes in colon carcinoma-bearing mice. Cancer Res 1992;52:5135-43.

177. Sengupta S, Sasisekharan R. Exploiting nanotechnology to target cancer. Brit J Cancer 2007;96:1315-9.

178. Sengupta S, Eavarone D, Capila I, Zhao G, Watson N, Kiziltepe T, Sasisekharan R. Temporal targeting of tumour cells and neovasculature with a nanoscale delivery system. Nature 2005;436:568-72.

179. Mier W, Hoffend J, Haberkorn U, Eisenhut M. Current strategies in tumor-targeting. In: M Los, SB Gibson, eds. Apoptotic pathways as targets for novel therapies in cancer and other diseases. New York, NY: Springer Science+Business Media, Inc.; 2005.

180. Magnon C, Galaup A, Rouffiac V, Opolon P, Connault E, Rose M, Perricaudet M, Roche A, Germain S, Griscelli F, Lassau N. Dynamic assessment of antiangiogenic therapy by monitoring both tumoral vascularization and tissue degeneration. Gene Ther 2007;14:108-17.

181. Bazan-Peregrino M, Seymour LW, Harris AL. Gene therapy targeting to tumor endothelium. Cancer Gene Ther 2007;14:117-27.

182. Hurwitz H, Fehrenbacher L, Novotny W, Cartwright T, Hainsworth J, Heim W, Berlin J, Baron A, Griffing S, Holmgren E, Ferrara N, Fyfe G, Rogers B, Ross R, Kabbinavar F. Bevacizumab plus irinotecan, fluorouracil, and leucovorin for metastatic colorectal cancer. New Engl J Med 2004;350:2335-42.

183. Zhang Y, Sun C, Kohler N, Zhang M. Self-assembled coatings on individual monodisperse magnetite nanoparticles for efficient intracellular uptake. Biomedical Devices 2004;6:33-40.

184. Tamura T. Microbiological assay of folates. In: MF Picciano, ELR Stokstad, JF Gregory, eds. Folic acid metabolism in health and disease: Contemporary issues in clinical nutrition. New York, NY: Wiley-Liss; 1990.

185. Protocol: DNA extraction from onion. (Accessed January 27, 2006, at http://dwb.unl.edu/Teacher/NSF/C08/C08Links/www.framingham.k12.ma.us/fhs/depts/science/Biotechnology/protocols.html#oniondna.)

186. Introduction to DNA extractions. Access Excellence @ the National Museum. (Accessed August 4, 2005, at http://www.accessexcellence.org/AE/AEC/CC/DNA_extractions.html.)

BIOGRAPHICAL SKETCH

Iris Vanessa Enriquez Cartagena was born on May 16, 1979 in Ponce, Puerto Rico to parents Iris and Pedro Enriquez. She and her parents moved to El Paso, Texas when she turned one. Her younger sister, Laura Susana, was born in El Paso, Texas a little after she turned four at which point her family moved to Spangdahlem, Germany. Iris and her family spent five exciting and very fun years in Germany before moving down to Melbourne, Florida where Iris attended Holland Elementary, De Laura Junior High School, and Satellite High School. While at De Laura, Iris became very interested in math and was nominated to interview for a special NASA program entitled NURTURE, which stood for NASA's Unique Residential Tutoring program for Up-and-coming Replacement Engineers. Iris was one of the 50 students chosen out of the 500 from Brevard County that applied for the program. Iris visited NASA at the Kennedy Space Center four times a year from grades 9 through 12 and shadowed engineers in various disciplines. On her last two visits, Iris shadowed materials science engineers in the Failure Analysis Department and fell in love with the discipline.

Iris was accepted to the Department of Materials Science and Engineering at the University of Florida in January of 1997. She graduated from Satellite High School in May of 1997 and started school in June of that year. At the beginning of her junior year, Iris began a three co-op rotation with the Kimberly-Clark Corporation in Neenah, Wisconsin. While at Kimberly-Clark, her interests in materials science and polymers science grew and developed. Once Iris returned from her co-op rotation, she finished up her senior year. Iris graduated *cum laude* from the Department of Materials Science and Engineering with a specialty in polymers science in August of 2002 and decided to pursue graduate school.

Iris was accepted to the graduate program in the Department of Materials Science and Engineering in August of 2002 and was awarded the NSF Alliance for Graduate Education and

the Professoriate Fellowship. She began pursuing her doctorate degree in materials science and engineering and joined Dr. Goldberg's research group in January 2003. Since then, Iris has been working on the development of DNA mesospheres for intratumoral chemotherapy applications. In May of 2004, she was awarded her master's of science degree and in October of 2005 she married James Schumacher. In August 2007, Iris was awarded a Doctorate of Philosophy in Materials Science and Engineering from the University of Florida, specializing in biomaterials. After graduation, Iris plans to move to Atlanta with her husband James, to pursue a career in materials science and engineering/biomaterials science at the Kimberly-Clark Corporation.